

PREPARATION AND LUMINESCENCE PROPERTIES OF ALKALI
ALUMINUM BORATE GLASSES DOPED WITH TRIVALENT RARE
EARTH IONS



A Thesis Submitted in Partial Fulfillment of the Requirements for the
Degree of Doctor of Philosophy in Physics
Suranaree University of Technology
Academic Year 2021

การเตรียมและสมบัติการเรืองแสงของแก้วลิเทียมมอลูมิเนียมบอเรต
ที่เจือด้วยไอออนของธาตุหายาก



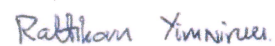
นางสาววิภากร ฤทธิสุทธิ์

วิทยานิพนธ์นี้เป็นส่วนหนึ่งของการศึกษาตามหลักสูตรปริญญาวิทยาศาสตรดุษฎีบัณฑิต
สาขาวิชาฟิสิกส์
มหาวิทยาลัยเทคโนโลยีสุรนารี
ปีการศึกษา 2564

PREPARATION AND LUMINESCENCE PROPERTIES OF ALKALI ALUMINUM
BORATE GLASSES DOPED WITH TRIVALENT RARE EARTH IONS

Suranaree University of Technology has approved this thesis submitted in partial fulfillment of the requirements for the Degree of Doctor of Philosophy.

Thesis Examining Committee



(Prof. Dr. Rattikorn Yimnirun)

Chairperson



(Assoc. Prof. Dr. Prapan Manyum)

Member (Thesis Advisor)



(Assoc. Prof. Dr. Saroj Rujirawat)

Member



(Assoc. Prof. Dr. Jakrapong Kaewkhao)

Member



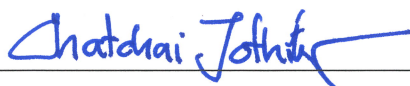
(Dr. Pinit Kidkhunthod)

Member



(Prof. Dr. Santi Maensiri)

Dean of Institute of Science



(Assoc. Prof. Dr Chatchai Jothityangkoon)

Vice Rector for Academic Affairs

and Quality Assurance

WIPAKORN RITTISUT : PREPARATION AND LUMINESCENCE PROPERTIES OF ALKALI ALUMINUM BORATE GLASSES DOPED WITH TRIVALENT RARE EARTH IONS. THESIS
ADVISOR : ASSOC. PROF. PRAPUN MANYUM, Ph.D. 188 PP.

Keyword: Lanthanides, Photoluminescence

The goal of this thesis is to investigate physical, luminescence, and optical properties of $25\text{Li}_2\text{O}-5\text{Al}_2\text{O}_3-\text{XGd}_2\text{O}_3-(69-\text{X})\text{B}_2\text{O}_3-1.0\text{R}_2\text{O}_3$ doped with Cerium (Ce^{3+}), Samarium (Sm^{3+}), Europium (Eu^{3+}), Terbium (Tb^{3+}), and Dysprosium (Dy^{3+}) prepared by conventional melt quenching technique at $1,200\text{ }^\circ\text{C}$ for 3 hours. It is interesting to understand the role of Gd_2O_3 in lithium aluminum borate glass systems, which has been known as a good host for various rare-earth oxides. The results show that doping with Cerium (Ce^{3+}), Samarium (Sm^{3+}), Europium (Eu^{3+}), Terbium (Tb^{3+}), and Dysprosium (Dy^{3+}) in high concentration increase the glasses molar volume due to the increasing of NBOs in the glasses network. The emitted of absorption spectra study indicate photon absorbing of glasses in the visible light and near infrared region. The emission spectra of Cerium, Samarium, Europium, Terbium and Dysprosium doped glasses show strongest emission at the wavelength of 350, 600, 614, 543 and 575 nm, respectively. The optimum concentration of Ce^{3+} , Sm^{3+} , Eu^{3+} , Tb^{3+} and Dy^{3+} for the strongest emission of $\text{Li}_2\text{O}-\text{Al}_2\text{O}_3-\text{Gd}_2\text{O}_3-\text{B}_2\text{O}_3-\text{R}_2\text{O}_3$ is 0.5, 0.50, 3.0, 4.0 and 1.0 mol%, respectively. CIE 1931 chromaticity investigation show that Sm^{3+} , Eu^{3+} , Tb^{3+} and Dy^{3+} doped glasses emit the light with color orange, reddish orange, green and white respectively. These kinds of luminescence functionality novel phosphor glasses could be a potential candidate for solid-state material applications.

School of Physics
Academic Year 2021

Student's Signature Wipakorn
Advisor's Signature P. Manyum

ACKNOWLEDGEMENTS

My thesis could not be accomplished without help and support from many people. Especially, I would like to acknowledge Assoc. Prof. Dr. Prapan Manyum, Prof. Dr. Rattikorn Yimnirun, Assoc. Prof. Dr. Jakrapong Kaewkhao, Assoc. Prof. Dr. Saroj Rujirawat and Dr. Pinit Kidkhunthod, thesis defense committee, for giving their valuable time and guiding good research aspects for my thesis defense and also give me many advices to make me better.

I would like to thank my advisors Assoc. Prof. Dr. Prapan Manyum, Prof. Dr. Rattikorn Yimnirun, Assoc. Prof. Dr. Jakrapong Kaewkhao for the opportunity they gave me to do this PhD in their groups, as well for all the advices, humanity, kindness, trust and support to develop my thesis work (courses, conferences, facilities, discussions and PhD funding). Because of all the help, patience, comprehension and care they showed during this time I feel very grateful and I could not think of better advisors.

I am grateful to Dr. Pinit Kidkhunthod for his management of beam time in my work at BL-5.2 Synchrotron Light Research Institute.

I would like to big thank Dr. Nuanthip Wantana, Dr. Pijika Mool-amkha, Dr.Ornuma Kalawa and Dr. Jintara Padchasri have helped me in completing this thesis from providing technical helps to valuable encouragements.

I would like to acknowledge my scholarship which is the Science Achievement Scholarship of Thailand (SAST) for financial support since bachelor's degree. It is impossible to list all my fellow graduate students that were a great support during my Ph.D. study, for all the great times we had together.

Thanks for your understanding, your never- ending encouragement, and for always being there for me. Your support has meant more to me than you could possibly realize. I would like to thank Mr. Adithep Butraburee and my family for being so supportive while I was working on my thesis.

Wipakorn Rittisut

CONTENTS

	Page
ABSTRACT IN THAI.....	I
ABSTRACT IN ENGLISH.....	II
ACKNOWLEDGEMENTS	III
CONTENTS	IV
LIST OF TABLES	VII
LIST OF FIGURES	VIII
CHAPTER	
I INTRODUCTION	1
1.1 Motivation.....	1
1.2 Research objectives.....	3
1.3 Expected objectives	4
1.4 Scope and Limitations of the Study	4
1.5 References.....	5
II REVIEW OF LITERATURES	7
2.1 Glass.....	7
2.2 Ingredients for making glass.....	11
2.3 Luminescence.....	14
2.4 Comparison of the fluorescence and phosphorescence phenomena.....	18
2.5 Basics of trivalent rare earth.....	20
2.6 Rare earth ions-doped glasses	22
2.7 Fundamentals of borate glasses.....	24
2.8 Previous study of glass system	29
2.9 Composition of the present glass	36
2.10 References.....	39

CONTENTS (Continued)

	Page
III RESEARCH METHODOLOGY	49
3.1 Research procedure.....	50
3.2 Sample preparation.....	50
3.3 Characterization techniques	53
3.4 Physical properties.....	53
3.5 Structural properties	55
3.6 Optical and spectral properties	57
IV CERIUM DOPED BORATE GLASS.....	62
4.1 Introduction.....	62
4.2 Experimental.....	64
4.3 Result and discussion.....	66
4.4 References.....	80
V SAMARIUM DOPED BORATE GLASS.....	84
5.1 Introduction.....	84
5.2 Experimental.....	87
5.3 Result and discussion.....	89
5.4 References.....	108
VI EUROPIUM DOPED BORATE GLASS	113
6.1 Introduction.....	113
6.2 Experimental.....	115
6.3 Result and discussion.....	116
6.4 References.....	133
VII TERBIUM DOPED BORATE GLASS.....	137
7.1 Introduction.....	137
7.2 Experimental.....	139
7.3 Result and discussion.....	141

CONTENT (Continued)

	Page
7.4 References	156
VIII DYSPROSIUM DOPED BORATE GLASS.....	160
8.1 Introduction.....	160
8.2 Experimental.....	162
8.3 Result and discussion.....	163
8.4 References.....	178
IX CONCLUSIONS AND FUTURE RESEARCH.....	182
9.1 CERIUM DOPED BORATE GLASS.....	182
9.2 SAMARIUM DOPED BORATE GLASS.....	183
9.3 EUROPIUM DOPED BORATE GLASS.....	184
9.4 TERBIUM DOPED BORATE GLASS.....	185
9.5 DYSPROSIUM DOPED BORATE GLASS.....	186
CURRICULUM VITAE.....	188

LIST OF TABLES

Table	Page
2.1 The basic properties of the trivalent rare earth.....	24
3.1 Chemical composition of LAGdxBR1.0 series.....	50
3.2 Chemical composition of LAGd2.5BRx glass series.....	51
4.1 Glass composition of glasses doped CeF ₃ 0.5 mol% increasing Gd ₂ O ₃	70
4.2 Assignment of FTIR bands of the glass system.....	73
4.3 Decay time comparison of LACB glasses with variation of Gd ₂ O ₃	80
5.1 The variation of energy transfer parameter of LAGdxBSm1.0 glasses.....	95
5.2 CIE chromaticity coordinates.....	106
6.1 The values of lifetime, energy transfer efficiencies of Eu ³⁺ glasses.....	132
7.1 The CIE color coordinates, correlated color temperature of LATB glass.....	150
7.2 The values of lifetime, energy transfer efficiencies of Tb ³⁺ glasses.....	155
8.1 The values of lifetime, energy transfer efficiencies of Dy ³⁺ glasses.....	170
8.2 The CIE coordinates, correlated color temperature for LAGd2.5BDy1.0.....	171
8.3 Dy ³⁺ ions concentration, the values of lifetime.....	177

LIST OF FIGURES

Figure	Page
2.1 The Crystal and glass of silica (SiO ₂) in two dimensions.....	8
2.2 illustrates a schematic enthalpy versus temperature plot for a glass-forming.....	9
2.3 Phase transition of general materials	10
2.4 Schematic representation of the oxide glass networks.....	12
2.5 Schematic representation of the network modifiers.....	13
2.6 Schematic representation of the network Intermediates	14
2.7 Electronic excitation.....	16
2.8 Types of luminescence and their energy sources	18
2.9 A simple model for Photoluminescence.....	19
2.10 Rare-earth ions of focus in this thesis	21
2.11 Energy levels of Ln ³⁺ and technologically crucial radiative transitions.....	21
2.12 Poly-borate groupings.....	27
2.13 structure of both crystalline and vitreous B ₂ O ₃	28
3.1 Glass Manufacturing Process.....	52
3.2 Flow chart for samples characterization.....	53
3.3 Densitometer	54
3.4 Refractometer.....	55
3.5 Powder X-ray Diffraction.....	56
3.6 X-ray absorption spectroscopy	57
3.7 Fourier-transform infrared spectroscopy.....	58
3.8 Diagram of the UV-Vis NIR spectrometer.	59
3.9 Shimadzu 3600 UV-Vis-NIR spectrophotometer	60
3.10 Agilent technology Cary Eclipse fluorescence spectrometer.....	61
3.11 X-ray induced luminescence.....	61
4.1 Schematic illustration of the prepared glasses	65

LIST OF FIGURES (Continued)

Figure	Page
4.2 The glass samples of LAGB series with different concentration of CeF_3	66
4.3 Density, molar volume, refractive index and XRD analysis of the LAGB.....	67
4.4 The absorption spectra of glasses doped with CeF_3	68
4.5 PL spectra of Ce^{3+} doped and the energy level diagram.....	68
4.6 Photograph of samples with different concentrations of Gd_2O_3	69
4.7 Variation of density, molar volume and XRD of 0.5 mol% Ce-doped.	71
4.8 FTIR spectra of samples.	72
4.9 Optical absorbance and indirect bandgap of 0.5 mol% Ce-doped	74
4.10 The excitation and emission spectra of glass with different Gd_2O_3	75
4.11 X-ray induced scintillation spectra of LACB series glasses.....	76
4.12 Cerium L_{III} XANES spectra of 0.5Ce: LAXGB glasses	78
4.13 The decay curve under 286 nm excitation of LACB glasses.....	79
5.1 Schematic illustration of the prepared glasses	88
5.2 Images of glasses in the LAGdxBSm1.0 and LAGd2.5BSmx series.....	89
5.3 Density, molar volume, refractive index of the LAGdxBSm1.0 series.	90
5.4 XRD pattern of LAGdxBSm1.0 and LAGd2.5BSmx glass series.....	91
5.5 FTIR spectra with different concentrations of Gd_2O_3 doped glasses.....	92
5.6 The excitation and emission spectra of LAGdxBSm1.0 glasses.....	94
5.7 The partial energy level diagram and decay curves	94
5.8 The variation of energy transfer parameter and decay times.....	96
5.9 The I-H fitting curves ($S= 6, 8, 10$) with varying Sm^{3+} glasses.	98
5.10 The optical absorption spectra of the LAGd2.5BSmx glasses.	99
5.11 The excitation and emission spectra of LAGd2.5BSmx glasses.....	101
5.12 X-ray induced scintillation spectra of LAGd2.5BSmx glasses.....	102
5.13 Luminescence decay profiles of LAGd2.5BSmx glasses	104
5.14 CIE chromaticity coordinates for LAGd2.5BSm glasses	105
5.15 Normalized Sm L_{III} -edge XANES spectra.....	107

LIST OF FIGURES (Continued)

Figure	Page
6.1 Photograph of LAEUB glass series.....	116
6.2 Density, molar volume, refractive index of the LAEUB series.	117
6.3 X-ray diffraction pattern and FTIR transmittance spectra of glasses.....	118
6.4 The comparison of Eu L ₃ -edge XANES spectra of LAEUB series glass	119
6.5 The excitation and emission spectra of LAEUB glasses	120
6.6 Relationship between the intensity and concentration of LAEUB glasses.	122
6.7 The decay time and X-ray induced luminescence of LAEUB series	123
6.8 Density and molar volume relation of LAGB doped with Eu ₂ O ₃	124
6.9 Photograph of LAGB glass series.....	125
6.10 The optical absorption spectra of the LAGB glass series.	125
6.11 The excitation and emission spectra of LAGB glasses	127
6.12 Relationship between the intensity and concentration of LAGB glasses.....	128
6.13 Luminescence decay profiles of LAGB series	129
6.14 The decay spectral and I-H fitting curves.	131
6.15 The CIE coordinate diagram of LAGB series.	133
7.1 Glass Manufacturing Process.....	140
7.2 Cut and polished of LATB glasses.....	140
7.3 Density and molar volume relation of LATB doped with Tb ₂ O ₃	141
7.4 X-ray diffraction pattern and FTIR spectra of LATB glasses	141
7.5 The excitation and emission spectra of LATB glasses.....	144
7.6 Relationship between the intensity and concentration of LATB glasses.	144
7.7 The XANES spectra and X-ray induced luminescence of LATB glasses	145
7.8 Lifetime curve and 1931 CIE chromaticity diagram of LATB glasses.	146
7.9 The optical absorption and excitation spectra of the LABG glass series.	147
7.10 The emission spectra of LAGB glasses.....	148
7.11 The emission spectra of LAGB with different concentrations of Tb ³⁺	149
7.12 The decay profiles and energy diagram of Gd ³⁺ /Tb ³⁺	150

LIST OF FIGURES (Continued)

Figure	Page
8.1 Photograph of glasses with different Gd_2O_3 and Dy_2O_3 concentrations.....	164
8.2 Densities, molar volumes, and refractive index of glasses.....	164
8.3 XRD pattern of LAGdxBDy1.0 and LAGd2.5BDyx glasses.....	165
8.4 The excitation and emission spectra of LAGdxBDy1.0 glasses.....	167
8.5 The radioluminescence of LAGdxBDy1.0 glasses doped with Gd_2O_3	167
8.6 Relationship between the decay time and energy transfer of glasses.....	168
8.7 The decay curves and I-H fitting curves (S= 6, 8, 10).	169
8.8 The CIE chromaticity diagram of the best condition: LAGdxBDy1.0.....	170
8.9 The optical absorption of the LAGd2.5BDyx series.....	172
8.10 FTIR spectra of LAGd2.5BDy0 and LAGd2.5BDy1.0 glasses.....	173
8.11 The excitation and emission spectra of LAGd2.5BDyx glasses.....	173
8.12 Luminescence decay curves of Dy^{3+} doped glass.....	175
8.13 The comparison of normalized Dy L_{III} -edge XANES spectra of glasses	177

CHAPTER I

INTRODUCTION

1.1 Motivation

Glass is a very important amorphous solid that has been utilized in various structural applications over centuries. Nevertheless, it was not until the twentieth century that the significance of glass was redefined, with the introduction of modern electronics like the radio, television, and smartphones. This also encouraged scientists to investigate novel glass compositions in order to achieve higher electrical characteristics while meeting present commercial demand. Oxide-based glasses including SiO_2 (Mohan et al., 2013), GeO_2 (Gunji et al., 2020; Khalid et al., 2020), TeO_2 (Stambouli et al., 2013), P_2O_5 (Kaura et al., 2019; Shoaib et al., 2019) are characteristics of extensively used glass compositions today. Rare-earth (RE) doped glasses are another prominent glass composition that has attracted the interests of many scientists and engineers. The 4f (Karl et al., 2001) electronic configuration of rare earth ions in different glass substrates makes it possible to emit from ultraviolet to infrared, which has spread to many potential applications, including display equipment, fiber amplifiers, high-intensity optical equipment, optical information processing, optoelectronic equipment, non-invasive temperature sensor and solar cell. In laser technology, the RE-doped glasses have been considered as good luminescent materials for their application in solid-state lasers due to their visible emissions, facile manufacturing processes, and good thermal stability (Elbatal et al., 2007).

This is of a particular interest especially borate glasses systems, which belong to rare earth doped glasses and play a major role due to their applications for scintillating material, in terms of their visible emissions, luminescent and photonic applications (Wantana et al., 2019; Rajaramakrishna et al., 2019) such as color displays, mercury-free fluorescent lamps, infrared solid-state lasers, LEDs. Borate glass is a good

choice because it has high thermal stability, good strength, low melting point, various coordination numbers and excellent transparency (Vijayakumar et al., 2014). However, borate glass has some poor properties such as hygroscopic character (Park et al., 2013) and their performance is adversely affected absorption of moisture without being stable. Therefore, it is possible to improve many properties of multicomponent borate glasses and change the hygroscopic property of their glass network. As for the glass composition, Li_2O , Al_2O_3 , Gd_2O_3 , and B_2O_3 host glasses systems have been extensively studied in the literature because of its high stability, clear transparent and enhancing the intensity of emission spectra, especially Li containing materials are also considered as ideal scintillators for neutron detection (Zaman et al., 2016; Rittisut et al., 2021).

Currently, the largest global market for lithium is its use in glass for high temperature applications, where thermal shock resistance, lowering viscosity and melting temperature offering higher performance, energy savings and molding advantages are important. Moreover, lithium in borate glass contributes to the conversion of sp^2 planar BO_3 units into more stable sp^3 tetrahedral BO_4 units and non-bridging oxygen (NBO) can be generated. The addition of Al_2O_3 is important in this structure and mainly confers thermal stability and durability superior to most other elements. On the other hand, Gd_2O_3 (Onderisinova et al., 2015) could act as a network modifier and could enhance the emission for the oxide glass, but further improvement of fast and efficient energy transfer from host to luminescence core is required. Accordingly, borate host glasses such as lithium aluminum gadolinium borate system glasses have some significant properties such as high transparency, high thermal stability, high bond strength, low melting point, high refractive index, good Ln^{3+} solubility and low energy gap. Moreover, adding some rare earth elements, e.g., cerium, samarium, europium, terbium, dysprosium and erbium into the host glass would improve the optical properties of the glass. The luminescence studies of trivalent rare earth ions in glasses can provide information on transition probabilities, lifetimes, excited state, increase in density, hardness, refractive index, bond strength, lowering of melting point, and reduction of softening mark of glass, which are very important for the design and development of various optical and luminescent devices. This could

be achieved by integrating borate glasses doubly doped with rare earth ions with overlapping emission absorption levels. For this reason, the type and level of lanthanides in the host must be tailored. By utilizing the lanthanide-encoded borate host matrix, one can deliver an organization with improved luminescence efficiency. Mainstream researchers have so far concluded that the only means to deliver glasses with fast and improved energy transfer, and thus efficient luminescence, is to use a glass scaffold co-doped with lanthanides, as the co-doped organization has an advantage over the singly doped scaffold.

1.2 Research objectives

In this work, main of borate glass with composition of $25\text{Li}_2\text{O}-5\text{Al}_2\text{O}_3-\text{XGd}_2\text{O}_3-(69-\text{X})\text{B}_2\text{O}_3-1.0\text{R}_2\text{O}_3$ (where $\text{X}= 0-10.0$ mol% and R is trivalent rare-earth ions: Cerium, Samarium, Europium, Terbium and Dysprosium) were prepared for the study of their physical, chemical group, optical, photoluminescence and radioluminescence properties. The main objectives of this thesis are as follows:

- 1.Synthesis of $25\text{Li}_2\text{O}-5\text{Al}_2\text{O}_3-\text{XGd}_2\text{O}_3-(69-\text{X})\text{B}_2\text{O}_3-1.0\text{R}_2\text{O}_3$ glass series (R stands for trivalent rare earths: Cerium, Samarium, Europium, Terbium and Dysprosium) by conventional melt quenching technique.

- 2.Find the best concentration of Gd_2O_3 doped with trivalent rare earth ions in borate glass as host matrix in term of this structural, physical, group chemical, optical, photoluminescence and radioluminescence properties.

- 3.To choose suitable pair of Ln^{3+} for the present matrix to enhance luminescence.

- 4.Determine the influence of concentration and type of dopants, such as trivalent rare earth ions, in improving the luminescence properties of the glass.

- 5.Investigate the influence of dual trivalent rare earths doped borate glasses as potential candidates for photonic applications.

- 6.To study the luminescence and scintillation properties of dual trivalent rare earths doped borate glasses by conventional photoluminescence and X-ray luminescence.

7. Analysis of mechanical properties and characteristic structure of $25\text{Li}_2\text{O}-5\text{Al}_2\text{O}_3-2.5\text{Gd}_2\text{O}_3-(67.5-X)\text{B}_2\text{O}_3-\text{XR}_2\text{O}_3$ glasses using XRD, FTIR, XAS, decay time, and UV-Vis techniques.

1.3 Expected objectives

1. The series of $25\text{Li}_2\text{O}-5\text{Al}_2\text{O}_3-\text{XGd}_2\text{O}_3-(69-X)\text{B}_2\text{O}_3-1.0\text{R}_2\text{O}_3$ glasses can be prepared by the melt-quenching technique.

2. To understand the role of Cerium, Samarium, Europium, Terbium and Dysprosium in borate glasses systems.

3. At least two papers carrying out in this work will be published in the international Journals.

1.4 Scope and Limitations of the Study

In this study, series of lithium aluminum borate glasses singly and doubly doped with Gd^{3+} and trivalent rare earth ions were prepared by mixing and melting appropriate amounts of $25\text{Li}_2\text{O}-5\text{Al}_2\text{O}_3-\text{XGd}_2\text{O}_3-(69-X)\text{B}_2\text{O}_3-1.0\text{R}_2\text{O}_3$ glasses, where X 0, 2.5, 5.0, 7.5, and 10.0 mol%. The trivalent rare earth oxide (R_2O_3) was inserted as a transition into the borate to improve the host organization, and Li_2O , Al_2O_3 , Gd_2O_3 , and B_2O_3 were used as modifiers to reduce the hygroscopic properties. The rare earth oxides of trivalent series (Cerium, Samarium, Europium, Terbium and Dysprosium) were selected as dopants in order to investigate their effect on the structural, physical, chemical, optical, photo-luminescent and radio-luminescent properties of the glasses. The densities were first measured using a simple Archimedes method. The structure of the prepared samples was confirmed by X-Ray Diffraction (XRD) measurement. The optical properties of the glass series were resolved using the UV-Visible-NIR spectrometer, then the band gap was calculated from the UV-Visible-NIR spectra. The primary highlights for doped and undoped assays were monitored by Fourier transform infrared spectroscopy (FTIR). Their luminescence properties were determined by photoluminescence and X-ray luminescence spectrometers. The oxidation state of the rare earth oxide doped borate glasses was evaluated by X-ray absorption near edge

structure spectroscopy (XANES). This research will be valuable for further basic studies in the glass science particularly the application of the rare earth doped glass for optical applications. Additionally, this dissertation can lead and encourage other fields of improvement in photonics (photonics: includes the generation, emission, transmission, modulation, signal processing, switching, amplification, detection, and sensing of light).

1.5 References

- ElBatal, F. H., Selim, M. S., Marzouk, S. Y., and Azooz, M. A. (2007). UV-vis absorption of the transition metal-doped $\text{SiO}_2\text{-B}_2\text{O}_3\text{-Na}_2\text{O}$ glasses. *Physica B: Physics of Condensed Matter*, 398, 126:134.
- Gunji, R. M., Mattos, G. R. S., Bordon, C. D. S., Gomez-Malagon, L. A., and Kassab, L. R. P. (2020). Efficiency enhancement of silicon solar cells covered by $\text{GeO}_2\text{-PbO}$ glasses doped with Eu^{3+} and TiO_2 nanoparticles. *Journal of Luminescence*, 223, 117244.
- Karl, G., Eyring, L., and Lander, G. H. (2001). Handbook of the physics and chemistry of Rare Earths. *Elsevier Science*.
- Kaura, P., Singh, D., and Singh, T. (2019). Sm^{3+} and Gd^{3+} Co-doped lead phosphate glasses for g-rays shielding and sensing. *Journal of Luminescence* (209), 74:88.
- Khalid, M., Lancaster, D. G., and Ebendorff-Heidepriem, H. (2020). Spectroscopic analysis and laser simulations of $\text{Yb}^{3+}/\text{Ho}^{3+}$ co-doped lead-germanate glass. *Optical Materials Express*, 10, 2819:2833.
- Mohan, M. M., Moorthy, L. R., and Jayasankar, C. K. (2013). Structural and optical properties of Sm^{3+} ions in potassium niobate silicate glasses. *International Journal of Advanced Research*, 3, 2:27.
- Onderisinova, Z., Kucera, M., Hanus, M., and Nikl, M. (2015). Temperature-dependent nonradiative energy transfer from Gd^{3+} to Ce^{3+} ions in co-doped LuAG : Ce, Gd garnet scintillators. *Journal of Luminescence*, 167, 106:113.
- Park, J. M., Ha, D. H., and Lee, S. W. (2016). Luminescence properties of Dy^{3+} doped lanthanum-calcium-silicaborate glass scintillator. *Journal of the Korean Physical Society*, 69, 1105:1109.

- Rajaramakrishna, R. , Nijapai, P. , Kidkhunthod, P. , Kim, H. J. , Kaewkhao, J. , and Ruangtaweeep, Y. (2019). Molecular dynamics simulation and luminescence properties of Eu^{3+} doped molybdenum gadolinium borate glasses for red emission. *Journal of Alloys and Compounds*, 813, 151914.
- Rittisut, W., Wantana, N., Butburee, A., Ruangtaweeep, Y., Padchasri, J., Rujirawat, S., and Kaewkhao, J. (2021). Luminescence properties of Ce^{3+} -doped borate scintillating glass for new radiation detection material. *Radiation Physics and Chemistry*, 185, 109498.
- Shoaib, M., Rooh, G., Chanthima, N., Rajaramakrishna, R., Kim, H. J., Wongdeeying, C., and Kaewkhao, J. (2019). Intriguing energy transfer mechanism in oxide and oxy-fluoride phosphate glasses. *Optical Materials*, 88, 429444.
- Stambouli, W., Elhouichet, H., Gelloz, B., and Férid, M. (2013). Optical and spectroscopic properties of Eu-doped tellurite glasses and glass ceramics. *Journal of Luminescence*, 138, 201:208.
- Vijayakumar, R., Maheshvaran, K., Sudarsan, V., and Marimuthu, K. (2014). Concentration dependent Luminescence studies on Eu^{3+} doped Telluro fluoroborate glasses. *Journal of Luminescence*, 154, 160:167.
- Wantana, N., Kaewnuam, E., Ruangtaweeep, Y., Valiev, D., Stepanov, S., Yamanoi, K., Kim, H. J. , and Kaewkhao, J. (2019). Radio, cathodo and photoluminescence investigations of high density $\text{WO}_3\text{-Gd}_2\text{O}_3\text{-B}_2\text{O}_3$ glass doped with Tb^{3+} . *Radiation Physics and Chemistry*, 164, 108350.
- Zaman, F., Kaewkhao, J., Rooh, G., Srisittipokakun, N., and Kim, H. J. (2016). Optical and luminescence properties of $\text{Li}_2\text{O-Gd}_2\text{O}_3\text{-MO-B}_2\text{O}_3\text{-Sm}_2\text{O}_3$ (MO Bi_2O_3 , BaO) glasses. *Journal of Alloys and Compounds*, 676, 275:285.

CHAPTER II

REVIEW OF LITERATURES

This chapter present relevant literature with a focus on glass materials and describes different host systems. The chapter also gives a brief look at doping optical glasses with trivalent rare-earth (RE) ions and luminescence, as well as their role in the development of new materials. It also gives an overview of glass that shows both photoluminescence and X-ray luminescence.

2.1 Glass

Glass is one of the oldest materials known to mankind. Glass has been used to create a wide range of utilitarian and ornamental items over the years. Glass's history as a creative craft has been partly influenced by technological developments in its fabrication and decorating, and in part by the history of taste and fashion. However, it is believed that the first glass was obtained about 400 BC. It was discovered by accident when calcium carbonate stones and sand were heated together (Schubert et al., 1997). A successful process for molding them was discovered approximately 300 years after the first registration, and this technique has been utilized ever since. The next progression in the history of glass occurred in the 15th century in Venice. Murano, the Venetian-island, became a center for glassmaking as early as the 13th century. Initially, Venetian glassmakers used numerous antique and medieval artistic techniques to create brightly colored and ornate pieces with themes typical of the Italian Renaissance. During the 1600s, Newton and Galileo encouraged optical research, and glasses have grown in importance because they are necessary in optical investigations. It is vital to recall that clear glasses were required at the time, and colorless glasses were still difficult to procure. Early in the 17th century, Bohemia became a significant glass-producing region, and it remained there until the early twentieth century. By the

17th century, England began producing glass in the Venetian tradition, which was distinguished by its simplicity. In 1675, glassmaker George Ravenscroft reported that adding lead oxide to Venetian-type glass produced a solid, heavier glass. Lead crystal, as it was afterwards known, became a popular variety of glass for fine dinnerware. Around 1800, different chemicals were used to make glass. As a result of the industrial revolution in 1850, the first glass plant opened in Jena in 1884 (Zacharias et al., 1932). Following that, the glasses were regularly investigated, from preparation to applications. "Glass is an amorphous solid with complete absence of long-range order and periodicity (Figure 2.1), displaying a glass transition area" according to the most widely recognized definition.

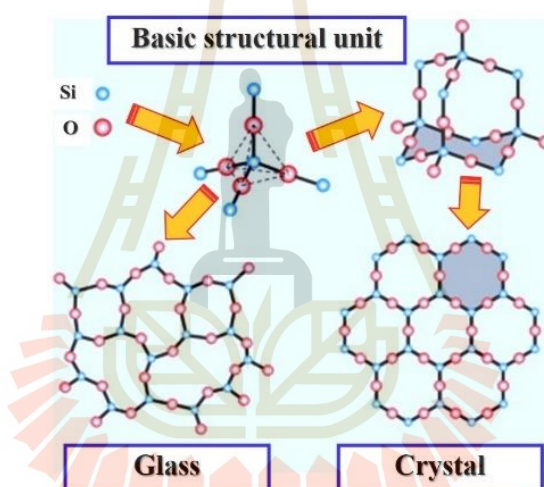


Figure 2.1 The Crystal and glass of silica (SiO₂) in two dimensions.

Glass, according to Zanotto and Mauro, is a nonequilibrium, non-crystalline condensed state of matter having a glass transition. Glasses have a structure that is similar to that of their supercooled liquid parents, and they naturally relax toward that state. Their ultimate fate is to crystallize in the face of infinite time (Zanotto et al., 2017). According to Zanotto and Mauro, one of the most well-known diagrams in glass science is the enthalpy and temperature diagram, which ranges from above the melting point to absolute zero, as seen in Figure 2.2. The concept that glass flows to a significant extent over long periods of time is not substantiated by empirical or theoretical research. From a more practical standpoint, glass should be regarded a

solid because it is rigid in everyday life. Owing to the unavailability of a first-order phase transition, some individuals believe glass to be a liquid. Volume, entropy, and enthalpy have all proven discontinuous throughout the glass transition range. However, the glass transition could be represented as related to a second-order phase transition in which the basic thermodynamic variables including such thermal expansivity and heat capacity are continuous (Stolkey et al., 1949) and the glass transition indicated in Figure 2.2. Notwithstanding this, the equilibrium theory of phase transformations in solids does not totally apply to glass, and thus the glass transition cannot be classified as one of the classical equilibrium phase transformations in solids. Even though the atomic structure of glass is similar to that of a super-cooled liquid, glass prefers to behave as a solid below the glass transition temperature (between T_m and T_g the super-cooled liquids (SCL)). A super-cooled liquid behaves like a liquid, but it is below the freezing point of the material and will crystallize relatively fast if a crystal is introduced as a core.

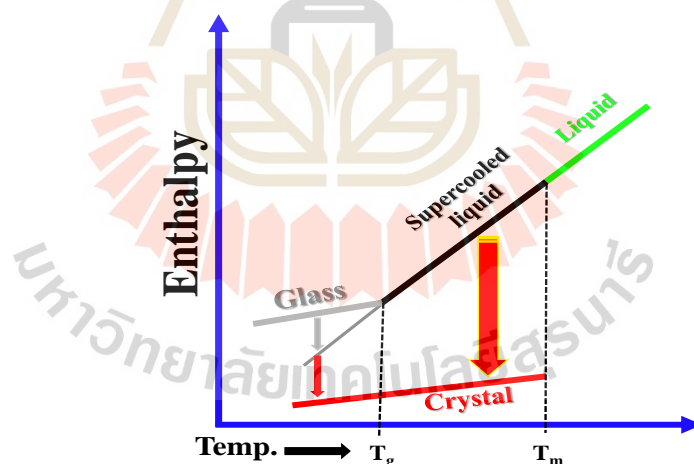


Figure 2.2 illustrates a schematic enthalpy versus temperature plot for a glass-forming material with four different states: liquid (L), supercooled liquid (SCL), glass (G), and crystal (C). T_m indicates the melting point or liquidus temperature, whereas T_g represents the glass transition temperature.

The difference in heat capacity during a glass transition and a melting transition of comparable materials is often of the same order of magnitude, indicating that the

change in active degrees of freedom is equivalent as well. In both a glass and a crystal, only the vibrational degrees of freedom remain active, while rotational and translational motion is halted. This explains why crystalline and non-crystalline materials display rigidity on most experimental time scales (Fedorov et al., 2015; Höland et al., 2012).

They can be found naturally (for example, obsidian) or obtained scientifically. The initial glasses created were not fully pure, but they exhibited some combinations of crystalline minerals and were deemed to be of low transparency quality. However, in the 1950s, researcher (Stolkey et al., 1949) modified his mind on glass with some crystalline phase. Although his study was unintentional, Stolkey discovered that after warming his glass, it had lost its transparency but gained greater mechanical resistance. From that moment forward, research into this new material was started, and it was discovered that glass-ceramics must be created under regulated, highly specific conditions. However, Stolkey's discovery was kept secret for over a decade, but after that, corning glass works publicized the discovery of Stolkey's substance, motivating other researchers to pursue this study route. Since the 1980s, scientists have been studying glass-ceramics, which includes a combination of glass and crystals, and focused on their production to acquire transparent materials with nanocrystals, which are important for photonic applications such as rare earth doped materials used in optical amplifiers, fibers based on the up-conversion process, and infrared solid-state lasers.

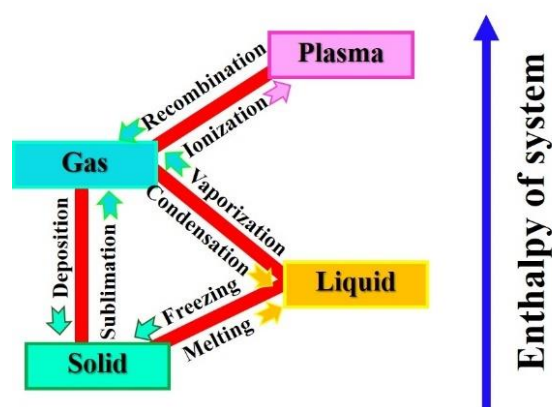


Figure 2.3 Phase transition of general materials.

The phase transition of the general materials is displayed in Figure 2.3. Glass is an amorphous (non-crystalline) solid substance, and its structure is given in Figure 2.3. Glasses are often brittle and often optically clear. Glass is often used for windows, bottles, and eyeglasses. The term "glass" originated in the late Roman Empire. The late-Latin name *glesum* is said to have arisen in the Roman glassmaking capital of Trier, situated in modern Germany, from a Germanic word for a translucent, shiny material. A glass is strictly defined as an inorganic fusion product that has been cooled through its glass transition to the solid state without crystallizing. Many glasses incorporate silica as their main component and glass forming. Moreover, the term glass is frequently used to refer to any amorphous solids (including melts that easily produce amorphous solids, polymers, resins, and other silica-free amorphous solids). Furthermore, in addition to typical melting processes, any additional method of preparation is examined, such as ion implantation and the sol-gel approach. Glass science and physics often exclusively deal with inorganic amorphous solids, whereas polymer science, biology, and other scientific fields deal with plastics and comparable organics.

2.2 Ingredients for making glass

Zachariasen group published the first study on these components in 1932, which is regarded as a landmark in glass research. In this research, he presents his beliefs on glass and categorizes the four main categories of cations that glass networks are composed of network formers, network modifiers, intermediates and minor ingredients.

2.2.1 Glass formers or network formers

Glass formers may be considered of as the glass's backbone, and modifying this element or compound would profoundly modify the ultimate material's characteristics. Some common cations that are in network formers are SiO_2 , B_2O_3 , GeO_2 , P_3O_5 , V_2O_5 , and As_2O_3 . These oxides are essential in the creation of glass because they build the foundation of the random three-dimensional network of glass. They have a high valence state (a surplus or shortage of electrons that allows them to bind easily with other atoms) and will covalently bond with oxygen. To achieve specific

characteristics in the glass, network ions that change the glass network and intermediates are introduced. For example, boron oxide, B_2O_3 , is a glass-forming oxide formed of flat triangles with boron atoms slightly out of the plane of the oxygen atoms. Boron oxide is a key component of various commercial glass kinds, notably borosilicate and aluminum-borosilicate glasses (Shelby et al., 1979).

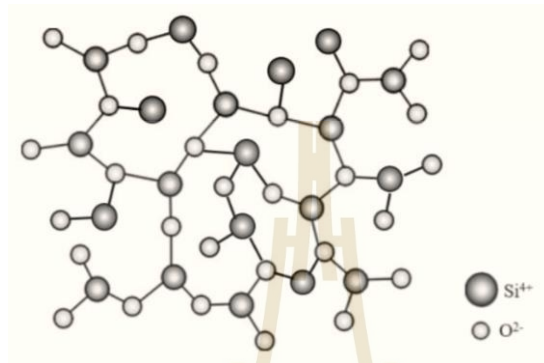


Figure 2.4 Schematic representation of structural units that build up an oxide glass network.

2.2.2 Network Modifiers

Additivity relationships essentially characterize the features of adjusted glass because glass typically behaves like a solution, which means that each element contributes to the bulk properties of the glass in an amount about proportionate to its concentration. Glass modifiers, which have a loose link with oxygen atoms, disrupt the typical bonding between glass-forming components and oxygen. The formation of "non-bridging oxygens" diminishes the relative quantity of strong bonding inside the glass. This implies that glass modifiers often have a major impact on glass characteristics. As a result of poorer overall bonding within the material, such effects as a decrease in melting point, surface tension, and viscosity might occur. Glass modifiers influence the coefficient of thermal expansion, chemical durability, and refractive index, making glass simpler to work with at lower temperatures while having no effect on transparency. Some examples include lithium oxide (Shelby et al., 1987), calcium oxide, potassium oxide, lead oxide, sodium oxide and zinc oxide have been used to fine-tune the features of glass to suit a variety of specialized advanced applications (Uhlmann et al., 1969).

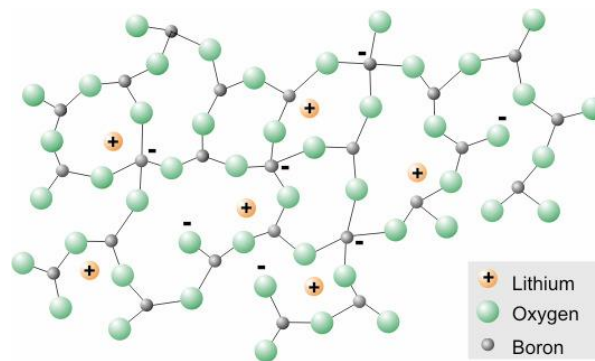


Figure 2.5 Schematic two-dimensional representation of the random structure of network modifiers (lithium) in borate glass.

2.2.3 Network Intermediates

Depending on the glass composition, the intermediates oxide in glasses include (titanium, aluminum, zirconium, beryllium, magnesium, and zinc) can perform as both network formers and modifiers. These oxides are provided in high concentrations to maintain structural continuity by connecting to the fundamental glass network.

2.2.4 Minor ingredients

A variety of additional chemicals are added to adjust the properties of the produced glass to meet the specifications. Here are several examples:

- Boron: The inclusion of boron affects the thermal and electrical characteristics of the glass, allowing Pyrex glassware to endure severe temperatures.
- Lead: To manufacture crystal glasses, lead is added. Because of its good reflecting characteristics, the glass generated thus looks to sparkle, and it is used to form decorative patterns on conventional glass.

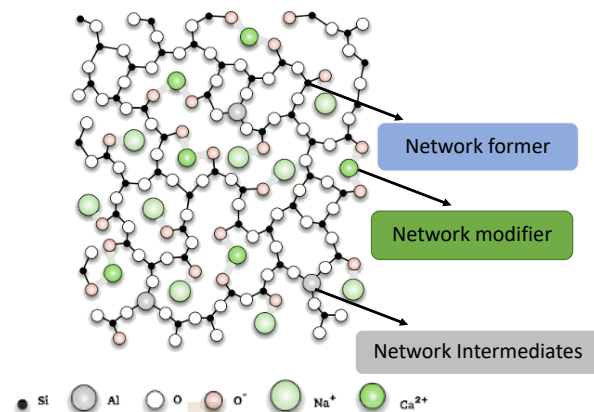


Figure 2.6 Schematic two-dimensional representation of the random network Intermediates in borate glass.

- Lanthium Oxide: It is utilized to manufacture high-quality lenses in glasses because of its excellent light-reflective characteristics. Thorium oxide was once utilized however, it is no longer used owing to its radioactive features.

- The addition of a wide range of chemicals can be used to color the glass. A clear glass is extremely tough to create. Glass is also colored using metals and oxides. For examples iron oxide: blue green, iron oxide and chromium: richer green, Sulphur and iron salts: amber, yellow, etc.

2.3 Luminescence

The emission of optical radiation (infrared, visible, or ultraviolet light) by matter is referred to as luminescence (Ying et al., 2019). It signifies the transformation of converted from one object to another, in this example, light. This occurrence is distinct from illumination, which is the emission of radiation by a material due to its high temperature (>500°C). Luminescence may happen in a variety of materials and under a variety of conditions. Atoms, various types of chemicals, polymers, organic or inorganic crystals, amorphous structures, and even living organisms will luminesce under the best conditions. The emission of luminescence in a solid material (phosphor) is caused by a radiative electronic transition in which an electron jumps from a higher energy level to a lower energy state, with the amount of energy released as photons (light emission). Nonetheless, for such a process to occur, the electron should first be

excited into a higher energy state by an external source of energy. There are two ways to return to the ground state, radiative decay and non-radiative decay. When an excited electron decays by producing photons, a process known as luminescence emission, it is referred to as radiative decay. When an excited electron decays to the ground state via producing phonons, this is referred to as non-radiative decay. In this scenario, the absorbed energy is lost as heat in the system, resulting in no emission. These two processes are antagonistic to one another. An efficient phosphor, but at the other hand, suppresses non-radiative decay and transforms the majority of the absorbed excitation energy into photons. These processes are depicted in Figure 7, which depicts the interactions of photons, electrons, and phonons in rare earth activated phosphors. In most rare earth-based phosphors, the luminescence process begins with electron absorption of energy on the 4f-4f transition. Due to losses that occur during the relaxation process, most phosphor materials emit at a lower energy than the absorbed energy. The difference between the maximums of the lowest excitation band and the emission band is referred to as the Stokes shift. Most elements' atoms have a varying number of electrons distributed throughout multiple shells and orbitals. Electrons are a fundamental particle. The luminescence is caused by electronic transitions. When the system absorbs energy, electrons are activated and raised to a higher energy level. Some electrons in the ground state are in the so-called HOMO state prior to stimulation (Highest Occupied Molecular Orbital). They are in the LUMO (Lowest Unoccupied Molecular Orbital) after reaching an excited state in Figure 2.7. Using photoluminescence as an illustration, the specifics of this works will be described.

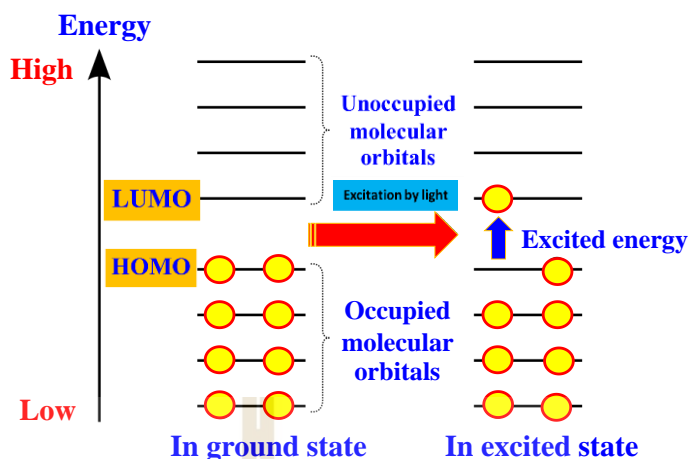


Figure 2.7 Electronic excitation.

The various energetic states of an atom or molecule are referred to as "energy levels". Because energy is quantized, electrons can only occupy discrete energy levels depending on the molecule or atom, which means that energy can only be received and released in specified proportions. Equation 2.1 could be used to compute the difference between two levels (where E_2 is the higher energy level and E_1 the lower one).

$$\Delta E = E_2 - E_1 \quad (2.1)$$

Photons, the particles that make up electromagnetic radiation or light, must have a particular energy value in order to excite electrons. Equation 2 may be used to determine the energy of a photon, where h is the Planck constant and ν is the frequency of the light.

$$E_{\text{photon}} = h\nu \quad (2.2)$$

The difference in energy levels equals the required excitation energy for electrons. Only light with a certain energy, as well as a specific frequency and wavelength, is possible to excite. The appropriate frequency and wavelength may be determined by equalizing equations 2.1 and 2.2 and using equation 2.3 (where c stands for the speed of light) (see eq. 4). UV-radiation is frequently used to excite.

$$\lambda = c/\nu \quad (2.3)$$

$$\Delta E = E_{\text{photon}} \Leftrightarrow E_2 - E_1 = h\nu \quad (2.4)$$

$$\nu = (E_2 - E_1)/h \text{ and } \lambda = hc/(E_2 - E_1)$$

Electrically excited states of this kind are unstable. Electrons return to their ground states. At the same time, the excitation energy can be released again. Radiative decay processes and non-radiative decay processes are the two types of decay processes. Non-radiative decay mechanisms include vibrational relaxation, quenching with surrounding molecules, and internal conversion. These methods will be covered in more detail later. Radiative decay can sometimes take the form of fluorescence and phosphorescence. The energy released in the form of electromagnetic radiation, which is commonly referred to as photons. Because part of the energy is already released by non-radiative decay, the light emitted has a longer wavelength and a lower energy than the absorbed light. This is why excitation with non-visible UV-radiation can result in visible emission. This change toward a longer wavelength is referred to as the Stokes shift.

There are many types of luminescence that may be classified based on the energy source that initiates the luminescence process. Figure 2.8 displays a summary of several types of luminescence and their energy sources. Most of these luminescence mechanisms have significant scientific and industrial applications, like electroluminescence, which is the basic working principle of light-emitting diodes and is induced by the recombination of electrons and holes after applying an electric field across a material, and chemiluminescence, which is induced by a chemical process and is responsible for glow sticks glowing. Nonetheless, the focus of this article is on photoluminescence, which is the basis of the powerful non-destructive spectroscopic technique, photoluminescence spectroscopy, which is extensively used in both academia and industry. The emission of light from a material as a result of light absorption is referred to as photoluminescence. The name is noteworthy because it combines the Latin term "luminescence" with the Greek prefix "photo," which means "light". Any light induced by photon absorption is referred to as photoluminescence.

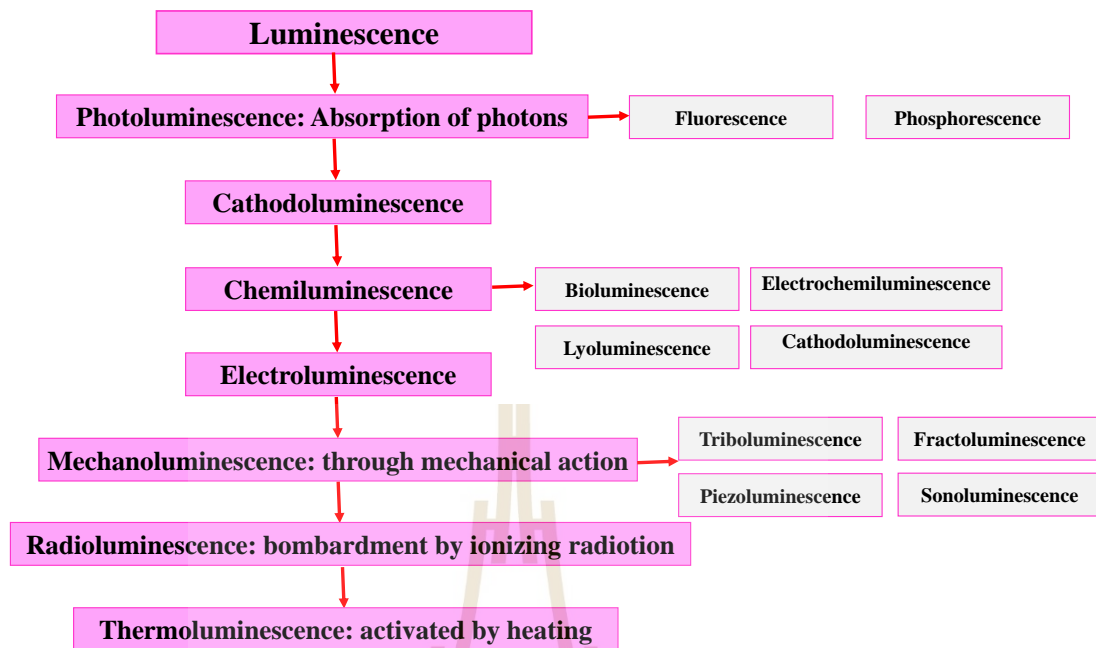


Figure 2.8 Types of luminescence and their energy sources.

2.4 Comparison of the fluorescence and phosphorescence phenomena

The phenomenon known as luminescence happens when a substance absorbs energy and then, as a result of that absorption, emits radiation in the visible or near-visible spectrum (excitation). Fluorescence and phosphorescence are the two types of luminescence that may be classified based on the typical time scale (τ) between excitation and radiation emission. The time scales involved in fluorescence are very fast, in the order of 10^{-8} s, which is almost the same as the relaxation time of an isolated gaseous ion, but phosphorescence it is in milliseconds. In the case of phosphorescence, the emission continues even after the excitation has ceased, which is known as afterglow. Because of the metastable state transition leading to light emission, the phosphorescence decay period increases. Photoluminescence or fluorescence occurs when a photon-excited activator emits electromagnetic radiation from the ground state. Radiative decay describes the process through which light is emitted as a result of the relaxing of an excited state. Non-radiative decay describes the process of de-excitation to the ground state without the emission of photons. The

radiative lifetime of excited states depends on the radiative state and the ion. It can be from a few hundred picoseconds to a few hundred milliseconds. The most interesting part is that the fluorescent emission occurs in a part of the spectrum where the glass can't absorb light. The fluorescence of an active ion in a material is affected by the way the binding forces in the region are not the same. The luminescence process is illustrated in Figure 9. A luminescent material, often known as a phosphor, is mainly composed of a host lattice that has been purposefully doped with defects. Phosphors are typically powders, but in certain cases, thin films. The impurities that are intentionally doped into the host matrix are designated as activator ions. Excitation energy is absorbed in phosphors through either the host lattice or activator ions. Energy can also be transferred through the host matrix. In most occurrences, the emission in phosphors (Gupta et al., 2021) is caused by activator ions. The activator ions have energy levels that can be populated either directly or indirectly through energy transfer. Additionally, the host matrix ought to be transparent enough to allow visible light to pass through to the phosphor's surface. The performance of devices that use phosphor materials made from rare earth ions has been greatly improved by using a wide range of these materials.

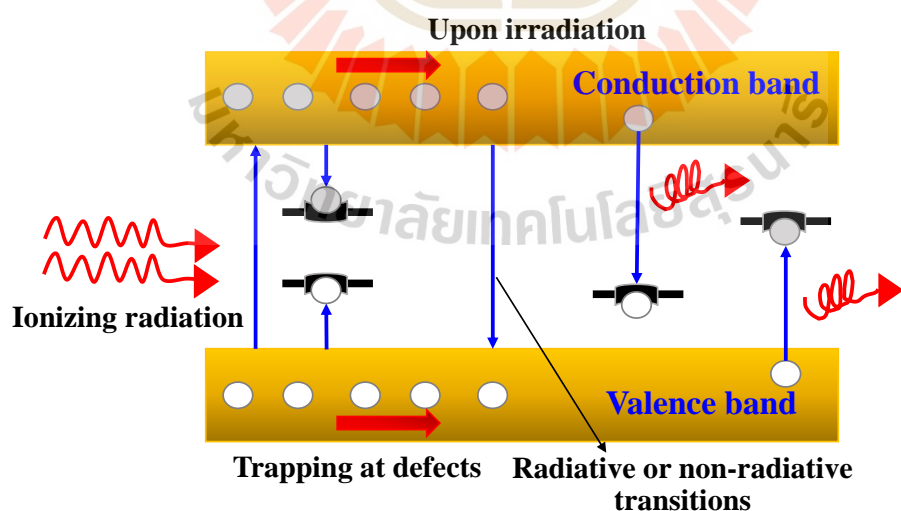


Figure 2.9 Illustration of a simple model for Photoluminescence.

2.5 Basics of trivalent rare earth

The optical absorption and emission spectra of trivalent lanthanide ions are induced by intra-shell 4f electronic structure among various energy levels associated with the 4f orbitals. The elements with Z ranging from 57 to 71 (La to Lu) in the periodic table are called lanthanides (Ln). The rare earth elements of particular interests for this thesis are highlighted in Figure 2.10. The ground-state electronic configuration of neutral lanthanide is $[\text{Xe}] 4f^n 6s^2$ and the first excited configuration is $[\text{Xe}] 4f^{n-1} 5d^1 6s^2$, where [Xe] represents the ground-state electronic configuration of Xe, n represents the number of n=4 in the 4f subshell. As a result, comprehending the photoluminescence emissions of Ln^{3+} ions require a more in-depth investigation of their electrical structure. The lanthanide atoms tend to lose two electrons from their 6s shell followed by losing a 5d electron (or perhaps a 4f electron) by successive ionization to obtain their stable oxidation state as trivalent ions (Ln^{3+}). Among the $4f^n$ configuration lanthanum ($4f^0$), gadolinium ($4f^7$) and lutetium ($4f^{14}$) are having empty, half-filled and fully filled 4f shell, respectively, and are most stable ones. Apart from trivalent, some of the RE ions can exist in divalent or tetravalent state in a matrix depending on the preparation method. There is similarity between the spectra of Ln^{3+} compounds and those of the atoms: both types of spectra are sharp. The distinctive property of the Ln^{3+} spectra is because of the fact that the filled 5s and 5p shells of the ligand shield the $4f^n$ electrons from the ligand environment. The $4f^n$ electrons slightly feel the vibrational motions within the ligand environment. Photoemission experiments of the trivalent lanthanide compounds have shown that the 4f state lies lower than the valence band at least 5 eV. Hence, such states behave like free atoms. The $f \rightarrow d$ inter-configurational optical transitions and the transitions of trivalent ions are of major interest. The interaction between the 5d electrons and ligand ions alters the bond strength when the 4f–5d excitation occurs, resulting in broad, rather than sharp, absorption and emission bands.

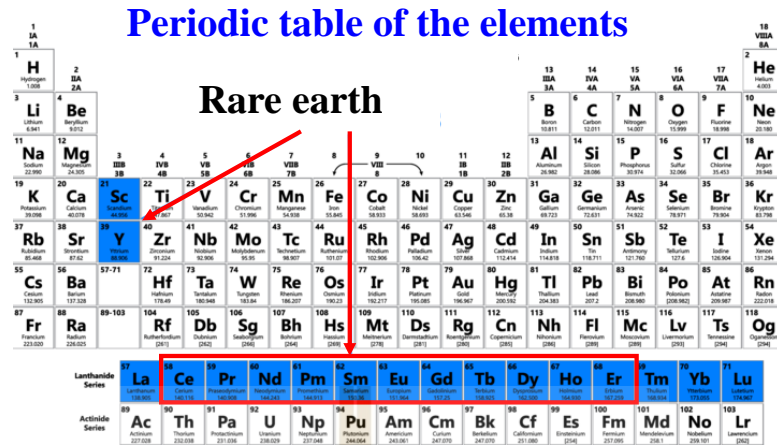


Figure 2.10 Rare-earth ions of focus in this thesis.

Figure 2.11 show the energy level diagrams of all Ln^{3+} ion whose 4f orbitals are partially filled: $n=1$ (cerium) to $n=13$ (ytterbium). The radiative transitions, crucial for technology, are labeled. The shielding effect implies that the Ln^{3+} ion energy levels are not function of the host, the levels are, however, broadened by the Stark effect thanks to the applied crystal field. Stark splitting is caused by the low-point symmetries of the rare-earth (RE) sites in amorphous matrices. In order to obtain a strong emission in the visible and near-infrared (NIR) regions, the ion may be carefully selected.

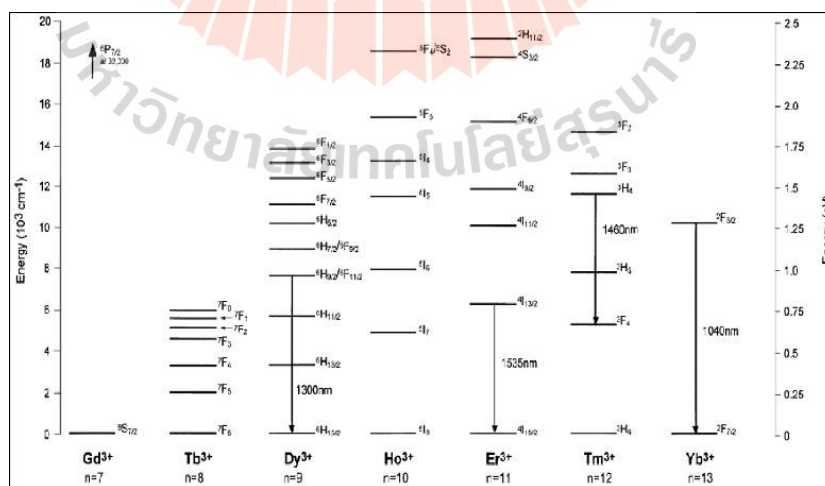
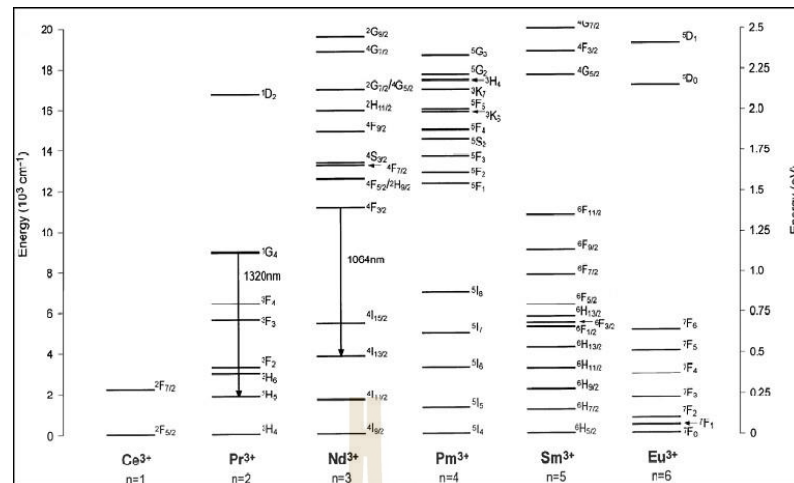


Figure 2.11 Energy levels of Ln^{3+} and technologically crucial radiative transitions.



is that they absorb and emit light in a wide range of wavelengths, from ultraviolet Gd^{3+} (Xu et al., 2018; Sun et al., 2013; Chun et al., 2004) through visible (e.g., Sm^{3+} , Eu^{3+} , Pr^{3+} , Tb^{3+} , Dy^{3+} , Tm^{3+} , Er^{3+} , etc.) and infrared (e.g., Ho^{3+} , Nd^{3+} , Er^{3+} , Yb^{3+} , etc.). In this research, nine trivalent rare earth ions were investigated (some of the basic properties of the rare earths in Table 2. Pr^{3+} is a trivalent rare earth ion with a complicated energy level diagram composed of many metastable multiples (i.e., $^3P_{0,1,2}$, 1D_2 and 1G_4) that allow for multiple emissions in the blue, green, orange, red, and infrared areas depending on the host matrix (Rai et al., 2007). The predominant emission lines in Eu^{3+} (Khan et al., 2018) occur between the 5D_0 level and the 7F_J multiples, while the main emission lines in Tb^{3+} (Fu et al., 2018) occur between the 5D_4 level and the 7F_J multiples. Blue fluorescence from this ion has been seen from the 5D_3 level to the 7F_J multiples. Ce^{3+} (Bahadur et al., 2013) on the other hand is a broad band emitter whose 4f configuration consists of only two multiples, the ground state ($^2F_{5/2}$) and the excited state ($^2F_{7/2}$). Furthermore, the properties of their emissions are substantially influenced by the material in which they are located.

Ln-doped glasses have attracted a lot of attention because of their promising optical characteristics, which alter noticeably when a host is significantly doped with Ln^{3+} , such as by ~ 1 wt% (Samek et al., 1992). In some cases, depending on the quality of the dopant, the difference might be rather apparent. The Ln^{3+} ions are important for studying glasses' fluorescence because they are used the most. In some cases, depending on the grade of the dopant, the difference might be rather noticeable. The Ln^{3+} ions are important for studying glasses' fluorescence because they are used the most. The splitting of the multiple terms of Ln^{3+} ions, leading to a fine structure, depends on the strength of the crystal-field and the symmetry of the site accommodating the Ln^{3+} ions. It affects the optical spectra of Ln^{3+} ions in glasses to be unevenly widened. The optical absorption and emission spectra are inhomogeneously enhanced, and the radiative transition probability was shown by non-exponential radiative decays to change from site to site as a function of the in-place network modifier. With multi-phonon emission, the probability of non-radiative decay

is computed by the vibrations of high frequencies caused by the network former of the glass (Reisfeld et al., 1980).

Table 2.1 Some of the basic properties of the trivalent rare earth.

Element	Atomic number	Electronic structure (outer electrons only)		Color caused by Ln ³⁺ absorption	Ionic radius Ln ³⁺
		Ln	Ln ³⁺		
Lanthanum: La	57	5d ¹ 6s ²	[Xe]	Colorless	1.061
Cerium: Ce	58	4f ¹ 5d ² 6s ²	4f ¹	Colorless	1.034
Praseodymium: Pr	59	4f ³ 6s ²	4f ²	Green	1.013
Neodymium: Nd	60	4f ⁴ 6s ²	4f ³	Reddish	0.995
Promethium: Pm	61	4f ⁵ 6s ²	4f ⁴	Pink/ yellow	0.979
Samarium: Sm	62	4f ⁶ 6s ²	4f ⁵	Yellow	0.964
Europium: Eu	63	4f ⁷ 6s ²	4f ⁶	Nearly colorless	0.950
Gadolinium: Gd	64	4f ⁷ 5d ¹ 6s ²	4f ⁷	Colorless	0.938
Terbium: Tb	65	4f ⁹ 6s ²	4f ⁸	Nearly colorless	0.923
Dysprosium: Dy	66	4f ¹⁰ 6s ²	4f ⁹	Yellow	0.908
Holmium: Ho	67	4f ¹¹ 6s ²	4f ¹⁰	Pink/ yellow	0.894
Erbium: Er	68	4f ¹² 6s ²	4f ¹¹	Pink	0.881
Thulium: Tm	69	4f ¹³ 6s ²	4f ¹²	Pale green	0.869
Ytterbium: Yb	70	4f ¹⁴ 6s ²	4f ¹³	Colorless	0.858
Lutetium: Lu	71	4f ¹⁴ 5d ¹ 6s ²	4f ¹⁴	Colorless	0.848

2.7 Fundamentals of borate glasses

There are a variety of chemical compositions that may be used to create different types of glasses. Oxide glasses outperform their non-oxide counterparts due to the ease with which they react with ambient oxygen. When cooled from their molten state, oxide minerals such as SiO₂, B₂O₃, GeO₂, and P₂O₅ create glasses on their

own, without the incorporation of various chemicals. This oxide glass has a lot of interest because of its interesting characteristics, including excellent solid solubility for RE dopants and strong thermal stability, as well as a lower melting point than most other oxide glasses. On the other hand, some borate glass matrixes have been criticized for being fragile, chemically unstable, and having a high phonon energy ($\sim 1300\text{--}1500\text{ cm}^{-1}$). These disadvantages decrease the luminescence and scintillation properties of the material, which in turn reduces the material's efficiency. This is a barrier to the material's use in applications using lightning devices. This challenge has been significantly resolved by adding alkali elements such as Li, Na, and K into a borate matrix, in which they are influences in oxide glass. Researchers are working to improve un-doped borate glasses' optical characteristics. As a result, the glasses doped with Ln^{3+} have intrigued the scientific community. It is possible to modify the properties and structures of the Ln^{3+} dopant by using an optimized network matrix (borate host) and dopant. Chemical stability, structural and compositional variation, reduced toxicity, biocompatibility and increased luminosity for lightning devices make Borate glasses with Ln^{3+} dopants the ideal choices. The borate glasses doped with a single lanthanide have shown improved emissions, but the challenges are fast and effective energy transfer (ET) from the host to the luminescence center and quenching caused by dopant activation. This problem can be resolved by methods like as co-doping, which offer great performance parameters for lightning applications such as UV light transparency, remarkable optical damage thresholds, great thermal and chemical durability, and increased luminescence efficiency. The non-radiative resonant ET from Ln^{3+} donor to Ln^{3+} acceptor can increase the luminescence of Ln^{3+} ions doped in glass. The donor's emission should overlap the acceptor's absorption for an effective ET, which is completely reliant on the host and dopants. Because luminescence and scintillation can be exploited in photonic devices, the primary goal is to find a suitable borate host and a combination of Ln^{3+} (donor and acceptor). The luminescence and scintillation of the glass matrixes may be studied utilizing glasses incorporating dopant oxides, especially rare-earth oxides. Depending on the quantitative features of the dopants and the glass host, a certain amount of dopant ions with different valence

levels can be found in the glass. Consequently, the incorporation of Ln^{3+} into the glass matrix is expected to enhance and extend the applications of the glass matrix in photonic devices, and this work is considered to be extremely significant. The materials with controlled properties are of great interest for scientific and technological reasons. The investigation of borate glasses, driven by scientific curiosity and technological applications, have led to a detailed understanding of their structure and unique features. Despite the fact that traditional glasses, such as silicates and borosilicate, are capable of meeting a wide range of technological requirements, they are occasionally limited in their abilities. On the other hand, the borate glasses may offer an advantage over other glasses.

2.7.1 Borate glass formation

In general, the production of glass depends on the cooling rate of the process, the tendency of the materials to form glass, their chemical composition, and their structure. Borate glasses are manufactured by cooling from a molten state without fulfilling the requisite for crystallization. There is one or more than one element functioning as a primary source for the production of every glass; these elements are collectively referred to as a glass former or network former. Borates, when cooled from their molten state, are known to form glasses on their own (without combining with other chemicals), and as a result, is believed to be an effective glass forming.

2.7.2 Structure features of borate glass

Borate glasses play a significant role in technology and contribute to a better understanding of the correlation between the structure and the physical characteristics of the glasses. The structures of boron-based glasses can be investigated using IR, NMR and Raman spectroscopy techniques, simplified structural models and statistical thermodynamic model. Krogh-Moe discovered that borate glasses and borate crystals all share the same well-defined and stable poly-borate groupings. Some of these poly-borate groupings are depicted in Figure 2.12.

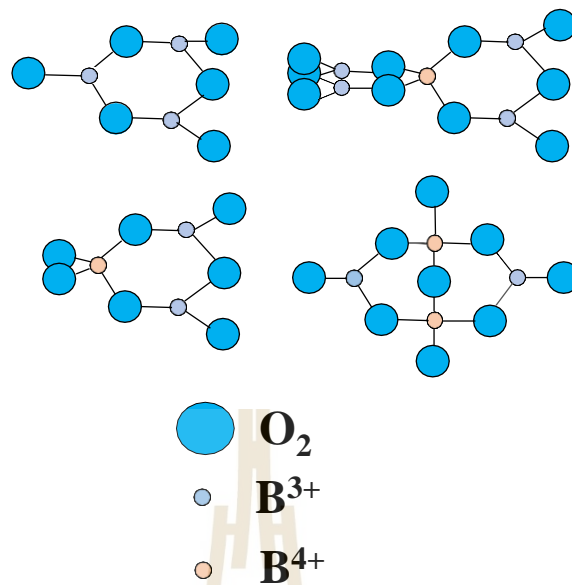


Figure 2.12 Polyborate groupings.

Youngman and Zwanziger have reported while using the boron NMR spectra that the structure for vitreous B_2O_3 comprises 1:1 ratio of boroxol rings to B_2O_3 units. Gooding and Turner's plot on the alkali-dependent thermal expansion coefficient of sodium borate glasses demonstrated a marked reduction in expansion coefficient with the increasing density. According to several studies, B_2O_3 glass is typically composed of three coordinated boron, with the BO_3 triangle serving as the basic structural unit and boron positioned slightly above the plane of three O ions. The boron atoms in various structural units in several borate glasses are represented in Figure 2.13, coordinating with three (or four) O atoms. Both crystalline and vitreous glassy B_2O_3 have planar $[BO_{3/2}]$ triangles in their structures. The B-O-B angle in amorphous B_2O_3 is found to be between 120° and 130° , with the majority of the triangles arranged in boroxol rings containing three oxygens within and three outside the ring. In Figure 2.13, boroxol rings are randomly interconnected with loose $[BO_{3/2}]$ triangles in the glass.

When alkali and alkaline earth cations are added, the structure of borates changes in the following ways:

- O^{2-} breaks boron-oxygen-boron bonds to form one NBO. Boron's coordination was still three.

- The B coordination changes from 3 to 4, leading to the creation of the BO_4 tetrahedron.

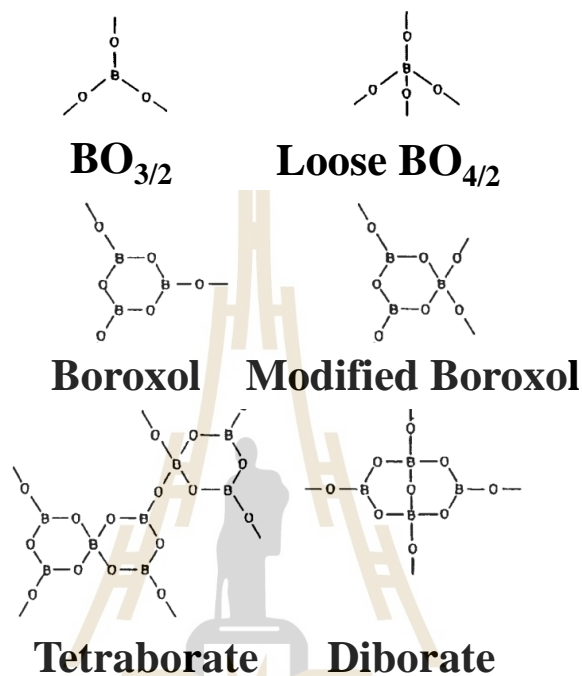


Figure 2.13 Structure of both crystalline and vitreous B_2O_3 .

Wong et al., 1976 and Jellison et al., 1978 found the alkali oxide conversion of $[\text{BO}_{3/2}]$ to $[\text{BO}_{4/2}]^-$. Because there are four bonds between the BO_4 groups and the remainder of the structure, they are responsible for the structure's compactness and strength. The scientific community is interested in borate glasses because of the boron anomaly. According to Biscoe and Warren (Biscoe et al., 1938), increasing Na_2O from 0 to 16 mol% reduces thermal expansion coefficient owing to the replacement of boric oxide by sodium oxide. This was caused by the conversion of B from a 3-fold boron (B_3) coordination to a 4-fold boron (B_4) coordination, as well as the creation of NBOs. The boron anomaly happens when the concentration of alkali is higher than 16 mol% and the thermal expansion coefficient (TEC) goes up while the viscosity goes down. This happens because adding more alkali oxide makes NBOs form.

2.8 Previous study of glass system

2.8.1 Previous Study on borate glasses

In order to determine the structure of $\text{Li}_2\text{O}-\text{MgO}-\text{B}_2\text{O}_3$ (LMB) glasses. Glass has excellent structural characteristics, according to several reports (Rao et al., 2004). (Oprea et al., 2004) investigated the optical characteristics of $\text{Bi}_2\text{O}_3-\text{B}_2\text{O}_3$ glasses and reported that the UV absorption edge and refractive index are significantly affected by the glass composition. It has been shown that the presence of mixed alkali in manganese-doped borate glasses has a big effect on a number of physical properties.

(Shailajha et al., 2015) investigated the excellent structural and optical properties of sodium-calcium-phosphor borate glasses containing CuO. Additionally, the glass's direct optical band gap has been found to decrease with the addition of CuO. (Dalal et al., 2005) have looked into how adding iron to lithium borate glasses changes their structure and how they conduct electricity. The results show that iron doping increased density and molar volume. (Saddeek et al., 2011) researched the optical properties of $x\text{B}_2\text{O}_3-25\text{Li}_2\text{O}-(75-x)\text{Bi}_2\text{O}_3$ glasses. They determined that the optical basicity and refractive index decreased when bismuth content was added, but the optical energy gap increased. (Saeed et al., 2018) studied the physical and optical characteristics, including density, polaron radius, optical basicity, optical band gap, Urbach energy, electronic polarizability, and refractive index of the barium-doped borate glasses. They found that as barium content increases, density increases while polaron radius decreases. Subhadra et al., 2011 investigated vanadium-doped lithium-potassium-bismuth-borate glasses, in which the optical band gap was reduced as the Bi_2O_3 concentration increased. Shaban et al., 2017 prepared and examined lithium-borate glasses ($\text{Li}_2\text{O}-\text{MoO}_3-\text{Al}_2\text{O}_3-\text{B}_2\text{O}_3$), obtaining the indirect optical band gap, density, molar volume, and refractive index. Rao et al., 2011 found that the physical properties of zinc-lithium-sodium-borate glasses with different concentrations of CuO dopant changed in ways like density, refractive index, ionic concentration, molar refractivity, polaron radii and inter-ionic distance, and electronic polarizability.

Recent studies have shown that boron and aluminum speciation depend on the modifier type and content as well as the Al/B ratio. It has been demonstrated that

adding Al_2O_3 to sodium borate glasses can result in improvements in the mechanical properties such as hardness and, more importantly, fracture resistance. In fact, replacing Na_2O with Li_2O led to the discovery of a $24\text{Li}_2\text{O}-21\text{Al}_2\text{O}_3-55\text{B}_2\text{O}_3$ glass, which has the best crack resistance of any oxide glass of alumina to borate glasses leads to significant changes in the boron speciation, as 4-coordinated aluminum also requires charge stabilization, either through alkali cations or through the formation of 5- and 6-fold coordinated aluminum.

The alkali oxide in aluminum-borate glasses is selectively consumed to charge compensate the four-coordinated aluminum (with the presence or absence of a minor concentration of increased coordinated aluminum species relying on the ionic field strength of the network modifying cation (Rao et al., 2002), and the remaining part is consumed to charge compensate the four-coordinated boron, which indicates that the content of Al_2O_3 will affect the relative fraction of BO_4 and BO_3 groups. This structural was confirmed to be valid in our study on $25\text{Na}_2\text{O}-x\text{Al}_2\text{O}_3-(75-x)\text{B}_2\text{O}_3$ ($x = 0-30$ mol%) glasses, where it was observed that the glass transition temperature (T_g) decreased almost linearly as the $\text{Na}_2\text{O}/\text{Al}_2\text{O}_3$ ratio decreased from 5 to 1, leading to a rise of 5 with further decrease in $\text{Na}_2\text{O}/\text{Al}_2\text{O}_3$ ratio (Januchta et al., 2017). As demonstrated by all of these investigations, there is a wide range of structural possibilities in borate glass. Optical and physical properties may be adjusted by incorporating various elements and oxides. In addition, and most importantly, it is confirmed to be cost-effective when compared to the other glasses.

2.8.2 Previous study on single Ln^{3+} -doped borate glasses

Single Ln^{3+} -doped borate compounds have attracted attention since 1967, when the first calcium-borate polycrystalline red phosphors activated by dysprosium were published (Kazanskaya et al., 1974), demonstrating radio thermo luminescence detecting characteristics. The studies of Ln^{3+} -doped borate glasses began in 1975. Since then, technological interest in these glasses has increased. Over the last few decades, researchers have focused on researching single RE-doped borate glasses. The functional glasses $\text{Li}_2\text{O}-\text{MgO}-\text{B}_2\text{O}_3$ doped with a series of REs such as Gd, Dy, Pr, Ce, Eu, and Tb are reported to have thermoluminescence characteristics.

Rajesh et al., 2012 studied the luminescence properties of Dy^{3+} ion strontium lithium bismuth borate (SLBiB) glasses, confirming the increased white light emission by assessing oscillator strength, transition probabilities, branching ratios, and emission cross section. Balakrishna et al. 2012 investigated the structural and photoluminescence properties of the different modifier-containing oxides on Li-B glasses with Dy content addition. The goal of this study was to find out what Dy dopant does, especially if it only changes the shape or also makes the material more photoluminescent.

The optical and luminescent properties of Dy^{3+} contained in $(65-x)\text{B}_2\text{O}_3-10\text{CaO}-25\text{Na}_2\text{O}:x\text{Dy}_2\text{O}_3$ were investigated by F. Zaman (Zaman et al., 2019) and colleagues using two complementary spectroscopic methods (UV-Vis-NIR and PL). Luminescence and scintillating glasses characteristics of Dy^{3+} -added silico borate glasses were studied by J. Kaewkhao (Kaewkhao et al., 2016). The luminescence effect has been demonstrated by photoluminescence excitation. Deopa et al., 2017 demonstrated the photoluminescence and ET characteristics of glasses with lithium-lead- aluminum-borate and Dy^{3+} content added used for white light emitting diode (W-LED) and laser applications. The intensity characteristics of the life-time decay parameters were calculated in order to validate the energy transfer and photoluminescence. Kaewnuam et al., 2017 reported scintillation, W-LEDs, and laser applications of Dy^{3+} -doped lithium yttrium borate glass $(60\text{Li}_2\text{O}-10\text{Y}_2\text{O}_3-(30-x)\text{B}_2\text{O}_3)$, where yellow and blue emissions were found, the Y/B ratio was measured, and CIE chromicity was analyzed Zaman et al., 2019 performed comparative studies of gadolinium-based borate glasses doped with Dy^{3+} for white light applications. The research demonstrated that Ba-borate glasses are more efficient than Bi-borate glasses. Alajerami et al., 2012 synthesized samarium and Dy-activated borate glasses via melt-quenching method and analyzed luminescence excitation and emission spectra. Venkateswarlu and coworkers (Venkateswarlu et al., 2014) published a spectral study of Sm^{3+} and dysprosium in $\text{B}_2\text{O}_3\text{-ZnO-MgO}$ glasses. In this work, the energy-level diagram of the emission mechanism involved in Sm^{3+} glasses were thoroughly explained. According to studies published by D.D. Ramteke, the structural and luminescent characteristics of lithium borate glasses are affected by

the concentration of Sm^{3+} ions. The physical and optical properties, such as density, molar volume, and optical band gap, have been calculated and analyzed. The LGBi/Ba Sm^{3+} -doped borate glasses have a strong optical absorption spectrum, outstanding photoluminescence properties, and transparency; these characteristics make them a suitable candidate for luminescence applications. Wantana et al., 2017 reported good luminescence and scintillation applications of calcium gadolinium borate glass doped with Sm^{3+} ion using rapid melt quenching. Rani et al., 2019 previously investigated the lasing uses of samarium-doped barium lead alumino fluoro borate glasses. The reddish-light emission and spectroscopic studies of alkaline-earth chloro borate glasses doped with Sm^{3+} for visible photonic applications were reported in this study. On the basis of these findings, it is concluded that the trivalent Ln^{3+} activators drastically modify the structure and hence improve the luminescence properties of borate glasses.

2.8.3 Previous study on Co Ln^{3+} -doped borate glasses

Borate glasses containing Ln^{3+} co-doping have the potential to be used in luminescence applications. Co-doping these glasses with a particular Ln^{3+} dramatically improves both their luminescence and scintillation properties. It is consequently important to determine the important conditions where enhanced luminescence occurs, and the energy transfer as a function of the dopants and their composition. The selection of Ln^{3+} ions and the proportions of those ions, as well as an understanding of the energy transfer mechanisms among those ions and to the luminescence centers, may be quite challenging to investigate. Keeping in mind these important properties, we present the synthesis and characterization of co-doped Ln^{3+} borate glasses, driven by scientific curiosity and technological applications. The standard melt-quenching technique was used to create the transparent luminescent LMgGBDy and LMgGBSm glasses with 0.5 mol% optimized Gd^{3+} and varying content of Ln^{3+} (Dy^{3+} and Sm^{3+}) borate glasses. The melt quenching process was used to create transparent luminescent LMgGBDy and LMgGBSm glasses with 0.5 mol% optimum Gd^{3+} and variable Ln^{3+} (Dy^{3+} and Sm^{3+}) content. The density and molar volume of the indicated glasses increased as a consequence of rising Dy_2O_3 and Sm_2O_3 caused by the production of NBOs. The photoluminescence excitation and emission spectra proved

that the Dy^{3+} dopant concentration quenches at 0.5 mol%. In LMgGBDy glasses, and 0.3 mol% Sm^{3+} dopant in LMgGBSm glasses. The energy transfer in the glasses has been determined by the decreased emission of Gd^{3+} at $\lambda_{\text{exc}} = 275$ nm and the increased emission of Dy^{3+} and Sm^{3+} in LMgGBDy and LMgGBSm glasses, respectively. Using the J–O theory, the radiative emission parameters, total radiative transition probabilities, emission cross section, experimental branching ratio, and radiative lifetimes were computed for samples doped with 0.5 mol% Dy^{3+} and 0.3 mol% Sm^{3+} in LMgGBDy and LMgGBSm glasses, respectively. The energy transfer efficiency from Gd^{3+} to Dy^{3+} in LMgGBDy and Gd^{3+} to Sm^{3+} in LMgGBSm glasses was found to be increasing with the decreasing lifetime of the samples. Moreover, it was demonstrated that electric dipole-dipole interaction is an effective energy transfer mechanism in both glass systems. The CIE chromaticity coordinates calculated from the emission spectra also indicated the presence of white-light emission in LMgGBDy and orange luminescence in LMgGBSm glasses. So Dy^{3+} -doped glasses could be applied as white-light emitters and Sm^{3+} -doped glasses as orange-visible lasers. Borate glasses co-doped with an appropriate pair of donor-acceptor, sensitizers, and activators have been created in a variety of forms, making them ideal for a wide range of applications, including nonlinear optics, lasers, solar energy, photodetectors, light-emitting diodes, and radiation dosimeters.

Zhou et al., 2019 investigated the luminescent properties of mono- and bi-doped $\text{Dy}^{3+}/\text{Eu}^{3+}$ calcium borosilicate synthesized using the standard high temperature melt-quenching process. Co-doping with rare earths changes the network in ways like changing BO_3 to BO_4 , sending out white light, and causing Dy^{3+} to break down, even though the CIE color coordinates change from cyan to white.

Pisarska et al., 2014 investigated the energy transfer from Dy^{3+} to Tb^{3+} ions as well as the luminescence properties of melt-synthesized $\text{Dy}^{3+}\text{-Tb}^{3+}$ co-doped glasses $72\text{PbO-}18\text{B}_2\text{O}_3\text{-(}6.5x\text{)Al}_2\text{O}_3\text{-}3\text{WO}_3\text{-}0.5\text{Dy}_2\text{O}_3\text{-}x\text{Tb}_2\text{O}_3$. Prior to melting at high temperatures, glass components were preheated in an argon-free atmosphere. The energy transfer notion has been confirmed by the yellow transition of Dy^{3+} and the

green transition of Tb^{3+} at 543 nm. The efficiency of energy transfer via nonradioactive decay was measured to be 16%.

Yang et al., 2014 have researched the visible photon multiplication process in Ce^{3+} - Tb^{3+} bi-doped borate glasses manufactured by high temperature melting for improved solar cells. It is demonstrated that the excitation wavelength range widened from the long wavelength region (UVA) to the medium wavelength region (visible and UVB), consequently increasing emission intensity. So, the glass system could play an active role as an effective layer for UV to Vis spectrum radiation to improve the performance of solar cells.

Sontakke et al., 2015 investigated the case of the energy transfer processes that take place between Ce^{3+} and Yb^{3+} in borate glass that was melted using the melt quenching method. It was found how to distinguish between the electron transfer and the energy transfer phenomenon that occurs between dopants in glass matrix. This is especially helpful when taking into consideration the recent developments on Ln^{3+} -doped materials for spectral modification, sustained luminescence, and potential applications.

The optical and physical characteristics of co-doped Dy^{3+} - Pr^{3+} bi-doped $27.5Li_2O: (72.5-X) B_2O_3: 0.5Dy_2O_3: XPr_6O_{11}$ glasses are prepared and studied using melt quenching technique by Pawar et al., 2016. The amorphous nature of glass samples, as well as the presence of functional groups, were determined using XRD and FTIR investigations. UV-VIS-NIR optical absorption spectra indicate direct and indirect transitions, as well as seven absorption bands at various wavelength ranges. The energy transfer phenomenon from praseodymium to dysprosium is demonstrated by an increase in luminescence at 663 nm. The CIE chromaticity confirms that these glasses may be used in W-LED applications.

Lakshminarayana et al., 2017 investigated optical absorption, luminescence, and the energy transfer phenomena in Dy^{3+}/Tb^{3+} -co-doped borate glasses synthesized using the melt quenching techniques. The non-exponential life time decay curves from the Inokuti-Hirayama (IH) model were examined, and the non-radiative ET from dysprosium and terbium with an efficiency of 45% is owing to an electric dipole-dipole

mechanism. The measured color coordinates (x , y) and CCT show a yellowish green region and might be used to make meaningful luminescent display devices and state-light emitting diodes.

Loos et al., 2017 studied the luminescence as a function of temperature and the energy transfer properties of single- and double-doped melted terbium and europium $51\text{ZrF}_4\text{-}20\text{BaF}_2\text{-}20\text{NaF}\text{-}3.5\text{LaF}_3\text{-}3\text{AlF}_3\text{-}0.5\text{InF}_3\text{-}2\text{Ln}^{3+}(\text{Tb:Eu})\text{F}_3$. The glass samples have good temperature stability from 15 K to 700 K, and the rate of energy transfer from Tb^{3+} to Eu^{3+} increases as temperature increases. As the temperature is raised, the color changes from orange to red (15 K to 350 K) and from red to yellow (350 K to 700 K). Loos et al., 2017 investigated the luminescence as a function of concentration and energy transfer in $51\text{ZrF}_4\text{-}20\text{BaF}_2\text{-}20\text{NaF}\text{-}3.5\text{LaF}_3\text{-}3\text{AlF}_3\text{-}0.5\text{InF}_3\text{-}2\text{Ln}^{3+}(\text{Tb:Eu})\text{F}_3$ glasses doped with $\text{Tb}^{3+}/\text{Eu}^{3+}$. Energy transfer from excited Tb^{3+} at 485 nm to improved Eu^{3+} emissions has been confirmed. Dipole-dipole interactions are responsible for the energy transfer. There is also a faster radiative decay rate and a chromaticity shift from green to orange/red.

C.R. Kesavulu (Kesavulu et al., 2017) researched the non-radiative energy transfer process in gadolinium calcium silica borate glasses from Gd^{3+} to Nd^{3+} . These glasses can be used advantageously in NIR lasers at 1059 nm, according to structural, thermal, absorption, emission, and decay time analyses. Yao et al., 2017 studied the structural, optical, and energy transfer characteristics of $\text{Tb}^{3+}\text{-Sm}^{3+}$ bi-doped $\text{Na}_2\text{O}\text{-CaO}\text{-P}_2\text{O}_5\text{-B}_2\text{O}_3\text{-ZrO}_2$ glasses produced by high temperature melting. It was observed that as the Sm^{3+} increased, thus increased the energy transfer efficiency from $\text{Tb}^{3+}/\text{Sm}^{3+}$ and the probability of energy transfer. Electric quadrupole-quadrupole interaction, color coordinate, and CCT from yellow to yellow have all been confirmed. This finding demonstrated great potential of these glasses in UV-modified WLEDs and photonic devices.

Wantana et al., 2018 studied the strong energy transfer emission from Gd^{3+} to Eu^{3+} produced by UV irradiation in calcium silico borate glasses. According to the photoluminescence, X-ray scintillation, and fluorescence lifetime analyses, these glasses may be used in laser systems with a sufficient lasing threshold and energy

performance gain. Mohammed et al., 2018 investigated the optical and dielectric characteristics of borate glasses doped with samarium and terbium. In comparison to the other chosen compositions, the glass with co-dopant content (Tb0.5-Sm0.5) exhibits enhanced emission, i.e., five emission bands. CIE chromicity has confirmed the yellow emission.

2.9 Composition of the present glass

In order to make this certain glass, the following components were combined: borate (B_2O_3), lithium oxides (Li_2O), aluminum oxides (Al_2O_3), gadolinium oxides (Gd_2O_3), cerium trifluoride (CeF_3), terbium oxides (Tb_2O_3), Europium oxides (Eu_2O_3), dysprosium oxides (Dy_2O_3), and samarium oxides (Sm_2O_3). The properties of the present materials are explained below.

2.9.1 Borate (B_2O_3)

In the present glass components, borate is an essential component that is operating primarily as a glass former and partially as a fluxer. Borate's dual role in the manufacturing and producing process may be summarized as follows: In the current investigation, borate was chosen as the material of choice for a number of apparent reasons, including its ease of availability, its low processing temperature glass-forming temperature, and, most significantly, its inexpensive cost. It has the privilege of being able to tolerate enormous concentrations of Ln^{3+} , however the drawback of having a very high phonon energies, which brings the luminous efficiency of the material down. It is expected that borate, when mixed with other components in a stoichiometrically appropriate ratio, will function as an excellent host for Ln^{3+} activators.

2.9.2 Lithium oxides (Li_2O)

Lithium oxide is considered as appropriate modifiers therefore, it is incorporated to improve the mechanical stability of the host. It also functions as a fluxer, significantly lowering the temperature at which glass melts. Once lithium oxide is added to the glass host, a number of NBOs are produced. The creation of color (luminescence) centers is enhanced by the ionic bonds formed as a result of NBOs

with excitation (Alajerami, et al., 2012). Furthermore, due to the production of borate rings when Li^+ ions are added, two BO_4 units are swapped with one mono BO_4 unit.

2.9.3 Aluminum oxides (Al_2O_3)

Aluminum oxide is a good glass structure modifier. It has high field strength and might result in a strongly-bonded glass structure. In borate glasses, it generates more NBOs. When aluminum was added to the borate system, the luminescence intensity increased and the glass network improved throughout the excitation (Ichoja et al., 2018).

2.9.4 Gadolinium oxides (Gd_2O_3)

Among the Ln^{3+} series, Gd is of particular importance because it may facilitate energy transfer from host to activators to luminescence centers. Moreover, in the existing glasses, it may perform as a modifier as well as an efficient sensitizer for the dopant Ln^{3+} . Its excitation ($^8\text{S}_7 \rightarrow ^6\text{G}_J$) and emission ($^6\text{P}_{7/2} \rightarrow ^8\text{S}_{7/2}$) are in the UV region and exhibit no visible emission, but it can be sensitized by another Ln^{3+} dopant or modified in a host network to show visible emission through spectrum conversion. It possesses a higher permittivity, improved thermal stability, and a large energy band gap (5.4 eV).

2.9.5 Cerium trifluoride (CeF_3)

The cerium ions (Ce^{3+}) can act as a dynamic sensitizer for certain rare earth ions. Further, Ce^{3+} ions exhibit intense and broad f-d absorption and emission bands varying from ultraviolet to visible region due to the large energy gap between their ground state (4f) and excited state (5d). The cerium ions are mainly used as the activators in different halides or oxide-based scintillators as the emission centre due to its high light yield and short luminescence decay time. Glass Scintillators doped with Ce^{3+} can be used in the fields such as medical imaging, nuclear and high-energy physics experiments, astrophysics, homeland security, neutron detection, radiochemistry etc.

2.9.6 Samarium oxides (Sm_2O_3)

Existing usually in trivalent state, samarium is the only transition element in lanthanide series and may act as an efficient activator in the present glasses. Triply ionized Sm^{3+} is given significant importance in Ln^{3+} family due to its closely spaced

energy states. It has ${}^6H_{5/2}$, ${}^4G_{5/2}$ and ${}^6F_{11/2}$ as ground, lowest excited, and highest ground states, respectively. These are separated at approximately 7200 cm^{-1} . There is almost no chance of multiphonon relaxation and limited chance of nonradiative decay between these states in the hosts having more phonon energy (1400 cm^{-1}) such as borates. It gives an intense orange emission due to ${}^4G_{5/2} \rightarrow {}^6H_{7/2}$, while light blue, orange-red and red due to ${}^6H_{5/2}$, ${}^6H_{9/2}$, ${}^6H_{11/2}$ transitions. In the enhancement of luminescence of inorganic materials Sm^{3+} is considered as important activator. In the current decade Sm^{3+} doped glasses draw considerable interest in the field of dense optical storage, color displays and in deep water communication.

2.9.7 Europium oxides (Eu_2O_3)

Europium (atomic number 63: $[\text{Xe}] 4f^7 6s^2$) is anion in the class of lanthanide which have the electron configuration, $[\text{Xe}]-4f^6$. Eu^{3+} ion is special among the lanthanides (RE^{3+}) ions to investigate the local ion symmetry of RE^{3+} ions in different glass matrices. The Eu^{3+} emission spectrum is composed of several multiple transitions ${}^5D_0 \rightarrow {}^7F_J = 0, 1, 2, 3$ and 4 for Eu^{3+} ion. The most intense emission of Eu^{3+} is placed at wavelength around 610 nm which is red color emitting and can be attributed to ${}^5D_0 \rightarrow {}^7F_2$ hypersensitive transition, which shows red emission (613 nm) emitted due to hypersensitive ${}^5D_0 \rightarrow {}^7F_2$ Europium (Eu^{3+}) ions have been doped into glasses for development of a laser gain medium in a red laser device. The index, characterizing the spectral changes in the glasses containing Eu^{3+} ions, is the red-to-orange fluorescence intensity ratio R/O. It is the ratio of the intensity of the ${}^5D_0 \rightarrow {}^7F_2$ (red) to ${}^5D_0 \rightarrow {}^7F_1$ (orange) transition and allows to determine the degree of asymmetry in the environment of Eu^{3+} ions in the matrix.

2.9.8 Terbium oxides (Tb_2O_3)

In oxide-based glasses activated by Tb^{3+} ions have been demonstrated to be delightful candidates for gain medium in the green region at 543 nm , since the ${}^5D_4 \rightarrow {}^7F_5$ transition of Tb^{3+} -doped materials provides a four-level laser system with a lower threshold pump power to obtain strong green pulsed laser operation at 543 nm . Bjorklund were demonstrated for the first time for green laser action at 547 nm and correspond to ${}^5D_4 \rightarrow {}^7F_5$ transition from Tb^{3+} -doped chelate in solution at room

temperature. Moreover, the experimental branching ratios of the $^5D_4 \rightarrow ^7F_5$ (543 nm) transition are usually more than 50%, which makes the Tb^{3+} -doped materials a promising ion for green laser applications.

2.9.9 Dysprosium oxides (Dy_2O_3)

In lanthanides series, Dy is regarded a useful element as a glass dopant and functions as an efficient activator in the existing glasses. In modification of glass and, consequently, in its luminescence, Dy plays a key function. The investigation of Dy doped glass luminescence is extremely important in the visible and NIR regimes. Previously, the understanding of dysprosium spectra was viewed as critical due to complicated electronic structure's configuration and closely lying energy levels. Consequently, little research has been paid to luminescence from dysprosium. However, the basic $^4F_{9/2} \rightarrow ^6H_{13/2}$ and $^4F_{9/2} \rightarrow ^6H_{15/2}$ transitions from dysprosium may be obtained by choosing an appropriate host. Although a considerable portion of work on spectrum analyses of Dy^{3+} ion doped materials has been carried out, still, its promising optical properties (profound emission) still attract growing interest in solid state laser. Research effort has been carried out to examine the luminescence of crystals and glasses doped with Dy^{3+} . All this research confirmed the role of dysprosium as an activator for enhancement of the luminescence.

2.10 References

- Alajerami, Y. S. M. and Hashim, S. (2012). The effect of titanium oxide on the optical properties of lithium potassium borate glass. *Journal of Molecular Structure*, 1026, 159:167.
- Alajerami, Y. S. M., Hashim, S., Hassan, W. M. S., Ramli, A. T., and Kasim, A. (2012). Optical properties of lithium magnesium borate glasses doped with Dy^{3+} and Sm^{3+} ions. *Physica B: Condensed Matter*, 407, 2398:2403.
- Annapurna, K. and Buddhudu, S. (1991). Characterization of fluorophosphate optical glasses. *Journal of Solid State Chemistry*, 93, 454:460.
- Babu, P. and Jayasankar, C. K. (2000). Spectroscopic properties of Dy^{3+} ions in lithium borate and lithium fluoroborate glasses. *Optical Materials*, 15, 65:79.

- Babu, P., Jang, K. H., and Kim, E. S. (2009). Spectral investigations on Dy³⁺-doped transparent oxyfluoride glasses and nanocrystalline glass ceramics. *Journal of Applied Physics*, 105, 013516.
- Babu, P., Jang, K. H., Kim, E. S., Shi, L., Vijaya, R., Lavin, V., Jayasankar, C. K., and Seo, H. J. (2010). Optical properties and energy transfer of Dy³⁺-doped transparent oxyfluoride glasses and glass-ceramics. *Journal of Non-Crystalline Solids*, 356, 236:243.
- Babu, S. S., Babu, P., and Jayasankar, C. K. (2009). Optical properties of Dy³⁺-doped phosphate and fluorophosphate glasses. *Optical Materials*, 31, 624:631.
- Bahadur, A., Dwivedi, Y., and Rai, S. B. (2013). Optical properties of cerium doped oxyfluoroborate glass. *Spectrochimica Acta Part A: Molecular and Biomolecular Spectroscopy*, 110, 400:403.
- Balakrishna, A., Rajesh, D., and Ratnakaram, Y. C. (2012). Structural and photoluminescence properties of Dy³⁺ doped different modifier oxide-based lithium borate glasses. *Journal of Luminescence*, 132, 2984:2991.
- Baryshnikov, G., Minaev, B. and Agren, H. (2017). Theory and Calculation of the Phosphorescence Phenomenon. *Chemical Reviews*, 117, 6500:6537.
- Basavapoornima, C. H. and Jayasankar, C. K. (2014). Spectroscopic and photoluminescence properties of Sm³⁺ ions in Pb-K-Al-Na phosphate glasses for efficient visible lasers, *Journal of Luminescence*, 153, 233:241.
- Biscoe, J. and Warren, B. E. (1938). X-ray diffraction study of soda-boric oxide glass. *Journal of the American Ceramic Society*, 21, 287:293
- Caldino, U., Lira, A., and Meza-Rocha, A. N. (2015). White light generation in Dy³⁺-and Ce³⁺/Dy³⁺ doped zinc sodium aluminosilicate glasses. *Journal of Luminescence*, 167, 327:332.
- Chun, J., Peizhen, D., Junzhou, Z., and Fuxi, G. (2004). Radioluminescence of Ce³⁺-doped B₂O₃-SiO₂-Gd₂O₃-BaO glass. *Physics Letters A*, 323, 323:328.
- Dalal, S., Khasa, S., Dahiya, M. S., Agarwal, A., Yadav, A., Seth, V. P., and Dahiya, S. (2015). Effect of substituting iron on structural, thermal and dielectric properties of lithium borate glasses. *Materials Research Bulletin*, 70, 559:566.

- Danmallam, I. M., Ghoshal, S. K., Ariffin, R., Jupri, S. A., Sharma, S., and Bulus, I. (2019). JuddOfelt evaluation of europium ion transition enhancement in phosphate glass. *Optik*, 196, 163197.
- Deopa, N. and Rao, A. S. (2017). Photoluminescence and energy transfer studies of Dy³⁺ ions doped lithium lead alumino borate glasses for W-LED and laser applications. *Journal of Luminescence*, 192, 832:841
- Deopa, N. and Rao, A. S. (2018). Spectroscopic studies of single near ultraviolet pumped Tb³⁺ doped Lithium Lead Alumino Borate glasses for green lasers and tricolour w-LEDs. *Journal of Luminescence*, 194, 56:63.
- Fedorov, P. P., Luginina, A. A., and Popov, A. I. (2015). Transparent oxyfluoride glass ceramics. *Journal of Fluorine Chemistry*, 172, 22:50.
- Fu, Z., Xu, P., Yang, Y., Li, C., Lin, H., Chen, Q., Yao, G., Zhou, Y., and Zeng, F. (2018). Study on luminescent properties of Ce³⁺ sensitized Tb³⁺ doped gadolinium borosilicate scintillating glass. *Journal of Luminescence*, 196, 368:372.
- Gedam, R. S. and Ramteke, D. D. (2013). Influence of CeO₂ addition on the electrical and optical properties of lithium borate glasses. *Journal of Physics and Chemistry of Solids*, 74, 1399:1402.
- Gupta, I., Singh, S., Bhagwan, S., and Singh, D. (2021). Rare earth (RE) doped phosphors and their emerging applications: A review. *Ceramics International*, 47, 19282:19303.
- Höland, W. and Beall, G. H. (2012). Glass-Ceramic Technology. *John Wiley & Sons*.
- Ichoja, A., Hashim, S., Ghoshal, S. K., Hashim, I. H., and Omar, R. S. (2018). Physical, structural and optical studies on magnesium borate glasses doped with dysprosium ion. *Journal of Rare Earths*, 36, 1264:1271.
- Januchta, K., Youngman, R., Goel, A., Bauchy, M., Rzoska, S., Bockowski, M., and Smedskjaer, M. (2017). Structural origin of high crack resistance in sodium aluminoborate glasses. *Journal of Non-Crystalline Solids*, 460, 54:65.
- Jayasankar, C. K., Venkatramu, V., and Babu, S. S. (2004). Luminescence properties of Dy³⁺ ions in a variety of borate and fluoroborate glasses containing lithium, zinc, and lead. *Journal of Alloys and Compounds*, 374, 22:26.

- Jayasimhadri, M., Jang, K., and Lee, H. S. (2009). White light generation from Dy³⁺-doped ZnO-B₂O₃-P₂O₅ glasses. *Journal of Applied Physics*, 106, 013105.
- Jellison, G. E. and Bray, P. J. (1978). Structural Determinations for Sodium Borate Glasses Using B10 and B11 NMR, in Borate Glasses. *Springer*. 353:367
- Jubera, V., Chaminade, J. P., Garcia, A., Guillen, A., and Fouassier, C. (2003). Luminescent properties of Eu³⁺-activated lithium rare earth borates and oxyborates. *Journal of luminescence*, 101, 1:10.
- Kaewjaeng, S., Kaewkhao, J., Limsuwan, P., and Maghanemi, U. (2012). Effect of BaO on optical, physical and radiation shielding properties of SiO₂-B₂O₃-Al₂O₃-Na₂O glass system. *Procedia Eng*, 32, 1080:1086.
- Kaewkhao, J., Wantana, N., Kaewjaeng, S., Kothan, S., and Kim, H. J. (2016). Luminescence characteristics of Dy³⁺ doped Gd₂O₃-CaO-SiO₂-B₂O₃ scintillating glasses. *Journal of rare earths*, 34, 583:589.
- Kaewnuam, E., Wantana, N., Kim, H. J., and Kaewkhao, J. (2017). Development of lithium yttrium borate glass doped with Dy³⁺ for laser medium, W-LEDs and scintillation materials applications. *Journal of Non-Crystalline Solids*, 464, 96:103.
- Kazanskayaet, V., Kuzmin, V. V., Minaeva, E. E., and Sokolov, A. D. (1974). Magnesium borate radiothermoluminescent detectors. in Proceedings of the fourth international conference on luminescence dosimetry. *Krakow-Poland*. 27:31.
- Kesavulu, C. R., Kim, H. J., Lee, S. W., Kaewkhao, J., Wantana, N., Kaewnuam, E., Kothan, S., and Kaewjaeng, S. (2017). Spectroscopic investigations of Nd³⁺ doped gadolinium calcium silica borate glasses for the NIR emission at 1059 nm. *Journal of alloys and compounds*, 695, 590:598
- Khan, I., Rooh, G., Rajaramakrishna, R., Sirsittipokakun, N., Kim, H. J., Wongdeeying, C., and Kaewkhao, J. (2018). Development of Eu³⁺ doped Li₂O- BaO- GdF₃- SiO₂ oxyfluoride glass for efficient energy transfer from Gd³⁺ to Eu³⁺ in red emission solid state device application. *Journal of luminescence*, 203, 515:524.
- Kim, H. J., Rooh, Gul, Park, H., and Kim, S. (2015). Luminescence and scintillation properties of the new Ce- doped Tl₂LiGdCl₆ single crystals. *Journal of luminescence*, 164, 86:89.

- Lakshminarayana, G. Kaky, K. M., Baki, S. O., Lira, A., Caldiño, U., Kityk, I. V., and Mahdi, M.A. (2017). Optical absorption, luminescence, and energy transfer processes studies for Dy³⁺/Tb³⁺-codoped borate glasses for solid-state lighting applications. *Optical Materials*, 72, 380:391.
- Lakshminarayana, G. and Qiu, J. (2009). Photoluminescence of Pr³⁺, Sm³⁺ and Dy³⁺-doped SiO₂-Al₂O₃-BaF₂-GdF₃ glasses. *Journal of Alloys and Compounds*, 476, 470:476.
- Lewis, J. M., O'Brien, C. P., Affatigato, M., and Feller, S. A. (2001). Physical properties of alkali and mixed lithium-cesium vanadate glasses prepared over an extended range of compositions. *Journal of Non-Crystalline Solids*, 293, 663:668.
- Linganna, K., Srinivasa Rao, C. H., and Jayasankar, C. K. (2013). Optical properties and generation of white light in Dy³⁺-doped lead phosphate glasses. *Journal of Quantitative Spectroscopy and Radiative Transfer*, 118, 40:48.
- Loos, S., Steudel, F., Ahrens, B., and Schweizer, S. (2017). Concentration-dependent luminescence and energy transfer in Tb³⁺/Eu³⁺ doped borate and fluorozirconate glasses. *Journal of luminescence*, 187, 298:303.
- Loos, S., Steudel, F., Ahrens, B., and Schweizer, S. (2017). Temperature-dependent luminescence and energy transfer properties of Tb³⁺ and Eu³⁺ doped barium borate glasses. *Journal of luminescence*, 181, 31:35.
- Luewarasirikul, N., Kim, H. J., and Meejitpaisan, P. (2017). White light emission of dysprosium doped lanthanum calcium phosphate oxide and oxyfluoride glasses. *Optical Materials*, 66, 559:566.
- Mohammed, A. B., Lakshminarayana, G., Baki, S. O., Bashar, K. A., Kityk, I. V., and Mahdi, M.A. (2018). Optical and dielectric studies for Tb³⁺/Sm³⁺ co-doped borate glasses for solid-state lighting applications. *Optical Materials*, 86, 387:393.
- Nachimuthu, P., Jagannathan, R., and Kumar, V. N. (1997). Absorption and emission spectral studies of Sm³⁺ and Dy³⁺ ions in PbO-PbF₂ glasses. *Journal of Non-Crystalline Solids*, 217, 215:223.
- Nagli, L., Bunimovich, D., and Katzir, A. (1997). The luminescence properties of Dy-doped high silicate glass. *Journal of Non-Crystalline Solids*, 217, 208:214.

- Oprea, I. I. and Hesse, H. (2004). Optical properties of bismuth borate glasses. *Optical Materials*, 26, 235:237.
- Park, J. M., Ha, D. H., Kaewjeang, S., Maghanemi, U., Kothan, S., Kaewkhao, J., and Kim, H. J. (2016). Luminescence properties of Ce^{3+} doped gadolinium-calcium-silicaborate glass scintillator. *Radiation Measurements*, 90, 166:169.
- Pawar, P. P., Munishwar, S. R., and Gedam, R. S. (2016). Physical and optical properties of Dy^{3+}/Pr^{3+} Co-doped lithium borate glasses for W-LED. *Journal of Alloys and Compounds*, 660, 347:355.
- Pisarska, J., Kos, A., Sołtys, M., Zur, L., and Pisarski, W. A. (2014). Energy transfer from Dy^{3+} to Tb^{3+} in lead borate glass. *Materials letters*, 129, 146:148
- Ragab, M., Mahani, Y., Samir, Y., and Marzouk, A. (2013). AC conductivity and dielectric properties of $SiO_2-Na_2O-B_2O_3-Gd_2O_3$ glasses. *Journal of Alloys and Compounds*, 579, 394:400.
- Raj, V. K. and Kumar, K. (2007). Upconversion in Pr^{3+} doped tellurite glass. *Optical Materials*, 29, 873:878.
- Rajesh, D., Ratnakaram, Y. C., Seshadri, M., Balakrishna, A., and Krishna, T. S. (2012). Structural and luminescence properties of Dy^{3+} ion in strontium lithium bismuth borate glasses. *Journal of luminescence*, 132, 841:849.
- Ramteke, D. D. and Gedam, R. S. (2014). Study of $Li_2O-B_2O_3-Dy_2O_3$ glasses by impedance spectroscopy. *Solid State Ion*, 258, 82:87.
- Rani, P. R., Venkateswarlu, M., Mahamuda, S.K., Swapna, K., Deopa, N., Rao, A. S., and Prakash, G. (2019). Structural, absorption and photoluminescence studies of Sm^{3+} ions doped barium lead alumino fluoro borate glasses for optoelectronic device applications. *Materials Research Bulletin*, 110, 159:168.
- Rao, R. B., Rao, D. K., and Veeraiah, N. (2004). The role of titanium ions on structural, dielectric and optical properties of $Li_2O-MgO-B_2O_3$ glass system. *Materials chemistry and physics*, 87, 357:369.
- Rao, T. R., Krishna, C. H. R., Thampy, U. S., and Reddy, Y. P. (2011). Physical and Spectral Investigations of Cu^{2+} -Doped Alkali Zinc Borate Glasses. *Applied Magnetic Resonance*, 40, 339:350.

- Reisfeld, R. (1980). Multiphonon Relaxation in Glasses, in *Radiationless Processes*. Springer. 489:498
- Rittisut, W., Wantana, N., Butburee, A., Ruangtawee, Y., Padchasri, J., Rujirawat, S., and Kaewkhao, J. (2021). Luminescence properties of Ce^{3+} -doped borate scintillating glass for new radiation detection material. *Radiation Physics and Chemistry*, 185, 109498.
- Saddeek, Y. B. (2011). Study of elastic moduli of lithium borobismuthate glasses using ultrasonic technique. *Journal of Non-Crystalline Solids*. 357, 2920:2925.
- Saeed, A., Elbashar, Y. H., and Khameesy, S. U. (2018). A novel barium borate glasses for optical applications. *Silicon*, 10, 569:574.
- Saleh, Y., Alajerami, M, Hashim, S., Saridan, W. M., Hassan, W., Ramli, A. T., and Kasim, A. (2012). Optical properties of lithium magnesium borate glasses doped with Dy^{3+} and Sm^{3+} ions. *Physica B: Condensed Matter*, 407, 2398:2403.
- Samek, L., Wasylak, J., and Marczych, K. (1992). Optical properties of fluorozirconate glasses activated with rare earth elements. *Journal of Non-Crystalline Solids*, 140, 243:248.
- Sankar, R. and Subba R. (1998). Luminescence studies on doped borates, $\text{A}_6\text{MM}'(\text{BO}_3)_6$. *Journal of Alloys and Compounds*, 281, 126:136.
- Schubert, U. (1997). Introduction to glass science and technology. *Angewandte Chemie*, 109, 2637:2637.
- Shaaban, K. H., Abo-Naf, S. M., and Hassouna, M. E. M. (2019). Physical and structural properties of lithium borate glasses containing MoO_3 . *Silicon*, 11(5), 2421-2428.
- Shailajha, S., Geetha, K., Vasantharani, P., and Kadhar, S. P. (2015). Effects of copper on the preparation and characterization of Na–Ca–P borate glasses. *Spectrochimica Acta Part A: Molecular and Biomolecular Spectroscopy*, 138, 846:856.
- Shamshad, L., Rooh, G., and Kirdsiri, K. (2017). Effect of alkaline earth oxides on the physical and spectroscopic properties of Dy^{3+} -doped $\text{Li}_2\text{O}-\text{B}_2\text{O}_3$ glasses for white emitting material application. *Optical Materials*, 64, 268:275.
- Shelby, J. E. (1974). Viscosity and thermal expansion of alkali germanate glasses. *Journal of the American Ceramic Society*, 57, 436:439.

- Shelby, J. E. (1979). Effect of morphology on the properties of alkaline earth silicate glasses. *Journal of Applied Physics*, 50, 8010:8015.
- Shelby, J. E. (1983). Properties and structures of RO-GeO₂ glasses. *Journal of the American Ceramic Society*, 66, 414:416.
- Shelby, J. E. (1983). Thermal expansion of alkali borate glasses. *Journal of the American Ceramic Society*, 66, 225:227.
- Shelby, J. E. and Ruller, J. (1987). Properties and structure of lithium germanate glasses. *Glass Physics and Chemistry*, 28, 262:268.
- Sontakke, A. D., Ueda, J., Katayama, Y., Dorenbos, P., and Tanabe, S. (2015). Experimental insights on the electron transfer and energy transfer processes between Ce³⁺-Yb³⁺ and Ce³⁺-Tb³⁺ in borate glass. *Applied Physics Letters*, 106, 131906
- Srihari, T. and Jayasankar, C. K. (2017). Fluorescence properties and white light generation from Dy³⁺-doped niobium phosphate glasses. *Optical Materials*, 69, 87:95.
- Stookey, S. D. (1949). Photosensitive glass. *Industrial & Engineering Chemistry*, 41(4), 856-861.
- Subhadra, M. and Kistaiah, P. (2011). Effect of Bi₂O₃ Addition on Electron Paramagnetic Resonance, Optical Absorption, and Conductivity in Vanadyl-Doped Li₂O- K₂O- Bi₂O₃- B₂O₃ Glasses. *The Journal of Physical Chemistry A*, 115, 1009:1017.
- Sujay, R., Julia R. W., and Nils, G. W. (2018). Life under the Microscope: Single-Molecule Fluorescence Highlights the RNA World. *Chemical Reviews*, 118, 4120:4155.
- Sun, X., Jiang, D., Chen, S., Zhen, G., Huang, S., Gu, M., Zhang, Z., and Zhao, J. (2013). Eu³⁺ activated borogermanate scintillating glass with a high Gd₂O₃ content. *Journal of the American Ceramic Society*, 96, 1483:1489.
- Thomazini, D., Lanciotti J. A., and Sombra, S. B. (2001). Structural properties of lithium borate glasses doped with rare earth ions. *Cerâmica*, 47, 302.
- Uhlmann, D. R. and Shaw, R. R. (1969). The thermal expansion of alkali borate glasses and the boric oxide anomaly. *Journal of Non-Crystalline Solids*, 1, 347:359.
- Ullah, I., Shah, S. K., Rooh, G., Srisittipokakun, N., Khan, A., Kaewkhao, J., Kim, H. J., and Kothan, S. (2020). Spectroscopic study and energy transfer behavior of Gd³⁺ to

- Dy³⁺ for Li₂O-MgO-Gd₂O₃-B₂O₃-Dy₂O₃ glasses for white emission material. *Journal of luminescence*, 226, 117380.
- Venkata Krishnaiah, K., Upendra Kumar, K., and Jayasankar, C. K. (2013). Spectroscopic properties of Dy³⁺-doped oxyfluoride glasses for white light emitting diodes. *Optical Materials Express*, 3, 61:70.
- Venkateswarlu, M., Naresh, V., Rajavaram, R., and Rudramadevi, B. H. (2014). Spectral analysis of Sm³⁺& Dy³⁺: B₂O₃-ZnO-MgO optical glasses. *Journal of Engineering Research and Applications*, 4, 103:113.
- Vijaya, N. and Jayasankar, C. K. (2012). Structural and spectroscopic properties of Eu³⁺-doped zinc fluorophosphate glasses. *Journal of Molecular Structure*, 1036, 42:50.
- Wantana, N., Kaewjaeng, S., Kothan, S., Kim, H. J., and Kaewkhao, J. (2017). Energy transfer from Gd³⁺ to Sm³⁺ and luminescence characteristics of CaO-Gd₂O₃-SiO₂-B₂O₃ scintillating glasses. *Journal of luminescence*, 181, 382:386.
- Wantana, N., Kaewnuam, E., Damdee, B., Kaewjaeng, S., Kothan, S., Kim, H. J., and Kaewkhao, J. (2018). Energy transfer based emission analysis of Eu³⁺ doped Gd₂O₃-CaO-SiO₂-B₂O₃ glasses for laser and X-rays detection material applications. *Journal of Luminescence*, 194, 75:81.
- Wantana, N., Ruangtaweep, Y., Kaewnuam, E., Kang, S. C., Kim, H. J., Kothan, S., and Kaewkhao, J. (2020). Development of WO₃-Gd₂O₃-B₂O₃ high density glasses doped with Dy³⁺ for photonics and scintillation materials application. *Solid State Sciences*, 101, 106135.
- Xu, P., Fu, Z., Fan, S., Lin, H., Li, C., Yao, G., Chen, Q., Zhou, Y., and Zeng, F. (2018). Study on the sensitization of Gd³⁺ on Ce³⁺/Tb³⁺ co-doped GBS scintillating glass. *Journal of Non-Crystalline Solids*, 481, 441:446.
- Yang, P., Chen, B., Shen, L., Yue, B. P., and Lin, H. (2014). Visible photon multiplication in Ce³⁺-Tb³⁺ doped borate glasses for enhanced solar cells. *Journal of Physics D: Applied Physics*, 47, 445101
- Yao, L. Q. (2017). Optical properties and energy transfer in Tb³⁺/Sm³⁺ co-doped Na₂O-CaO-P₂O₅-B₂O₃-ZrO₂ glasses. *Journal of Alloys and Compounds*. 692, 346:350.

- Ying Z., Xianchun Z., Yao Z., Zhang, Q., and Dai, Q. (2019). CdWO₄:Eu³⁺ Nanostructures for Luminescent Applications. *ACS Appl. Nano Mater*, 2, 7095:7102.
- Zachariasen, W. H. (1932). The atomic arrangement in glass. *Journal of the American Chemical Society*, 54, 3841:3851.
- Zaman, F., Rooh, G., Srisittipokakun, N., Ahmad, T., Khan, I., Shoaib, M., and Kaewkhao, J. (2019). Comparative investigations of gadolinium-based borate glasses doped with Dy³⁺ for white light generations. *Solid State Sciences*, 89,50:56.
- Zanella, G., Zannoni, R., Dalligna, R., Polato, P., and BETTINELLI, M. (1995). Development of a terbium lithium glass for slow neutron detection. *Nuclear Instruments and Methods in Physics Research*, 359, 547:550.
- Zanotto, E. D. and Mauro, J. C. (2017). The glassy state of matter: Its definition and ultimate fate. *Journal of Non-Crystalline Solids*, 471, 490:495.
- Zeng, Q., Pei, Z., Su, Q., and Huang, S. (1999). Luminescence and Its Temperature Effects on Sm²⁺ in Alkaline Earth Borates. *Physica Status Solidi*. 212, 207:219.
- Zhao, J., Huang, L., Liang, T., Zhao, S., and Xu, S. (2019). Luminescent properties of Eu³⁺ doped heavy tellurite scintillating glasses. *Journal of luminescence*, 205, 342:345.

CHAPTER III

RESEARCH METHODOLOGY

3.1 Research procedure

3.1.1 Characterization and Instrumentation

- The Center for Scientific and Technological Equipment, SUT:
 - Power X-ray diffraction: PXRD (Bruker D2 diffractometer with Cu-K α radiation)
 - Fourier-transform infrared spectroscopy (FTIR)
- Synchrotron Light Research Institute (Public Organization):
 - X-ray absorption spectroscopy (XAS)
- Center of Excellence in Glass Technology and Materials Science
 - 4-digit sensitive microbalance (AND, HR 200)
 - UV-Visible spectrophotometer (UV-VIS: Shimadzu UV-3600)
 - Photoluminescence (PL: Cary-Eclipse with a Xenon flash lamp)
 - X-ray luminescence (XL: Ocean Optics QE65 Pro spectrometer)

3.1.2 Population/Samplings/ Location of research

- The Center for Scientific and Technological Equipment (Suranaree University of Technology)
- Synchrotron Light Research Institute (Public Organization)
- Center of Excellence in Glass Technology and Materials Science (Nakhon Pathom Rajabhat University)

3.1.3 Materials use

- Lithium carbonate: Li₂CO₃
- Aluminum oxide: Al₂O₃
- Gadolinium (III) oxide: Gd₂O₃
- Boric acid: H₃BO₃

- Cerium (III) fluoride: CeF_3
- Samarium (III) oxide: Sm_2O_3
- Terbium (III) oxide: Tb_2O_3
- Europium (III) oxide: Eu_2O_3
- Dysprosium (III) oxide: Dy_2O_3

3.2 Sample preparation

3.2.1 Preparation of Gd_2O_3 -doped (host glass)

Series of single and double doped borate glasses with Gd_2O_3 and trivalent rare-earth oxide were prepared by mixing and melting appropriate amounts of high purity Li_2CO_3 , H_3BO_3 , Gd_2O_3 , Al_2O_3 , and R_2O_3 (R is trivalent rare-earth oxide: Cerium, Samarium, Europium, Terbium and Dysprosium) as starting materials. A series of $25\text{Li}_2\text{O}-5\text{Al}_2\text{O}_3-\text{XGd}_2\text{O}_3-(69-\text{X})\text{B}_2\text{O}_3-1.0\text{R}_2\text{O}_3$ glasses with different compositions (where X are 0, 2.5, 5.0, 7.5, and 10.0 mol%) is called the LAGdxBR1.0 glasses series are listed in Table 3.1.

Table 3.1 Chemical composition of LAGdxBR1.0 series.

Sample name	X (mol%)	Composition (mol%)
LAGd0BR1.0	0	$25\text{Li}_2\text{O}-5\text{Al}_2\text{O}_3-0\text{Gd}_2\text{O}_3-69.0\text{B}_2\text{O}_3-1.0\text{R}_2\text{O}_3$
LAGd2.5BR1.0	2.5	$25\text{Li}_2\text{O}-5\text{Al}_2\text{O}_3-2.5\text{Gd}_2\text{O}_3-66.5\text{B}_2\text{O}_3-1.0\text{R}_2\text{O}_3$
LAGd5.0BR1.0	5.0	$25\text{Li}_2\text{O}-5\text{Al}_2\text{O}_3-5.0\text{Gd}_2\text{O}_3-64.0\text{B}_2\text{O}_3-1.0\text{R}_2\text{O}_3$
LAGd7.5BR1.0	7.5	$25\text{Li}_2\text{O}-5\text{Al}_2\text{O}_3-7.5\text{Gd}_2\text{O}_3-61.5\text{B}_2\text{O}_3-1.0\text{R}_2\text{O}_3$
LAG10.0BR1.0	10.0	$25\text{Li}_2\text{O}-5\text{Al}_2\text{O}_3-10.0\text{Gd}_2\text{O}_3-59.0\text{B}_2\text{O}_3-1.0\text{R}_2\text{O}_3$

3.2.2 Preparation of R_2O_3 doped

The best condition of the host glass was selected to fabricate for trivalent rare-earth oxide dopant. The glass samples with chemical composition $25\text{Li}_2\text{O}-5\text{Al}_2\text{O}_3-2.5\text{Gd}_2\text{O}_3-(67.5-\text{X})\text{B}_2\text{O}_3-\text{XR}_2\text{O}_3$ were chosen (where 2.5 mol% of Gd_2O_3 is the best condition for the luminescence results and X is the varying R_2O_3 composition of 0, 0.05, 0.1, 0.3, 0.5, 1.0, and 1.5 mol%). They were named as LAGd2.5BRx glasses with varying concentration of trivalent rare-earth oxide (see Table 3.2).

Table 3.2 Chemical composition of LAGd2.5BRx glasses series.

Sample name	X (mol%)	Composition (mol%)
LAGd2.5BR0	0	25Li ₂ O-5Al ₂ O ₃ -2.5Gd ₂ O ₃ -67.5B ₂ O ₃ -0R ₂ O ₃
LAGd2.5BR0.05	0.05	25Li ₂ O-5Al ₂ O ₃ -2.5Gd ₂ O ₃ -67.45 B ₂ O ₃ -0.05R ₂ O ₃
LAGd2.5BR0.1	0.1	25Li ₂ O-5Al ₂ O ₃ -2.5Gd ₂ O ₃ -67.4 B ₂ O ₃ -0.1R ₂ O ₃
LAGd2.5BR0.3	0.3	25Li ₂ O-5Al ₂ O ₃ -2.5Gd ₂ O ₃ -67.2 B ₂ O ₃ -0.3R ₂ O ₃
LAGd2.5BR0.5	0.5	25Li ₂ O-5Al ₂ O ₃ -2.5Gd ₂ O ₃ -67.0 B ₂ O ₃ -0.5R ₂ O ₃
LAGd2.5BR1.0	1.0	25Li ₂ O-5Al ₂ O ₃ -2.5Gd ₂ O ₃ -66.5 B ₂ O ₃ -1.0R ₂ O ₃
LAGd2.5BR1.5	1.5	25Li ₂ O-5Al ₂ O ₃ -2.5Gd ₂ O ₃ -66.0 B ₂ O ₃ -1.5R ₂ O ₃

Figure 3.1 shows that both glasses systems were created utilizing a melt quenching procedure and scientific grade great quality Li₂CO₃, H₃BO₃, Gd₂O₃, Al₂O₃, and R₂O₃ as precursor materials. Approximately 20 g batches were homogeneously combined in an alumina crucible during the process. The powder was then melted in an electrical furnace at 1200°C for 90 minutes. The molten glass was then placed onto a graphite plate, annealed at 500°C for 3 hours, and gently cooled to ambient temperature to reduce thermal stress. All glasses were cut and polished to a rectangle shape of 1.0 x 1.5 x 0.3 cm³. The density of the glass samples was initially determined by the basic Archimedes technique using water as an immersion liquid, and the molar volumes were then measured using a 4-digit sensitive microbalance (AND, HR 200). The molar volume (V_M) of the glasses was calculated using the $V_M = Mw/D$ relationship, where Mw and D were the overall molecular weight of the glass composition and the density of the glass samples respectively. In order to confirm that the glass samples were completely amorphous and transparent, the PXRD (Bruker D2 diffractometer with Cu-K α radiation) analysis was performed. UV-vis and NIR (Shimadzu UV-3600) spectrophotometers are used to analyze the optical absorption spectra (wavenumber range 200-2500 nm). A Xenon flash lamp was used to record the excitation and emission spectra and the decay data at room temperature were measured by a spectrofluorophotometer (Cary-Eclipse). The measurements were carried out by an experimental setup consisting of Cu target x-ray generator (Inel, XRG3D-E), fiber optic

spectrum analyzer (Ocean Optics QE65 Pro), and brass sample holder. The X-ray induced optical luminescence (XOL) spectra of the glasses were studied using an Ocean Optics QE65 Pro spectrometer and a Cu target Xray generator, Inel XRG3D-E, which was operated at 50 kV and 30 mA power. All measurements (in Figure 3.2) were carried out at room temperature. X-ray absorption near-edge structure (XANES) method was used to determine the oxidation state of the glass samples. The experimental XANES data collected in fluorescence mode were compared with those of bent Ge (220) crystals using a crystal analyzer spectrometer.

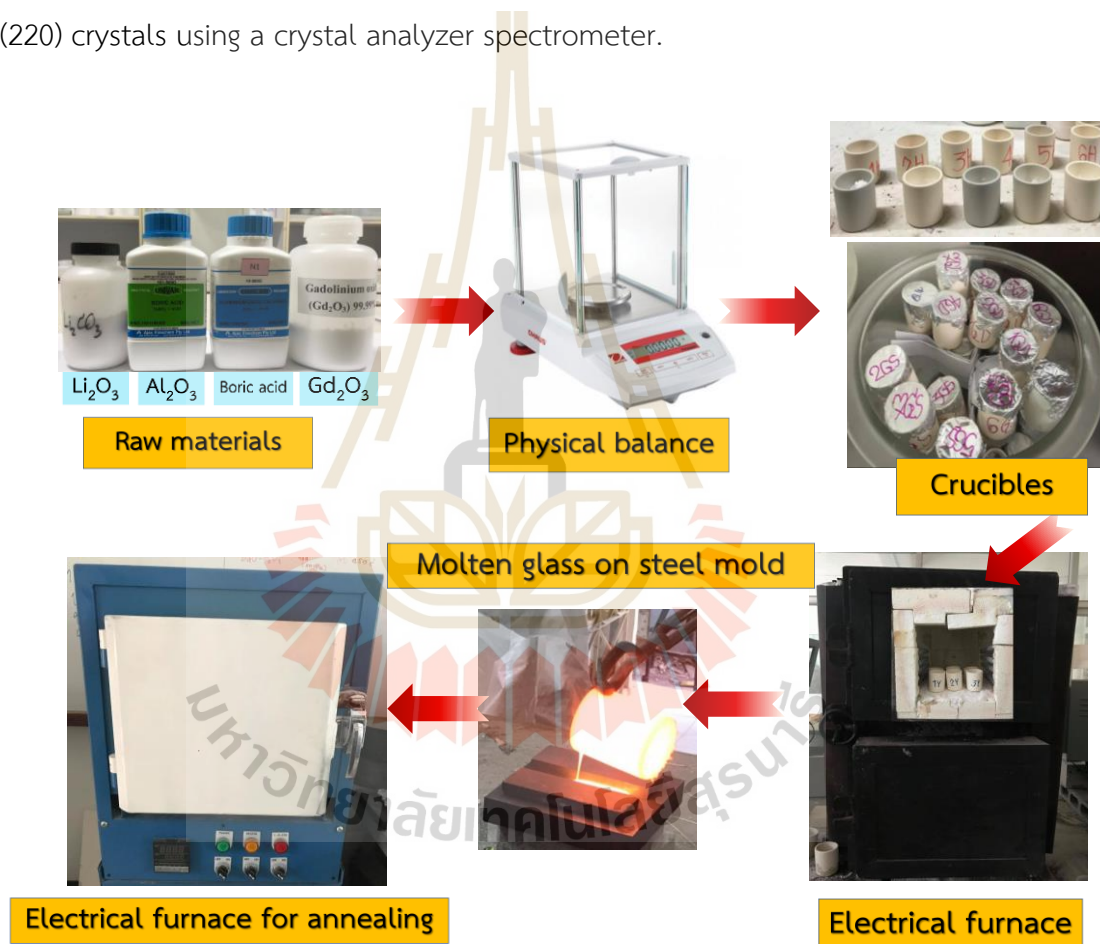


Figure 3.1 Glass Manufacturing Process.

3.3 Characterization techniques

The following properties of the prepared glasses were explored using different characterizations techniques (Figure 3.2).

3.3.1 Flow chart for samples preparation and characterization

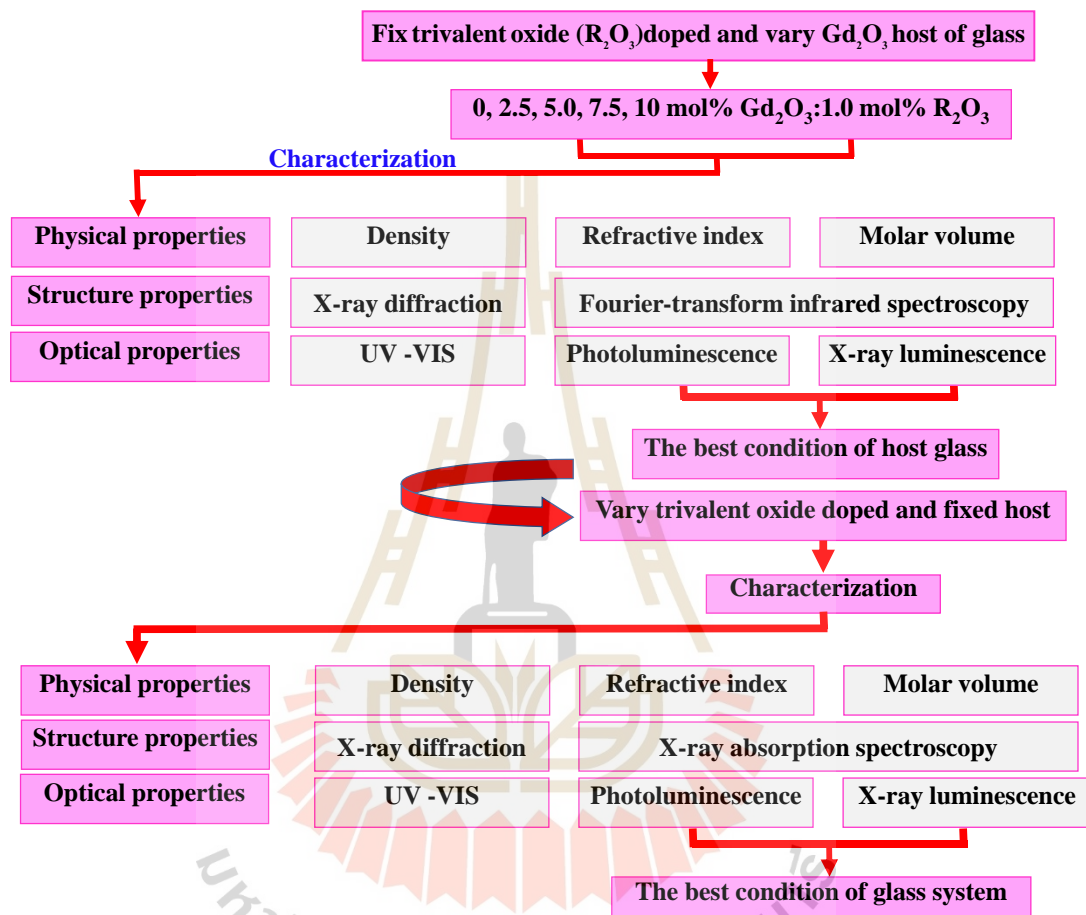


Figure 3.2 Flow chart for samples characterization.

3.4 Physical properties

3.4.1 The density & Molar volumes

The density of glass varies greatly because of the atoms that make up the glass. Because different types of glass contain different combinations of metal oxides, they have different densities. Importantly, the physical properties of glasses, such as their density, Ln^{3+} ion content in the glasses, and refractive index of the glasses doped with Ln^{3+} , have been calculated following the procedure given below. The density (ρ) of

the glasses was determined using the Archimedes principle, where the immersion liquid was taken as distilled water. Figure 3.3 shows density measurement equipment with an accuracy of 0.0001g. The sample was weighed in air and water using a balance at room temperature and the density was computed by Eq. (3.1).

$$\rho = \frac{W_{\text{air}}}{W_{\text{air}} - W_{\text{liq}}} \quad (3.1)$$

where is the weight of the glass sample in air while in liquid (water). The density of water is 0.999 g/cm³ at room temperature. Molar volumes (V_m) of the prepared samples were determined by equation (3.2),

$$V_m = \frac{M}{\rho} \quad (3.2)$$

Where M is the total molecular weight of the glass.



Figure 3.3 Densitometer (Dietheim Limited, HR-200).

3.4.2 Refractive index

The refractive indices (n) of the glasses were determined with an Abbe refractometer with a measuring accuracy of 0.0001 as shown in Figure 3.4 at a wavelength of 589.3 nm using a sodium lamp as a source with monobromonaphthalene as a contact liquid between the glass and the prism of the refractometer.

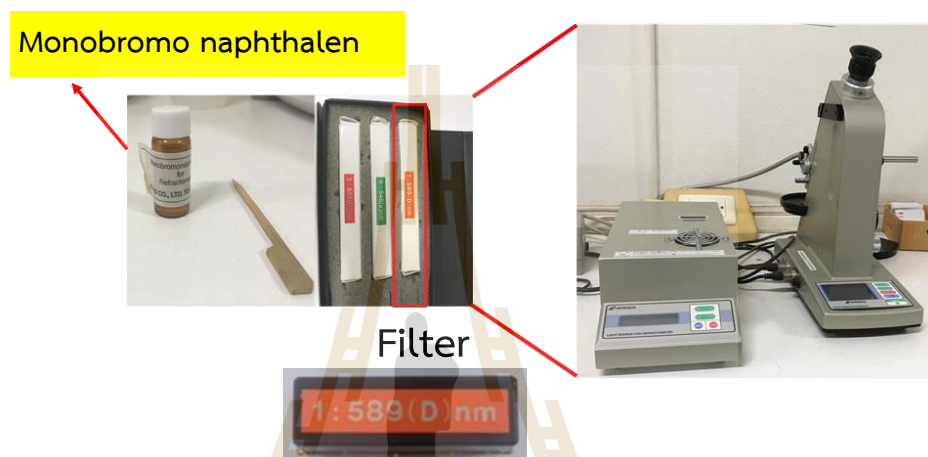


Figure 3.4 Abbe refractometer (ATAGO) with a sodium vapor lamp as a light source having wavelength of 589.3 nm (D line) with monobromonaphthalene as a contact layer.

3.5 Structural properties

X-RAY Diffraction, Fourier Transform Infrared spectroscopy and X-ray absorption spectroscopy are used to find out about the structure of glass samples in this dissertation.

3.5.1 X ray diffraction

X-ray diffraction is a standard technique for material characterization to obtain microstructural information for crystalline and non-crystalline materials. This non-destructive method could provide information such as crystal structure, lattice parameter, crystal size, composition, etc., which are useful for ceramics, metal alloys, semiconductors, polymers, nano-materials research. In this work, the structure of glass was examined on a D2 Advance Bruker with $\text{Cu K}\alpha$ and $\lambda = 0.15406$ nm. The step size of 0.02 and step time of 0.4 were used to record the XRD patterns in the 2θ of 10° to

80°. X-ray diffraction (XRD) is the principal technique used for phase identification of a crystalline material and determining the unit-cell dimensions. X-ray diffraction depends on the crystalline sample, and the constructive interference of X-rays is produced from X-ray tubes. Then it is filtered to provide monochromatic X-rays and directed directly to the sample. The interaction between the incident radiation and the sample leads to constructive interference. The geometrical interpretation of the XRD phenomenon (constructive interferences) has been given by W.L. Bragg (Bragg, 1929). Figure 3.5 shows a photograph of an X-ray diffractometer.

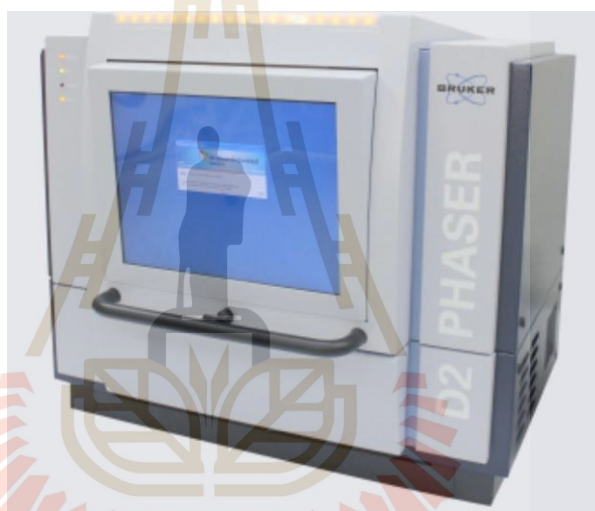


Figure 3.5 Powder X-ray Diffraction (Bruker D2 PHASER).

3.5.2 X-ray absorption spectroscopy (XAS)

X-ray absorption spectroscopy (XAS) is a high-efficiency technique for determining the chemical and structural information in the local environment of the absorber. The XAS spectrum consists of X-ray absorption near edge structure (XANES) and extended X-ray absorption fine structure (EXAFS). The XANES spectrum often gives information on the coordination geometry (e.g., octahedral, tetrahedral coordination) and oxidation state of the absorbing atom. XANES measurements can be carried out in transmission or fluorescent modes. The samples are for the fluorescence mode experiment. The photon hits the sample and it is absorbed by the core electron. After

that, the core electron ejects from its core-shell, leading to the occurrence of a core hole that is in a highly excited state. Then, the phenomenon of X-ray fluorescence or Auger electron emission occurs to relax the core hole state. In terms of higher-energy excitation, the primary relaxation process is X-ray fluorescence. The $\mu(E)$ is calculated using the equation (3.3)

$$\mu(E) = C \left(\frac{F}{I_0} \right) \quad (3.3)$$

Where C is approximately constant, F is the intensity of the fluorescence X-rays, and I_0 is the intensity of the incident X-ray beam. In this work, the oxidation states of Ce, Sm, Tb, Eu, and Dy (L3-edge) were collected in the fluorescence mode. XANES measurement was conducted in the electron energy of 1.2 GeV and a beam current of 80-150 mA at the SUT-NANOTEC-SLRI XAS (BL5.2), the Synchrotron Light Research Institute (SLRI), Thailand (Figure 3.6).

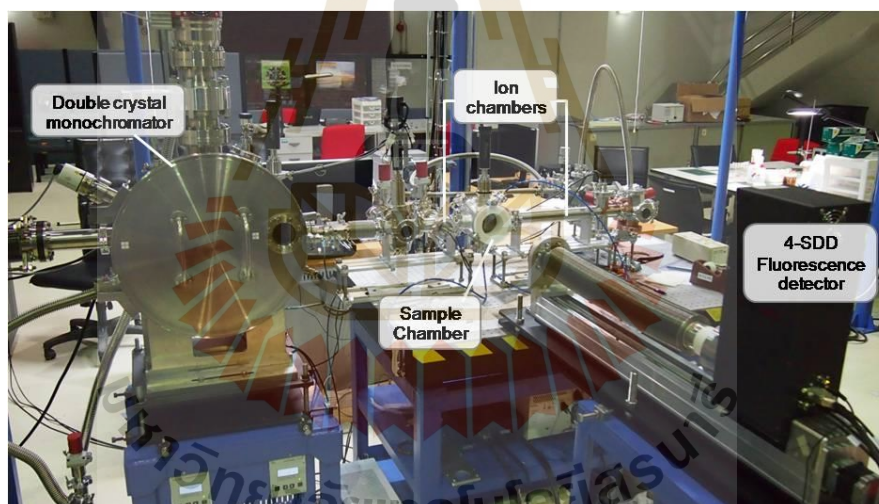


Figure 3.6 X-ray absorption spectroscopy (SUT-NANOTEC-SLRI beamline setup (BL5.2)).

3.6 Optical and spectral properties

3.6.1 Fourier-transform infrared spectroscopy

Fourier transform infrared analysis of glasses has been analyzed in order to identify the spectral contribution of each component in the structure and to point out the role of the lanthanide ions in the glass network. Fourier transform infrared spectroscopy is one of the effective tools for resolving the structure of local

arrangements in glasses. These non-destructive techniques provide extensive information about the structure and vibrational properties of glasses. The quantitative interpretation of the absorption bands of the IR spectra according to the value of the stretching force constant and reduced mass of the vibrating cation-anion has been discussed. Interpretation of the IR absorption curves shows that the co-ordination number determines the nature of the spectra. Infrared spectroscopy exploits the fact that molecules absorb specific frequencies that are characteristic of their structure. These absorptions have resonant frequencies, i.e., the frequency of the absorbed radiation matches the frequency of the bond or group that vibrates. The energies are determined by the shape of the molecular potential energy surfaces, the masses of the atoms, and the associated vibronic coupling. In particular, in the Born–Oppenheimer and harmonic approximations, i.e., when the molecular Hamiltonian corresponding to the electronic ground state can be approximated by a harmonic oscillator in the neighborhood of the equilibrium molecular geometry, the resonant frequencies are determined by the normal modes corresponding to the molecular electronic ground state potential energy surface. Nonetheless, the resonant frequencies can be related to the strength of the bond and the mass of the atoms at either end of it in a first approach. Thus, the frequency of the vibrations can be associated with a particular bond type.



Figure 3.7 Fourier-transform infrared spectroscopy.

3.6.2 UV-Visible spectrophotometer

The UV-Vis NIR technique is used to identify the optical properties of the sample in the wave length range of 200–2500 nm, with a measurement accuracy of 1 nm. This range of wave lengths covers the visible and infrared spectrums. When monochromatic em radiations are made incident on the sample, it absorbs, scatters, transmits, and reflects some part of the light, and the incident intensity of the light can be determined with the help of a detector. This model has a radiation source, like a deuterium or halogen lamp, a filter, a sample cell, a photo diode detector, and a readout (computer system), as shown in block diagrams Figure 3.8 and Figure 3.9. Tauc et al. and E.A. Davis et al. theoretically investigated the absorption edges of the absorption spectra. They proposed a correlation between the absorption coefficient and the band gap energy for direct and indirect allowed transitions. To determine the optical band gap and the nature of direct and indirect transitions theoretically, the formula proposed by Tauc is given by Eq. (3.4)

$$\alpha = \alpha_0 (h\nu - E_g)^n \quad (3.4)$$

where α_0 is a constant, $n = 1/2$, $n = 2$ for allowed direct and indirect transitions respectively, E_g is the optical energy gap between the valence and conduction band. Tauc's formula holds true for glass host, therefore the indirect optical band gap (E_g) can be evaluated by putting $n = 2$ in Eq. (3.4) and drawing the absorption coefficient $(\alpha h\nu)^{1/2}$ versus photon energy $h\nu$.

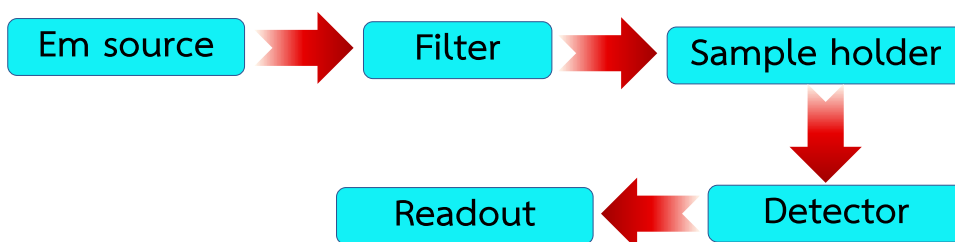


Figure 3.8 Block diagram of the UV-Vis NIR spectrophotometer.



Figure 3.9 Shimadzu 3600 UV-Vis-NIR spectrophotometer.

3.6.3 Photoluminescence technique

A photoluminescence spectrometer with a measurement accuracy of 1 nm is employed to study the spectral characteristics of the samples. The de-excitation of electrons to the ground state causes the emission of light called luminescence or heat. Luminescence spectra were recorded by adjusting the excitation monochromator at a specific wavelength and scanning the emission monochromator over a range of wavelengths. Excitation spectra are recorded by fixing the emission monochromator at a chosen wavelength and the excitation monochromator is scanned over the desired wavelength range. In the present work, an Agilent technology Cary Eclipse fluorescence spectrometer capable of performing in the wavelength region of 200 to 900 nm with a spectral resolution of 1.0 nm has been used. The block diagram of the luminescence spectrometer is displayed in Figure 3.10.

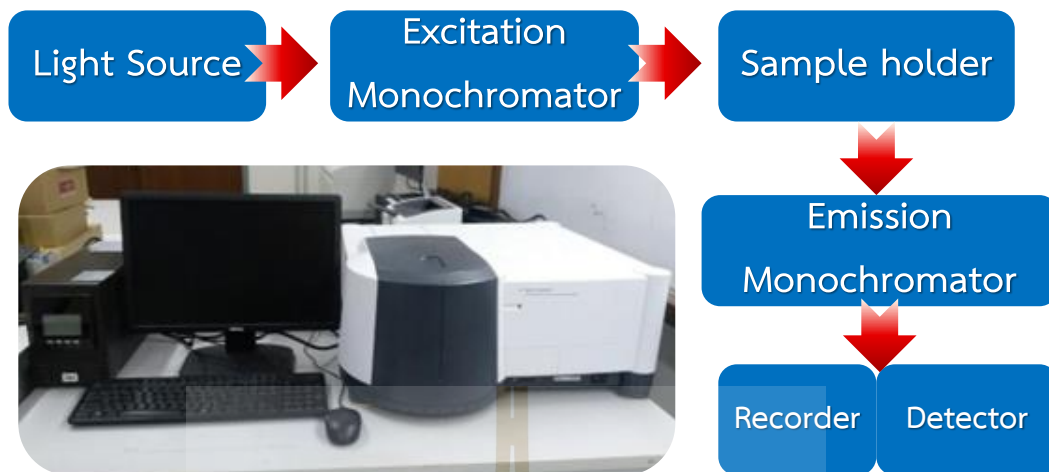


Figure 3.10 Agilent technology Cary Eclipse fluorescence spectrometer.

3.6.4 X-ray luminescence technique

Luminescence induced by X-ray was recorded using the same procedure as that for Photoluminescence technique, except the radiation induced source was used as a Cu target with an x-ray generator (Intel, XRG3D-E: X-Ray generator) instead of visible light. The power of the X-ray source was operated at 50 kV and 20 mA for all developed samples. The spectrometer (QE65 Pro, Ocean Optics) with optical fiber was employed for the detection of emission spectra instead of the phototube. Figure 3.10 shows the experimental tools of the induced x-ray luminescence spectrometer.

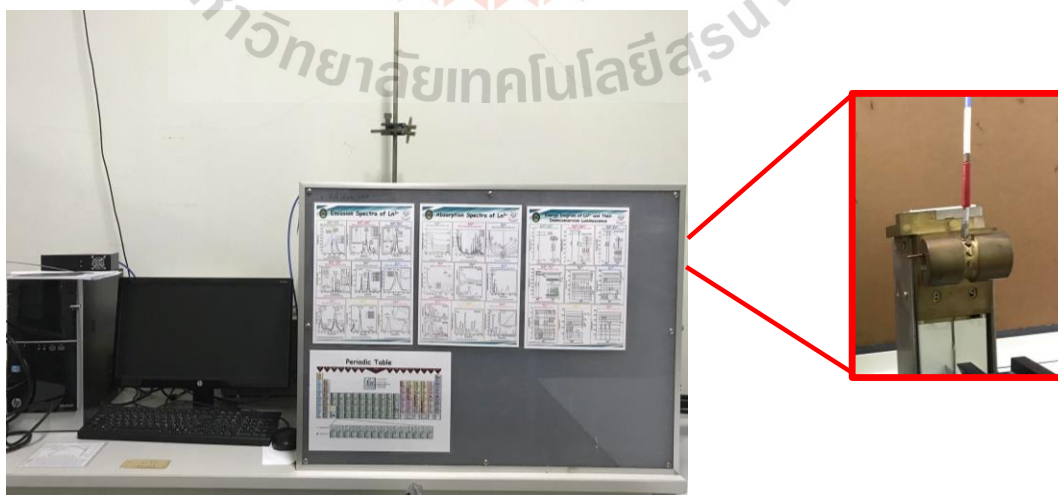


Figure 3.11 X-ray induced luminescence.

CHAPTER IV

CERIUM DOPED BORATE GLASS

A series of glasses composed (Ce^{3+} and Gd^{3+}) co-doped lithium aluminum borate glasses with composition $25\text{Li}_2\text{O}-5\text{Al}_2\text{O}_3-\text{XGd}_2\text{O}_3-(69.5-\text{X})\text{B}_2\text{O}_3-0.5\text{CeF}_3$ glasses were successfully synthesized by using a conventional melt-quenching technique and characterized through physical, structural and luminescence properties. The optimal doping concentration of CeF_3 contents is 0.5 mol% and varying Gd_2O_3 concentration for studying the combined effect of dual doped glass. Further, the phenomenon of energy transfer from the host glass in luminescence center was observed by x-rays induced luminescence spectra, as well as from Gd^{3+} to Ce^{3+} ions are confirmed by photoluminescence emission spectra. The strongest emission intensity of Ce^{3+} emission is obtained when the scintillating glass contains 5.0 mol% of Gd_2O_3 concentration. From the nano-second decay time of glass exhibit a high potential for using as scintillating materials.

4.1 Introduction

Borate-glasses pertaining rare earth (RE) doped glasses play a lot of significance owing to their applications for scintillating material, solid state, luminescent applications (Nikl et al., 2000; Zhang et al., 2018; Yoshimura et al., 2009). Borate glass is a good choice because of their have high thermal stability, good strength, low melting point, different coordination numbers, good solubility of rare earth (RE) ions and excellent transparency (Pascuta et al., 2008; Park et al., 2016; Ogieglo et al., 2013). However, borate glass has some poor properties such as hygroscopic character (Park et al., 2013). The borate glasses have a detrimental effect on their performance by absorbing moisture without being stable. Therefore, it can enhance many properties

of borate glasses and alter, even decrease the hygroscopic property of their glass network such as Li_2O , Na_2O , and K_2O leading to a solution that is the addition of alkali oxides. In addition, Li_2O , Gd_2O_3 , and B_2O_3 host glasses systems have been extensively studied in the literature because its high stability, clear transparent, energy transfer from Gd^{3+} to the trivalent rare earth activator and improve the intensity of emission spectra, especially Li- containing materials are also considered ideal scintillators for neutron detection (Zaman et al., 2016; Spector et al., 1993). Moreover, lithium in borate glass contributes to the conversion of sp^2 planar BO_3 units into more stable sp^3 tetrahedral BO_4 units and non-bridging oxygen (NBO) can be produced (Sun et al., 2015). Lithium is an important alkali cation and Al_2O_3 is important in that structure, mainly imparting thermal stability and durability superior to most other elements. Adding some of the rare-earth elements are show special properties to the glass such as super-fluorescent (a fast luminescence decay time in nanosecond units), especially Ce^{3+} ions doped have been studied of considerable interest for potential applications as scintillators (Bahadur et al., 2013) Further, most scintillation materials need high efficiencies of luminescence and dopant or activators from preferred inorganic scintillation sites for excited electrons from the activator before falling to the ground state. So that, co doped between Ce^{3+} and Gd^{3+} form activated borate glasses have become very popular for using in neutron detection reports by Bollinger, et al. 1962. Due to the 4f-4f transition states of the Gd^{3+} are overlapped with the 4f-5d transition state of the Ce^{3+} , which its present the charge transfer of the 4f \rightarrow 5d character. Thus, the energy transfer from the Gd^{3+} to Ce^{3+} ions show many unique advantages such as high quantum efficiency, high light yield and short lifetime of glass could be a potential candidate for radiation scintillating materials (Park et al., 2013).

In this paper, we focus on the co-doped with rare earth (Ce^{3+} and Gd^{3+}) of lithium aluminum borate host glass matrix. The composition ratio $25\text{Li}_2\text{O}-5\text{Al}_2\text{O}_3-\text{XGd}_2\text{O}_3-(70-\text{Y}-\text{X})\text{B}_2\text{O}_3-\text{YCeF}_3$, have been fabricated by using the melt-quenching technique. In the first step, the doping concentration of the CeF_3 was varied from 0 to 1.5 mol%. The optimal doping concentration of Ce^{3+} ions was 0.5 mol% CeF_3 show photoemission with high-intensity, designated name as LACB glasses after step the varying concentration of Gd_2O_3 where $\text{X}= 0, 2.5, 5.0,$ and 10 mol%. Therefore, we

studied the physical, structural, luminescence and scintillation properties of glass system by using an optical spectrometer, X-ray absorption near-edge structure (XANES) and X-ray luminescence system will help us understand the impact of dual-dope the host glass matrix in the borate with two lanthanide trioxides.

4.2 Experimental Procedure

4.2.1 Preparation of CeF₃ doped

The compositions of borate glasses investigated in the present work are 25Li₂O-5Al₂O₃-5Gd₂O₃-(65-Y)B₂O₃-YCeF₃ fixed 5.0 mol% of Gd₂O₃ so called as LAGB series and varying concentration of CeF₃ in mol%, where Y= 0, 0.05, 0.3, 0.5, 1.0, and 1.5 mol%. The cerium fluoride-containing scintillation glass host has greatly higher the luminescent intensity. This the optimal concentration CeF₃ of glass host gives the high PL intensity and chose then for varying Gd₂O₃ concentration.

4.2.2 Preparation of Gd₂O₃ doped

For Gd³⁺ doping, a proportional portion about Gd₂O₃ substance with difference X from 0 to 10.0 mol%, call the LACB series of glass (0 mol% Gd, 2.5 mol% Gd, 5.0 mol% Gd, 7.5 mol% Gd and 10 mol% Gd) have been substituted for those particular stoichiometric measures of dopant contents. Both glasses series were prepared by using the melt quenching technique at 1,200°C (Figure 4.1). The starting materials of lithium carbonate (Li₂CO₃), boric acid (H₃BO₃), gadolinium oxide (Gd₂O₃), and cerium fluoride (CeF₃) were weighed using an electronic balance having an accuracy of the order of 0.0001g. In the process, about 20 g batches of a homogeneous mixture of raw material were prepared. All the chemicals were of laboratory reagent grade. The alumina crucible containing the mixture was placed in an electric furnace. The electric furnace was kept at a temperature 1,200°C for 90 minutes. Then the glass melt was poured onto a graphite plate followed by annealing at 500°C for 3 hours to relieve thermal stress and cooled slowly to room temperature. The two opposite faces of the glasses were ground approximately on the cutter machine and then on the polishing machine (1.0x1.5x0.3 cm³). The sample thickness was measured with a micrometer, with a resolution of 0.001 mm. From the final glass materials at room temperature,

their densities were first measured according to a simple Archimedes method using water as an immersion liquid and then molar volumes were calculated. The optical absorption spectra of polished samples are measured with a UV-vis -NIR spectrophotometer (Shimadzu UV-3600) in the wavenumber range 200-800 nm. Optical band gaps were calculated for indirect transitions from the absorption spectra of each sample. Photoluminescence (PL) spectra were recorded using a spectrofluorophotometer (Cary-Eclipse) with a Xenon flash lamp as an excitation light source. The pattern of X-ray diffraction (XRD) was recorded using a Bruker D2 phaser XRD-6100 with $\text{CuK}\alpha$ radiation at 30 kV and 30 mA with a range of $2\theta = 10^\circ\text{--}80^\circ$. The X-ray luminescence spectra were measured by an experimental setup consisting of Cu target x-ray generator (Inel, XRG3D-E), fiber optic spectrometer (Ocean Optics, QE65 Pro) and brass sample holder. Glass was radiated by x-ray which operates at 50 kVp source and 30 mA current. The luminescence decay curve of glasses was studied by using the Deltapro™ fluorescence life time system (HORIBA scientific) with 286 nm DeltaDiode light source (DD-290) and picosecond photon detector (PPD-850). X-ray absorption spectroscopy (XAS) was performed at Synchrotron Light Research Institute (beamline 5.2). The Ce L_{III} X-ray absorption near-edge structure (XANES) was recorded for the glass samples in fluorescence mode. Standard CeF_3 and CeO_2 samples were used for reference.

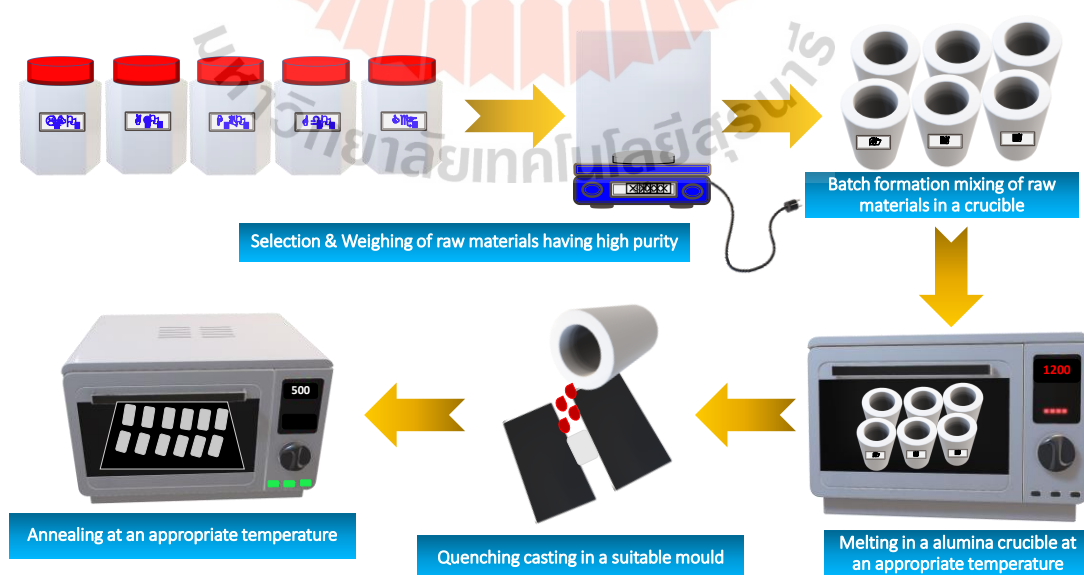


Figure 4.1 Schematic illustration of melt quenching technique along with a photograph of the prepared glasses.

4.3 Results and discussion

4.3.1 A series of LAGB: 5.0 mol% Gd_2O_3 with varying concentrations of CeF_3

With no noticeable coloration, the glass samples with varying CeF_3 concentrations from 0 to 0.5 mol% demonstrate excellent inline transmission. While the concentration of 1.0 mol% CeF_3 is a yellow shaded material in presented in Figure 4.2.

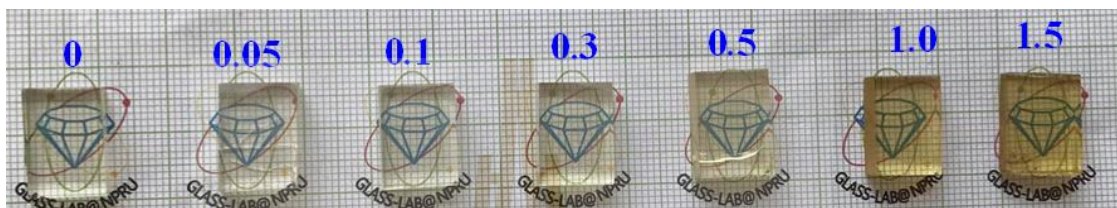


Figure 4.2 The glass samples of LAGB series with different concentration of CeF_3 .

In Figure 4.3(a) shows the density (approximate) and molar volume (V_m) of $25Li_2O-5Al_2O_3-5Gd_2O_3-(65-Y)B_2O_3-YCeF_3$ glass samples as a variable concentration factor of CeF_3 . With an increase in the volume of CeF_3 doped in the glass system, the density increased. The density of LAGB doped CeF_3 glass provides in a range of 2.662 to 2.732 g/cm^3 . As seen in the glass chemical system, the CeF_3 is heavier than the substitution of B_2O_3 by CeF_3 doping, resulting in an increase in overall glass weight that raises density (Park et al., 2013; Zaman et al., 2016). With an increase in CeF_3 concentration between 0.05-0.10 mol%, molar glass volume was decreased. The vacancies, interstitial space of the glass network can be added by the small quantity sum of CeF_3 dopant. Hence the volume per mole of glass decrease. The overabundance of Ce^{3+} will disrupt the O_2 cation bonding and make non-bridging oxygen (NBO) or non-connecting oxygen (NCO) with glass sample doped with CeF_3 above 0.10 mol%. These NBOs activate the molar-related interstitial space of the glass network. These NBOs allow the interstitial space in the glass network to extend with an increase in CeF_3 concentration from 0.10-1.50 mol% in comparison to the molar volume (Kaewnuam et al., 2019). The refractive index values were plotted versus the concentration of CeF_3 , displayed in Figure 4.3(b). The results show the refractive index increase with increase the concentration of CeF_3 corresponding to density result. Due to the growth of NBOs in the glass matrix, it is predicted. The XRD results for all glass

samples as seen in Figure 4.3(c), the amorphous existence of the samples is confirmed by the absence of crystallization peaks in the spectra. In addition, the transparent glass without crystallization was observed.

The optical absorption edge is seen to clearly demonstrate the amorphous essence of glass samples recorded at room temperature in the wavelength of 200-800 nm, as shown in Figure 4.4. As CeF_3 content rises, it is noted that the direction of the absorption edge shifted to shorter wavelengths. In the entire UV zone, Gd-doped glass samples have large absorption. Hence, it is reasonable to consider these absorption bands are due to host glass.

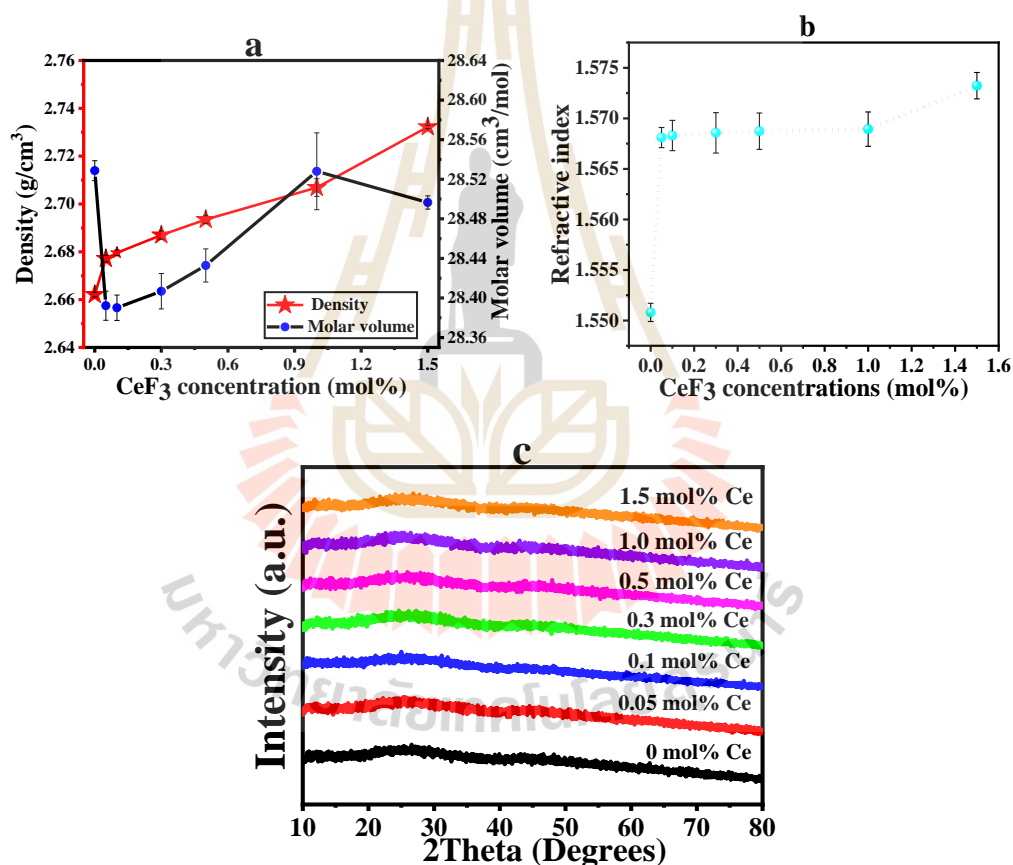


Figure 4.3 Density, molar volume, refractive index and XRD analysis of the LAGB glass system as a function of the mol% of CeF_3 (mol%) defined from a, b, and c.

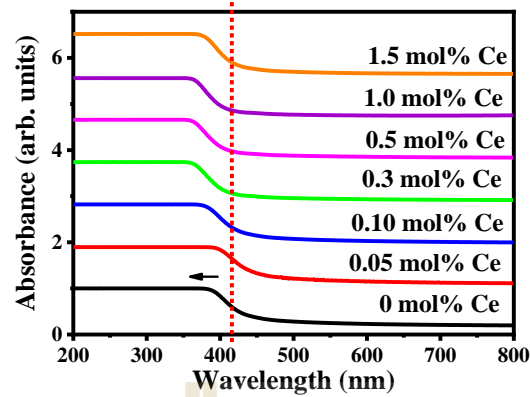


Figure 4.4 The absorption spectra of lithium aluminum gadolinium borate glasses (LAGB) doped with increasing CeF_3 amount doped in glass.

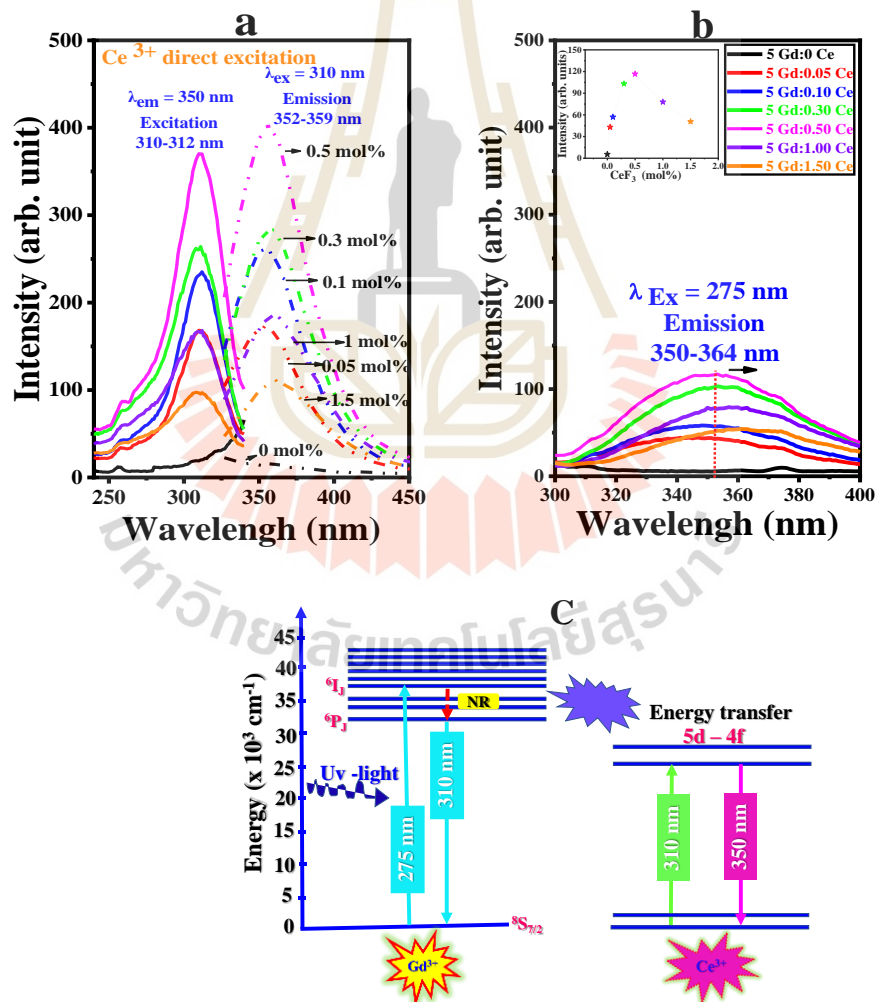


Figure 4.5 PL spectra of the non-doped and Ce (0.05–1.5 mol%)-doped samples with fixed concentration of 5.0 mol% Gd_2O_3 (a, b) and the energy level diagram for the transitions of Ce^{3+} (c).

Figure 4.5(a) indicates photoluminescence of excitation/emission spectra in non-doped and (0.05–1.5 mol%) CeF_3 doped glasses. No emission bands were observed in the non-doped sample, while the (0.05–1.5 mol%) CeF_3 -doped sample have a large emission bands centered at 350 nm. It is respected the emission spectra due to the 5d–4f electron transition character of Ce^{3+} ions. Addition, the broad excitation band centered at about 312 nm (4f–5d allowed transition of Ce^{3+} ions) have to trend increases with the increasing CeF_3 concentration up to 0.5 mol% (the maximum intensity). Figure 4.5(b) shows the Gd^{3+} excitation at 275 nm due to the $^8\text{S}_{7/2}$ to $^6\text{I}_J$ transition Gd^{3+} to Ce^{3+} energy transfer phenomena, was obtained and show emission bands centered between 350–364 nm when excited with UV. The emission intensity increased with increasing Ce^{3+} concentration from 0.05 to 0.5 mol% and consequently dropped due to concentration quenching phenomena. In comparison, direct excitation (310 nm) for Ce^{3+} emission intensity has been higher than under excitation for Gd^{3+} (275 nm), peak in the range 352–364 nm and the 4f–4f transition states of the Gd^{3+} are overlapped with 4f–5d transition state of the Ce^{3+} , which present the charge transfer of the 4f→5d character. All process of luminescence transitions under Ce^{3+} directly and Gd^{3+} excitation was shown in Figure 4.5(c). Then, we investigated the optimum doping concentration for CeF_3 amount doped in (LAGB) glass. CeF_3 is observed here to be 0.5 mol%, the best condition for the next experiment.

4.3.1 A series of LACB: 0.5 mol% CeF_3 with varying concentrations of Gd_2O_3



Figure 4.6 Photograph of samples with different concentrations of Gd_2O_3 .

In this part, we have presented a detailed spectroscopic analysis for the best concentration of glass with doped $Y = 0.5 \text{ mol\%}$, $25\text{Li}_2\text{O}-5\text{Al}_2\text{O}_3-5\text{Gd}_2\text{O}_3-(64.5-X)\text{B}_2\text{O}_3-0.5\text{CeF}_3$ (LACB series). Because the glass scintillation should be of high detection

performance with x-rays, great care is being taken to ensure that Ce^{3+} doped glasses are a successful host with optimum numbers of Gd_2O_3 . As a result of the energy conversion from Gd^{3+} to Ce^{3+} when excited with UV or X-rays (Wantana et al., 2018). There is an improved amount of the light yield of Ce^{3+} -doped LAGB glasses. In Figure 4.6 plays all glass samples appearance, with the chemical composition of x ranging from 0 up to 10 mol% fraction of $25Li_2O-5Al_2O_3-xGd_2O_3-(69.5-x)B_2O_3-0.5CeF_3$. In relation, Table 4.1, we summed up some properties of the glass samples, where the increase of Gd_2O_3 is marginally seen.

Table 4.1 Glass composition (mol%), density, molar volume, refractive index, indirect bandgap, and decay time of lithium aluminum gadolinium borate (host) doped CeF_3 0.5 mol% glasses with increasing of Gd_2O_3 amount doped in glass.

Gd_2O_3 (mol%)	0	2.5	5.0	7.5	10.0
Density (g/cm^3)	2.2390 ± 0.0201	2.4096 ± 0.0251	2.5787 ± 0.0198	2.6553 ± 0.02512	2.8799 ± 0.0205
Molar volume (cm^3/mol)	27.3792 ± 0.1026	28.4796 ± 0.2025	29.4508 ± 0.1521	31.3585 ± 0.1820	31.4560 ± 0.1625
Refractive index	1.6535 ± 0.0013	1.5433 ± 0.0019	1.5667 ± 0.0017	1.5641 ± 0.0020	1.5274 ± 0.0025
Indirect bandgap (eV)	2.3620	2.7284	2.8955	3.0211	3.0559
Decay time (ns)	17.44 ± 1.07	15.70 ± 1.37	15.20 ± 1.35	16.03 ± 0.56	16.98 ± 1.07

The increasing Gd_2O_3 content increases the density and molar volume, which means the Gd_2O_3 portion is a glass modifier. The Gd_2O_3 molecular weight (362.5 g/mol) is higher and at the same concentration of 0.5 mol% CeF_3 samples. Glasses then indicate a raise in their density was varied in glass (Figure.4.7(a)). Although the rise in the molar volume is due to disruptions in the block network in the glass, more non-bridging oxygen is more generated and its volume thus increases (Zhu et al., 2013).

Figure 4.7(b) indicates the XRD pattern for all samples has no continuous or discrete sharp peak, and consists only of diffuse bands, which specifically show the glassy quality of the glass samples prepared.

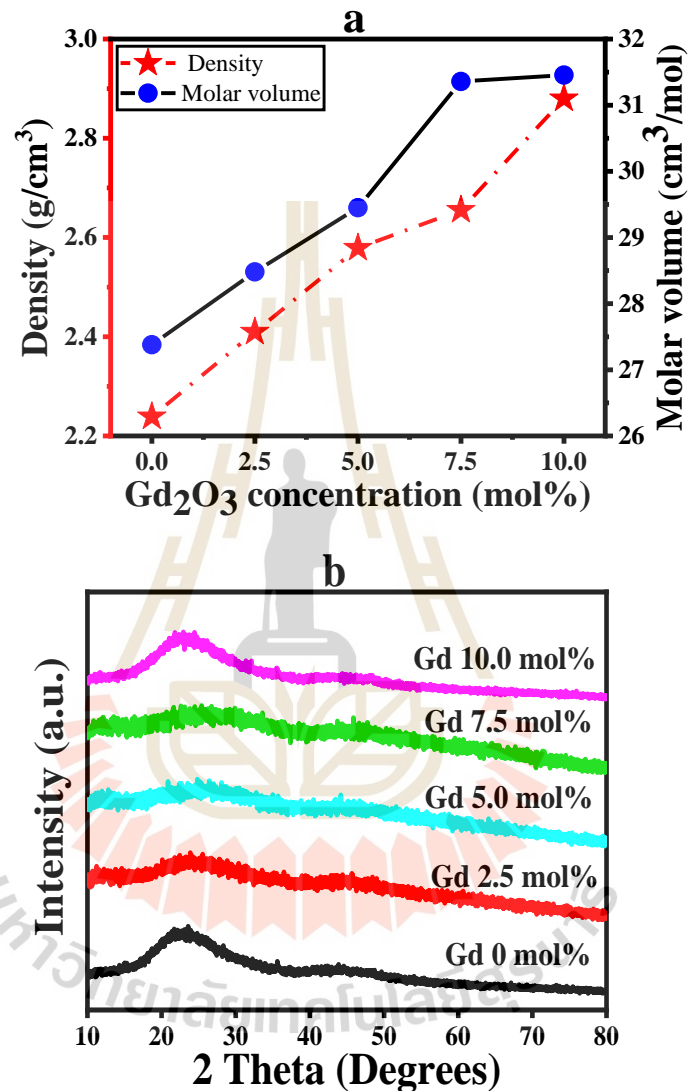


Figure 4.7 Variation of density, molar volume (a) and XRD results (b) of 0.5 mol% Ce-doped with different concentration of Gd₂O₃ glass sample.

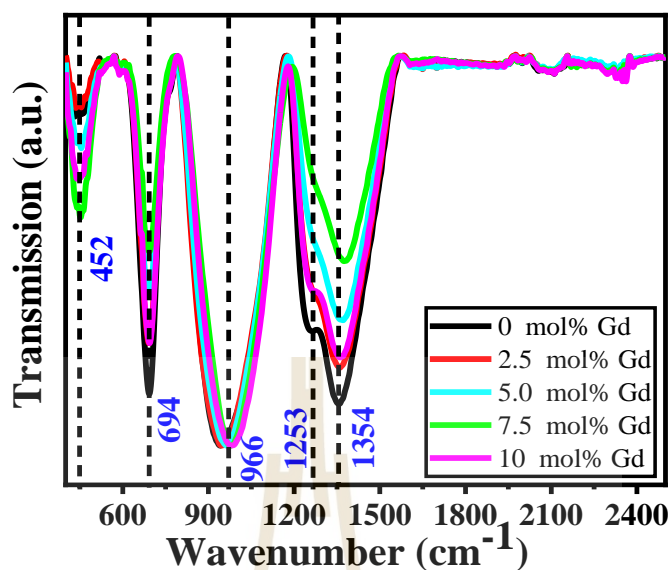


Figure 4.8 FTIR spectra of non-doped powders (0 mol% Gd_2O_3) and powders from doped Gd_2O_3 (0, 2.5, 5.0, 7.5, and 10 mol%) samples. Characteristic peaks are presented in Table 4.2.

Figure 4.8 displays Fourier transform infrared spectroscopy (FTIR) spectra of samples from non-doped Gd_2O_3 and variable Gd_2O_3 contents of existing glass-systems. The FTIR spectrum, which includes the main two traditional bands owing to the presence of borate groups, reveals the extended vibrations of trigonal BO_3 units (NBOs) at 1354 cm^{-1} (Konijnendijk et al., 1975) and B–O tetrahedral stretching units [BO_4] at 966 cm^{-1} (Konijnendijk et al., 1975; Furukawa et al., 1980; Silim et al., 2006) of all the samples. There is also an additional band of roughly 694 cm^{-1} as B–O–B links bend through the borate network. Although the vibrations of these NBOs occur 0 mol% of Gd_2O_3 in the study, Gd_2O_3 increases. Its intensity of observed peaks tends to decline in samples, suggesting that NBOs are becoming extinct, to 7.5 mol% of Gd_2O_3 . We may also assume the gadolinium tends to suppress NBOs. This also goes well with density observations that density shows an increasing trend as we move from sample 0 to 7.5 mol% of Gd_2O_3 . When the glasses are doped with 7.5 mol% of Gd_2O_3 , the intensity of the band due to [BO_3] units are observed to decrease and in correspondence to a new band is rise at 452 cm^{-1} band. This band is attributed to the vibration of cerium cations

at their network sites (Silim et al., 2006). In some studies, the creation of cerium units in combination with the network is mentioned (Khanna et al., 2014). Thus, no shift of place with 0.5 mol% CeF_3 fixing (452 cm^{-1}) leads to conclude that the range is mostly attributable to modifier vibrations than the former CeF_3 units (Balachandera et al., 2013) network. It gives knowledge on different structural groups in nature and allows to know changes with the compositional variety of the glass samples in their configurations. As the concentration of Gd_2O_3 is further increased, it is also noticed that the peak intensity decreases by 1354 cm^{-1} , corresponding to a band intensity of 966 cm^{-1} with changes towards higher wavenumbers ($960\text{-}982 \text{ cm}^{-1}$). This is attributable $[\text{BO}_4]$ classes increased and glass systems (Konijnendijk et al., 1976; Gautam et al., 2012) reduced by $[\text{BO}_3]$ units. The $[\text{BO}_3]$ group is converted to the $[\text{BO}_4]$ group and oxides of Gd_2O_3 are added in the borate network.

Table 4.2 Assignment of FTIR bands of the glass system ($25\text{Li}_2\text{O}\text{-}5\text{Al}_2\text{O}_3\text{-}X\text{Gd}_2\text{O}_3\text{-(}69.5\text{-}X)\text{B}_2\text{O}_3\text{-}0.5\text{CeF}_3$).

IR bands wave number (cm^{-1})	Assignments
452	presence of lithium oxide in the glass samples
694	Bending vibration O-B-O
966	B-O stretching of tetrahedral BO_4
1253	B-O asymmetric stretching vibration in BO_3 from varied types of borate groups
1354	Stretching vibration of NBOs of BO_4 unit

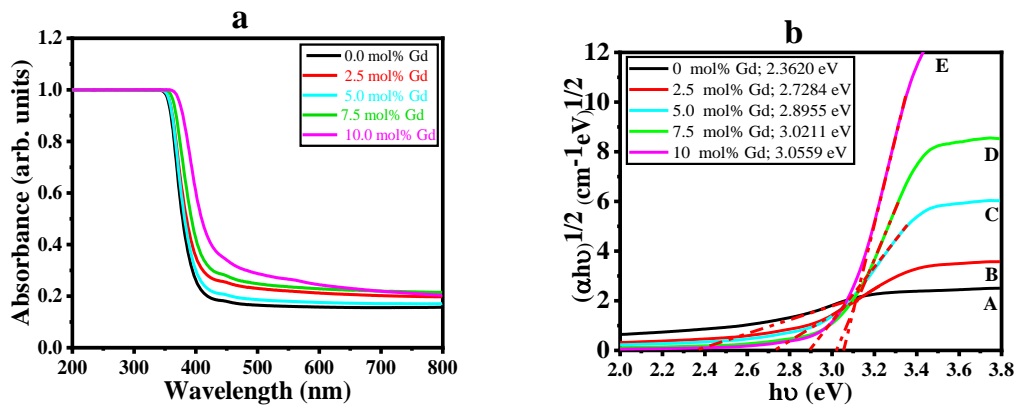


Figure 4.9 Optical absorbance (a) and indirect bandgap (b) of the investigated 0.5 mol% Ce-doped with different concentration of Gd_2O_3 in the UV-VIS region.

The optical absorption range for all glass samples with various amounts of Gd_2O_3 (0-10 mol%) as shown in Figure 4.9(a), the sharp of absorption edge in the spectra is no sharp, which confirms the amorphous existence of all the glass samples. All the samples show high transmittance. Figure 4.9(b) were plotted between $(\alpha h\nu)^{1/2}$ and $h\nu$ using for determination of the optical band gap of prepared glass samples where α , h and ν are the absorption coefficient, Planck constant and frequency, respectively. (Ravangvong et al., 2020; Shoab et al., 2019; Sinha et al., 1996)

The optical band gap (E_g) of glass was calculated by following the equation;

$$\alpha h\nu = B (h\nu - E_g)^{1/2}$$

The optical band gaps of glasses were found at 2.3620, 2.7284, 2.8955, 3.0211, and 3.0559 eV for 0, 2.5, 5.0, 7.5, and 10 mol% concentrations of gadolinium, respectively as listed in Table 4.2. From Figure 4.9, it can be seen that for glasses doped with 0 to 10 mol% the absorption edge shifts slightly towards longer wavelengths. The optical bandgap for the highest Gd_2O_3 content occurs at the highest 3.0559 eV in 10 mol% of Gd_2O_3 . By increasing the Gd_2O_3 content in the glass matrix are shown in the optical band gap energy increases.

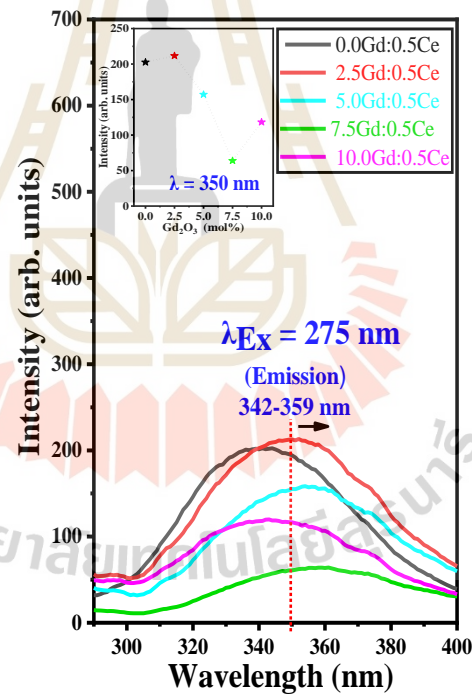
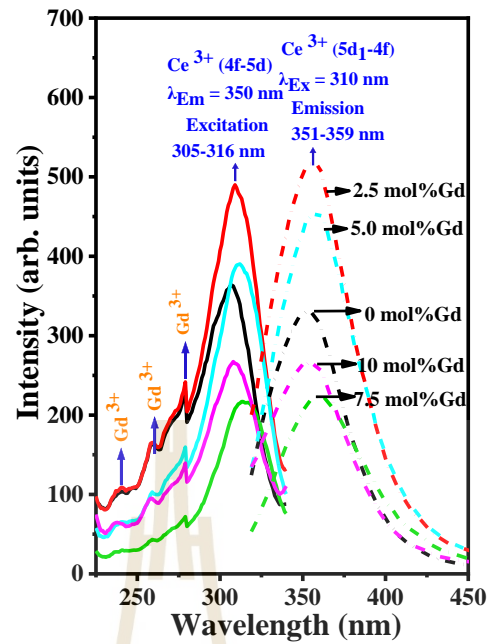


Figure 4.10. excitation and emission spectra of glass samples with different Gd_2O_3 concentrations prepared in the atmosphere.

The luminescence spectra under Ce^{3+} show the peak emission wavelength around 350 nm. The excitation spectrum of Ce^{3+} ion consists of asymmetric broadband with a maximum at 312 nm in the 2.5 mol% (high intensity) doped with Gd_2O_3

are influenced by concentration quenching appear. The excitation peaks of the Gd^{3+} were observed at 254 nm, 275 nm, and 312 nm that represent the major emission peak of Gd^{3+} at 312 nm, corresponding to the transition from Gd^{3+} (Figure 4.10(a)) respect. The excitation of the 4f state of the Gd^{3+} at $\lambda_{exc} = 275$ nm, an indicative of the effective energy transfer (ET) can be attributed to the sharp 4f-4f transition of the Gd^{3+} in the UV region and overlapping with the broad 4f-5d transition state of the Ce^{3+} . Therefore, the energy transfer from Gd^{3+} to Ce^{3+} was studied by 275 nm excitation illustrated in Figure 4.10(b). As the highest luminescence intensity was observed from the sample series LACB glass prepared at 2.5 mol% of Gd_2O_3 , providing the best condition with high energy transfer between the Gd^{3+} to Ce^{3+} ions. Moreover, the energy levels diagrams of Gd^{3+} and Ce^{3+} ions and their relative transition are described in Figure 4.5(c). Since Gd^{3+} ion is stimulated by 275 nm of UV radiation, the original upper energy level population relaxes to its lower energy levels before it exceeds the ${}^6P_{7/2}$ level by phonon help and 310 nm of characteristic Gd^{3+} ion emission occurs are shown in Figure 4.5(c).

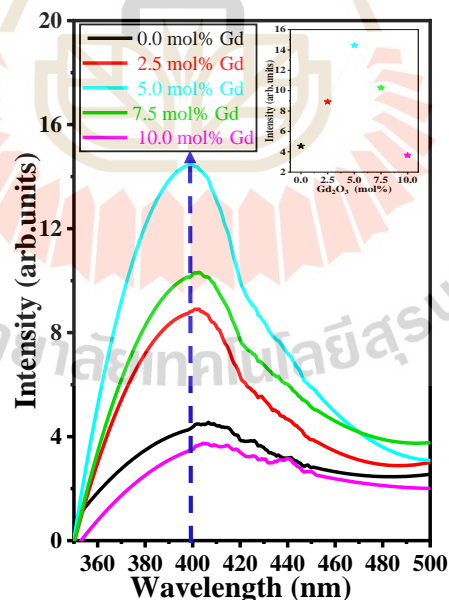


Figure 4.11 X-ray induced scintillation spectra of LACB series glasses by fixed 0.5 mol% CeF_3 concentrations with increasing of Gd_2O_3 concentration doped glass are show a dark (0 mol%), red (2.5 mol%), sky blue (5.0 mol%), green (7.5 mol%), and pink (10.0 mol%).

In Figure 4.11, the x-ray excited emission spectra of 0.5 mol% Ce^{3+} as a function of Gd_2O_3 content are given. We have developed a concept of transfer efficiency has increased: the optimum concentration Gd^{3+} ions allowed efficient migration of energy into these glass matrices following by a single-step energy transfer towards emission centers created by the Ce^{3+} . The glass samples have the similar shape and the measurements have been made under identical settings. The emission band center, approximately 398 nm ($4f \rightarrow 5d$ transitions of Ce^{3+}), was observed. For the 0.5 mol% Ce concentration that provides a large the maximum radioluminescence intensity was achieved with Gd^{3+} concentration at 5.0 mol% after that the intensity decreased, causing the concentration quenching effect. Which is not the same concentration of Gd_2O_3 in the photoluminescence spectra (Figure 4.10). Therefore, the optimal concentrations of Gd_2O_3 for the PL and RL are different as 2.5 mol% and 5.0 mol%, respectively. It can be clarified that the host material and activator ion have various interaction mechanisms with excitation by UV and X-ray. On the way, the UV source will specifically activate the electrons of the trivalent lanthanide ions, while the X-rays excite electrons of both the trivalent lanthanide ions and the host in glass systems. X-ray excitation (creates electrons and holes) in host glass results to electron hole pairs, then recombination process will be happened and transfer energy to activator ions for light emission.

To confirm the oxidation state change of Ce ions in $25\text{Li}_2\text{O}-5\text{Al}_2\text{O}_3-\text{XGd}_2\text{O}_3-(69.5-\text{X})\text{B}_2\text{O}_3-0.5\text{CeF}_3$, we measured Ce L_{III} -edge X-ray absorption near-edge structure (XANES) spectra of CeF_3 and Ce_2O_3 as standard curves show in Figure 4.12(a). It is obvious that the CeF_3 had only one sharp peak at 5723 eV. The reference sample Ce_2O_3 had two peaks of the maximal points at 5729.5 and 5739.5 eV. It can be found that the valence state and corresponding ratios of Ce (3+ or 4+) ions in obtained LACB glasses could be estimated by comparing its XANES spectrum (calculated with Athena software). All the glass samples exhibited only peak with different Gd_2O_3 concentrations which demonstrated that Ce ions in the sample glass have two valence states, trivalent (Ce^{3+}) and tetravalent (Ce^{4+}), respectively. The calculated results are shown in Figure 4.12(b).

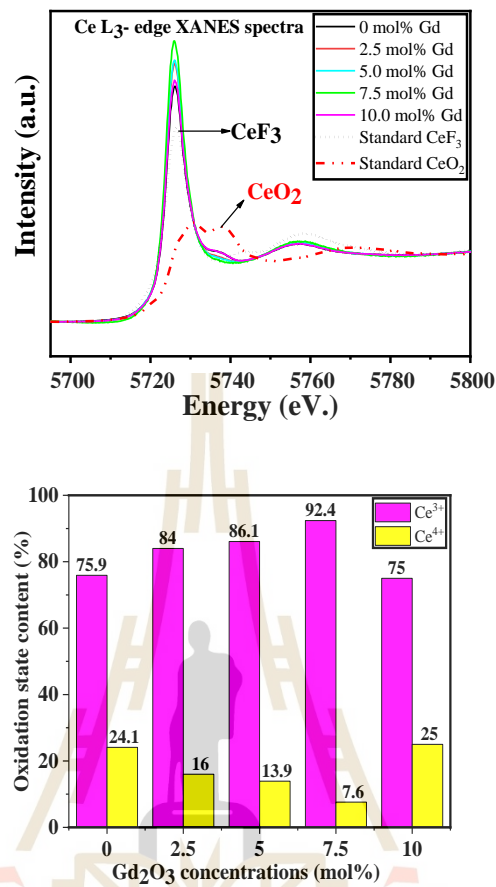


Figure 4.12 Cerium L_{III} XANES spectra of 0.5Ce: LAXGB glasses along with fitting curves constructed by combination of XANES analysis using CeF₃ and CeO₂ standard.

It can be seen that the relative content of Ce³⁺ ions in glasses increases with the increase of Gd₂O₃ doping concentration, and the highest relative content of Ce³⁺ is about 92.4% for the 7.5 mol% Gd₂O₃ in LACB glass sample. It is proved that only Ce³⁺ could luminescence efficiently, while Ce⁴⁺ shows no luminescence due to resonant energy transfer and metal-metal charge transfer along with self-absorption from far UV to 500 nm visible regions. It can be noticed that the photoluminescence intensity of LACB sample raises with the increase of Gd₂O₃ doping concentration, reaching the peak value at doping with 2.5 mol% Gd₂O₃, but decreases with the further increase of Gd₂O₃ doping concentrations. With the increase of Gd₂O₃ doping concentration in the LACB glasses sample, trivalent Ce³⁺ ions incorporated into the

LACB glasses lattice became saturated and exceeded the limitation, suggesting that concentration quenching effect.

Figure 4.13 represents the nano-second decay time spectra of LACB series glasses. Details of the decay constants for different Gd_2O_3 -concentration in LACB glasses are given in Table 4.3. Decay time spectra were fitted with three exponential functions using the below equation:

$$I(t) = B_1 \cdot \exp(-t/T_1) + B_2 \cdot \exp(-t/T_2) + B_3 \cdot \exp(-t/T_3)$$

Where $I(t)$ is the emission intensity as a function of time t , B_1 , B_2 , and B_3 are constant, T_1 , T_2 , and T_3 are the short and long-time decay constants.

The decay time of glass was observed using 286 nm excitation with 2 ns of pulse rate. Fixed 0.5 mol% cerium concentrations with increasing of Gd_2O_3 amount doped glass are presented in Figure 4.13. All data corresponding to behavior was conducted for the three exponential components. It is well fitted by an exponential decay equation, as shown in Table 4. 3. In particular, the decay time value decreases from 17.45 to 15.20 ns with increasing Gd_2O_3 concentration from 0 to 10.0 mol% in the glass samples.

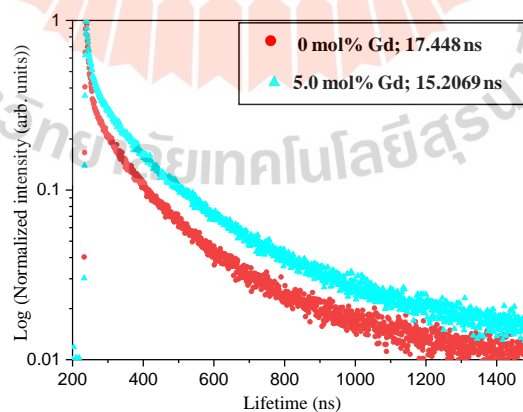


Figure 4.13 The typical luminescence decay curve under 286 nm excitation of LACB glasses doped with 0 and 5.0 mol% of Gd_2O_3 .

Moreover, Table 4.3 clearly shows that maximum light is emitted with fast decay constant (almost 100%) for all samples therefore, it is concluded that direct electron-hole capture by Ce^{3+} ions is a dominant energy transfer mechanism in this glass.

Table 4.3 Decay time comparison of LACB glasses with variation of Gd_2O_3 .

Sample name	$T_1(ns)$	$T_2(ns)$	$T_3(ns)$
0 mol% Gd	17.44±1.07 (55.44%)	94.42±5.83 (37.0%)	3.56±0.28 (7.55%)
2.5 mol% Gd	16.59±1.37 (61.71%)	101.70±6.84 (30.64%)	4.96±0.27 (10.77%)
5.0 mol% Gd	15.20±1.35 (58.6%)	85.28±5.25 (30.64%)	4.96±0.27 (10.77%)
7.5 mol% Gd	15.70±0.56 (57.73%)	1.18±0.10 (5.83%)	5.21±1.99 (36.43%)
10.0 mol% Gd	16.03±1.07 (57.44%)	101.10±5.84 (35.55%)	4.56±0.27 (7.00%)

4.4 Reference

- Bahadur, A., Dwivedi, Y., and Rai, S. B. (2013). Optical properties of cerium doped oxyfluoroborate glass. *Spectrochimica Acta Part A: Molecular and Biomolecular Spectroscopy*, 110, 400:403.
- Balachandera, L., Ramadevudub, G., Shareefuddina, M., Sayannac, R., and Venudharc, Y. (2013). IR analysis of borate glasses containing three alkali oxides. *Science Asia*, 39, 278.
- Bollinger, L. M., Thomas, G. E., and Ginther, R. J. (1962). Neutron detection with glass scintillators.

- Furukawa, T. and White, W. B. (1980). Raman spectroscopic investigation of the structure and crystallization of binary alkali germanate glasses. *J. Mater.Sci*, 15, 1648.
- Gautam, C., Yadav, A. K., and Singh, A. K. (2012). A review on infrared spectroscopy of borate glasses with effects of different additives. *ISRN Ceram 2012*, 1–17.
- Kaewnuam, E., Wantana, N., Kaewkhao, J, and Kim, H. J. (2019). X-ray Induced Luminescence and Physical Properties of Lithium Lanthanum Borate Glass Doped with Ce^{3+} for Radiation Detection Material. *Materials Today: Proceedings*, 17, 1787:1793.
- Khan, I., Rooh, G., Rajaramakrishna, R., Sirsittipokakun, N., Kim, H. J., Wongdeeying, C., and Kaewkhao, J. (2018). Development of Eu^{3+} doped Li_2O - BaO - GdF_3 - SiO_2 oxyfluoride glass for efficient energy transfer from Gd^{3+} to Eu^{3+} in red emission solid state device application. *Journal of Luminescence*, 203, 515:524.
- Khanna, A. , Saini, A. , Chen, B. , Gonzalez, F., and Ortiz, B. (2014). Structural characterization of PbO - B_2O_3 - SiO_2 glasses. *European Journal of Glass Science and Technology Part B*, 55, 65:73.
- Konijnendijk, W. L. and Stevals, J. M. (1975). Structure of borate and borosilicate glasses by Raman spectroscopy. *Journal of Non-Crystalline Solids*, 18, 307.
- Konijnendijk, W. L. and Verweij, H. (1976). Structural aspects of vitreous PbO - B_2O_3 studied by Raman scattering. *Journal of the American Ceramic Society*, 59, 459:461.
- Nikl, M., Nitsch, K., Mihokovan, N., Solovieva E., Mares, J. A., Fabeni, P., Pazzi, G. P., Martini, M. A., Vedda, A., and Baccaro, S.(2000). Efficient radioluminescence of the Ce^{3+} - doped Na- Gd phosphate glasses. *Applied Physics Letters*, 77, 2159:2161.
- Ogieglo, J. M., Katelnikovas, A., Zych, A., Justel, T., Meijerink, A., and Ronda, C. R. (2013). Luminescence and Luminescence Quenching in $Gd_3(Ga,Al)_5O_{12}$ Scintillators Doped with Ce^{3+} . *Journal of Applied Physics*, 117, 2479:2484.

- Park, J., Kim, H., Kim, S., Limsuwan, P., and Kaewkhao, J. (2012). Luminescence property of rare-earth doped bismuth borate glasses. *Procedia Engineering*, 32, 855:861.
- Park, J. M, Ha, D. H., Kaewjeang, S., Maghanemi, U., Kothan, S., Kaewkhao, J., and Kim, H. J. (2016). Luminescence properties of Ce³⁺ doped gadolinium-calcium-silicaborate glass scintillator. *Radiation Measurements*, 90, 166:169.
- Pascuta, P., Borodi, G., and Culea, E. (2008). Influence of europium ions on structure and crystallization properties of bismuth borate glasses and glass ceramics. *Journal of Non-Crystalline Solids*, 354, 5475:5479.
- Ravangvong, S., Chanthima, N., Rajaramakrishna, R., Kim, H. J., Sangwaranatee, N., and Kaewkhao, J. (2019). Dy³⁺ ions doped (Na₂O/NaF)-Gd₂O₃-P₂O₅ glasses for solid state lighting material applications. *Solid State Science*, 97, 105972.
- Ravangvong, S., Chanthima, N., Rajaramakrishna, R., Kim, H. J., and Kaewkhao, J. (2020). Effect of sodium oxide and sodium fluoride in gadolinium phosphate glasses doped with Eu₂O₃ content. *Journal of Luminescence*, 219, 116950.
- Shoaib, M., Rooh, G., Chanthima, N., Rajaramakrishna, R., Kim, H. J., Wongdeeying, C., and Kaewkhao, J. (2019). Intriguing energy transfer mechanism in oxide and oxy-fluoride phosphate glasses. *Optical Materials*, 88, 429:444.
- Shoaib, M., Rooh, G., Rajaramakrishna, R., Chanthima, N., Kiwsakunkran, N., Kim, H. J., Kaewkhao, J., and Tuscharoen, S. (2019). Comparative study of Sm³⁺ ions doped phosphate-based oxide and oxy-fluoride glasses for solid state lighting applications. *Journal of Rare Earths*, 37, 374:382.
- Silim, H. A. (2006). Composition effect on some physical properties and FTIR spectra of alumina borate glasses containing lithium, sodium potassium and barium oxides. *Egyptian Journal of Solids*, 29, 293.
- Sinha, S. P. (1966). Complexes of the rare earths. *Complexes Rare Earths*, 17:23.
- Spector, G. B., Mccollum, T., and Spowart, A. R. (1993). Advances in terbium-doped, lithium loaded scintillator glass development. *Nuclear Instruments and Methods in Physics Research*, 326, 526:530.

- Sun, X. Y., Yang, Q. M., and Gao, P. (2015). Luminescence, energy transfer properties of Tb³⁺/ Gd³⁺-coactivated oxyfluoride borogermanate scintillating glasses. *Journal of luminescence*, 165, 4045.
- Wantana, N., Kaewnuam, E., Chanthima, N., Kaewjaeng, S., Kim, H. J., and Kaewkhao, J. (2018). Ce³⁺ doped glass for radiation detection material. *Ceramics International*, 44, S172-S176.
- Yoshimura, E. M., Santos, C. N., Ibanez, A., and Hernande, A. (2009). Thermoluminescent and optical absorption properties of neodymium doped yttrium aluminoborate and yttrium calcium borate glasses. *Optical Materials*, 31, 795:799.
- Zaman, F., Rooh, G., Srisittipokakun, N., Kim, H. J., Kaewnuam, E., Meejitpaisan, P., and Kaewkhao, J. (2017). Scintillation and luminescence characteristics of Ce³⁺ doped in Li₂O-Gd₂O₃-BaO-B₂O₃ scintillating glasses. *Radiation Physics and Chemistry*, 130, 158-163.
- Zhang, Y., Chen, B., Xu, S., Li, X., Zhang, J., Sun, J., Zhang, X., Xia, H., and Hua, R. (2018). A universal approach for calculating the Judd-Ofelt parameters of RE³⁺ in powdered phosphors and its application for the β-NaYF₄:Er³⁺/Yb³⁺ phosphor derived from auto-combustion-assisted fluoridation. *Physical Chemistry Chemical Physics*, 20, 15876:15883.

CHAPTER V

SAMARIUM DOPED BORATE GLASS

The standard melt-quenching technique was used to create a novel series of Gd^{3+} and Sm^{3+} co-doped borate glasses with the LAGdxBSm1.0 and LAGd2.5BSmx series of glasses. All samples were analyzed by XRD, FTIR, and optical screening to determine their characteristics (absorption, excitation, and emission). The results confirmed the amorphous nature of the synthesized glass samples, while the FTIR revealed the existence of BO_3 and BO_4 vibrations in the samples. The series glass quality of LAGdxBSm1.0 doped in the host matrix was confirmed by the radioluminescence and photoluminescence results at the optimal doping concentration of 2.5 mol%. The decay times and energy transfer parameters for energy levels of Sm^{3+} to Sm^{3+} ions in borate glass were investigated to determine the relationship between doping concentration and luminescence characteristics. Glasses have been created into an appropriate lighting glass using $25Li_2O-5Al_2O_3-2.5Gd_2O_3-(67.5-X)B_2O_3-XSm_2O_3$ host matrix glass doped with varying concentrations of Sm^{3+} . Visible light and near-infrared absorption values in the glass samples demonstrate the existence of Sm^{3+} ions. The photoluminescence and radioluminescence spectra have high concentration quenching (0.5 mol%) and produce four emission peak wavelengths, with the maximum emission wavelength at 600 nm (soft orange color). Based on these results, the studied glass series could be a good choice for X-ray scintillators in medical, industrial, and other settings in the future.

5.1 Introduction

In the recent past, scientists have tried to prepare phosphor materials doped with multi-rare-earth glass matrix, together with developing host materials for useful optical devices such as fiber amplifiers, waveguide lasers, bulk lasers, infrared to visible

upconversion lasers, and phosphors. Several oxide components, such as SiO_2 (Mohan et al., 2013), GeO_2 (Gunji et al., 2020; Khalid et al., 2020), TeO_2 (Stambouli et al., 2013), P_2O_5 (Kaura et al., 2019; Shoaib et al., 2013), have been successfully used in glass production. As a glass-former, borate seems to be the best host material (Kirdsiri et al., 2019; Wantana et al., 2017). Rare-earth-doped borate glass is one of the best host materials for trivalent rare-earth ions because it is inexpensive, has good thermal stability, high phonon energy of $1200\text{--}1500\text{ cm}^{-1}$, low temperature for synthesis, radiation hardness, and interesting optical properties like high transparency from the visible to the near-infrared spectral region (Karthikeyan et al., 2005, ElBatal et al., 2007; Gedam et al., 2013; Ramteke and Gedam et al., 2014). Furthermore, borate-based glasses joined with other modifier oxides such as Li_2O and Al_2O_3 in a glass system are well known to increase several attributes such as durability, good mechanical ability, and glass-forming ability. Recent studies indicate that the properties of systems based on Gd_2O_3 (Onderisnova et al., 2015) containing rare-earth ions are significant in the field of luminescent materials because they can improve the energy transfer mechanism from sensitizer (Gd^{3+} ions) to luminescence activator, which not only enhances activator ion photoluminescence but also boosts the light yield of emission in the host.

Recently, many researchers have studied the energy transfer mechanism from Gd^{3+} to trivalent rare-earth such as Tb^{3+} (Kesavulu et al., 2017), Ce^{3+} (Rittisut et al., 2021), Dy^{3+} (Ullah et al., 2020), and Eu^{3+} (Khan et al., 2018) in some proper single host lattice for UV-based lighting applications. As a result, the rapid growth of essential luminescent materials, indicated by amorphous glass doped with multi-rare-earth (MRE) ions, has come to dominate several fields of glass research. Rare-earth -doped glass materials require a comprehensive view of luminescence characteristics like lifetimes, quantum yields, and energy transfer efficiencies. These appear extremely sensitive to their immediate surroundings and the distribution of the doped ions in the glass matrix, which substantially impacts its chemical composition. Hence, the rare-earth ion (REI) luminescence characteristics are being studied in different glass matrices to understand REI and ligand interactions to build optical devices with enhanced

performance. This luminescence will be caused by the shielding effects of their outer 5s and 5p orbitals on 4f-4f transitions (Moorthy et al., 2014). Therefore, rare-earth ion-doped glasses have received particular attention. Because of this, there are significant peaks in the absorption and emission spectra in the visible region. The manufacturing and optical study of samarium doped glasses have received little attention, therefore the trivalent samarium ion (Sm^{3+}) was selected for this study because of its luminescent characteristics in the visible region (Wantana et al., 2020; Kaewnuam et al., 2017; Zaman et al., 2016). Maximum emission peaks in the 550-700 nm region are appropriate for employing Sm^{3+} ion as a dopant for orange emission. The prominent peaks in the luminescence spectra of samarium combinations are transitions from the $^4\text{G}_{5/2}$ excited state to $^6\text{H}_J$ ($J = 5/2, 7/2, 9/2,$ and $11/2$) levels that make the glasses display reddish-orange light. The addition of co-doping with two rare-earth ions was used for efficient energy transfer between components (if their energy levels are close enough to be implicated in a transfer). Many systems have been investigated in order to assess energy transfer between two RE co-doped glasses. This is important not only for applications of sensitized luminescence but also for understanding how it works.

The objective of this work is to investigate the optical characteristics of Gd_2O_3 doped borate glasses in $25\text{Li}_2\text{O}-5\text{Al}_2\text{O}_3-\text{XGd}_2\text{O}_3-(69-\text{X})\text{B}_2\text{O}_3-1.0\text{Sm}_2\text{O}_3$ with different X concentrations of 0, 2.5, 5.0, 7.5, and 10.0 mol%. The optimal Gd_2O_3 concentration in the glass series was approximately 2.5 mol%, which gave a higher luminescence intensity than the other doping concentrations. This optimal concentration of Gd_2O_3 was then used as the host glass matrix of the borate for further study. To find the best proportion combination of dopant ions in a luminescence glass. We produced and studied lithium aluminum gadolinium borate glasses doped with varying concentrations of Sm_2O_3 in $25\text{Li}_2\text{O}-5\text{Al}_2\text{O}_3-2.5\text{Gd}_2\text{O}_3-(67.5-\text{X})\text{B}_2\text{O}_3-\text{XSm}_2\text{O}_3$, where $X = 0, 0.05, 0.1, 0.3, 0.5,$ and 1.0 mol%. This study investigated the physical, structural, luminescence, and scintillation properties of glass systems using optical spectrometer, X-ray absorption near-edge structure (XANES), and X-ray luminescence system to better understand the impact of dual-doping the host glass matrix with two lanthanide trioxide.

5.2 Experiment

The melt quenching method produced lithium aluminum borate glass samples doped with Gd^{3+} and Sm^{3+} ions. Standard chemicals from Sigma-Aldrich with the highest purity of Li_2CO_3 , H_3BO_3 , Gd_2O_3 , Al_2O_3 , and Sm_2O_3 were used as starting ingredients.

5.2.1 Doped with Gd_2O_3 concentration

First, a series of $25Li_2O-5Al_2O_3-XGd_2O_3-(69-X)B_2O_3-1.0Sm_2O_3$ glasses with different amounts of $X = 0, 2.5, 5.0, 7.5,$ and 10.0 mol% were made and called the LAGdxBSm1.0 glasses series.

5.2.2 Doped with Sm_2O_3 concentration

The optimal concentration of Gd_2O_3 (2.5 mol%) glass matrices were then doped with various amounts of Sm_2O_3 to produce a series of glass samples with a chemical composition as $25Li_2O-5Al_2O_3-2.5Gd_2O_3-(67.5-X)B_2O_3-XSm_2O_3$. These samples were labeled as LAGd2.5BSm0, LAGd2.5BSm 0.05, LAGd2.5BSm0.1, LAGd2.5BSm0.3, LAGd2.5BSm0.5, LAGd2.5BSm1.0, and LAGd2.5BSm1.5.

Figure 5.1 shows the standard melt quenching method used to produce all compounds. Alumina crucibles were used to grind each batch of recipes to a fine powder. Alumina crucible possesses a high melting point, strong hardness, and good chemical stability, making it a good material to withstand high temperatures and chemical corrosion. Electrically heated, the powder was melted. The melted compounds were then heated to about $1200\text{ }^\circ\text{C}$ and kept at that temperature for 90 minutes. Figure 5.2(a, b) shows transparent glass samples of uniform thickness. Each sample was obtained by pouring the melting glass on a graphite plate, then annealing at $500\text{ }^\circ\text{C}$ for 3 hours to relieve thermal stress before cooling it down slowly to room temperature. The samples were cut and then polished on a polishing machine until they were approximately $1.0 \times 1.5 \times 0.3\text{ cm}^3$. The samples were then characterized to determine their optical properties.

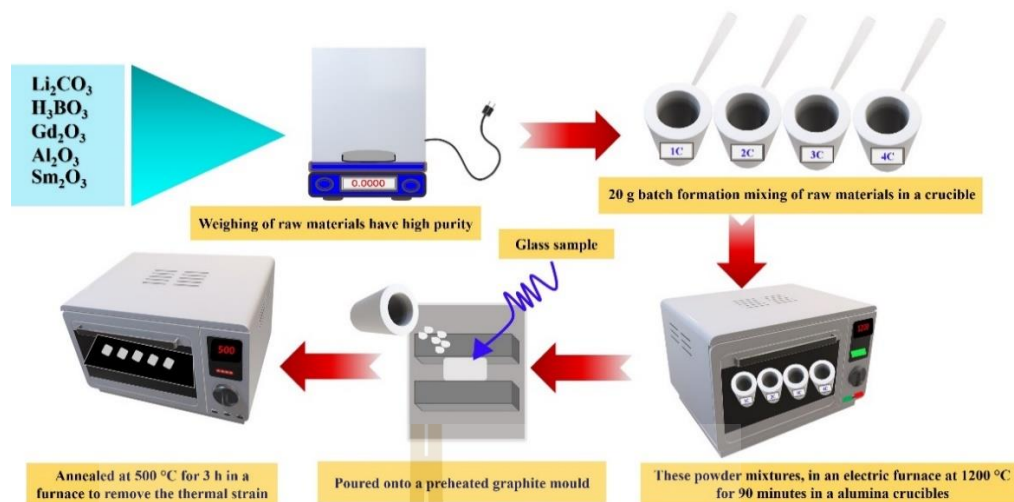


Figure 5.1 Schematic illustration of the melt quenching technique along with a photograph of the prepared glasses.

5.2.3 Measurements

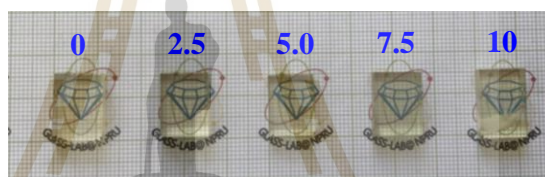
The density of the glass samples was initially determined by the basic Archimedes technique using water as an immersion liquid, and the molar volumes were then measured using a 4-digit sensitive microbalance (AND, HR 200). The molar volume (V_M) of the glasses was calculated using the $V_M = Mw/D$ relationship, where Mw and D are the overall molecular weight of the glass composition and the density of the glass samples, respectively. The PXRD (Bruker D2 diffractometer with Cu-K radiation) analysis was performed in order to confirm that the glass samples were completely amorphous and transparent. The UV-vis and NIR (Shimadzu UV-3600) spectrophotometers are used to analyze the optical absorption spectra (wavenumber range 200–2500 nm). A Xenon flash lamp was used to record the excitation, emission spectra, and decay data at room temperature by a spectrofluorophotometer (Cary-Eclipse). The measurements were carried out by an experimental setup consisting of a Cu target x-ray generator (Inel, XRG3D-E), fiber optic spectrum analyzer (Ocean Optics QE65 Pro), and a brass sample holder. The X-ray-induced optical luminescence spectra of the glasses were studied using an Ocean Optics QE65 Pro spectrometer and a Cu target X-ray generator, Inel XRG3D-E, which was operated at 50 kV and 30 mA power. All measurements were carried out at room temperature. The X-ray absorption near-edge structure (XANES) method was used to determine the oxidation state of the glass

samples. The experimental XANES data collected in fluorescence mode were compared with those of bent Ge (220) crystals at the Sm LIII-edge using a crystal analyzer spectrometer.

5.3 Result and discussion

The present glass series of LAGdxBSm1.0 and LAGd2.5BSmx are doped gently with Gd^{3+} and Sm^{3+} . Both glasses exhibit a soft yellow color, free of bubbles, homogeneous, and high transparency, as seen in Figure 5.2(a, b). It can be seen in these photographs that the color of the glass sample changes from colorless to bright yellow when Gd_2O_3 and Sm_2O_3 are added to the mixture.

(a) LAGdxBSm1.0 : $25Li_2O \cdot 5.0Al_2O_3 \cdot XGd_2O_3 \cdot (69-X)B_2O_3 \cdot 1.0Sm_2O_3$



(b) LAGd2.5BSmx : $25Li_2O \cdot 5.0Al_2O_3 \cdot 2.5Gd_2O_3 \cdot (67.5-X)B_2O_3 \cdot XSm_2O_3$

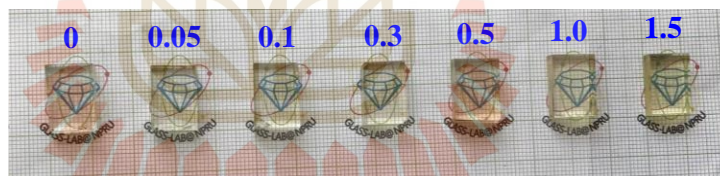


Figure 5.2 Images of glasses in the (a) LAGdxBSm1.0 and (b) LAGd2.5BSmx series.

Figure 5.3(a, b) shows the dependence of Gd^{3+} and Sm^{3+} ions concentration on density, refractive index, and molar volume of the LAGdxBSm1.0 and LAGd2.5BSmx glass series. Glass density is commonly described in terms of competition between the masses and volumes of the various compound structures. It is clearly shown that all density, refractive index, and molar volume tend to increase with the increase of Gd_2O_3 and Sm_2O_3 content in the LAGdxBSm1.0 and LAGd2.5BSmx glass series. Figure 5.3(a) shows that increasing the Gd_2O_3 content up to 7.5 mol% increased the density and refractive index from 2.313 g/cm^3 to 2.788 g/cm^3 and 1.535 to 1.570, respectively. However, milky white phenomena were observed at a high Gd_2O_3 concentration of 10

mol%, resulting in an opaque glass. Similar results were observed for Sm_2O_3 dopant from 0 to 1.5 mol%, as shown in Figure 5.3(b). However, increasing density (1.010 g/cm^3 to 2.412 g/cm^3), and molar volume (27.603 to $28.390 \text{ cm}^3/\text{mol}$) were observed for Sm_2O_3 dopant. The density increment is attributed to the fact that Gd_2O_3 ($M_w = 362.4982 \text{ g/mol}$) and Sm_2O_3 ($M_w = 348.7182 \text{ g/mol}$) have higher molecular mass than B_2O_3 ($M_w = 69.6202 \text{ g/mol}$). In addition, the density and molar volume of glass samples increase linearly with the increasing concentration of Gd_2O_3 and Sm_2O_3 , indicating an increase in the rigidity of the glass network. In the case of glass, the increase in density is attributable to an increase in the number of bridging oxygen molecules present in the glass. Furthermore, an increase in molar volume leads to an increase in bond length, or the inter-atomic distance between atoms in the molecule.

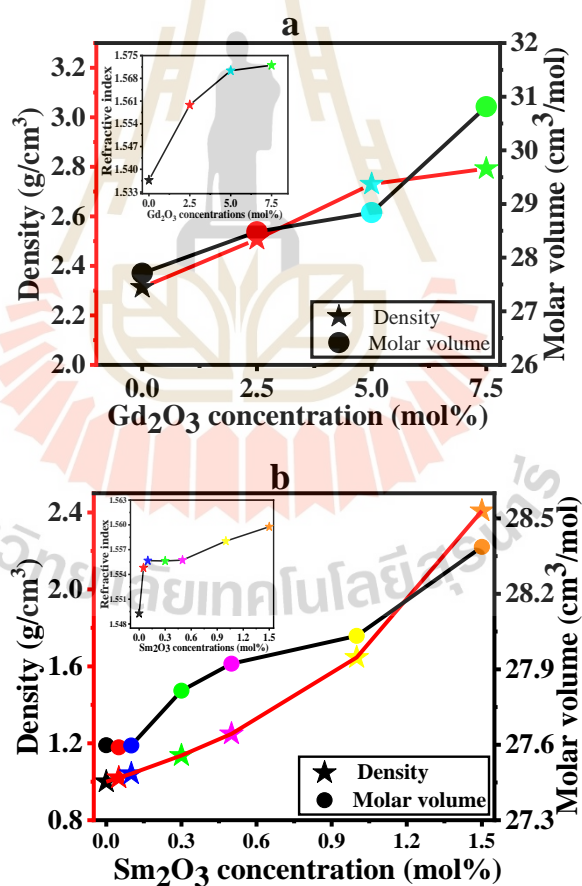


Figure 5.3(a, b) The variation of density (g/cm^3), refractive index, and molar volume parameters as a function of Gd_2O_3 and Sm_2O_3 concentration in the LAGdxBSm1.0 and LAGd2.5BSmx series.

The X-ray diffraction spectra of the studied glasses in the range of $2\theta = 10\text{--}80^\circ$ are depicted in Figure 5.4(a, b). The amorphous character of glass samples is confirmed by the fact that the spectra contain only humps and no strong crystallization peak, indicating the amorphous nature of all the glass samples.

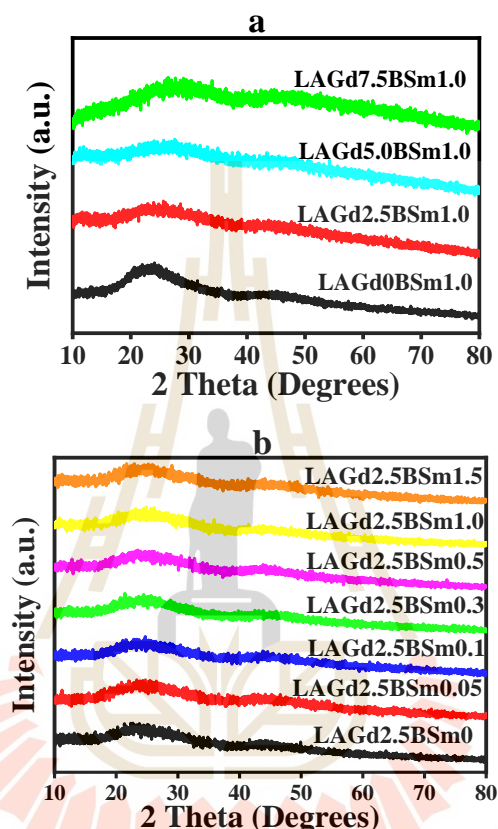


Figure 5.4 XRD pattern of (a) LAGd x BSm1.0 and (b) LAGd2.5BSm x glass series with different amounts of Gd₂O₃ and Sm₂O₃ added (in mol%).

Figure 5.5 shows the FTIR spectrum of all glasses with different Gd₂O₃ concentrations in the mid-infrared (MIR) spectrum range (500–4000 cm⁻¹). It is noted that the LAGd x BSm1.0 base glasses show several peaks at 455, 698, 939, 1272, and 1358 cm⁻¹. The first vibration part, infrared absorbed with a wavenumber of 455 cm⁻¹, was used to bend the vibration of Li⁺ ions with a glass network (Pawar et al., 2016). The bond at 698 cm⁻¹ is caused by the B-O-B linkage of the trigonal BO₃ in the borate group. In the central at 939 cm⁻¹ is due to the units of BO₄. As the amount of Gd₂O₃ in the glass is increased, the intensity of this band increases, peaking at 2.5 mol%. After

that, the intensity declines. For 2.5 mol% Gd_2O_3 doped glasses, the increase in the intensity of this band implies an increase in BO_4 groups, which represents the largest number of BO_4 groups in the samples (Dalal et al., 2015). In the region $1200\text{--}1600\text{ cm}^{-1}$ (central at 1272 (Kaur et al., 2014) and 1358 cm^{-1} (Thakur et al., 2015)), the array of bands is due to the B–O bond expanding relaxation of the trigonal BO_3 units. The smaller bands with a wavenumber higher than 2200 cm^{-1} are attributed to OH-bonds and water molecules.

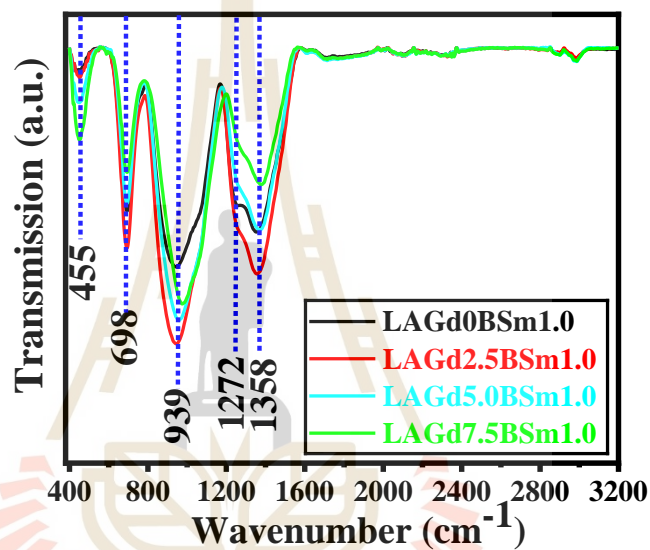


Figure 5.5 FTIR spectra with different concentrations of Gd_2O_3 doped glass samples.

Figure 5.6(a) illustrates the photoluminescence excitation spectra of LAGdxBSm1.0 glasses containing Gd_2O_3 concentrations of 0 to 7.5 mol% glassy matrix. The emission wavelength was obtained at 600 nm by measuring the emission wavelength with the highest intensity. Thirteen excitation bands peaking at 275 nm ($^8S_{7/2}\text{--}^6I_{9/2}$), 311 nm ($^8S_{7/2}\text{--}^6P_{7/2}$), 345 nm ($^6H_{5/2}\text{--}^4D_{7/2}$), 361 nm ($^6H_{5/2}\text{--}^4D_{3/2}$), 375 nm ($^6H_{5/2}\text{--}^6P_{7/2}$), 403 nm ($^6H_{5/2}\text{--}^6P_{3/2}$), 415 nm ($^6H_{5/2}\text{--}^6P_{5/2}$), 439 nm ($^6H_{5/2}\text{--}^4G_{9/2}$), 462 nm ($^6H_{5/2}\text{--}^4I_{13/2}$), 475 nm ($^6H_{5/2}\text{--}^4M_{15/2}$), 500 nm ($^6H_{5/2}\text{--}^4G_{7/2}$), 526 nm ($^6H_{5/2}\text{--}^4F_{3/2}$) and 562 nm ($^6H_{5/2}\text{--}^4G_{5/2}$) (Wantana et al., 2020; Zaman et al., 2016) were observed. The broad and strong excitation peak occur because of the CTB from $Sm^{3+}\text{--}O^{2-}$ and the narrow peak at 275 nm is expected to be a signature of the Gd^{3+} ion luminescence excitation spectrum (Gupta et al., 2015). Furthermore, two strong bands were identified, matching to the

275 nm ($^8S_{7/2}$ - $^6I_{9/2}$) and 311 nm ($^8S_{7/2}$ - $^6P_{7/2}$) transitions. The other peaks (eleven excitation peaks) are known for their characteristic excitation of Sm^{3+} . Since the excitation spectrum of the glasses shows the strongest peaks at 275 nm and 403 nm, these glasses were then excited by these wavelengths to investigate their emission spectra, as shown in Figure 5.6(b, c). The excitation wavelength at 275 nm was used to study the energy transfer from Gd^{3+} - Sm^{3+} luminescence. The emission spectra of the glass samples doped with Gd_2O_3 demonstrate five emission bands at 311 ($^6P_{7/2}$ - $^8S_{7/2}$), 562 ($^4G_{5/2}$ - $^6H_{5/2}$), 600 ($^4G_{5/2}$ - $^6H_{7/2}$), 648 ($^4G_{5/2}$ - $^6H_{9/2}$), and 705 ($^4G_{5/2}$ - $^6H_{11/2}$) nm. In addition, there is a second harmonic generation of UV-luminescence Gd^{3+} located at 622 nm (Wantana et al., 2017). Figure 5.6(b) indicates that when energy transfer from Gd^{3+} to Sm^{3+} occurs, the energy transitions from $^6P_{7/2}$ initial state to $^8S_{7/2}$ decline with the increase in Gd^{3+} fluorescence intensity at 311 nm. A clear indication that energy is being transferred. Figure 5.6(c) depicts the emission spectra of the LAGdxBSm1.0 glass series doped with Gd_2O_3 under an excitation wavelength of 403 nm (under direct excitation of Sm^{3+}). Four distinct emission spectra were detected at 563, 600, 646, and 705 nm, corresponding to the transitions from excited state $^4G_{5/2}$ - $^6H_{5/2}$ (yellow), $^4G_{5/2}$ - $^6H_{7/2}$ (orange), $^4G_{5/2}$ - $^6H_{9/2}$ (orange-reddish), and $^4G_{5/2}$ - $^6H_{11/2}$ (red) emission, respectively. The highest intensity peak represents 600 nm and is further used to study the photoluminescence properties of synthesized glasses. We can conclude that the highest intensity of emission spectra ($\lambda_{ex} = 275$ and 403 nm) belongs to 600 nm ($^4G_{5/2}$ - $^6H_{7/2}$: orange emission). The emission intensity increases with increasing Gd_2O_3 concentration up to 2.5 mol%, then the intensity slightly decreases. The concentration at 2.5 mol% is the optimal condition. Figure 5.6(d) shows the radioluminescence (RL) measurements of the LAGdxBSm1.0 glasses irradiated by X-rays from a power source of 50 kV and 30 mA. The LAGdxBSm1.0 glasses exhibit four bands at 561, 598, 644, and 704 nm, corresponding to $^4G_{5/2}$ - $^6H_{5/2}$, $^4G_{5/2}$ - $^6H_{7/2}$, $^4G_{5/2}$ - $^6H_{9/2}$, and $^4G_{5/2}$ - $^6H_{11/2}$ transitions, respectively. These four emission peaks of the radioluminescence spectra have locations and tendencies to intensity variations similar to photoluminescence. It can be seen that the LAGdxBSm1.0 glass series doped with 2.5 mol% of Gd_2O_3 has the strongest radioluminescence characteristic at 598 nm wavelength. The optimal Gd_2O_3 concentration in the $25Li_2O$ - $5Al_2O_3$ - XGd_2O_3 -($69-X$) B_2O_3 - $1.0Sm_2O_3$ host glasses is $X = 2.5$

mol%, which will be used to investigate the optimal Sm_2O_3 concentration in future experiments.

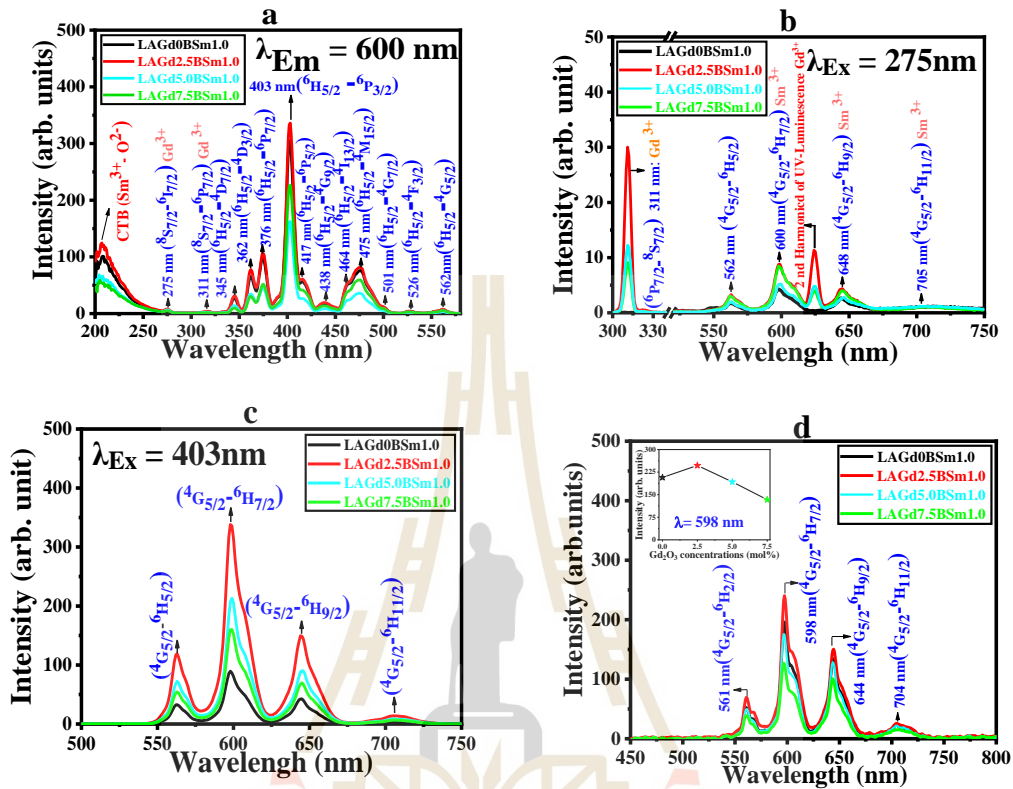


Figure 5.6 The (a) excitation (λ_{em} at 600 nm), (b,c) emission (λ_{ex} at 275 and 403 nm), and (d) the radioluminescence of LAGdxBSm1.0 glasses.

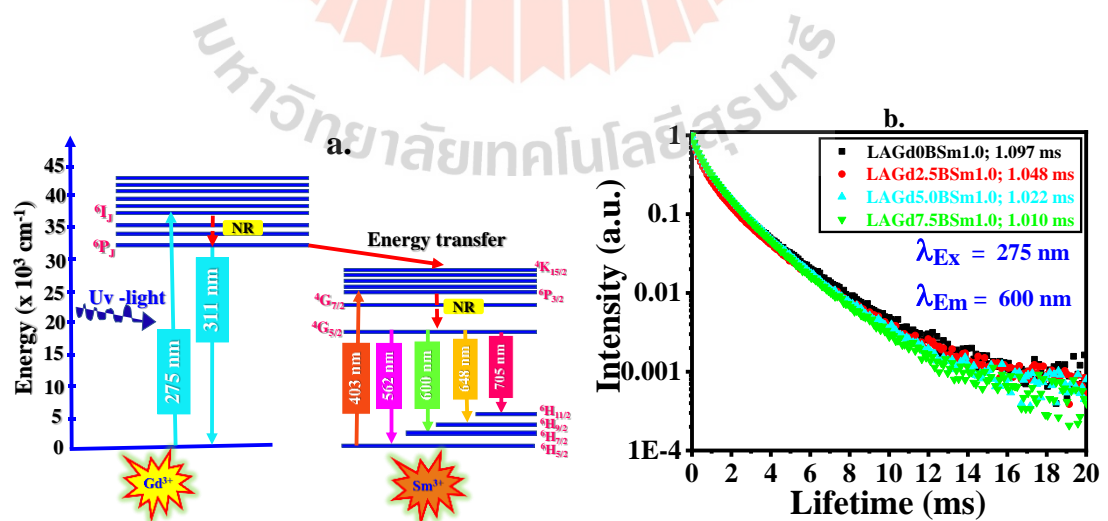


Figure 5.7 The partial energy level diagram (a) and PL decay curves of LAGdxBSm1.0 glasses for 600 nm emission with 275 nm excitation wavelength.

Figure 5.7(a) shows a modified energy level diagram with a potential energy transfer mechanism in Gd^{3+}/Sm^{3+} co-doped glasses, which assists in understanding the energy transfer process (Zaman et al., 2016). The ${}^6I_{7/2}$ level of the Gd^{3+} ion was initially populated upon 275 nm excitation; followed by non-radiative relaxation, the electrons should reach the ${}^6I_{7/2}$ state of Gd^{3+} , and the Gd^{3+} ions may return to the ground state in two ways. First, the Gd^{3+} ions in the ${}^6P_{7/2}$ state may transfer energy to the Sm^{3+} states through the resonance energy transfer mechanism. After then, the Sm^{3+} acceptor decreased its state by NR to obtain a luminescence level of ${}^4G_{5/2}$. Later, Sm^{3+} took the transition from ${}^4G_{5/2}$ level to ${}^6H_{5/2}$, ${}^6H_{7/2}$, ${}^6H_{9/2}$ and ${}^6H_{11/2}$ level by emitting the visible light with 562, 600, 648 and 705 nm, respectively. Second, the Gd^{3+} ions in the ${}^6P_{7/2}$ state may emit through the ${}^6P_{7/2}$ - ${}^8S_{7/2}$ (ground state) transitions. Moreover, the excitation with a wavelength of 403 nm, it lifted the Sm^{3+} from ground ${}^6H_{5/2}$ to ${}^6P_{3/2}$ state and Sm^{3+} lowered the state down to ${}^4G_{5/2}$ by NR. The Sm^{3+} ion emitted light with four wavelengths from the ${}^4G_{5/2}$ level, similarly to the emissions under 275 and 311 nm excitation. On excitation of the Sm^{3+} ions above the ${}^4G_{5/2}$ level, the electrons decay to the ${}^4G_{5/2}$ level by fast non-radiative relaxation. Cross-relaxation between lanthanide ions is possible if they have two energy levels with the same energy gap. It can be done by measuring the decay curves for different Gd^{3+} concentrations in borate glasses under 275 nm of illumination and monitoring the emission peak of 600 nm. As can be seen in Figure 5.7(b), the non-exponential function may be used to describe the decay profile of Gd_2O_3 doped LAGdxBSm1.0 glasses from the excited state. As a consequence, the glasses with the Gd_2O_3 doped have decay curves of 1.097, 1.048, 1.022, and 1.010 ms with the most prominent orange-red emission band (${}^4G_{5/2}$ - ${}^6H_{7/2}$ transition). Due to a non-radiative transition from energy transfer, their durations decrease as the Gd_2O_3 concentration increases. Under the excitation of Gd^{3+} , donor and acceptor are most likely, resulting in a non-exponential decay curve. Because the fluorescence decay curves are non-exponential, the Inokuti–Hirayama (IH) model (Inokuti et al., 1965) is used to reveal the dominant mode of interaction. These curves were fitted with the IH model using dipole-dipole interactions ($S = 6$). Figure 5.8 shows the lifetime and the energy transfer parameter (Q) as a function of Gd^{3+} concentration. The obtained Q value, representing the amount of Sm^{3+} - Sm^{3+} energy transferred, increases as

Gd^{3+} concentration increases. Fluorescence decay intensity (I) is determined by the following equation:

$$I(t) = I_0 \exp\left\{-\frac{t}{\tau_0} - Q\left(\frac{t}{\tau_0}\right)^{3/S}\right\} \quad (5.1)$$

where t is the time after excitation, τ_0 is the intrinsic decay time of the donors in the absence of acceptors. The value of $S = 6, 8,$ or 10 depending on the main mechanism of the interactions (dipole–dipole, dipole–quadrupole, or quadrupole–quadrupole). Q is a parameter for energy transfer which is defined as:

$$Q = -\frac{4\pi}{3} \Gamma\left(1 - \frac{3}{S}\right) N_0 R_0^3 \quad (5.2)$$

N_0 is the concentration of acceptors, which is almost equal to the total concentration of Ln^{3+} ions, R_0 is the critical energy transfer distance, which is the distance between donor and acceptor when the rate of energy transfer is equal to intrinsic decay, and the gamma function $\Gamma(X)$ which is equal to 1.77 for dipole-dipole ($S = 6$), 1.43 for dipole–quadrupole ($S = 8$), and 1.3 for quadrupole–quadrupole ($S = 10$) interactions, respectively. The calculated values of the multipolar interaction parameter S can be reasonably approximated to 6 as shown in Table 5.1. The Q parameter can be determined by fitting the decay curves, as shown in Figure 5.9 (a, b, c, and d). We expect to see an increase in the Q parameter when the distance between optically active Ln^{3+} ions decreases due to increased concentration.

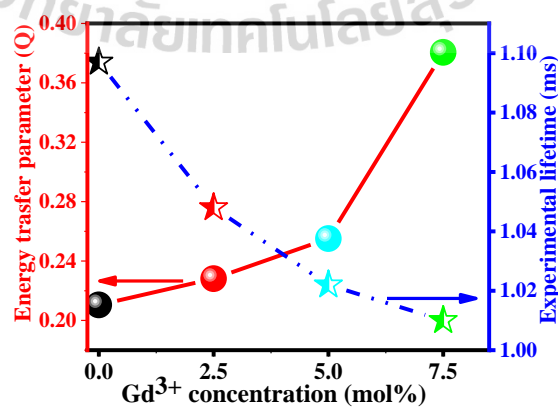


Figure 5.8 (a) Luminescence decay curves ($\lambda_{ex} = 275$ nm, $\lambda_{em} = 600$ nm) and (b) variation of energy transfer parameter (Q) with respect to concentration of Gd^{3+} ion.

This result confirms the energy transfer from donor to acceptor since the energy transfer is often defined as an exchange of electric interactions between the donor (Gd^{3+}) and acceptor (Sm^{3+}) and ($Sm^{3+}-Sm^{3+}$). An increased concentration of Gd^{3+} may result in non-exponential growth due to the formation of resonant excitation energy movements between $Sm^{3+}-Sm^{3+}$ ions. The host glass, which is essential for the persistent luminescence, can also be used to determine the energy transfer efficiencies in the produced series of glasses (calculated by using Eq. (5.3)).

$$\eta_{(Sm^{3+}-Sm^{3+})} = 1 - (\tau_{xSm^{3+}} / \tau_{0Sm^{3+}}) \quad (5.3)$$

where $\eta_{(Sm^{3+}-Sm^{3+})}$ is the energy transfer efficiencies, $\tau_{0Sm^{3+}}$ is the lifetime of Gd^{3+} in the host sample with 0 mol% concentration and $\tau_{xSm^{3+}}$ is the lifetime of Gd^{3+} with $x = 2.5, 5.0,$ and 7.5 mol% at a constant concentration of 1.0 mol% of Sm_2O_3 . The energy transfer efficiency was found to be 4.4667%, 6.8368%, and 7.9307%, whilst the amount of Gd_2O_3 concentration increases from 2.5 to 7.5 mol%, as shown in Table 5.1.

Table 5.1 Gd^{3+} ions concentration, lifetime (τ_{exp} ; ms), energy transfer efficiencies (η), energy transfer parameter (Q), and R-square of LAGdxBSm1.0 glasses.

Name of sample	Ln ³⁺ content		τ_x (ms)	τ_0 (ms)	η	Q	R-square
	mol%						
	Gd ³⁺	Sm ³⁺					
LAGd0BSm1.0	0	1.0	1.097	1.097	-	0.2104	-
LAGd2.5BSm1.0	2.5	1.0	1.048	1.097	4.4667	0.2281	0.9994
LAGd5.0BSm1.0	5.0	1.0	1.022	1.097	6.8368	0.2551	0.9995
LAGd7.5BSm1.0	7.5	1.0	1.010	1.097	7.9307	0.3805	0.9999

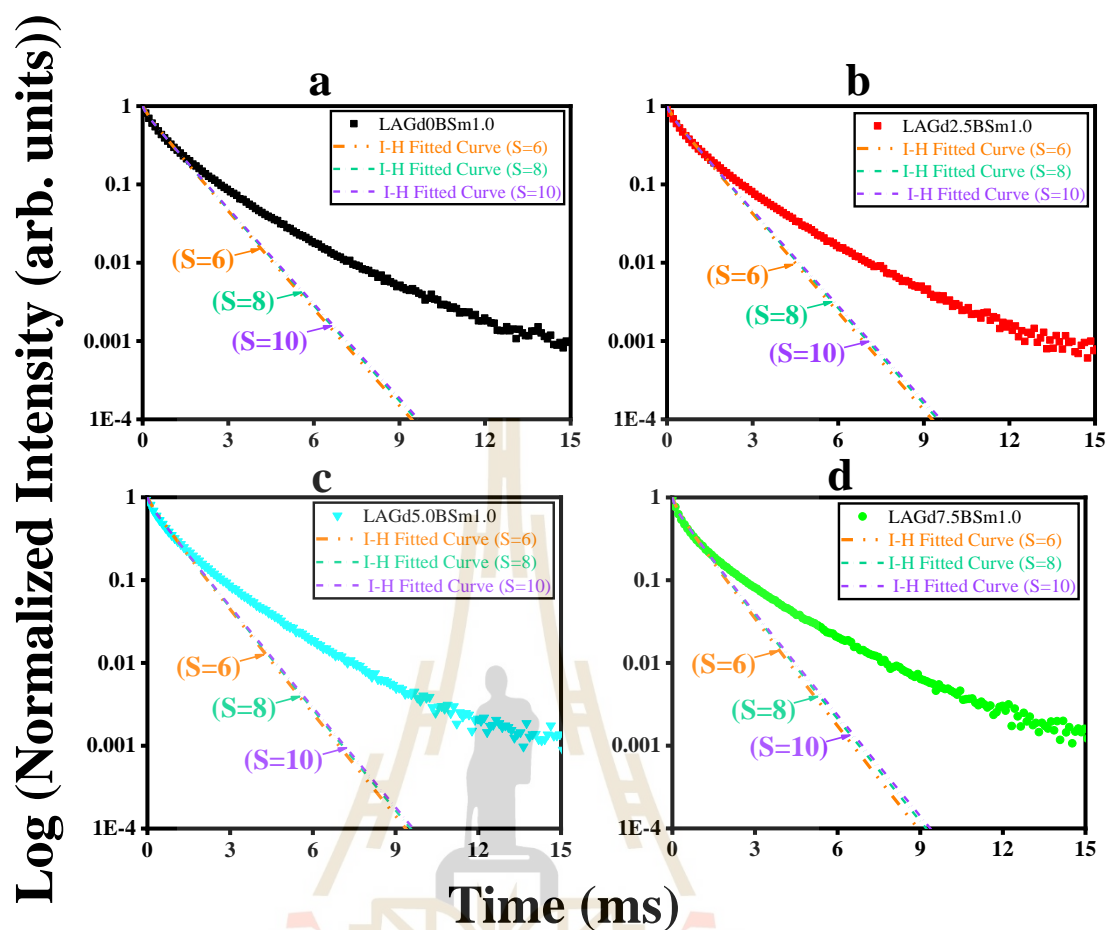


Figure 5.9 The I-H fitting curves ($S=6, 8,$ and 10) with varying Sm^{3+} concentrations in the as-prepared glasses.

Figure 5.10(a, b) depicts the absorption spectra of LAGd2.5BSm x glasses in the visible and near-infrared regions at ambient temperature. The nine bands, associated with typical transitions of the Sm^{3+} ions, were assigned to the following $4f-4f$ transitions from the ground state $^6\text{H}_{5/2}$ to the excited states $^6\text{P}_{3/2}$ (402 nm), $^4\text{I}_{11/2}$ (474 nm), $^6\text{F}_{5/2}$ (1376 nm), $^6\text{F}_{3/2}$ (1478 nm), $^6\text{H}_{15/2}$ (1531 nm), and $^6\text{F}_{1/2}$ (1583 nm) in the infrared range. The fundamental absorption edge of the glass series was increased with the increase of Sm^{3+} concentration and is attributed to the strong, wide absorption band of approximately 402 nm.

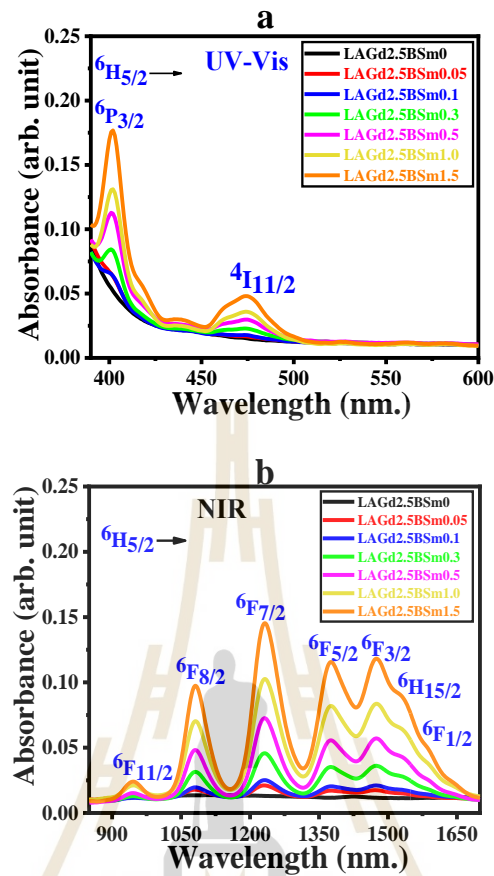


Figure 5.10 The optical absorption spectra of the LAGd2.5BSmx glasses.

The excitation spectra of LAGd2.5BSmx glasses are shown in Figure 5.11(a). There are thirteen major excitation bands in the 250–600 nm region of the excitation spectrum observed at 600 nm. These sharp excitation bands caused by f-f transitions of Gd^{3+} and Sm^{3+} ions are attributed to the following transitions: two transitions at 275 nm ($^8S_{7/2}-^6I_{9/2}$), 312 nm ($^8S_{7/2}-^6P_{7/2}$) of Gd^{3+} ion and other eleven transitions at 345 nm ($^6H_{5/2}-^4D_{7/2}$), 361 nm ($^6H_{5/2}-^4D_{3/2}$), 375 nm ($^6H_{5/2}-^6P_{7/2}$), 403 nm ($^6H_{5/2}-^6P_{3/2}$), 415 nm ($^6H_{5/2}-^6P_{5/2}$), 439 nm ($^6H_{5/2}-^4G_{9/2}$), 462 nm ($^6H_{5/2}-^4I_{13/2}$), 475 nm ($^6H_{5/2}-^4M_{15/2}$), 500 nm ($^6H_{5/2}-^4G_{7/2}$), 526 nm ($^6H_{5/2}-^4F_{3/2}$), and 562 nm ($^6H_{5/2}-^4G_{5/2}$) of Sm^{3+} ion. The excitation bands are similar to those reported in the literature (Jamalaiah et al., 2009; Wantana et al., 2020; Zaman et al., 2016; Khan et al., 2018).

These results suggest that incorporating Gd^{3+} could improve the luminescence of Sm^{3+} ions. Figure 5.11(b). shows the significant bands at 275 nm (Gd^{3+}) versus 401 nm (Sm^{3+}) of LAGd2.5BSmx glasses. Among these two, the intensity Gd^{3+} at 275 nm

decreases with an increase of Sm_2O_3 concentration, while the intensity of Sm^{3+} increases until 0.5 mol%. Therefore, the concentration quenching of LAGd2.5BSmx glass is 0.5 mol%. The bands at 275 nm ($^8\text{S}_{7/2}$ - $^6\text{I}_{9/2}$): Gd^{3+} and 401 nm ($^6\text{H}_{5/2}$ - $^6\text{P}_{3/2}$): Sm^{3+} have the highest excitation in the visible region. These wavelengths were then selected to excite the glass samples for the PL measurements. Different activator ion concentrations can impact the PL characteristics of a phosphor. Various concentrations of LAGd2.5BSmx glasses were produced in order to identify the best luminescence intensity.

The emission spectra of the LAGd2.5BSmx glasses under Gd^{3+} excitation with 275 nm is shown in Figure 5.11(c). These spectra show five emission bands in the visible region. The first region is a very strong band at 312 nm ($^6\text{P}_{7/2}$ - $^8\text{S}_{7/2}$). It has been reported that Gd_2O_3 containing glass shows strong emission around 310–312 nm (Gandhi et al., 2016; Gupta et al., 2015; Kalpana et al., 2016), which is very useful for producing narrow-band UVB (ultraviolet broadband) light. The second region includes four peaks at 562 ($^4\text{G}_{5/2}$ - $^6\text{H}_{5/2}$), 600 ($^4\text{G}_{5/2}$ - $^6\text{H}_{7/2}$), 648 ($^4\text{G}_{5/2}$ - $^6\text{H}_{9/2}$), and 705 ($^4\text{G}_{5/2}$ - $^6\text{H}_{11/2}$) nm. It is reported that the f-f transition of Sm^{3+} ions containing glass shows strong emission around 600-605 nm. At an excitation wavelength of 275 nm, the Gd^{3+} ions present in the host material emit at 312 nm, whereas the Sm^{3+} ions emit in the range of 550 to 750 nm. Sm^{3+} ions had no noticeable effect on the emission peaks in Figure 5.11.(c). When the Gd^{3+} emission (312 nm) is reduced at the same time as the Sm^{3+} emission (600 nm) is increased, this is really a clear indication of the energy transfer phenomenon from Gd^{3+} to Sm^{3+} occurring, as shown in Figure 5.11(d). The energy transfers between Gd^{3+} and Sm^{3+} have been extensively investigated in many other different host materials. Although electrons can be generated in Gd^{3+} , the luminescence from $\text{Gd}^{3+}/\text{Sm}^{3+}$ codoped glasses arises mainly due to the transitions from $^4\text{G}_{5/2}$ to $^6\text{H}_{7/2}$ in Sm^{3+} , which give rise to four emission bands in the visible region. Moreover, the excitation peaks of LAGd2.5BSmx glasses containing 2.5 mol% Gd_2O_3 may be seen in Figure 5.11.(e), which shows three excitation peaks. These peaks correspond to $^6\text{D}_{7/2}$ (at 246 nm), $^6\text{D}_{9/2}$ (at 253 nm), and strong peaks of $^6\text{I}_{9/2}$ (at 275 nm).

These peaks correspond to f-f transitions between the $^8\text{S}_{7/2}$ ground state and the $^6\text{D}_{7/2}$, $^6\text{D}_{9/2}$, $^6\text{I}_{9/2}$ of Gd^{3+} ions. When the Gd^{3+} excitation (λ_{Em} at 312 nm), the band

Gd^{3+} at 275 nm is decreased while the concentration of Sm^{3+} increases. The decay times of the glass system have been investigated in order to acquire a better understanding of the luminescence properties and energy transfer mechanisms of the system. Figure 5.11(f) shows the decay lifetimes of Gd^{3+} in LAGd2.5BSm x glasses under 275 nm excitation and at 312 nm emission wavelengths. The experimentally measured decaytimes are 1.861, 1.712, 1.668, 1.403, 1.351, 1.097, and 0.993 ms for 0, 0.05, 0.1, 0.3, 0.5, 1.0, and 1.5 mol% doped Sm^{3+} glasses, respectively, and decrease with increasing Sm^{3+} content in the samples. It further confirms the energy transfer from Gd^{3+} to Sm^{3+} .

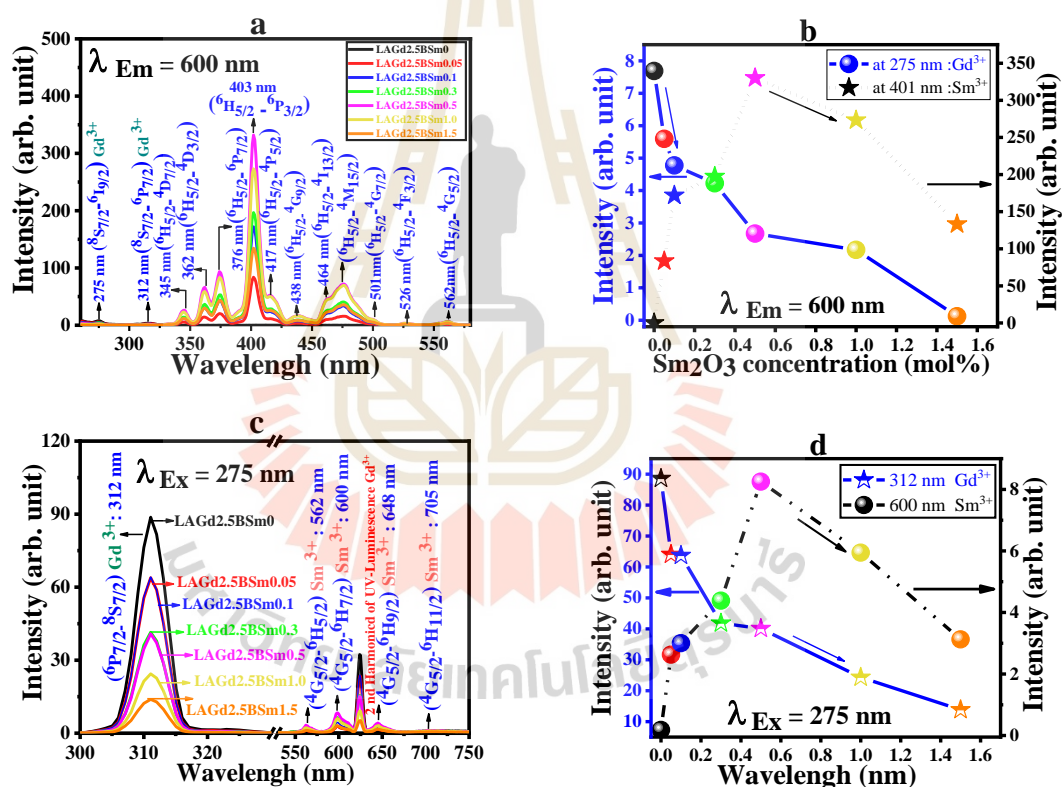


Figure 5.11 (continued) The photoluminescence excitation (a, b, and e), emission spectra (c, d) and (f) decay curve of the Gd^{3+} ion in glass series under 275 nm excitation and at 312 nm emission wavelengths of LAGd2.5BSm x glasses with different concentrations of Sm_2O_3 .

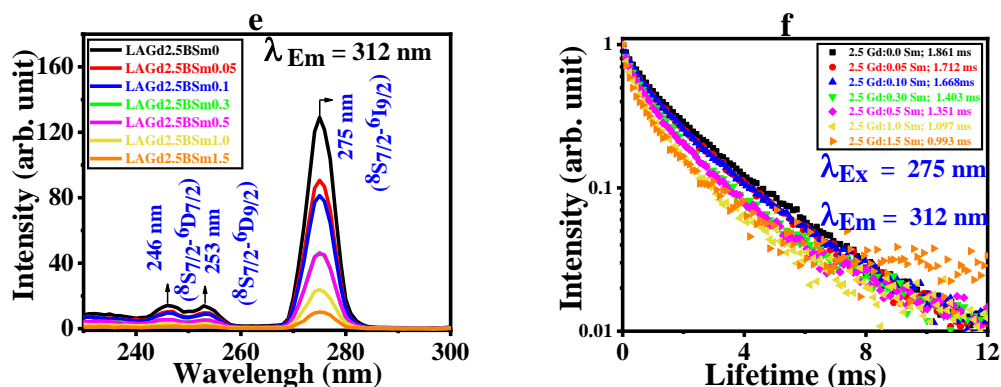


Figure 5.11 (continued) The photoluminescence excitation (a, b, and e), emission spectra (c, d) and (f) decay curve of the Gd³⁺ ion in glass series under 275 nm excitation and at 312 nm emission wavelengths of LAGd2.5BSmx glasses with different concentrations of Sm₂O₃.

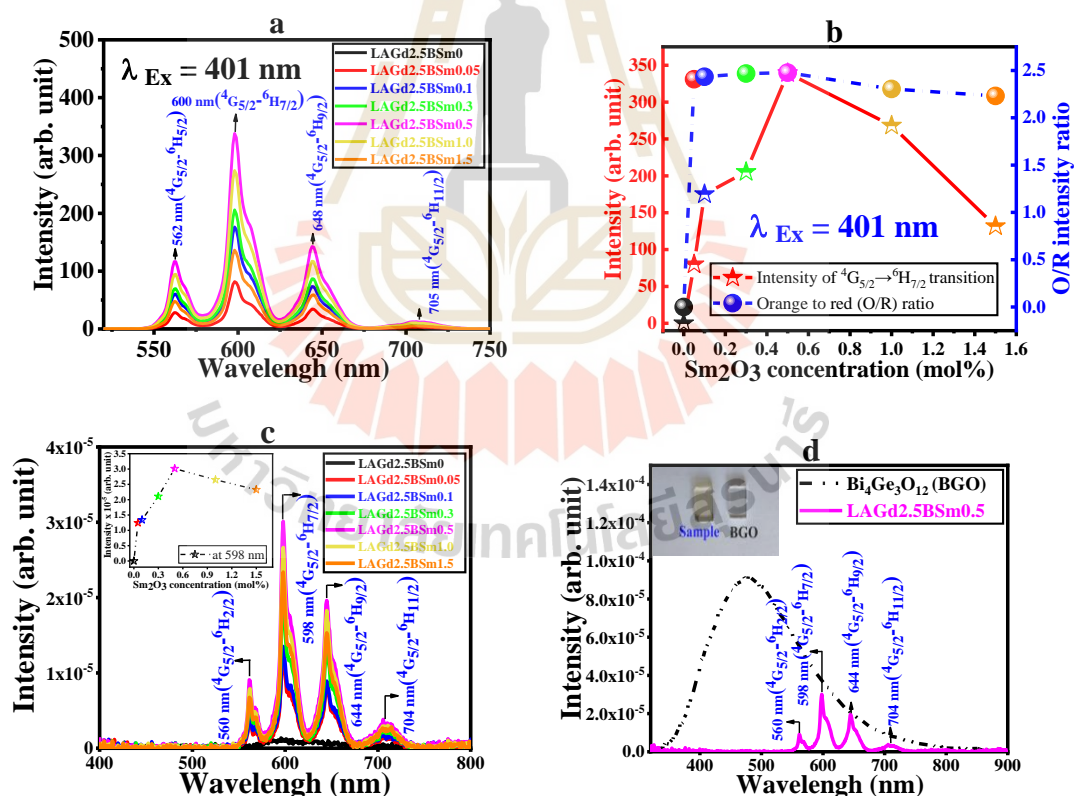


Figure 5.12 Emission spectra of LAGd2.5BSmx glasses (0- 1.5 mol%) at excitation wavelength 401 nm (a, b), radioluminescence spectra (c) and BGO and 0.5 mol% Sm₂O₃ doped glass for compared RL measurement (d).

Figure 5.12(a) shows the concentration-dependent photoluminescence spectra under an excitation wavelength of 401 nm, which has four prominent groups of emission lines in the range of 550 to 750 nm. These peaks can be attributed to the Sm^{3+} intra-4f orbital transition of ${}^4\text{G}_{5/2}$ - ${}^6\text{H}_{5/2}$ (yellow), ${}^4\text{G}_{5/2}$ - ${}^6\text{H}_{7/2}$ (orange-red), ${}^4\text{G}_{5/2}$ - ${}^6\text{H}_{9/2}$ (red), and ${}^4\text{G}_{5/2}$ - ${}^6\text{H}_{11/2}$ (deep red) transitions at the wavelengths of 562, 600, 648, and 705 nm, respectively. These luminescence bands are clearly the signature of the Sm^{3+} bands, with the maximum intensity at 600 nm. Figure 5.12(b) depicts the intensity variation of ${}^4\text{G}_{5/2} \rightarrow {}^6\text{H}_{7/2}$ transitions as well as the O/R ratio, which relates the luminescence intensity of ${}^4\text{G}_{5/2} \rightarrow {}^6\text{H}_{7/2}$ (orange)/ ${}^4\text{G}_{5/2} \rightarrow {}^6\text{H}_{9/2}$ (red), to the Sm^{3+} ion concentration in the LAGd2.5BSm x glasses. It is clearly seen that the 0.5 mol% of Sm^{3+} ion is the optimum concentration to give the highest emission intensity at 600 nm. Energy migration from one activator center to another can explain the concentration quenching observed beyond 0.5 mol% of Sm^{3+} in these glasses. The orange to red (O/R) ratio is found to be LAGd2.5BSm0 = 0, LAGd2.5BSm0.05 = 2.40775, LAGd2.5BSm0.1 = 2.43348, LAGd2.5BSm0.3 = 2.46724, LAGd2.5BSm0.5 = 2.47723, LAGd2.5BSm1.0 = 2.30484, and LAGd2.5BSm1.5 = 2.23098. The orange-to-red (O/R) ratio increases as the Sm^{3+} concentration increases up to 0.5 mol%. The ratio then falls due to the concentration quenching, indicating a strong local disorder in the glass network of the investigated glasses. There is no inversion symmetry site in the analyzed glass network if the O/R ratios are larger than unity. The O/R results indicate that it is possible to extract the orange light from the samples, which will be further supported by the results of CIE color 1935. Figure 5.12(c) displays the X-ray generated luminescence spectra of the LAGd2.5BSm x glass series in the 500–750 nm wavelength region. The glass samples were irradiated with X-rays at 50 kV and 30 mA. The LAGd2.5BSm x glass series produces four peaks at 560, 598, 644, and 704 nm wavelengths, which are ascribed to the characteristic Sm^{3+} (f-f transitions) at (${}^4\text{G}_{5/2}$ - ${}^6\text{H}_{5/2}$), (${}^4\text{G}_{5/2}$ - ${}^6\text{H}_{7/2}$), (${}^4\text{G}_{5/2}$ - ${}^6\text{H}_{9/2}$) and (${}^4\text{G}_{5/2}$ - ${}^6\text{H}_{11/2}$), respectively. The highest peak is seen at a wavelength of 598 nm. The best concentrations of Sm_2O_3 for the X-ray generated luminescence spectra pattern are 0.5 mol%, which is comparable to the photoluminescence spectra. The intensity of the glasses was increased by increasing the concentration of Sm_2O_3 to 0.50

mol%. After that, the intensity dropped due to the concentration quenching, which the host material can explain, and the activator ions exhibit distinct interaction mechanisms by X-rays and UV-visible radiation. In comparison, UV may directly excite electrons of lanthanide ions (Ln^{3+}), while X-ray can excite electrons of both Ln^{3+} ions and the host. Because of the X-ray excitation of the host glass, a significant number of secondary electrons are generated due to the hole-electron interaction. The lanthanide ions (Ln^{3+}) in the glass are excited indirectly and directly by electrons. Due to its long decay period of a few milliseconds, the created glass has the potential for X-ray scintillator applications in medical, industrial, and security imaging inspection systems. A glass doped with 0.5 mol% Sm^{3+} , LAGd2.5BSm0.5 was manufactured under cut and polish conditions in the same size and shape as a commercial $\text{Bi}_4\text{Ge}_3\text{O}_{12}$ (BGO) scintillator crystal in order to investigate the integral scintillation efficiency of the present glasses. Figure 5.12(d) demonstrates the X-ray luminescence spectra of the current glass samples when compared to BGO samples. The calculated integral scintillation efficiency of LAGd2.5BSm0.5 is 4.43% as compared with the BGO crystal.

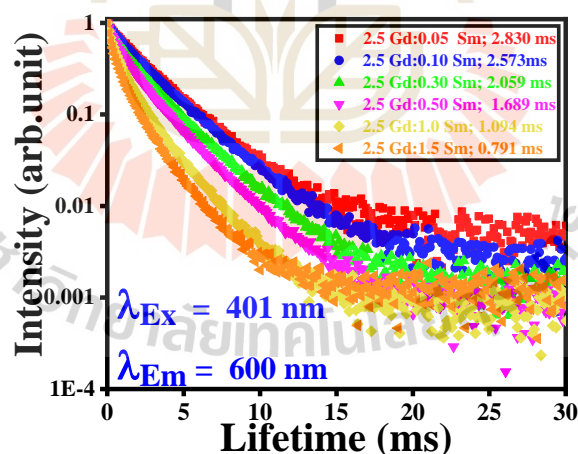


Figure 5.13 Luminescence decay profiles of the ${}^4\text{G}_{5/2}$ emission state in LAGd2.5BSm glasses for 600 nm emission with 401 nm excitation wavelength.

The PL decay curves of the Sm^{3+} transition from the ${}^4\text{G}_{5/2}$ level were studied using 600 nm emission and 401 nm excitation wavelengths. These decay profiles are depicted in Figure 5.13, as Sm^{3+} concentration grows from 0.05 to 1.5 mol%, the decay time reduces from 2.830 to 0.791 ms. The decay rate is about the same at low Sm^{3+}

ion concentrations (0.05 and 0.3 mol %) but rapidly drops when Sm^{3+} ion concentrations are above 0.5 mol%. It is clear that the effect of energy exchange between Sm^{3+} ions as the distance between Sm^{3+} ions is reduced with rising Sm^{3+} ion concentrations, increasing the energy depletion rate and decreasing the decay time.

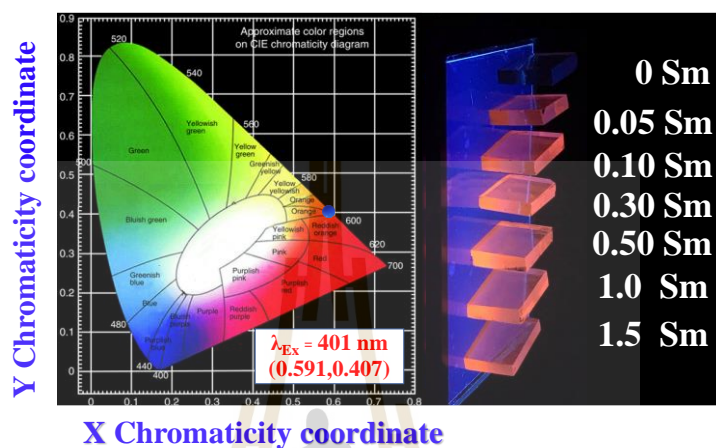


Figure 5.14 CIE chromaticity coordinates ($\lambda_{\text{ex}} = 401 \text{ nm}$) for LAGd2.5BSm ($\text{Sm}_2\text{O}_3 = 0.5 \%$) series glasses with varying Sm^{3+} concentrations. The insets are the corresponding digital luminescence photos under a 365 nm UV lamp excitation.

The LAGd2.5BSm x glass series with varying Sm^{3+} concentrations is shown in the CIE-1931 (Commission-international de-lighting) color coordinates diagram and color temperatures (CCT) in Figure 5.14. In order to define the color of the visible emission that the human eye sees, the Commission Internationale de l'Eclairage (CIE) coordinates were calculated. The CIE is the usual reference for identifying colors, and it is calculated by examining the human eye's sensitivity to different colors (wavelengths). In the CIE color chart, the predicted color coordinates for the present highlight emission intensity with CIE chromaticity coordinates $x = 0.55$ and $y = 0.44$ create orange light. In addition, the color coordinates did not change when the concentration of Sm^{3+} ions increased from 0.05% up to 1.5 mol%, as shown in Table 2. The correlated color temperature (CCT) measures the closest Planckian black body radiator to the operational point on the chromaticity diagram to evaluate the performance of a light source's production. The CCT can be calculated using McCamy's empirical formula, Eq. (5.4) (McCamy et al., 1992), and the result is listed in Table 5.2.

$$\text{CCT} = 437n^3 + 3601n^2 + (-6861)n + 5524.31 \quad (5.4)$$

$n = (x - 0.332)/(y - 0.186)$ where n is the slope line. Using the prevailing glasses, the correlated color temperature (CCT) value was determined to be 1725-1726 K, which is lower than that of daylight (6500 K) and close to that of the fluorescent warm white (2940 K). CCT values of Sm^{3+} in different glass hosts have been studied and published (Deopa et al., 2017). Based on these results, the LAGd2.5BSm x glass series may be utilized in the LED orange light.

Table 5.2 CIE chromaticity coordinates ($\lambda_{\text{ex}} = 401 \text{ nm}$) and correlated color temperature (CCT) of all LAGd2.5BSm x series glasses.

Sample name	Concentration of Sm_2O_3 (mol%)	CIE coordinates (x, y)	CCT (K)
LAGd2.5BSm0	0	(0.357, 0.492)	4971
LAGd2.5BSm0.05	0.05	(0.590, 0.407)	1726
LAGd2.5BSm0.1	0.10	(0.590, 0.407)	1726
LAGd2.5BSm0.3	0.30	(0.591, 0.406)	1725
LAGd2.5BSm0.5	0.50	(0.591, 0.407)	1725
LAGd2.5BSm1.0	1.00	(0.591, 0.407)	1725
LAGd2.5BSm1.5	1.50	(0.591, 0.407)	1726
10Li ₂ O-10PbO-(10-x)Al ₂ O ₃ - 70B ₂ O ₃ -xSm ₂ O ₃ (Deopa et al., 2017)	0.5	(0.564, 0.435)	1901
PKAPbNSm10 (Basavapoornima et al., 2014)	1.0	(0.59, 0.40)	1626
PPNSm (Praveena et al., 2008)	-	(0.59, 0.40)	2152
TZKC (Kesavulu et al., 2014)	2.0	(0.59, 0.40)	2152
PbFSm (Andrade et al., 2004)	-	(0.48, 0.34)	1919
Fluorescent, warm white	-	(0.440, 0.403)	2940
Incandescent bulb	-	(0.448, 0.408)	2854
Daylight (CIE standard)	-	(0.313, 0.329)	6500

The normalization and merging of XAS spectra and background reduction were examined using the Athena program on actual and theoretical L_{III} -edge XANES spectra. The normalized spectra of LAGd2.5BSm x glasses are compared with the reference spectra of Sm_2O_3 powder as shown in Figure 5.15. The dipole-allowed transition is ascribed to the Sm L_{III} -edge spectra with edge positions of LAGd2.5BSm x glasses and the Sm_2O_3 standard powder at about 6721.7 eV and 6721.2 eV (Kaewnuam et al., 2017). The energy difference between the LAGd2.5BSm x glasses and the Sm_2O_3 standard powder is around 0.5 eV, which is consistent with prior research. The peak of the white line in all spectra is centered at 6723 eV, which is more intense in these glass samples than in standard powder samples. The positions of the powder's edge and the white line for all glasses are identical and conform to the XANES pattern of Sm ion with a 3+ oxidation state. It has been established that the Sm ions in these glasses are Sm^{3+} ions, similar to those found in Sm_2O_3 powder.

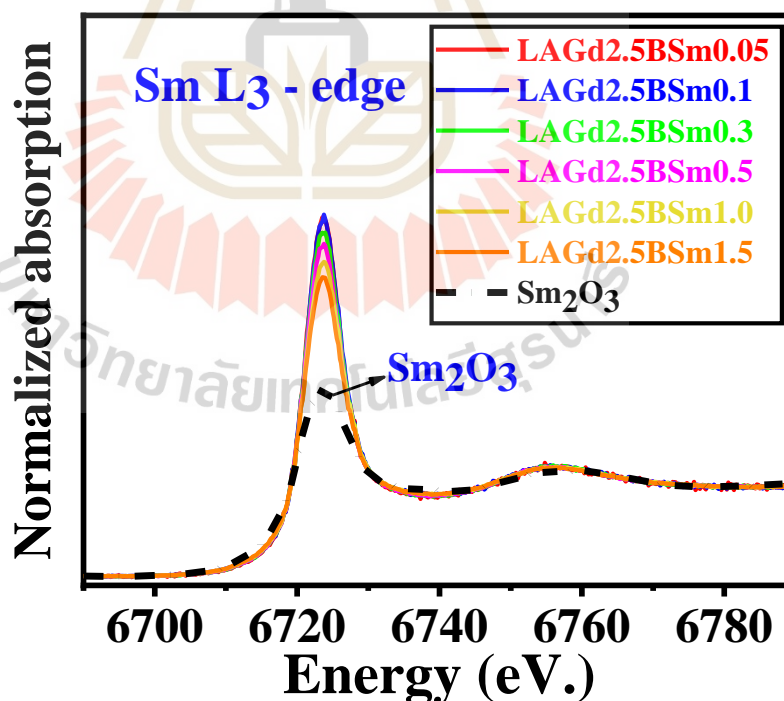


Figure 5.15 Normalized Sm L_{III} -edge XANES spectra are compared with Sm^{3+} in oxide from standard reference.

5.4 References

- Andrade, B. W. and Forrest, S. R. (2004). White organic light-emitting devices for solid-state lighting. *Advanced Materials*, 16, 1585:1595.
- Basavapoornima, C. H. and Jayasankar, C. K. (2014). Spectroscopic and photoluminescence properties of Sm^{3+} ions in Pb–K–Al–Na phosphate glasses for efficient visible lasers. *Journal of Luminescence*, 153, 233:241.
- Dalal, S., Khasa, S., Dahiya, M. S., Agarwal, A., Yadav, A., Seth, V. P., and Dahiya, S., (2015). Effect of substituting iron on structural, thermal and dielectric properties of lithium borate glasses. *Materials Research Bulletin*, 70, 559:566.
- Deopa, N. and Rao, A. S. (2017). Spectroscopic studies of Sm^{3+} ions activated lithium lead alumino borate glasses for visible luminescent device applications. *Optical Materials*, 72, 31:39.
- Deopa, N. and Rao, A. S. (2018). Spectroscopic studies of single near ultraviolet pumped Tb^{3+} doped lithium lead alumino borate glasses for green lasers and tricolour w-LEDs. *Journal of Luminescence*, 194, 56:63,
- ElBatal, F. H., Selim, M. S., Marzouk, S. Y., and Azooz, M. A. (2007). UV vis absorption of the transition metal-doped $\text{SiO}_2\text{-B}_2\text{O}_3\text{-Na}_2\text{O}$ glasses. *Physica B: Condensed Matter*, 398, 126:134.
- Gandhi, Y., Rajanikanth, P., Sundara Rao, M., Ravi Kumar, V., Veeraiah, N., and Piasecki, M. (2016). Effect of tin ions on enhancing the intensity of narrow luminescence line at 311 nm of Gd^{3+} ions in $\text{Li}_2\text{O-PbO-P}_2\text{O}_5$ glass system. *Optical Materials*, 57, 39:41.
- Gedam, R. S. and Ramteke, D. D. (2013). Influence of CeO_2 addition on the electrical and optical properties of lithium borate glasses. *Journal of Physics and Chemistry of Solids*, 74, 1399:1402.
- Gunji, R. M., Mattos, G. R. S., Bordon, C. D. S., Gomez-Malagon, L. A., and Kassab, L. R. P. (2020). Efficiency enhancement of silicon solar cells covered by $\text{GeO}_2\text{-PbO}$ glasses doped with Eu^{3+} and TiO_2 nanoparticles. *Journal of Luminescence*, 223, 117244.

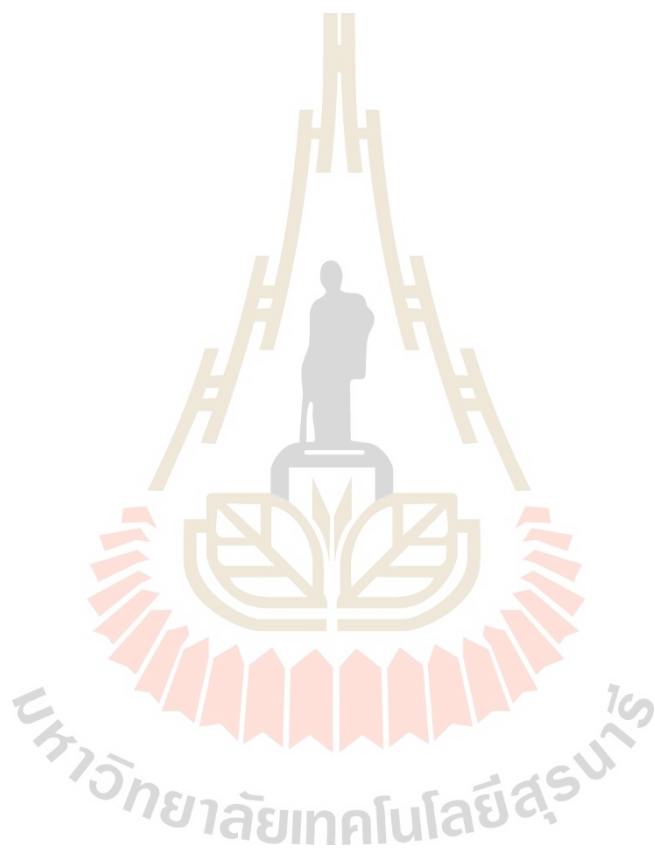
- Gupta, P., Bedyal, A. K., Kumar, V., Khajuria, Y., Sharma, V., Ntwaeaborwa, O. M., and Swart, H. C. (2015). Energy transfer mechanism from Gd^{3+} to Sm^{3+} in $K_3Gd(PO_4)_2:Sm^{3+}$ phosphor. *Materials Research Express*, 2 (7), 076202.
- Inokuti, M. and Hirayama, F. (1965). Influence of energy transfer by the exchange mechanism on donor luminescence. *The Journal of Chemical Physics*, 43 (6), 1978:1989.
- Jamalaiah, B. C., Suresh, Kumar J., Mohan Babu, A., Suhasini, T., and Rama Moorthy, L. (2009). Photoluminescence properties of Sm^{3+} in LBTAf glasses. *Journal of Luminescence*, 129 (4), 363:369.
- Kaewnuam, E., Kaewkhao, J., Wantana, N., Klysubun, W., Kim, H. J., and Sangwanateee, N. (2017). Comparative study of Sm^{3+} doped in $Li_2O_3-RE_2O_3-B_2O_3$ (RE= Y/La) glasses system for laser medium application. *Results in physics*, 7, 3698-3703.
- Kalpana, T., Gandhi, Y., Bhaskar, S., Sudarsan, V., Bragiel, P., Piasecki, M., Ravi Kumar, V., and Veeraiah, N. (2016). Influence of alumina on photoluminescence and thermoluminescence characteristics of Gd^{3+} doped barium borophosphate glasses. *Journal of Luminescence*, 179, 44:49.
- Karthikeyan, B., Philip, R., and Mohan, S. (2005). Optical and non-linear optical properties of Nd^{3+} -doped heavy metal borate glasses. *Optics Communications*, 246, 153:162.
- Kaur, P., Kaur, S., Singh, G. P., and Singh, D. P. (2014). Cerium and samarium codoped lithium aluminoborate glasses for white light emitting devices. *Journal of Alloys and Compounds*, 588, 394:398.
- Kaura, P., Singh, D., and Singh, T. (2019). Sm^{3+} and Gd^{3+} co-doped lead phosphate glasses for g-rays shielding and sensing. *Journal of Luminescence*. 209, 74:88.
- Kesavulu, C. R. and Jayasankar C. K. (2012). Spectroscopic properties of Sm^{3+} ions in lead fluorophosphate glasses. *Journal of Luminescence*, 132, 2802:2909.
- Kesavulu, C. R., Kim, H. J., Lee, S. W., Kaewkhao, J., Kaewnuam, E., and Wantana, N. (2017). Luminescence properties and energy transfer from Gd^{3+} to Tb^{3+} ions in gadolinium calcium silicoborate glasses for green laser application. *Journal of Alloys and Compounds*, 704, 557:564.

- Khalid, M., Lancaster, D. G., and Ebendorff, H. (2020). Spectroscopic analysis and laser simulations of $\text{Yb}^{3+}/\text{Ho}^{3+}$ co-doped lead-germanate glass. *Optical Materials Express*, 10, 2819:2833.
- Khan, I., Rooh, G., Mukamil, S., Kaewkhao, J., Shamshad, L., and Sangwanate, N. (2018). Investigation of the luminescence properties of Sm^{3+} activated mixed alkali borate glasses. *Materials Today: Proceedings*, 5(7), 15019:15023.
- Khan, I., Rooh, G., Rajaramakrishna, R., Sirsittapokakun, N., Kim, H. J., Kaewkhao, J., and Kirdsiri, K. (2019). Energy transfer phenomenon of Gd^{3+} to excited ground state of Eu^{3+} ions in $\text{Li}_2\text{O}-\text{BaO}-\text{Gd}_2\text{O}_3-\text{SiO}_2-\text{Eu}_2\text{O}_3$ glasses. *Spectrochimica Acta Part A: Molecular and Biomolecular Spectroscopy*, 210, 21-29.
- Kirdsiri, K., Rajaramakrishna, R., Damdee, B., Kim, H. J., Nuntawong, N., Horphathum, M., and Kaewkhao, J. (2019). Influence of alkaline earth oxides on Eu^{3+} doped lithium borate glasses for photonic, laser and radiation detection material applications. *Solid State Sciences*, 89, 57:66.
- Lakshminarayana, G., Kaky, K. M., Baki, S. O., Lira, A., Caldino, U., Kityk, I. V., and Mahdi, M. A. (2017). Optical absorption, luminescence, and energy transfer processes studies for $\text{Dy}^{3+}/\text{Tb}^{3+}$ - codoped borate glasses for solid-state lighting applications. *Optical Materials*, 72, 380:391.
- McCamy, C. S. (1992). Correlated color temperature as an explicit function of chromaticity coordinates. *Color Research and Application*, 17, 142:144.
- Mohan, M. M., Moorthy, L. R., and Jayasankar, C. K. (2013). Structural and optical properties of Sm^{3+} ions in potassium niobate silicate glasses. *Indian Journal of Applied Research*, 3, 23:27.
- Onderisinova, Z., Kucera, M., Hanus, M., and Nikl, M. (2015). Temperature-dependent nonradiative energy transfer from Gd^{3+} to Ce^{3+} ions in co-doped LuAG:Ce,Gd garnet scintillators. *Journal of Luminescence*, 167, 106:113.
- Pawar, P. P., Munishwar, S. R., and Gedam, R. S. (2016). Physical and optical properties of $\text{Dy}^{3+}/\text{Pr}^{3+}$ Co-doped lithium borate glasses for W-LED. *Journal of Alloys and Compounds*, 660, 347:355.

- Praveena, R., Venkatramu, V., Babu, P., and Jayasankar, C. K. (2008). Fluorescence spectroscopy of Sm^{3+} ions in $\text{P}_2\text{O}_5\text{-PbO-Nb}_2\text{O}_5$ glasses. *Physica B: Condensed Matter*, 403, 3527:3534.
- Ramteke, D. D. and Gedam, R. S. (2014). Study of $\text{Li}_2\text{O-B}_2\text{O}_3\text{-Dy}_2\text{O}_3$ glasses by impedance spectroscopy. *Solid State Ionics*, 258, 82:87.
- Ramteke, D. D., Ganvir, V. Y., Munishwar, S. R., and Gedam, R. S. (2015). Concentration effect of Sm^{3+} ions on structural and luminescence properties of lithium borate glasses. *Physics Procedia*, 76, 25:30.
- Rittisut, W., Wantana, N., Butburee, A., Ruangtaweep, Y., Padchasri, J., Rujirawat, S., Manyum, P., Kidkhunthod, P., Yimnirun, R., Kothan, S., Kim, H. J., Prasatkhetragarn, A., and Kaewkhao, J. (2021). Luminescence properties of Ce^{3+} -doped borate scintillating glass for new radiation detection material. *Radiation Physics and Chemistry*, 185, 109498.
- Shoib, M., Rooh, G., Chanthima, N., Rajaramakrishna, R., Kim, H. J., Wongdeeying, C., and Kaewkhao, J. (2019). Intriguing energy transfer mechanism in oxide and oxy-fluoride phosphate glasses. *Optical Materials*, 88, 429:444.
- Stambouli, W., Elhouichet, H., Gelloz, B., and Férid, M. (2013). Optical and spectroscopic properties of Eu-doped tellurite glasses and glass ceramics. *Journal of Luminescence*, 138, 201:208.
- Thakur, V., Kushwaha, H. S., Singh, A., Vaish, R., Punia, R., and Singh, L. (2015). A study on the structural and photocatalytic degradation of ciprofloxacin using $(70\text{B}_2\text{O}_3-29\text{Bi}_2\text{O}_3-1\text{Dy}_2\text{O}_3)-x(\text{BaO-TiO}_2)$ glass ceramics. *Journal of Non-Crystalline Solids*, 428, 197:203.
- Wantana, N., Kaewjaeng, S., Kothan, S., Kim, H. J., and Kaewkhao, J. (2017). Energy transfer from Gd^{3+} to Sm^{3+} and luminescence characteristics of $\text{CaO-Gd}_2\text{O}_3\text{-SiO}_2\text{-B}_2\text{O}_3$ scintillating glasses. *Journal of Luminescence*, 181, 382:386.
- Wantana, N., Kaewnuam, E., Kim, H. J., Kang, S. C., Ruangtaweep, Y., Kothan, S., and Kaewkhao, J. (2020). X-ray/proton and photoluminescence behaviors of Sm^{3+} -doped high-density tungsten gadolinium borate scintillating glass. *Journal of Alloys and Compounds*, 849, 156574.

Ullah, I., Shah, S. K., Rooh, G., Srisittipokakun, N., Khan, A., Kaewkhao, J., Kim, H. J., and Kothan, S. (2020). Spectroscopic study and energy transfer behavior of Gd^{3+} to Dy^{3+} for $Li_2O-MgO-Gd_2O_3-B_2O_3-Dy_2O_3$ glasses for white emission material. *Journal of Luminescence*, 226, 117380.

Zaman, F., Kaewkhao, J., Rooh, G., Srisittipokakun, N., and Kim, H. J. (2016). Optical and luminescence properties of $Li_2O-Gd_2O_3-MO-B_2O_3-Sm_2O_3$ ($MO = Bi_2O_3, BaO$) glasses. *Journal of Alloys and Compounds*, 676, 275:285.



CHAPTER VI

EUROPIUM DOPED BORATE GLASS

The physical, structural, optical and luminescence properties of lithium aluminum borate glasses as a function of Gd_2O_3 and Eu_2O_3 concentration were reported. The glasses composition of $25Li_2O-5Al_2O_3-YGd_2O_3-(70-Y-Z)B_2O_3-ZEu_2O_3$ system was successfully synthesized through a conventional melt-quenching technique. The various Gd_2O_3 concentration, 2.5 mol% is suitably added into the host composite: $25Li_2O-5Al_2O_3-2.5Gd_2O_3-(67.5-Z)B_2O_3-ZEu_2O_3$, supporting by X-ray induced luminescence and photoluminescence analysis. The influence of the Eu_2O_3 concentration doped glasses system has been investigated in different concentrations of Eu^{3+} ions. It was found that the emission intensity increase with an increase of Eu_2O_3 concentration up to 3.0 mol% (luminescence quenching). The maximum intensity peaks were located at 614 nm (red emission), which was due to $^5D_0 \rightarrow ^7F_2$ transitions of Eu^{3+} ions. The decay profile is measured to prove the occurrence of maximum energy transfer efficiency ($Eu^{3+}-Eu^{3+}$) obtained is as high as 15.36% for their potential candidature in solid state device applications.

6.1 Introduction

Nowadays, we recently tried to prepare the luminescent material doped with multi-rare-earth of borate glass system has been carried out in order to develop suitable host materials for useful photonic applications (Bergh et al., 2001; Im et al., 2009) such as color screens displays, infrared solid-state lasers, LEDs and radiation scintillating materials (Kaewnuam et al., 2017; Rahimi et al., 2020). Also, glasses doped with trivalent rare earth (RE^{3+}) ions are promising good choices due to their low synthesis cost, large-volume production, fast preparation period, easy manufacturing process, strength, and high ability to contain embedded ions. Oxide glasses such as

borate, phosphate, silicate and telluride glass system have attracted significant attention due to their excellent optical properties. Especially, borate glasses doped with RE³⁺ (Kaewnuam et al., 2017; Azizan et al., 2014; Kalpana et al., 2015) represent one of the best possible host materials that include better thermal chemical stability, high phonon energy ~1200-1500 cm⁻¹, low temperature for the synthesis, and radiation hardness. In addition, they are interesting optical properties such as high transparency from the visible to the near-infrared spectral region. Moreover, the borate glasses create an excellent host to incorporate trivalent rare-earth ions due to high solubility for lanthanide ions, resulting in the growing field of applications. Nonetheless, the borate glass system is also commonly recognized to improve some properties such as durability, raising mechanical strength, and boosting the glass-forming ability by the addition of some oxide such as Li₂O and Al₂O₃.

Currently, lanthanide oxides such as gadolinium oxide (Gd₂O₃), europium oxide (Eu₂O₃), or mixed lanthanide are a good choice of rare-earth dopants. Adding Gd₂O₃ in host glasses has become a very popular oxide material because it can improve the intensity of emission spectra (Ramteke et al., 2014; Ragab et al., 2013). We believe that the intensity of the photoemission increased with Gd³⁺ ion due to Gd³⁺ can enhance the energy transfer mechanism (Wattana et al., 2020) from Gd³⁺ ions to luminescence activator, high thermal neutron capture cross-section, and increase the light yield of emission. Furthermore, the trivalent rare-earth ions as europium ion (Eu³⁺) (Cao et al., 2020; Cao et al., 2022) is one of the super lanthanides because 4f-4f electron orbital and 4f-5d electronic transitions are shielded by 5s and 5p outer shells, which have the electron configuration [Xenon] 4f⁶ relatively simple energy level scheme is a very convenient spectroscopic probe. The photoluminescence (PL) demonstrated the presence of the wideband in the UV region ascribed to the transition from O²⁻ (2p₆ orbital) for electron transfer to Eu³⁺ ions (the empty orbital of 4f₆). This feature of Eu₂O₃ has garnered considerable attention from the researcher in various ways of the host glass. The motivation of this work, we synthesize and investigate the properties of Gd₂O₃ and Eu₂O₃ doped borate glass with varying lanthanide oxide concentrations. First, the optimum concentration of Gd₂O₃ (Y) doped borate glass designated as 25Li₂O-5Al₂O₃-YGd₂O₃-(60-Y)B₂O₃-1.0Eu₂O₃ (LAEUB) glasses were studied from 0, 2.5, 5.0, 7.5,

and 10.0 mol%. Second, the constant optimized concentration of Gd_2O_3 is selected for further experiments by varying Eu_2O_3 concentrations (Z). The glass samples of chemical composition $25Li_2O-5Al_2O_3-2.5Gd_2O_3-(67.5-Z)B_2O_3-ZEu_2O_3$ where, $Z = 0, 0.05, 0.5, 1.0, 2.0, 3.0,$ and 4.0 mol% designated name as LAGB glasses. The synthesized glasses are not only characterized in terms of structural and physical properties but also reveal the excellent desirable of X-ray-induced luminescence and photoluminescence properties. Therefore, the proposed glasses will be used in optical device applications such as LEDs, plasma display panels, solid-state devices, and radiation scintillating materials.

6.2 Experimental

6.2.1 Preparation of Gd_2O_3 doped

Lithium aluminum gadolinium borate glasses dual-doped with Gd^{3+} and Eu^{3+} having the chemical composition $25Li_2O-5Al_2O_3-YGd_2O_3-(69-Y)B_2O_3-1.0Eu_2O_3$ with difference Gd_2O_3 concentrations (Y) from 0, 2.5, 5.0, 7.5, and 10.0 mol%, call the “ LAEUB ” series of glass.

6.2.2 Preparation of Eu_2O_3 doped

The glass samples with various concentrations of Eu_2O_3 composition in $25Li_2O-5Al_2O_3-2.5Gd_2O_3-(67.5-Z)B_2O_3-ZEu_2O_3$ (where, concentrations of Eu_2O_3 ($Z = 0, 0.05, 0.5, 1.0, 2.0, 3.0,$ and 4.0 mol%)) designated name as “ LAGB ” glasses. The two glass systems were produced utilizing the lab grades of chemical $Li_2CO_3, H_3BO_3, Gd_2O_3, Al_2O_3,$ and Eu_2O_3 as starting ingredients, using standard melt quenching techniques. Through the processing in an aluminum crucible, around 20 g lots were fully integrated. In an electrical furnace, the thoroughly combined powder was melted at ~ 1200 °C for 90 minutes. Next step, the glass melted was poured onto a graphite plate followed by annealing at 500 °C for 3 hours to relieve thermal stress and cooled slowly to room temperature then cooled onto the polishers ($1.0 \times 1.50 \times 0.3$ cm³) to produce a clear sample of uniform thickness. The final glass material at room temperature was measured first by a simple method called Archimedes with water as a liquid immersion, and then molar volumes were estimated through a 4-digit sensitive microbalance (AND,

HR 200). The optical absorption spectra of polished samples are measured using a UV-vis and NIR (Shimadzu UV-3600) spectrophotometer in the region between 200 and 2500 nm of the wavenumber. The photoluminescence (PL) spectrum has been obtained in the 200-800 nm wavelength range, acquired at room temperature using a spectrometer (Cary-Eclipse) using a xenon flashlight as an excitation light source. The X-ray induced luminescence set up consisting of the Cu target x-ray generator (Inel, XRG3D-E), fiber optics spectrometer, and the brass-sample container was used to measure the X-ray luminescence spectrometer. Glass was radiated by X-ray (Cu target X-ray generator, Inel XRG3D-E, and operated at a power of 50 kV and 30 mA) with an Ocean Optics QE65 Pro spectrometer for signal readout. The Synchrotron Light Research Institute is routinely operated for X-ray absorption (XAS) spectroscopy (at beamline 5.2). For the glass samplings in the fluorescence mode the Eu L₃ edge: 6779 eV, the X-ray absorption near-edge structure (XANES) construction was recorded. The reference usage was given to standard Eu₂O₃ samples.

6.3 Results and discussion

6.3.1 Effect of Gd₂O₃ concentrations



Figure 6.1 Photograph of glass samples with varying Gd₂O₃ concentrations in 25Li₂O-5Al₂O₃-YGd₂O₃-(69.0-Y)B₂O₃-1.0Eu₂O₃ (LAEUB) glasses.

The effect of Gd₂O₃ concentration was studied, as shown in Figure 6.1. The obtained glasses are high transparent, completely free of bubbles, and soft yellow color depending on the increasing amount of Gd₂O₃ concentration. The density, molar volume, and refractive index of 25Li₂O-5Al₂O₃-Y Gd₂O₃-(69.0-Y)B₂O₃-1.0Eu₂O₃ glasses are represented in Figure 6.2 (a, b). The density and refractive index are found to increase trends linearly because Gd₂O₃ has a higher molecular weight (362.5 g/mol) than the several oxides in the borate glass system. Therefore, B₂O₃ is successively

replaced by Gd_2O_3 atom. While molar volume decreases with increasing Gd_2O_3 content, resulting in the decrease of the inter-atomic distance between the atoms or increased oxygen packing density, making the structure more compact. Consequently, it can be said that the compactness of the glass increased and more bridging oxygen (BO) occurred.

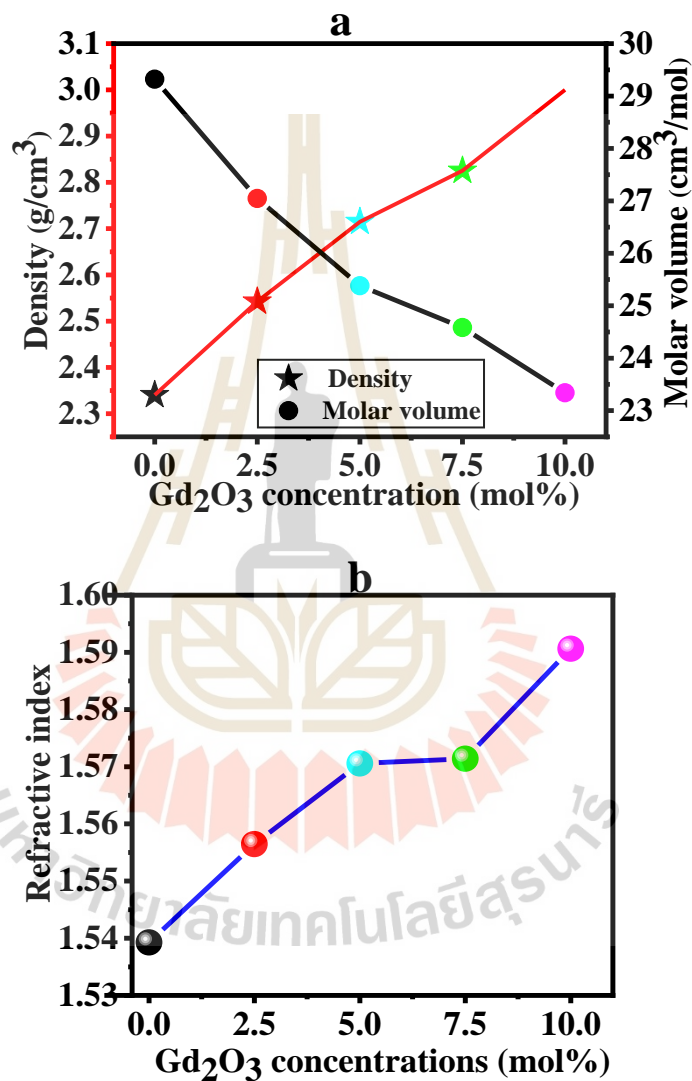


Figure 6.2 Density, molar volume (a), and refractive index (b) relation of $25Li_2O-5Al_2O_3-YGd_2O_3-(69.0-Y)B_2O_3-1.0Eu_2O_3$ glasses doped with varying concentrations of Gd_2O_3 ions.

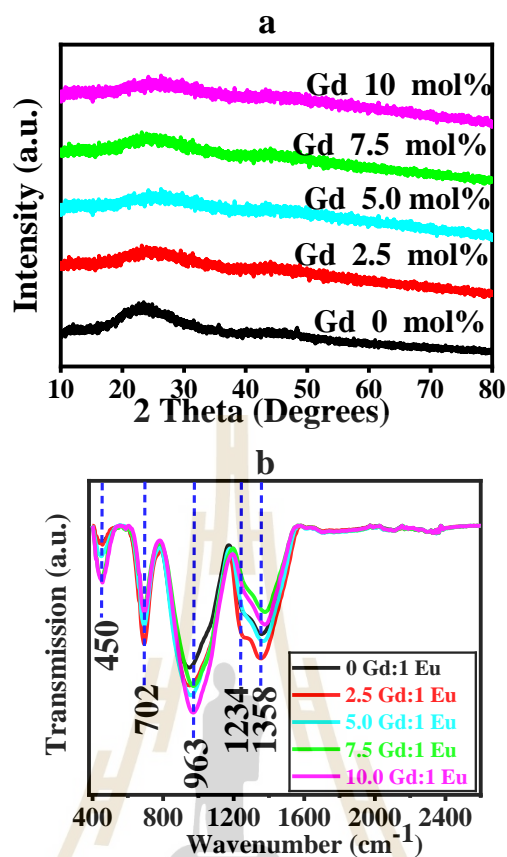


Figure 6.3 X-ray diffraction pattern (a) and FTIR transmittance (b) spectra of glasses.

The X-ray diffraction (XRD) spectra of Gd^{3+} doped on LAEUB glasses are depicted in Figure 6.3(a). The XRD patterns of the samples were measured in the range of 20° to 80° at room temperature. No peak is observed, although it exhibits a broad diffusion hump at a low scattering angle in the range 18° - 32° . Accordingly, the result can be confirmed that samples are amorphous structures. The coordination environment of B-O in the LAEUB series was confirmed by FTIR spectra by extending from 400 cm^{-1} to 2400 cm^{-1} region for the synthesis glasses are represented in Figure 6.3(b). The borate network structural analysis provided four infrared spectral regions. The following information is required, which is according to several previously reported. One of all spectra, the main vibrational modes are clearly shown at 450 cm^{-1} belong to lithium oxide in the glass samples (Rajesh et al., 2012). The second band near 702 cm^{-1} (Pawar et al., 2015; Azizan et al., 2014) indicates the B-O-B bending vibrations of bridges consisting of trigonal and tetrahedral boron. The third band between 800 and 1200 cm^{-1} which the center at 963 cm^{-1} may be obtained from the B-O bond

stretching of the tetrahedral BO_4 structural unit. Moreover, the absorption at 963 cm^{-1} is long to NBO vibrations in the glass network (Rajesh et al., 2012; Selvi et al., 2014) and tends to increase strength with increase Eu_2O_3 concentration dramatically, corresponding to the increasing of glass molar volume that can be explained by the NBO number addition. The last of spectra was located at $1200\text{--}1700\text{ cm}^{-1}$, representing asymmetric stretching relaxation of the B–O band of trigonal BO_3 units; the weak peak of B–O stretching vibrations has occurred at 1234 cm^{-1} , indicating that linkages between oxygen and different groups, belonging to B–O bridging between boroxol rings and trigonal BO_3 (Pawar et al., 2015). In addition, a band of asymmetric stretching relaxation at 1358 cm^{-1} belongs to the B–O bond of trigonal BO_3 units and various borate groups (Rajesh et al., 2012).

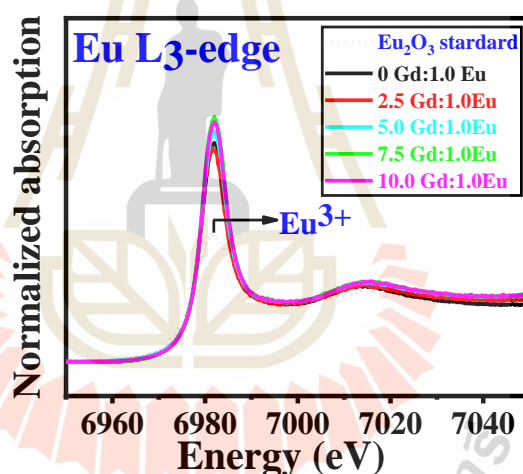


Figure 6.4 The comparison of Eu L_3 -edge XANES spectra of LAEUB series glass with Eu^{3+} in oxide form standard (dash double dotted line) reference spectra.

The X-ray absorption near-edge structure (XANES) spectroscopic was used to determine the oxidation state of materials. The experimental XANES data were compared by collecting fluorescence mode at the Eu L_3 -edge (6977 eV) based on a crystal analyzer spectrometer with bent Ge (220) crystals. In Figure 6.4, present the maximum energy of Eu L_3 -XANES spectra is observed at $\sim 6982\text{ eV}$ for Eu_2O_3 (Eu oxidation state is +3), indicating no difference within a LAEUB series. So, it is possible to conclude that all glass samples provided only one of the sharp peaks at 6982 eV white line (L_{III} edge of Eu^{3+} around 6977 eV with the sharp peak in the derivative

spectrum ~ 5 eV higher energy is expected), associated with the electronic transition from a $2p_{3/2}$ core- state to an empty $5d$ final state (Gaillard et al., 2005; Korthout et al., 2013). This energy position can be confirmed Eu atom remains a trivalent oxidation state: Eu^{3+} state of all LAEUB glass series used as a reference for the Eu_2O_3 measurements.

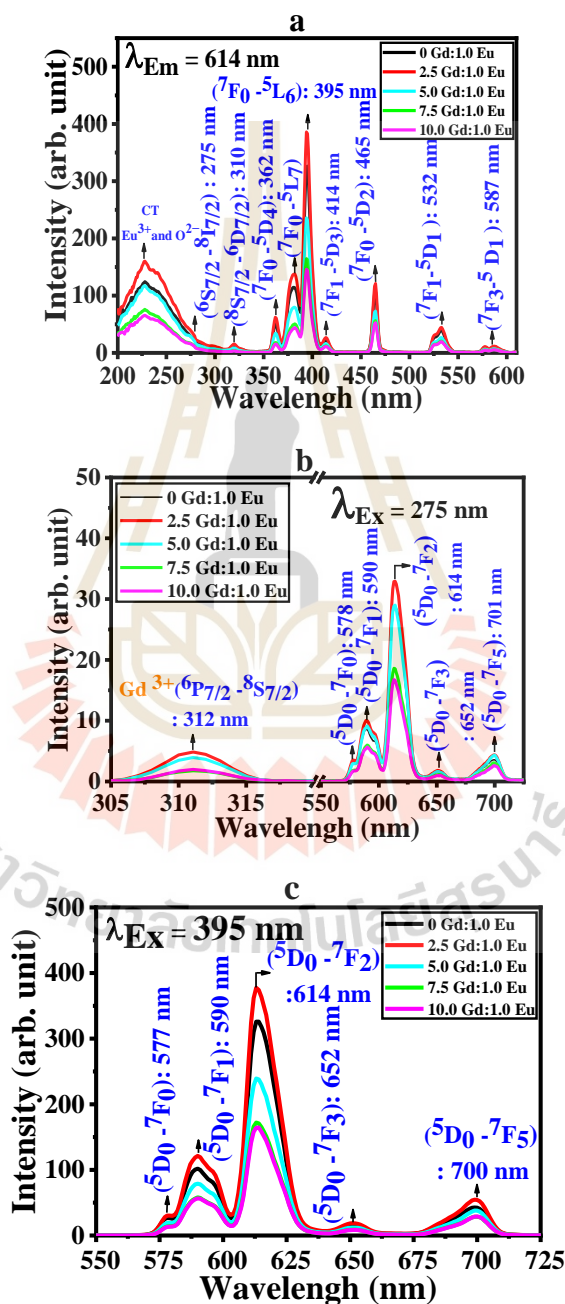


Figure 6.5 (a) Excitation spectra and (b, c) emission spectra of $25\text{Li}_2\text{O}-5\text{Al}_2\text{O}_3-\text{YGd}_2\text{O}_3-(69.0-\text{Y})\text{B}_2\text{O}_3-1.0\text{Eu}_2\text{O}_3$ glass system.

The detailed photoluminescence spectra results of lithium aluminum gadolinium borate glass phosphor dual-doped with Eu^{3+} and Gd^{3+} ions (LAEUB) were studied at room temperature and atmospheric pressure. The excitation spectra were recorded by selecting the emission wavelength at 614 nm and monitoring the spectral in the range of 200–600 nm. The characteristic of excitation spectra displays in Figure 6.5(a), ten bands can be assigned to 227, 275, 310, 362, 381, 395, 414, 465, 532 and 587 nm corresponds to the ${}^8\text{S}_{7/2} \rightarrow {}^6\text{D}_{7/2}$, ${}^6\text{S}_{7/2} \rightarrow {}^8\text{I}_{7/2}$, ${}^6\text{S}_{7/2} \rightarrow {}^6\text{D}_{7/2}$, ${}^7\text{F}_0 \rightarrow {}^5\text{D}_4$, ${}^7\text{F}_0 \rightarrow {}^5\text{L}_7$, ${}^7\text{F}_0 \rightarrow {}^5\text{L}_6$, ${}^7\text{F}_1 \rightarrow {}^5\text{D}_3$, ${}^7\text{F}_0 \rightarrow {}^5\text{D}_2$, ${}^7\text{F}_1 \rightarrow {}^5\text{D}_1$, and ${}^7\text{F}_3 \rightarrow {}^5\text{D}_1$ transitions of both Gd^{3+} and Eu^{3+} ion, respectively. A broadband emission band in the region from 200–250 nm (${}^8\text{S}_{7/2} \rightarrow {}^6\text{D}_{7/2}$) was observed monitored at 616 nm. The broadband peak with a maximum value at 227 nm is characteristic of the charge transfer band (CTB) transition between Eu^{3+} and O^{2-} (Wantana et al., 2018) because of the charge transfer behavior of the filled 2p^6 orbital of the O^{2-} to the partially filled 4f orbital of Eu^{3+} , which is easy to influence by the host environment. Figure 6.5(b, c) represents the emission spectra from the LAEUB series taken with excitation wavelengths at 275 and 395 nm of the sample, exhibiting a strong emission peak at 590 nm (orange colour) and 614 nm (red colour), which is characteristic of ${}^5\text{D}_0 \rightarrow {}^7\text{F}_1$ and ${}^5\text{D}_0 \rightarrow {}^7\text{F}_2$ transitions of Eu^{3+} ions of the host matrix. Among emission spectra (excitation wavelength at 275 nm) studied in Figure 6.5(b), shows the emission spectra for all glasses containing Gd_2O_3 consist of five prominent bands at 312, 577, 590, 614, 652, and 700 nm were assigned to the ${}^6\text{P}_{7/2} \rightarrow {}^8\text{S}_{7/2}$, ${}^5\text{D}_0 \rightarrow {}^7\text{F}_0$, ${}^5\text{D}_0 \rightarrow {}^7\text{F}_1$, ${}^5\text{D}_0 \rightarrow {}^7\text{F}_2$, ${}^5\text{D}_0 \rightarrow {}^7\text{F}_3$, and ${}^5\text{D}_0 \rightarrow {}^7\text{F}_5$ transitions, respectively. These transitions arise due to electric-dipole transition and magnetic dipole transitions. One can see from this Figure 6.5(b) that when the concentration of Gd_2O_3 increases there is an increase in the intensity of ${}^6\text{P}_{7/2} \rightarrow {}^8\text{S}_{7/2}$ up to 2.5 mol% and decrease for 5.0 mol% Gd_2O_3 which is an indication of the increasing energy transfer through cross-relaxation in the existing glass network. As the concentration of Gd^{3+} ions increases, the intermolecular distance reduces, and at 5.0 mol%, the Gd^{3+} ions are so near that there is a strong interaction between two active ions, resulting in the transfer of excitation energy from one Gd^{3+} ion to another. However, the emission spectra with $\lambda_{\text{ex}} = 275$ nm indicate the strongest peak at 614 nm and the emission

band excepted the sharp characteristic of Gd^{3+} ions at 311 nm (Gandhi et al., 2016; Kalpana et al., 2016). This data indicated that the emission intensity of Eu_2O_3 increases with increasing Gd_2O_3 at 2.5 mol%, this suitable concentration was chosen for further experiments.

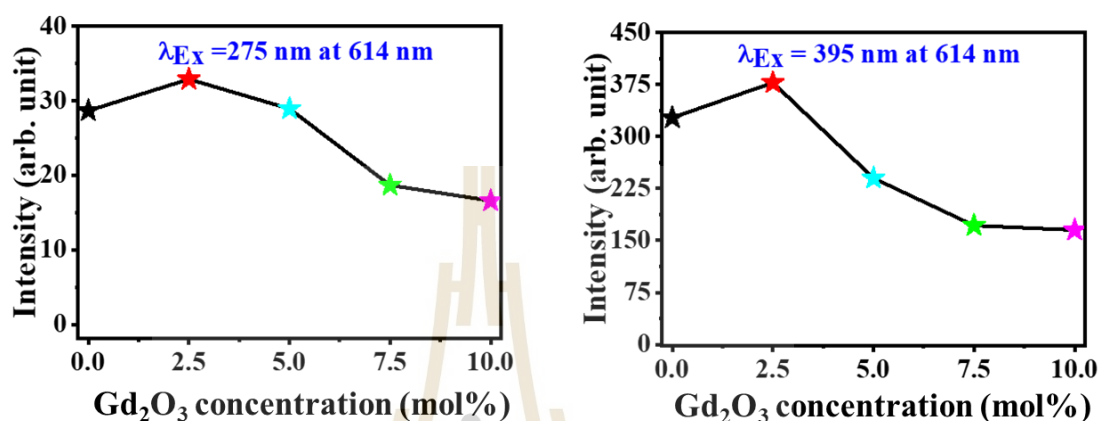


Figure 6.6 Relationship between the intensity of emission at 614 nm wavelength by excited 275 and 394 nm with varying concentrations of Gd_2O_3 with fixed Eu_2O_3 1.0 mol%.

To confirm the emission spectrum monitored at 614 nm, both excitation wavelengths ($\lambda_{Ex} = 275$ and 395 nm) were chosen to excite the glass samples, presented in Figure 6.6. The luminescence intensity increase with increasing Gd_2O_3 concentration by fixing Eu_2O_3 at 1.0 mol%. Whereas over 2.5 mol% of Gd_2O_3 causes the luminescence intensity to decrease. It is clearly shown that the optimum concentrations of Gd_2O_3 with the strongest emission in LAEUB host of glass are using 2.5 mol% Gd_2O_3 , providing the maximum luminescence intensity.

The luminescence lifetime curve for different concentrations of Gd_2O_3 in (LAEUB) glasses host series have been monitored at room temperature under excitation and emission wavelength 275 and 614 nm (Wantana et al., 2018), as illustrated in Figure 6.7(a). The emissions lifetime of the glass samples decreases (from 2.146 to 1.737 ms) with increasing Gd_2O_3 concentration which shows the energy transfer within the Gd_2O_3 . On the other hand, the higher concentration of Gd_2O_3 will significantly make the interaction between Gd^{3+} and Eu^{3+} ion. The energy transfer between the excited Gd^{3+} and Eu^{3+} ion is an event that occurs with high probability.

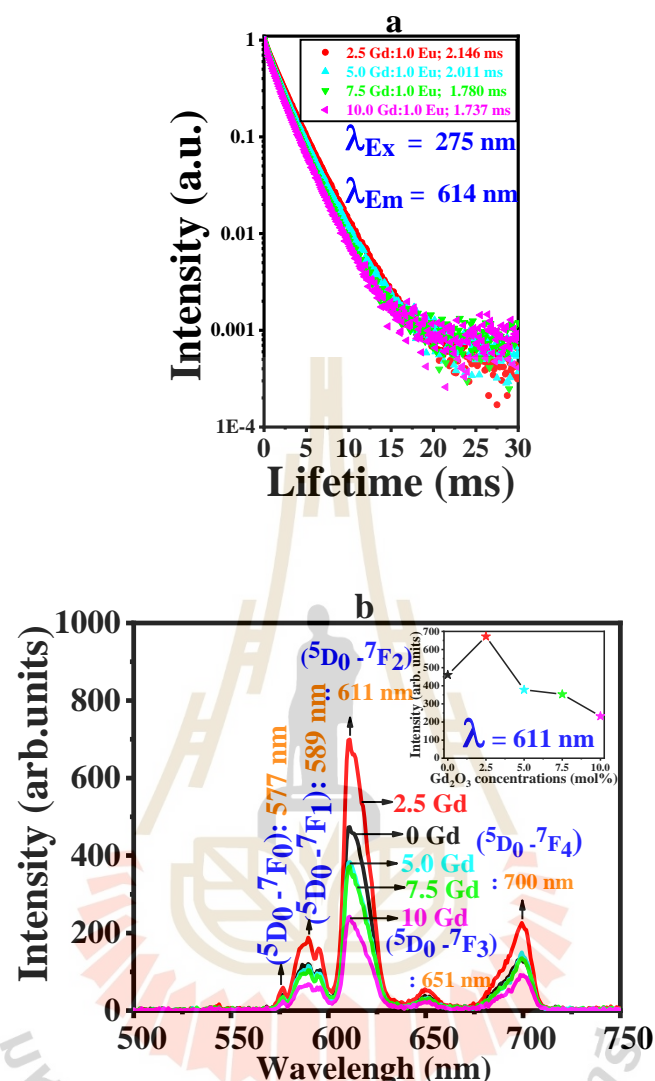


Figure 6.7 The decay rates (a) and X-ray induced luminescence (b) of 1.0 mol% Eu^{3+} ion in LAEUB series with varying concentrations of Gd_2O_3 system glasses.

The X-ray induced emission spectra of LAEUB host glass samples by using X-ray irradiation from a source operated with an energy of 50 keV and 30 mA is illustrated in Figure 6.7(b). The spectra contained a broad emission range of 400-800 nm, consist of 5 emission bands. Those wavelengths are similar to the results obtained in photoluminescence spectra with a little shift of peak position at the strong peak ~611 nm. This result could be explained by an incoming particle of ionizing radiation was trapped by some components in the LAEUB series. Then, the energy of the X-ray induces the electron to overcome the energy difference that contributed to the

ionization of glass samples. Moreover, relaxing or recombining the electron-hole releases the energy that eventually transfers to Eu^{3+} ions. It indicating LAEUB host of glass at 2.5 mol% concentration of Gd_2O_3 doped performs the best luminescence properties, which can be applied to be a scintillation material. Consequently, the Gd_2O_3 concentration of 2.5 mol% was chosen for the next experimental study.

6.3.2 Effect of Eu_2O_3 concentrations

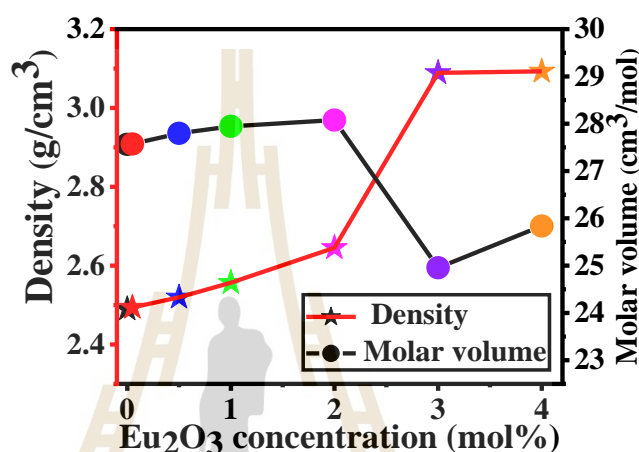


Figure 6.8 Density and molar volume relation of LAGB doped with Eu_2O_3 .

In the present study in Figure 6.8, the different values of the density (2.56 to $3.15 \text{ g}/\text{cm}^3$) of $25\text{Li}_2\text{O}-5\text{Al}_2\text{O}_3-2.5\text{Gd}_2\text{O}_3-(67.5-\text{Z})\text{B}_2\text{O}_3-\text{Z}\text{Eu}_2\text{O}_3$ (LAGB) with the increase of Eu_2O_3 concentration provides the great inline transmission with no visible coloration. The Eu_2O_3 ($\sim 352 \text{ g}/\text{mol}$) has heavier than B_2O_3 ($\sim 70 \text{ g}/\text{mol}$) so substituting B_2O_3 with Eu_2O_3 can occur, causing an increase in total molecular weight and glass density. The molar volume slightly increases from 27.59 to $28.11 \text{ cm}^3/\text{mol}$ with increasing Eu_2O_3 concentration while over $2.0 \text{ mol}\%$ the molar volume dramatically decreases from 28.11 to $24.92 \text{ cm}^3/\text{mol}$. We believe that the molar volume starts increasing at $3.0 \text{ mol}\%$ Eu_2O_3 content in glasses with starts bridging oxygen. The results show the increasing Eu_2O_3 contents can improve the compaction of the prepared glasses. The obtained glasses have transparent with no visible coloration and appeared homogeneous when examined visually in Figure 6.9.

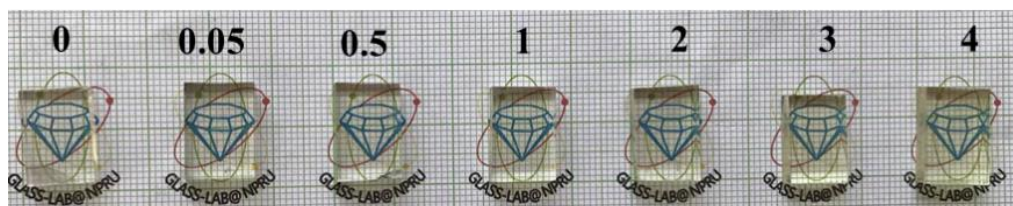


Figure 6.9 Photograph of glass samples with varying concentrations of Eu_2O_3 in $25\text{Li}_2\text{O}-5\text{Al}_2\text{O}_3-2.5\text{Gd}_2\text{O}_3-(67.5-Z)\text{B}_2\text{O}_3-Z\text{Eu}_2\text{O}_3$ (LAGB) glasses.

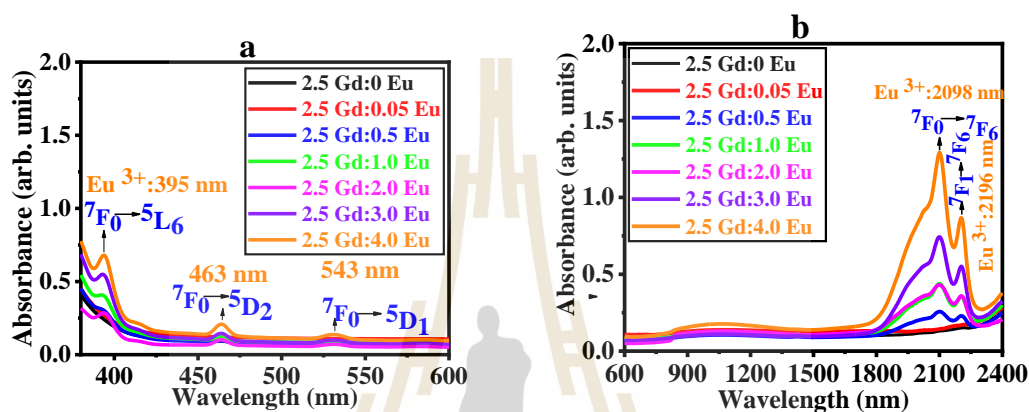


Figure 6.10 UV- Vis (a.) and NIR (b.) optical absorption spectra with different concentrations of Eu^{3+} doped LAGB glasses.

The absorption bands for LAGB glasses show the transitions from the ground state ${}^7\text{F}_0$ to different higher-level states. As shown in Figure 6.10(a, b), the various spectroscopic transitions observed are as follows: ${}^5\text{L}_6$ (395 nm), ${}^5\text{D}_2$ (463 nm), and ${}^5\text{D}_1$ (543 nm) for the UV-VIS range, and ${}^7\text{F}_6$ (2098 nm) and ${}^7\text{F}_6$ (2196 nm) for NIR range indicating with Eu_2O_3 variation in host matrix (Wantana et al., 2018). The increasing concentration of Eu_2O_3 contents demonstrates the intensity of all the transition increases. The transition from ${}^7\text{F}_0$ to ${}^5\text{L}_6$ provides the highest intensity and is hypersensitive for Eu^{3+} ion in the UV-Vis range.

The excitation spectra and emission spectra of Eu_2O_3 doped LAGB glasses by setup Gd^{3+} doped at 2.5 mol% (host) of glass samples and various concentrations of Eu_2O_3 , presented in Figure 6.11. Figure 6.11(a) shows the typical excitation spectra of Eu_2O_3 doped LAGB glasses, monitoring emission at 614 nm. A similar peak position of LAEUB series glass shows comparable results in Figure 6.5(a). The LAGB series without Eu_2O_3 doped (black line), disappeared a characteristic 4f-4f emission (broadband

situated below 227 nm) assigned to the Eu^{3+} charge transfer band (Zaman et al., 2018). A combination of a charging transfer transition (to $\text{Eu}^{3+}-\text{O}^{2-}$ charge transfer transition from a negative 2p orbit of oxygen to the empty 4f orbit of Eu^{3+}) is associated with the signature of broadband peaking at 227 nm. The emission spectra were evaluated as a function of Eu^{3+} ion concentrations by the exciting wavelength at 275 nm (for Gd^{3+}) and 395 nm (for Eu^{3+}) to investigate the emission spectra as shown in Figure 6.11(b, d).

Firstly, the emission spectra under direct excitation Gd^{3+} at 275 nm exhibit six bands at 312, 578, 590, 614, 652, and 701 nm were assigned to the ${}^6\text{P}_{7/2} \rightarrow {}^8\text{S}_{7/2}$, ${}^5\text{D}_0 \rightarrow {}^7\text{F}_0$, ${}^5\text{D}_0 \rightarrow {}^7\text{F}_1$, ${}^5\text{D}_0 \rightarrow {}^7\text{F}_2$, ${}^5\text{D}_0 \rightarrow {}^7\text{F}_3$, and ${}^5\text{D}_0 \rightarrow {}^7\text{F}_5$ transitions, respectively. In Figure 6.11(b) found the major emission peaks of Gd^{3+} at 312 nm and Eu^{3+} at 614 nm, which the maximum intensity of the emission peaks at 614 corresponds to the red emission of Eu^{3+} . It should be observed that the large band at 614 nm in this series glass is most likely composed of two superposed bands derived from Eu^{3+} ions (614 nm) and Gd^{3+} ions (624 nm). The emission at 624 nm may signal a lodged process of excited state absorption to ${}^6\text{G}_j$ levels of Gd^{3+} ions at 275 nm. LAGB glasses have an emission intensity of 312 nm (Gd^{3+}) as well as 614 nm (Eu^{3+}), as seen in Figure 6.11(c). The intensities of bands related to gadolinium transitions are reduced slightly, whereas the intensities of bands due to europium transitions increase significantly with increasing acceptor (Eu^{3+}) concentration, which shows that possible energy transfer from Gd^{3+} to Eu^{3+} occurred. The intensity of bands attributable to europium transitions increased at 614 nm, with a maximum intensity observed up to 3.0 mol%.

Secondly, the emission spectral under direct Eu^{3+} excitation at 395 nm in Figure 6.11(d) presents five bands assigned to the transition from ${}^5\text{D}_0$ to ${}^7\text{F}_j$ ($j = 0, 1, 2, 3,$ and 5) with excitation at 577, 590, 614, 652, and 700 nm (Zaman et al., 2018; Rajagukguk et al., 2016). The maximum intense exhibits at 614 nm red luminescence. The emission intensity increases with increasing Eu_2O_3 concentration and reaches maximum intensity at 3.0 mol%. Note that up to 3.0 mol% Eu_2O_3 leads to the emission decrease because influenced by concentration quenching phenomena.

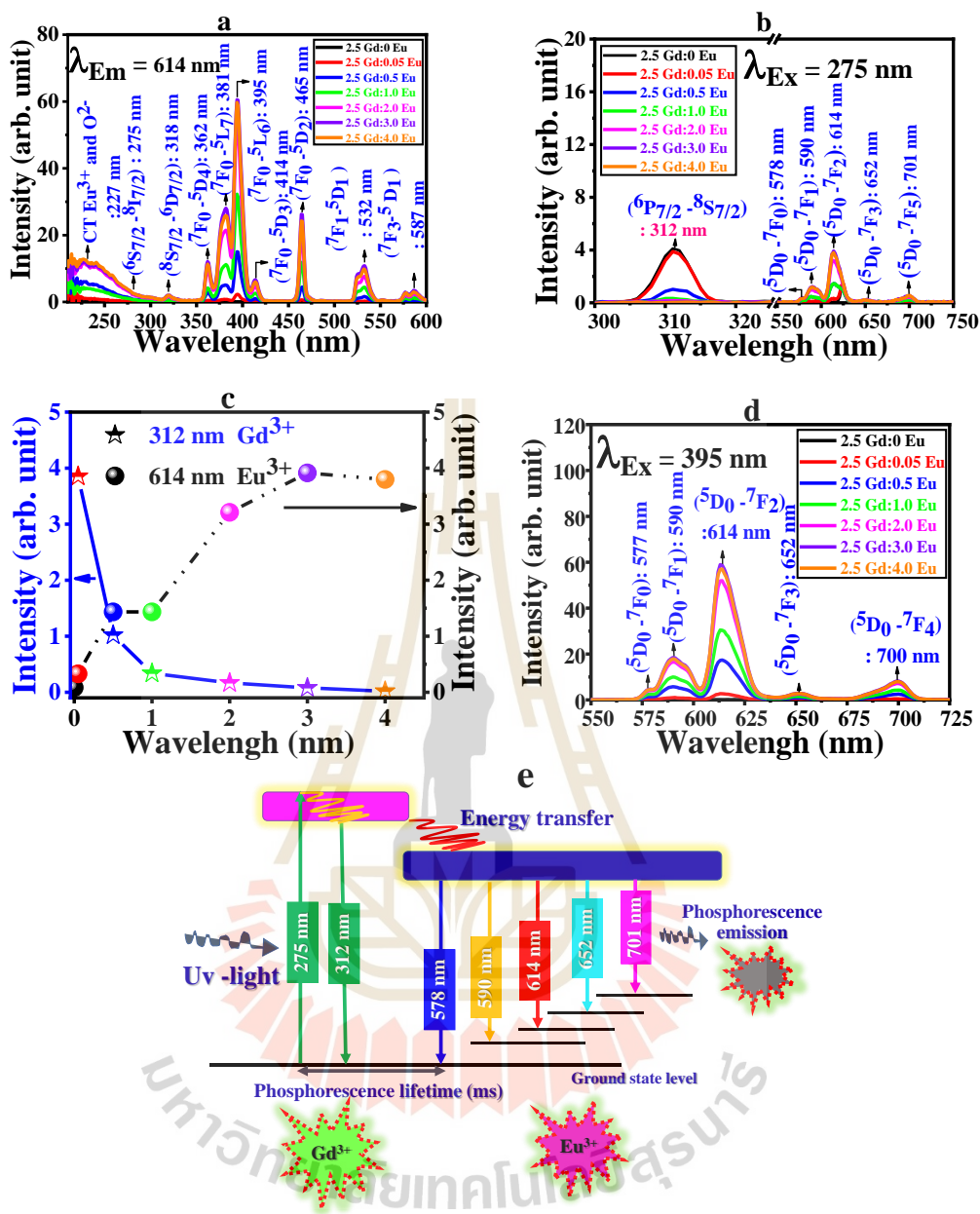


Figure 6.11 Excitation spectra (a), emission spectra $\lambda_{Ex} = 275$ (b, c), 395 nm (d) and energy level diagram (e) of LAGB glasses.

Moreover, Figure 6.11(e) depicts the schematic energy levels of Gd^{3+} to Eu^{3+} , which aids in understanding the energy transfer mechanism. The 6I_7 level of Gd^{3+} ion was initially populated upon 275 nm excitation. After non-radiative relaxation, the electrons should reach the $Gd^{3+} ^6P_{7/2}$ state, and the Gd^{3+} ions may return to the ground state in two ways. First, the Gd^{3+} ions in the $^6P_{7/2}$ state may transfer energy to the Eu^{3+} and the resonance energy transfer (ET) mechanism. Furthermore, Gd^{3+} ions in the

${}^6P_{7/2}$ state may emit through the ${}^6P_{7/2} \rightarrow {}^8S_{7/2}$ (ground state) transitions. In addition to the Eu^{3+} ions in Figure 6.11(e), the LAGB doped with Eu_2O_3 phosphor is stimulated at several wavelengths (577 nm, 590 nm, 614 nm, 652 nm, and 700 nm), and the Eu^{3+} ion is increased to distinct excitation levels from the ground level.

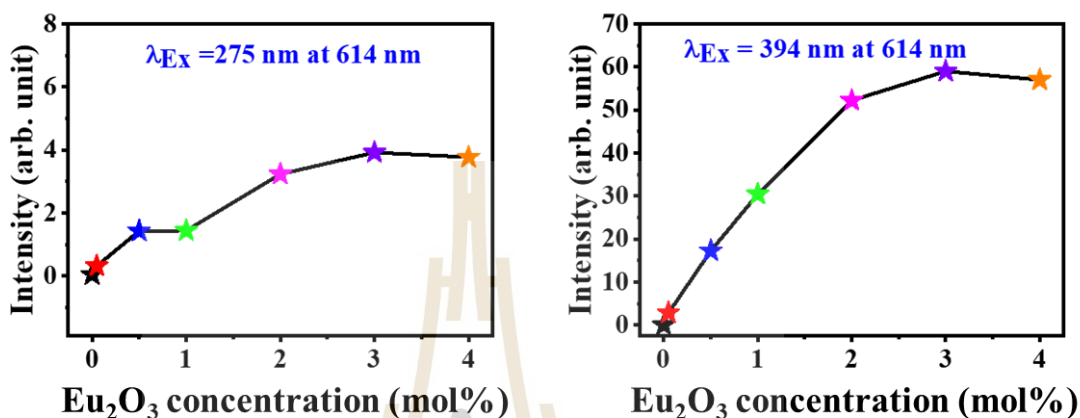


Figure 6.12 Relationship between the intensity of emission at 614 nm wavelength by excited 275 and 394 nm with varying concentration of Eu_2O_3 by fixed Gd_2O_3 2.5 mol%.

Figure 6.12, the photoluminescence of results of these emission signals can give useful information and confirm the concentration caused by concentration quenching conditions of Eu^{3+} ions in the LAEUB series. The emission spectrum monitored at 614 nm, under both excitation wavelengths ($\lambda_{\text{EX}} = 275$ and 394 nm) was chosen to excite the glass samples, presented in Figure 6.11(b, d). The appearance of the most intense band located at 614 nm is due to the main transitions from Eu^{3+} , which tend to increase with the increase of Eu^{3+} concentration. Whereas over 3.0 mol% of Eu_2O_3 causes the luminescence intensity to decrease. Both excitation wavelengths in the emission spectra clearly support the view that when the concentration of Eu_2O_3 is about 3.0 mol%. It was influenced by concentration quenching effect that provides Eu^{3+} emission intensities to decrease.

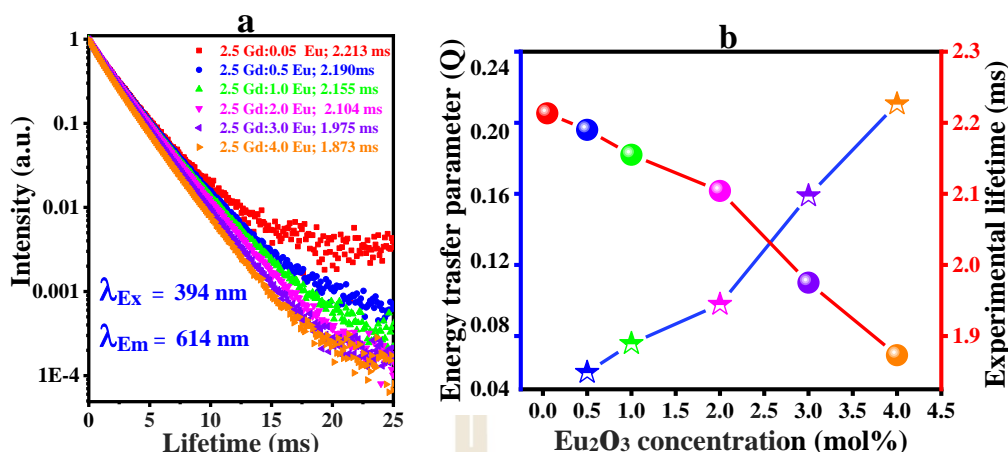


Figure 6.13 (a.) PL decay curves of LAGB series and (b.) variation of decay time, energy transfer parameter of $\text{Gd}^{3+} / \text{Eu}^{3+}$ codoped LAGB series glasses with Eu^{3+} concentration under $\lambda_{ex} = 394$ nm and $\lambda_{em} = 614$ nm.

The luminescence lifetime profiles were recorded for phosphor under excitation at $\lambda_{ex}=394$ nm and monitoring emission at $\lambda_{em}=614$ nm. The lifetime decay of $^5\text{D}_0$ level of Eu^{3+} -ions occurs in the red region in $25\text{Li}_2\text{O}-5\text{Al}_2\text{O}_3-2.5\text{Gd}_2\text{O}_3-(67.5-Z)\text{B}_2\text{O}_3-Z\text{Eu}_2\text{O}_3$ glasses doped with varying concentrations of Eu_2O_3 are presented in Figure 6.13(a). The observed decay curve values are decreased from 2.213 to 1.873 ms with an increase of Eu^{3+} concentration (in the order of millisecond) due to the characteristics of the $f \rightarrow f$ transition of Eu^{3+} given in Figure 6.13(a, b). While low concentrations of Eu_2O_3 provide a large average distance between different Eu^{3+} ions, leading to a low probability of $\text{Eu}^{3+} - \text{Eu}^{3+}$ energy transfer (Meert et al., 2014). It found that increasing Eu_2O_3 concentration causes a decrease in the intermolecular distance that can be increased the interaction between $\text{Eu}^{3+} - \text{Eu}^{3+}$ ions occurred. The energy transfer processes were studied, the non-exponential decay curves can be fitted to Inokuti-Hirayama (I-H) model (Inokuti et al., 1965). If there are higher concentrations of Eu^{3+} ions, it can be utilized to analyze the interaction between $\text{Eu}^{3+} - \text{Eu}^{3+}$ ions. As a result, the intensity of fluorescence decay can be given by following the Inokuti-Hirayama model using the equation (6.1).

$$I(t) = I_0 \exp\left\{-\frac{t}{\tau_0} - Q\left(\frac{t}{\tau_0}\right)^{3/5}\right\} \quad (6.1)$$

Where I_0 is the initial intensity at $t = 0$, t is time after excitation and τ_0 is intrinsic decay time of donors without the presence of acceptors, S is the multipolar interaction parameter, which when $S= 6, 8,$ and 10 corresponds to electrical dipole-dipole, dipole-quadrupole, and quadrupole-quadrupole interaction, respectively (in this work by taking $S = 6$), indicating dipole-dipole interaction between Eu^{3+} ions. During the fitting procedure of data at different Eu^{3+} concentrations, the parameter Q is the value of the direct donor to an acceptor, called the energy transfer parameter as shown in Figure 6.14(a, b, c, d, and e). The τ_0 values used in Eq. (6.1) correspond to the values under Eu^{3+} doped with 0.05 mol% conditions when there is no energy transfer ($Q=0$) and the experimental decay curves display flawless single exponential nature. The energy transfer parameter can be determined as follows equation (6.2).

$$Q = -\frac{4\pi}{3} \Gamma\left(1 - \frac{3}{S}\right) N_0 R_0^3 \quad (6.2)$$

where N_0 is the concentration of acceptors, which is almost equal to the total concentration of lanthanide ions, R_0 is critical energy transfer distance, which is the distance between donor and acceptor when the rate of energy transfer is equal to intrinsic decay and gamma function $\Gamma(X)$ can take on multiple values, for as dipole-dipole when $S = 6$ (Deopa et al., 2018) and $\Gamma(X) = 1.77$. The computed values of the multipolar interaction parameter S , as given in Table 6.1, can be roughly approximated to 6.

As discussed above in the case of higher concentration of Eu^{3+} ions in these glasses (Eu^{3+} concentrations ≥ 0.5 mol%: 0.5, 1, 2, 3, and 4 mol%), considering the non-exponential character of the decay is related to the interaction occurring between the active ions Eu^{3+} as shown in Figure 6.14(a, b, c, d, and e). For this reason, we have fitted this decay using I-H model. The decay curves for the Eu^{3+} (${}^5\text{D}_0 \rightarrow {}^7\text{F}_4$) transition show a non-exponential decay curves the values of energy transfer parameter (Q) that increases approximately linearly ($R^2 = 0.999$) behavior that is enhanced with increasing Eu^{3+} concentration (2.5Gd:0.5 Eu ($Q=0.05048$), 2.5Gd:1.0 Eu ($Q=0.06842$), 2.5Gd:2.0 Eu ($Q=0.09284$), 2.5Gd:3.0 Eu ($Q=0.16033$), and 2.5Gd:4.0 Eu ($Q=0.21755$)), verifies interactions mechanisms between dopant ions on a dipole-dipole basis (see table 6.1).

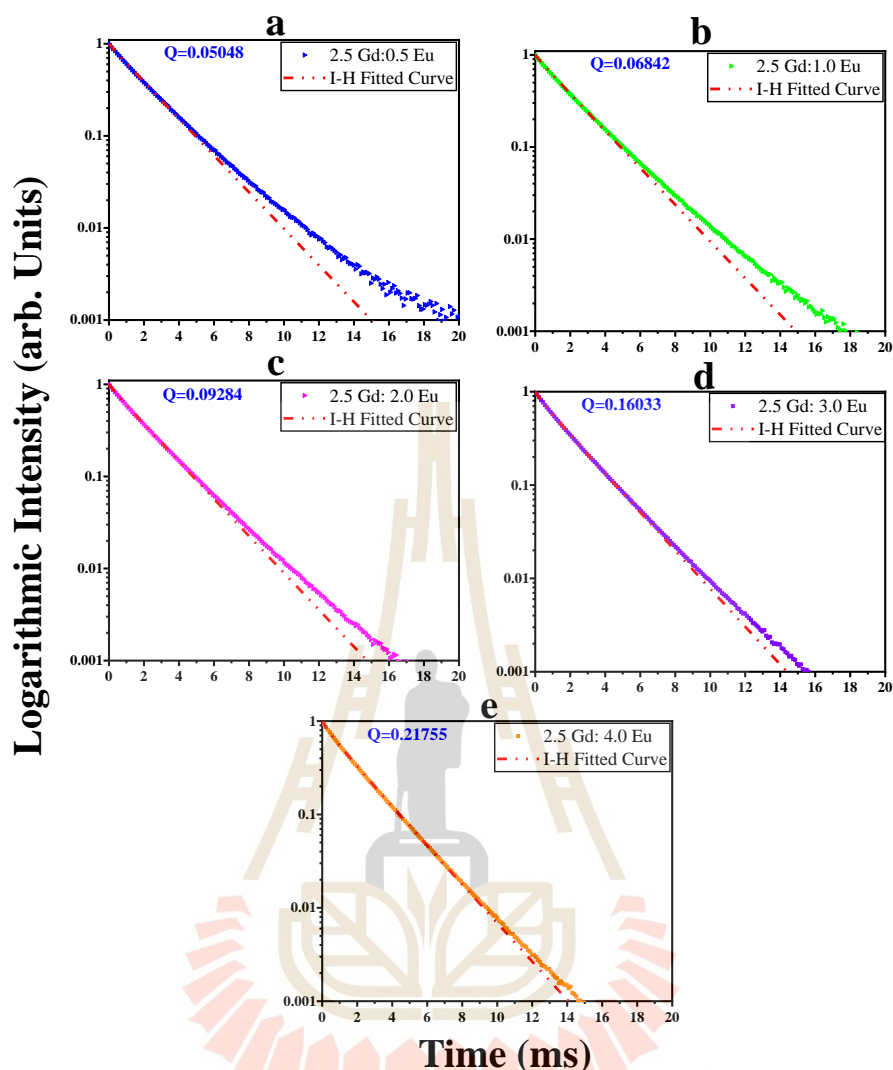


Figure 6.14 The decay spectral profiles of ${}^5D_0 \rightarrow {}^7F_2$ (614 nm) emission transition of Eu^{3+} ions in glasses series under 394 nm excitation along with I-H fitting curves.

The lifetime has one single exponential behavior at the lower Eu^{3+} concentration 0.05 mol% (2.213 ms), whereas the lifetime at a greater concentration of the other have non-exponential (2.190- 1.873 ms). Additional confirmation of the energy transfer from Gd^{3+} to Eu^{3+} is provided by this finding. Energy transfer is usually specified in terms of the exchange of dipole or multipole electric interactions between the donor (Gd^{3+}) and the acceptor (Eu^{3+}). Due to the development of resonant excitation energy movements between Eu^{3+} ions and hence some of the energy can be delivered in the quenching centers, a change from virtual single exponential to non-

exponential with increasing Eu^{3+} concentration might take place. One way of evaluating the energy transfer in the prepared series of glasses can be boosted up in the host glass, crucial for the persistent luminescence and calculated by using the Eq. (6.3) (Talewar et al., 2019):

$$\eta_{(\text{Eu}-\text{Eu})} = 1 - \tau_{x\text{Eu}} / \tau_{0\text{Eu}} \quad (6.3)$$

where $\eta_{(\text{Eu}-\text{Eu})}$ is the energy transfer efficiencies, where $\tau_{0\text{Eu}}$ is the lifetime of the Eu^{3+} in the sample with 0.05 mol% concentration, and $\tau_{x\text{Eu}}$ is the lifetime of Eu^{3+} with $x = 0.5-4.0$ mol% concentration. In Table 6.1, the energy transfer efficiency was found to be 1.03%, 2.62%, 4.92%, 10.75%, and 15.36%, whilst the amount of Eu_2O_3 increases between 0.5 to 4.0 mol%. Moreover, increased Eu^{3+} concentration may be caused by the resonant energy movement between Eu^{3+} to Eu^{3+} ions and provided the quenching center as well as the energy transfer parameter (Q) increases (Loos et al., 2017).

Table 6.1 The values of lifetime (τ_{exp} ; ms), energy transfer efficiencies (η), energy transfer parameter (Q), and R-square of ${}^5\text{D}_0 \rightarrow {}^7\text{F}_2$ (614 nm) transition of Eu^{3+} ions in LAGB glasses.

Name of sample	Ln^{3+} content mol%		τ_x (ms)	τ_0 (ms)	$\eta_{(\text{Eu}-\text{Eu})}$	Q	R-square
	Gd^{3+}	Eu^{3+}					
2.5Gd :0.05 Eu	2.5	0.05	2.213	2.213	-	-	-
2.5Gd : 0.5 Eu	2.5	0.5	2.190	2.213	1.03	0.05048	0.99941
2.5Gd : 1.0 Eu	2.5	1.0	2.155	2.213	2.62	0.06842	0.99958
2.5Gd : 2.0 Eu	2.5	2.0	2.104	2.213	4.92	0.09284	0.99998
2.5Gd : 3.0 Eu	2.5	3.0	1.975	2.213	10.75	0.16033	0.99989
2.5Gd : 4.0 Eu	2.5	4.0	1.873	2.213	15.36	0.21755	0.99906

In the final result, the glasses samples were excited with 275 and 394 nm for all the strong emissions in the red region, as shown in Figure 6.15 The emissions were used to analyze the color of emission, which indicates the Commission International de l'Eclairage (CIE) 1931 chromatic coordinates diagram (Kaewkhao et al., 2015). The

examination of CIE coordinates is (0.62, 0.35) and (0.64, 0.35) under excitation of $\lambda_{\text{ex}} = 275$ and 394 nm. Moreover, real naked-eye under UV-lamp excitation also observed the soft red-orange emissions of all the samples. The interesting inference is the emission that can be tuned to obtain required solid-state device applications for the samples depending upon the excitation.

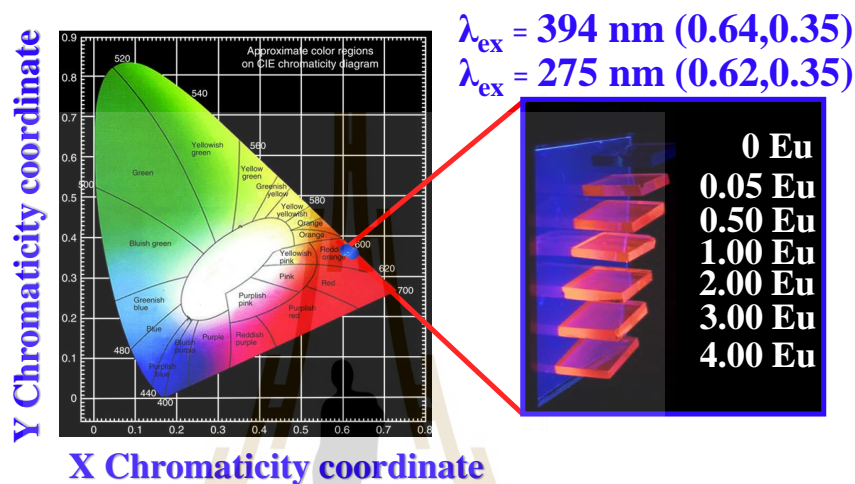


Figure 6.15 CIE coordinate diagram of $25\text{Li}_2\text{O}-5\text{Al}_2\text{O}_3-2.5\text{Gd}_2\text{O}_3-(67.5-Z)\text{B}_2\text{O}_3-\text{ZEu}_2\text{O}_3$ glasses doped with varying concentrations of Eu_2O_3 .

6.4 References

- Azizan, S. A., Hashim, S., Razak, N. A., Mhareb, M., Alajerami, Y., and Tamchek, N. (2014). Physical and optical properties of Dy^{3+} : $\text{Li}_2\text{O}-\text{K}_2\text{O}-\text{B}_2\text{O}_3$ glasses. *Journal of Molecular Structure*, 1076, 20:25.
- Azizan, S. A., Hashim, S., Razak, N. A., Mhareb, M., Alajerami, Y., and Tamchek, N. (2014). Physical and optical properties of Dy^{3+} : $\text{Li}_2\text{O}-\text{K}_2\text{O}-\text{B}_2\text{O}_3$ glasses. *Journal of Molecular Structure*, 1076, 20:25.
- Bergh, A., Craford, G., Duggal, A., and Haitz, R. (2001). The promise and challenge of solid-state lighting. *Physics today*, 54(12), 42-47.
- Cao, R., Lv, X., Jiaoa, Y., Rana, Y., Guoa, S., Aoa, H., Chena, T., and Fan, T. (2020). $\text{Ca}_3\text{La}_6\text{Si}_6\text{O}_{24}:\text{Eu}^{3+}$ orange-red-emitting phosphor: Synthesis, structure and luminescence properties. *Materials Research Bulletin*, 122, 110651.

- Cao, R., Liang, H., Chen, T., Wu, Z., Jiang, Z., Yi, X., and Wen, J. (2022). Study on luminescence characterizations of $\text{SrMg}_2\text{La}_2\text{W}_2\text{O}_{12}:\text{Eu}^{3+}$ red-emitting phosphor. *Journal of Physics and Chemistry of Solids*, 163, 110569.
- Deopa, N. and Rao, A. S. (2018). Spectroscopic studies of single near ultraviolet pumped Tb^{3+} doped lithium lead alumino borate glasses for green lasers and tricolour w-LEDs. *Journal of Luminescence*, 194, 56:63.
- Gaillard, C., Billard, I., Chaumont, A., Mekki, S., Ouadi, A., Denecke, M. A., Moutiers, G., and Wipff, G. (2005). Europium(III) and its halides in anhydrous room-temperature imidazolium-based ionic liquids: A combined TRES, EXAFS, and molecular dynamics study. *Inorganic Chemistry*, 44, 8355:8367.
- Gandhi, Y., Rajanikanth, P., Sundara Rao, M., Ravi Kumar, V., Veeraiah, N., and Piasecki, M. (2016). Effect of tin ions on enhancing the intensity of narrow luminescence line at 311 nm of Gd^{3+} ions in $\text{Li}_2\text{O}-\text{PbO}-\text{P}_2\text{O}_5$ glass system. *Optical Materials*, 57, 39-41.
- Hari Babu, B. and Ravi Kanth Kumar, V. V. (2016). Warm white light generation in γ -irradiated Dy^{3+} , Eu^{3+} codoped sodium aluminoborate glasses. *Journal of Luminescence*, 169, 16:23.
- Im, W. B., Fellows, N. N., Denbaars, S. P., Seshadri, R., and Kim, Y. (2009). $\text{LaSr}_2\text{AlO}_5$, A versatile host compound for Ce^{3+} -based yellow phosphors: structural tuning of optical properties and use in solid-state white lighting. *Chemistry of Materials*, 21, 2957:2966.
- Inokuti, M. and Hirayama, F. (1965). Influence of energy transfer by the exchange mechanism on donor luminescence. *The Journal of Chemical Physics*, 43, 1978:1989.
- Kaewkhao, J., Boonin, K., Yasaka, P., and Kim, H. J. (2015). Optical and luminescence characteristics of Eu^{3+} doped zinc bismuth borate (ZBB) glasses for red emitting device. *Materials Research Bulletin*, 71, 37:41.
- Kaewnuam, E., Kaewkhao, J., Wantana, N., Klysubun, W., Kim, H. J., and Sangwanate N. (2017). Comparative study of Sm^{3+} doped in $\text{Li}_2\text{O}_3-\text{RE}_2\text{O}_3-\text{B}_2\text{O}_3$ (RE = Y/La) glasses system for laser medium application. *Results in Physics*, 7, 3698:3703.

- Kaewnuam, E., Kim, H. J., and Kaewkhao, J. (2017). Development of lithium yttrium borate glass doped with Dy^{3+} for laser medium, W-LEDs and scintillation materials applications. *Journal of Non-Crystalline Solids*, 464, 96:103.
- Kalpana, T., Brik, M. G., Sudarsan, V., Naresh, P., Ravi Kumar, V., Kityk, I. V., and Veeraiah, N. (2015) Influence of Al^{3+} ions on luminescence efficiency of Eu^{3+} ions in barium boro-phosphate glasses. *Journal of Non-Crystalline Solids*, 419, 75:81.
- Kalpana, T., Gandhi, Y., Bhaskar, S., Sudarsan, V., Bragiel, P., Piasecki, M., Ravi Kumar, V., and Veeraiah, N. (2016). Influence of alumina on photoluminescence and thermoluminescence characteristics of Gd^{3+} doped barium borophosphate glasses. *Journal of Luminescence*, 179, 44:49.
- Korthout, K., Parmentier, A. B., Smet, P. F., and Poelman, D. (2013). A XAS study of the luminescent Eu centers in thiosilicate phosphors. *Physical Chemistry Chemical Physics*, 15, 8678:8683.
- Loos, S., Mungra, M., Ahrens, B., Leonard, R. L., Evans, A., Johnson, J. A., and Schweizer, S. (2017). Concentration- dependent luminescence and energy transfer in Tb^{3+}/Eu^{3+} doped borate and fluorozirconate glasses. *Journal of Luminescence*, 187, 298:303.
- Meert, K. W., Morozov, V. A., Abakumov, A. M., Hadermann, J., Poelman, D., and Smet, P. F. (2014). Energy transfer in Eu^{3+} doped scheelites: use as thermographic phosphor. *Optics Express*, 22, A961.
- Pawar, P. P., Munishwar, S. R., and Gedam, R. S. (2016). Physical and optical properties of Dy^{3+}/Pr^{3+} Co-doped lithium borate glasses for W-LED. *Journal of Alloys and Compounds*, 660, 347:355.
- Ragab, M., Mahani, Y., Samir, Y., and Marzouk, A. (2013). AC conductivity and dielectric properties of $SiO_2-Na_2O-B_2O_3-Gd_2O_3$ glasses. *Journal of Alloys and Compounds*, 579, 394:400.
- Rahimi, M., Zahedifar, M., Azimirad, R., and Faeghinia, A. (2020). Luminescence and scintillation properties of Eu^{2+} doped CaF_2 glass ceramics for radiation spectroscopy. *Journal of Luminescence*, 221, 117040.

- Rajagukguk, J., Kaewkhao, J., Djamel, M., Hidayat, R., and Ruangtaweep, Y. (2016). Structural and optical characteristics of Eu^{3+} ions in sodium-lead-zinc-lithium-borate glass system. *Journal of Molecular Structure*, 1121, 180:187.
- Rajesh, D., Ratnakaram, Y. C., Seshadri, M., Balakrishna, A., and Satya Krishna, T. (2012). Structural and luminescence properties of Dy^{3+} ion in strontium lithium bismuth borate glasses. *Journal of Luminescence*, 132, 841:849.
- Ramteke, D. D. and Gedam, R. S. (2014). Luminescence properties of Gd^{3+} containing glasses for ultra-violet (UV) light. *Journal of Rare Earths*, 32, 389:393.
- Selvi, S., Venkataiah, G., Arunkumar, S., Muralidharan, G., and Marimuthu, K. (2014). Structural and luminescence studies on Dy^{3+} doped lead boro-telluro-phosphate glasses. *Physica B: Condensed Matter*, 454, 72:81.
- Swapna, K., Mahamuda, S. K., Srinivasa Rao, A., Sasikala, T., Packiyaraj, P., Rama Moorthy, L., and Vijaya Prakash, G. (2014). Luminescence characterization of Eu^{3+} doped Zinc Alumino Bismuth Borate glasses for visible red emission applications. *Journal of Luminescence*, 156, 80:86.
- Talewar, R. A., Mahamuda, S., Swapna, K., and Rao, A. S. (2019). Near UV based Dy^{3+} ions doped alkaline-earth chloro borate glasses for white LED's and visible lasers. *Optics & Laser Technology*, 119, 105646.
- Wantana, N., Kaewnuam, E., Damdeeu, B., Kaewjaeng, S., Kothand, S., Kim, H. J., and Kaewkhao, J. (2018). Energy transfer based emission analysis of Eu^{3+} doped Gd_2O_3 - CaO - SiO_2 - B_2O_3 glasses for laser and X-rays detection material applications. *Journal of Luminescence*, 194, 75:81.
- Wantana, N., Kaewnuam, E., Ruangtaweep, Y., Kidkhunthod, P., Kim, H. J., Kothan, S., and Kaewkhao, J. (2020). High density tungsten gadolinium borate glasses doped with Eu^{3+} ion for photonic and scintillator applications. *Journal of Radiation Physics and Chemistry*, 172, 108868.
- Zaman, F., Rooh, G., Srisittipokakun, N., Wongdeeying, C., Kim, H. J., and Kaewkhao, J. (2018). Physical, structural and luminescence investigation of Eu^{3+} -doped lithium-gadolinium bismuth-borate glasses for LEDs. *Solid State Sciences*, 80, 161:169.

CHAPTER VII

TERBIUM DOPED BORATE GLASS

In this study, we developed the luminescence properties of Tb³⁺ and Gd³⁺ dual doped 25Li₂O- 5Al₂O₃- YGd₂O₃- (70- Y- Z) B₂O₃- ZTb₂O₃ glasses were prepared by a conventional melt-quenching method. As the concentrations of Gd³⁺ increase, both the radioluminescence and photoluminescence results increase, and then 2.5% Gd³⁺ doped glass sample under excitation wavelength with 222, 275, 377 nm providing the strong green emission intensity (at 543 nm) due to the optimum concentration happens. Analysis of the Tb L_{III}-edge XANES spectra data of LABT series glasses have confirmed the presence of Tb³⁺. The PL band with the highest intensity of Tb³⁺ ion in this glass is 4.0 mol% as it results from a maximum of both emission and excitation intensity. The experimental decay times calculated from the decay profiles have been observed to be declining gradually from 2.682 to 2.450 ms with the increase in Tb³⁺ ion concentration. The energy transfer in the borate glass from Gd³⁺ to Tb³⁺ is carried out by non-radiative processes with an efficiency close to 59.199%. The synthesized glass exhibits a high potential candidate for green luminescence applications.

7.1 Introduction

Glasses doped with rare-earth (RE) ions implanted in the luminescent host have been extensively studied in experimental and industrial processes (Bergh et al., 2001; Farouk et al., 2013). In the present study, we have chosen these glasses doped with rare-earth (RE) ions because of their prominent properties such as simple large-scale preparation, excellent mechanical strength, high variability in chemical composition, flexibility to add the active ion concentration, and high rare-earth solubility (Sun et al., 2010; Zhang et al., 2015). The variation of the physical properties, absorbance, fluorescence lifetime, photoluminescence, and radioluminescence properties of these

glasses are reported and discussed in the present work. Many glass systems hosts have been under the active research in the field of RE ion for many years. We can summary majority type of glass are following: soda-lime glass, borosilicate glass, lead glass, phosphate glass, chalcogenide glass, opal glass, glass-ceramics and borate glass. In this article, search for novel hosts, borate glasses (Singh et al., 2014) can be acknowledge as a good host to enhance optical properties within borate glass systems. We will introduce the glass system borate (B_2O_3) network formers (Shaaban et al., 2018) have got special candidate host for doped rare-earth ion due to higher bond strength, low dispersion, small cation size (valency = 3 of boron), low heat of fusion, good transparency, low refractive indices from the ultraviolet to near-infrared regions, good rare-earth ion solubility (Shaaban et al., 2018; Kaewnuam et al., 2017; Ibrahim et al., 2018) and better chemical stability and durability compared to many other hosts systems. We also believe that borate combined with lithium and aluminum oxides form of glass (Deopa et al., 2018; Singh et al., 2008; Aboutaleb et al., 2015) is a good stable host because adding alkaline oxide will boost many of the characteristics and conditions of preparation such as decreasing melting temperatures and improving chemical resistance. So that lithium is an important alkali cation and an important modifier is aluminum oxide. Moreover, special interest has been used as the gadolinium oxide (Kesavulu et al., 2016; Ragab et al., 2013; Zaman et al., 2016) additive to increase luminescence intensity and increase the efficient energy transfer between luminescence activators.

In designing new RE^{3+} optical applications, the choice of the appropriate host matrix and RE^{3+} ion is crucial. For other RE^{3+} with co-doped compounds have been paid on Dy^{3+} (Shamshad et al., 2017), Sm^{3+} (Ullah et al., 2021), Eu^{3+} (Wantana et al., 2018) doped gadolinium oxide component. So, when exposed to UV or X-rays, the light yield of trivalent rare-earth oxide-doped glasses will significantly increase due to energy conversion from Gd^{3+} to these ions of borate glass system. In particular, though, Gd^{3+} only serves as a sensitizer exhibits heavy linear luminescence due to the $4f-4f$ transformation as well as a high light yield in a variety of host materials (Ragab et al., 2013). That is maybe because of its basic electronic energy level scheme (the electron configuration of Gd: $[Xe] 4f^7 5d^1 6s^2$). Therefore, the Gd^{3+} ion contains seven unpaired

electrons that can be used as a spectroscopic examination for host-dopant energy transfer processes (Zaman et al., 2016; Shamshad et al., 2017). In addition, trivalent terbium (Tb^{3+}) ion-doped materials (Zu et al., 2021) as the optically active ions play a double role when a second rare-earth ion was introduced to the glass host. In the later system, was very interested in your research work such as i.e. Tb^{3+} - Eu^{3+} (Pisarska et al., 2014; Loos et al., 2017), Dy^{3+} - Tb^{3+} (Lakshminarayana et al., 2014; Pisarska et al., 2014) (the phenomenon of energy transfer from in lead borate glass occurs through a nonradiative process with an efficiency up to 16-18%). Trivalent Terbium (Tb^{3+}) is an effective ion that releases strong green light (around 545 nm) through its 5D_3 to 7F_5 transition with millisecond decay time (Yao et al., 2016). Numerous glasses co-doped with Gd^{3+}/Tb^{3+} (Sun et al., 2015) were investigated for obtaining the green color (Tb^{3+}) light through appropriate combinations of these luminescence properties that are useful in the color displays and light emitting diodes. Furthermore, they are also promising materials for green luminescence applications.

In this work, we were starting materials used for host glass preparation present for optimized Gd_2O_3 concentration of 2.5 mol% and a fixed concentration of Tb_2O_3 using as a 1.0 mol%. After that, we developed the lithium aluminum gadolinium borate glasses doped with Tb^{3+} to select the right proportion of dopant ions in a suitable luminescence glass. The chemical composition of $25Li_2O-5Al_2O_3-2.5Gd_2O_3-(67.5-Z)B_2O_3-ZTb_2O_3$ series glasses were prepared to study in the physical, chemical group, optical, photoluminescence, and radioluminescence properties. The influence of Tb_2O_3 concentration on these properties was also investigated to evaluate the optimum chemical composition of glass for the candidate for green-emitting luminescent devices.

7.2 Experimental

7.2.1 Preparation of Gd_2O_3 doped

Series of lithium aluminum borate glasses samples singly and doubly doped with Gd^{3+} and Tb^{3+} ions were prepared by mixing and melting appropriate amounts of Li_2CO_3 , H_3BO_3 , Gd_2O_3 , Al_2O_3 and Tb_2O_3 of high purity as starting materials. Firstly, a series

of $25\text{Li}_2\text{O}-5\text{Al}_2\text{O}_3-\text{YGd}_2\text{O}_3-(69-\text{Y})\text{B}_2\text{O}_3-1\text{Tb}_2\text{O}_3$ glasses with difference Y from 0, 2.5, 5.0, 7.5, and 10.0 mol% of composition so call the LATB glasses series of the host matrix.

7.2.2 Preparation of Tb_2O_3 doped

Then secondly, the glass samples of chemical composition $25\text{Li}_2\text{O}-5\text{Al}_2\text{O}_3-2.5\text{Gd}_2\text{O}_3-(67.5-\text{Z})\text{B}_2\text{O}_3-\text{ZTb}_2\text{O}_3$ (where, Z = 0, 0.1, 0.5, 1.0, 1.5, 2.0, 3.0, and 4.0 mol%) designated name as LAGB glasses with varying concentration of Tb_2O_3 . Both glasses systems were prepared by the conventional melt quenching technique as shown in Figure 7.1 In the process, about 20 g batches were mixed thoroughly by grinding in an alumina crucible. The well-mixed powder was melted in an electrical furnace. Then, they were melted at $\sim 1200^\circ\text{C}$ for 90 minutes. After that, the glass melt was poured onto a graphite plate followed by annealing at 500°C for 3 hours to relieve thermal stress and cooled slowly to room temperature and then on the polishing machine ($1.0 \times 1.5 \times 0.3 \text{ cm}^3$) to obtain a transparent glass sample of uniform thickness. From the final glass materials at room temperature, their densities were first measured according to a simple Archimedes method using water as an immersion liquid and then molar volumes were calculated via a 4-digit sensitive microbalance (AND, HR 200). The fully amorphous and transparent glass samples were obtained, which was confirmed by X-ray diffraction analysis using the power X-ray diffraction: PXRD (Bruker D2 diffractometer with Cu- $K\alpha$ radiation). The optical absorption spectra of polished samples are measured with a UV-vis and NIR spectrophotometer (Shimadzu UV-3600) in the wavenumber range 200-2500 nm. The excitation and emission spectra, as well as decay measurements, were recorded using a spectrofluorophotometer (Cary-Eclipse) with a Xenon flash lamp as an excitation light source in the 200–800 nm wavelength region, recorded at room temperature. The X-ray luminescence spectra were measure by an experimental set up consisting of Cu target x-ray generator (Inel, XRG3D-E), fiber optic spectrometer (Ocean Optics, QE65 Pro), and brass sample holder. Glass was radiated by X-ray induced optical luminescence (XOL) spectra were measured Cu target Xray generator (Inel XRG3D-E) which was operated at 50 kV and 30 mA power equipped with an Ocean Optics QE65 Pro spectrometer. The oxidation state of Tb was evaluated by performing XANES spectroscopy on the as-prepared samples using at Synchrotron Light Research Institute (beamline 5.2). The data were collected in the fluorescence

mode over the Tb L_{III} edge. A standard of terbium oxide (Tb_2O_3) was used as the reference sample. All measurements were carried out at room temperature.

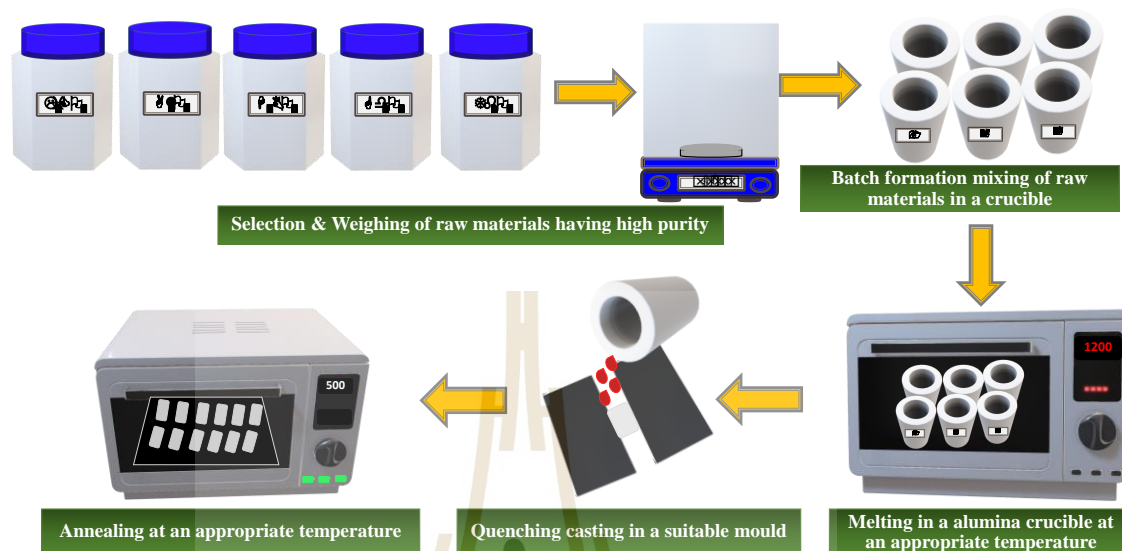


Figure 7.1 Glass Manufacturing Process.

7.3 Result and discussion

We created borate glass of the composition $25Li_2O-5Al_2O_3-XGd_2O_3-(69.0-X)B_2O_3-1.0Tb_2O_3$ so-called LATB and $25Li_2O-5Al_2O_3-2.5Gd_2O_3-(67.5-Z)B_2O_3-ZTb_2O_3$, LAGB glass series. Figure 7.2 shows images of optically polished Gd_2O_3 doped LATB glasses. It easily sees the change in the component of the glasses with doping observed that shades color of the glass sample changes from colorless to light soft yellow with the addition of Gd_2O_3 up to 10 mol%, we may have noticed that some areas start with white spots, stope doped due to the limits of the milky effect.

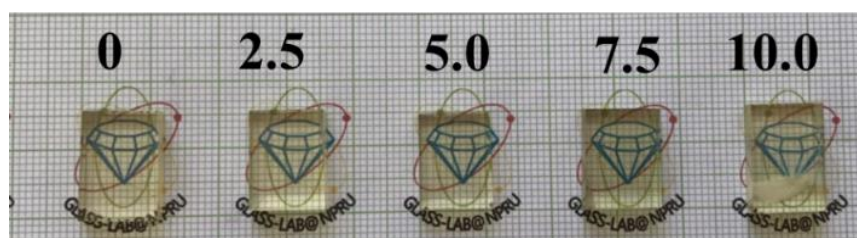


Figure 7.2 Cut and polished $25Li_2O-5Al_2O_3-XGd_2O_3-(69.0-X)B_2O_3-1.0Tb_2O_3$ glass sample from 0 to 10 mol% of Gd_2O_3 doped borate glass.

The physical properties such as density and molar volume were used to evaluate the level of structure compactness. Figure 7.3(a, b) displays that both parameters (density and molar volume) of the glass sample tend to increase with the increase of Gd_2O_3 and Tb_2O_3 concentrations. We believe that there is a change in the structural arrangement of the atoms with trivalent rare earth (Gd^{3+} and Tb^{3+}) addition in the $Li_2O: Al_2O_3: B_2O_3$ network. Borate can be replaced by gadolinium and terbium oxide due to the density of glass is like a total atomic mass of trivalent rare-earth ion as compared to other oxide components in glass accordingly, the substitution of B_2O_3 (Mw = 69.6202 g/mol) by Gd_2O_3 (Mw = 336.4822 g/mol) and Tb_2O_3 (Mw = 365.8488 g/mol) occur resulting in increasing the sample's overall molecular weight. In addition, this presented that the Gd^{3+} and Tb^{3+} ions in the glass broke bonds between boron and oxygen in its network, this so-called non-bridging oxygen (nBOs).

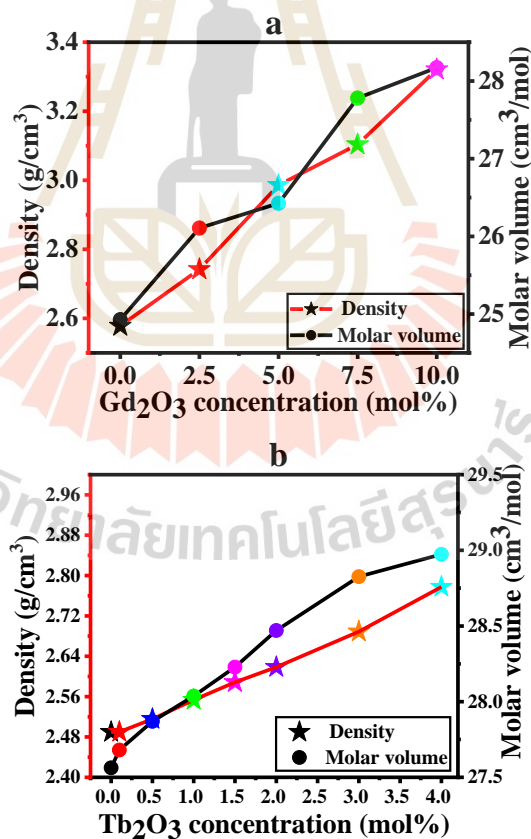


Figure 7.3 Densities and molar volume of lithium aluminum gadolinium-terbium borate glasses doped with different Gd_2O_3 (a) and Tb_2O_3 (b) concentrations.

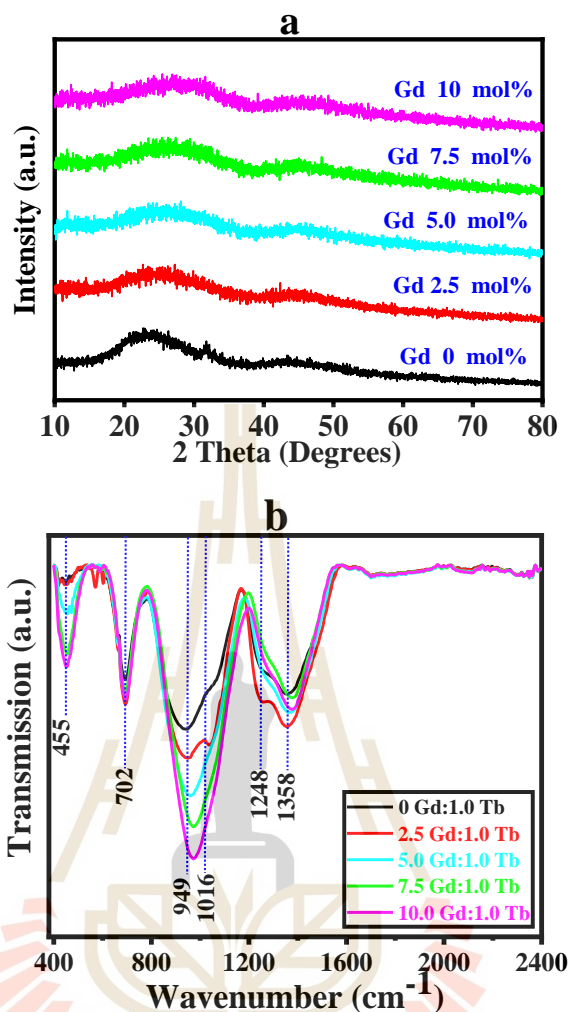


Figure 7.4 (a) X-ray diffraction and (b) FTIR spectra for the prepared LATB glass samples doped with different Gd_2O_3 concentrations.

The XRD pattern of the sample prepared LATB glass sample matrix was monitored in the range $10\text{--}80^\circ$ (2θ), as shown in Figure 7.4(a). The confirmations of the non-crystalline behavior of these glasses were determined using the XRD pattern. The XRD spectrum is absent only humps around in $18^\circ\text{--}50^\circ$ region and does not show any sharp Bragg peaks. This indicates that the prepared glasses host sample has a purely amorphous nature (Wantana et al., 2019).

Figure 7.4(b) presents the FTIR spectra of the prepared glass sample. Frequencies and assignments for FTIR spectra of the prepared glasses were confirmed around 455 , 702 , 949 , 1016 , 1248 , and 1358 cm^{-1} . The first of the vibrations part, absorbed infrared with 455 cm^{-1} wave number was used to bending vibrate of Li^+ ions

with glass network appear between 410-625 cm^{-1} (Azizan et al., 2014), assigned the vibrations of lithium in their oxygen linkage, exhibited in Figure 7.4(b). The shape of obtained spectra (at 702 cm^{-1}) increased with increasing Gd_2O_3 was used to bending vibrate the B-O-B linkage of trigonal BO_3 borate groups (Gedam et al., 2011). The stretching vibrations of B-O bonds of tetrahedral BO_4 units and NBO vibrations in glass network own the infrared absorption a huge kink was observed at 971 cm^{-1} this vibration tends to have more strength with rising of Gd_2O_3 concentration which corresponds to the increment of glass molar volume explained about the NBO number addition (Dalal et al., 2015). A tiny sharp band was observed at 1,248 and 1,358 cm^{-1} infrared represents the B-O stretching vibration of BO_3 units in pentaborate, pyroborate, orthoborate groups and the presence of asymmetric B-O stretching vibrations of BO_3 and BO_2O unit (Kaur et al., 2014; Thakur et al. 2015). All FTIR results point out that the BO_3 and BO_4 borate groups are the main structural unit in the glass system.

The room temperature excitation spectra of the LATB series glass samples are measured by monitoring the emission wavelength at 543 nm (Fig.5(a)). The Tb^{3+} doped in this glass are shown emitted bright green light under 275, 377, and 222 nm excitation. As can be seen from Figure 7.5(a), the excitation spectra of all the LATB glass series present peaks at 222, 275, 311, 341, 352, 370, 377, and 488 nm (Wantana et al., 2019) are related to the transitions of 4f-5d, ${}^6S_{7/2} \rightarrow {}^8I_{7/2}$, ${}^6S_{7/2} \rightarrow {}^6P_{7/2}$, ${}^7F_6 \rightarrow {}^5L_6$, ${}^7F_6 \rightarrow {}^5L_9$, ${}^7F_6 \rightarrow {}^5L_{10}$, ${}^7F_6 \rightarrow {}^5G_6 + {}^5D_3$, and ${}^7F_6 \rightarrow {}^5D_4$, respectively. Therefore, Figure 7.5(a) gives a variation of the excitation luminescence peaks were observed as two prominent signature peaks of Gd^{3+} ions in the host glasses at 275 (${}^8S_{7/2} \rightarrow {}^6I_j$) and 311 nm (${}^8S_{7/2} \rightarrow {}^6P_j$). Additionally, the other five transitions of Tb^{3+} ions can be assigned to main transitions from ground state 7F_6 to the higher-lying excited states 5D_3 (377 nm), 5D_4 (488 nm). A series of sharp excitation bands in the wavelength from 250 to 500 nm corresponds to the Tb^{3+} Intra-4f ($4f^8 - 4f^8$) transitions. The significant phenomena happen when this finding is compared with conventional Tb-doped phosphors. The extraordinary transition band 4f-5d of the Tb^{3+} ion can be observed on the excitation spectra of about 222 nm (Li et al., 2007). This occurrence is peculiar because the typical Tb-activated phosphor material glass often exhibits a high 4f-5d transition band

absorption of about 200-300 nm. Figure 7.5(b, c, and d) presents the emission spectra of LATB glasses series obtained by exciting at 275, 377, and 222 nm shows a strongest emission peak at 543 nm (green color), which is characteristic of $^5D_4 \rightarrow ^7F_5$ transition of Tb^{3+} ions of the host matrix. Among emission spectra were measured by exciting at 275 nm indicates the emission spectra in various Gd_2O_3 content as labeled in Figure 7.5(b). The emission peaking at 311nm corresponds to the $^6P_{7/2} \rightarrow ^8S_{7/2}$ transitions of Gd^{3+} ion energy level in UV region and other peaks belong to the characteristic emission of Tb^{3+} ion consist of four prominent bands at 488, 543, 586, and 620 nm were assigned to the $^5D_4 \rightarrow ^7F_6$, $^5D_4 \rightarrow ^7F_5$, $^5D_4 \rightarrow ^7F_4$ and $^5D_4 \rightarrow ^7F_3$ (Valieva et al., 2015) transitions, respectively. It found that the green emission of Tb^{3+} ion is greatly improved by Gd^{3+} ion doping and then the emission bands of Gd^{3+} (311 nm) decrease with increasing of Tb^{3+} ion concentration. These findings suggest that successful energy transfers are rendered into glasses from the host Gd^{3+} to dopant Tb^{3+} ion (Kesavulu et al., 2017). Some part of the absorption energy of Gd^{3+} ions has been emitted as a 311 nm light line emission. The other part of the energy transition from Gd^{3+} to Tb^{3+} ion has been contributed. Figure 7.5(c, d) describes the emission curve of the sample, fixing the excitation wavelength at 377 nm 222 nm. The spectrum displays a series of emission lines ascribed to the similar to the 275 nm emission band except for the sharp characteristic of Gd^{3+} ions at 311 nm. These data indicated that the emission intensity of Tb_2O_3 increases with increasing Gd_2O_3 concentration until 2.5 mol%, it slightly decreases. Hence, the optimum concentration of Gd_2O_3 content at 2.5 mol% was chosen.

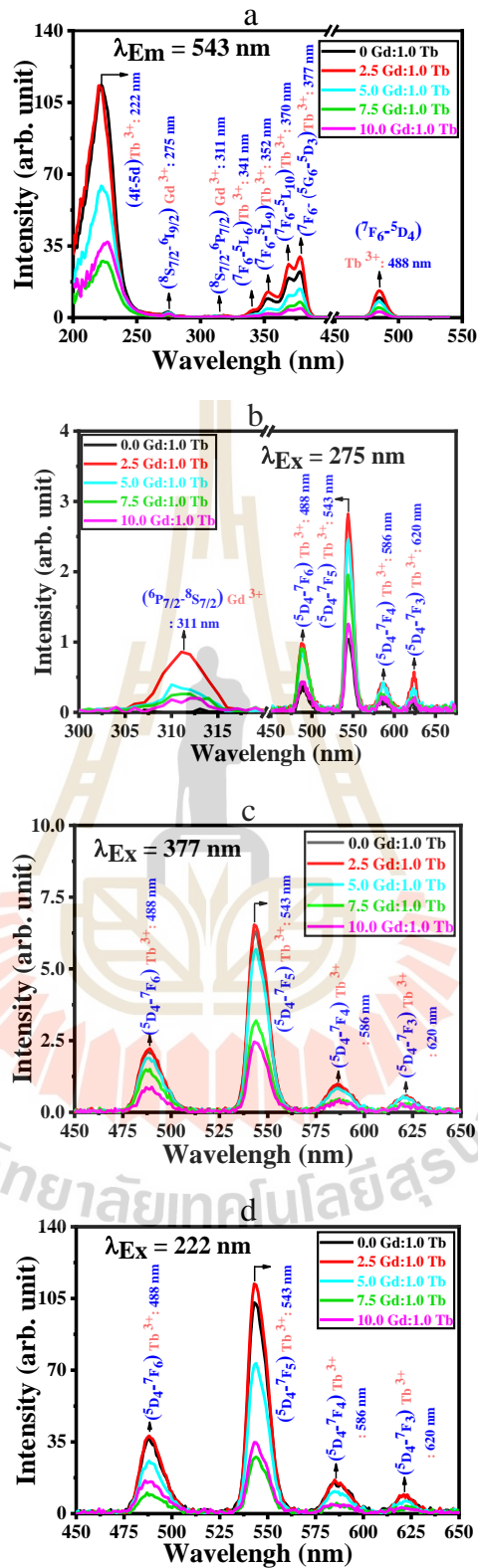


Figure 7.5 Photoluminescence spectra for Gd³⁺ and Tb³⁺ dual doped borate glass systems with different Gd₂O₃ concentrations.

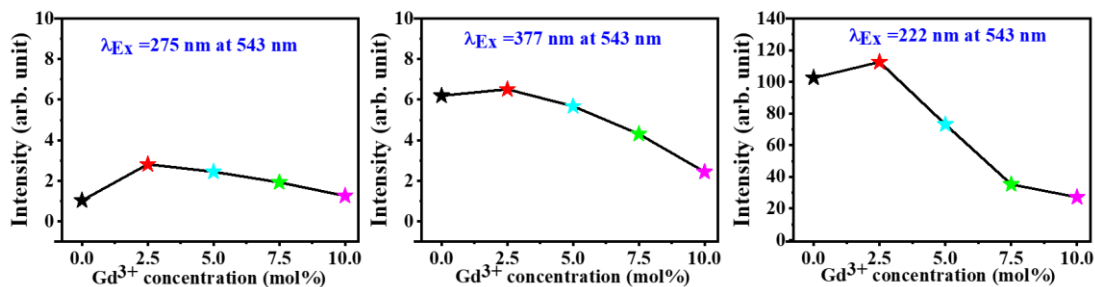


Figure 7.6 The emission spectra ($\lambda_{\text{ex}} = 222, 275, \text{ and } 377 \text{ nm}$) for Gd^{3+} and Tb^{3+} dual doped borate glass for different concentrations.

Figure 7.6 represents a variation of photoluminescence intensity with the Gd_2O_3 concentrations, the excitation spectra of Gd^{3+} and Tb^{3+} co-doped glass sample monitoring the emission wavelength (λ_{em}) with 543 nm and emission spectra under 3 excitations wavelength at $\lambda_{\text{ex}} = 222, 275, \text{ and } 377 \text{ nm}$ are introduced to the glass hosts in order to improve luminescence properties of Tb^{3+} , additional Gd^{3+} ions are usually incorporated in the glass host. The results clearly show the strongest intensity of emission spectra ($\lambda_{\text{ex}} = 222, 275, \text{ and } 377 \text{ nm}$) belongs to 543 nm ($^5\text{D}_4 \rightarrow ^7\text{F}_5$; green emission), increasing the emission output with the increase of Gd^{3+} concentration up to 2.5 mol%. Due to the optimum concentration, the energy transfer takes place among Tb^{3+} ions. In order to further enhance the luminescence of Tb^{3+} , additional Gd^{3+} ions are usually incorporated in the glass host.

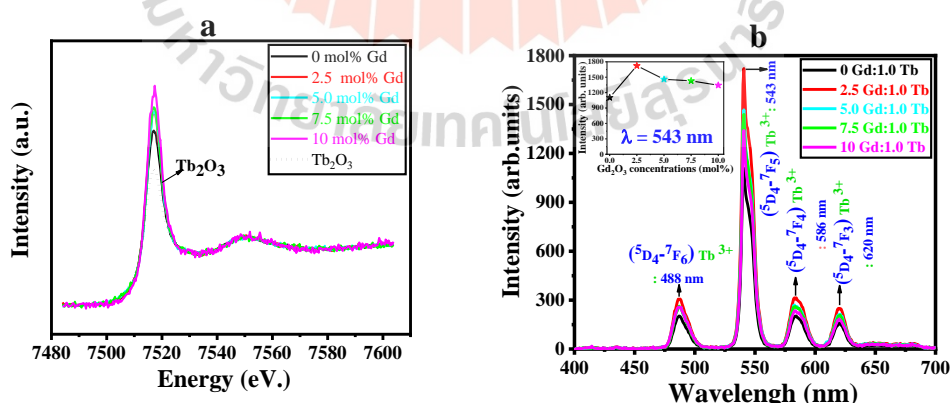


Figure 7.7 The XANES and X-ray induced luminescence spectra of LATB series glass.

Figure 7.7(a) displays the normalized Tb L_{III} -edge XANES presentation is indicated only in the energy range 7,480 and 7,600 eV of the LATB series with the $25\text{Li}_2\text{O}-5\text{Al}_2\text{O}_3-\text{YGd}_2\text{O}_3-(69.0-\text{Y})\text{B}_2\text{O}_3-1.0\text{Tb}_2\text{O}_3$ composition where $\text{Y} = 0-10 \text{ mol } \%$. Gd_2O_3

and standard Tb_2O_3 samples. For the XANES study, Tb_2O_3 was used as a standard and data were normalized at 7619 eV. The XANES data were analyzed using the Athena software. A first observation of the XANES spectra is that the features seem identically and the energies positions of the first main absorption bands centered at about 7,510 and 7,525 eV shift towards larger energies by increasing of the Gd_2O_3 in the host matrix. It is well known that terbium easily presents a mixture of valence states Tb^{3+} as in the chosen reference (Tb_2O_3). The white lines of Tb doped samples exhibit the dominant single maximum band at 7,519 eV relative to Tb^{3+} with no evidence of a marked shoulder on the right side of the maximum suggesting that the presence of Tb^{4+} , illustrating that Tb^{3+} ions exist predominantly in the samples.

The radioluminescence spectra for Gd^{3+} and Tb^{3+} dual doped of host glass with different Gd_2O_3 concentrations were shown in Figure 7.7(b). The present experimental aperture can detect sufficient signal from the un-doped Gd^{3+} by fixing 1.0 mol% Tb^{3+} in the LABT glass sample. At 1.0 mol% Tb-doped all samples presented the sharp emission lines exhibit four permanent peaks, which locate at a wavelength around 488 nm ($^5D_4 \rightarrow ^7F_6$), 543 nm ($^5D_4 \rightarrow ^7F_5$), 586 nm ($^5D_4 \rightarrow ^7F_4$), and 620 nm ($^5D_4 \rightarrow ^7F_3$) transition as observed the peaks with similar positions of photoluminescence and radioluminescence results. The LATB series glass doped with 2.5 mol% Gd^{3+} concentration is the higher intensity of radioluminescence pattern at the wavelength at 543 nm, which can indicate the same tend of photoluminescence result in Figure 7.5 The optimum concentrations of Gd^{3+} content in $25Li_2O-5Al_2O_3-XGd_2O_3-(69.0-X)B_2O_3-1.0Tb_2O_3$ host glass is $X=2.5$ mol%.

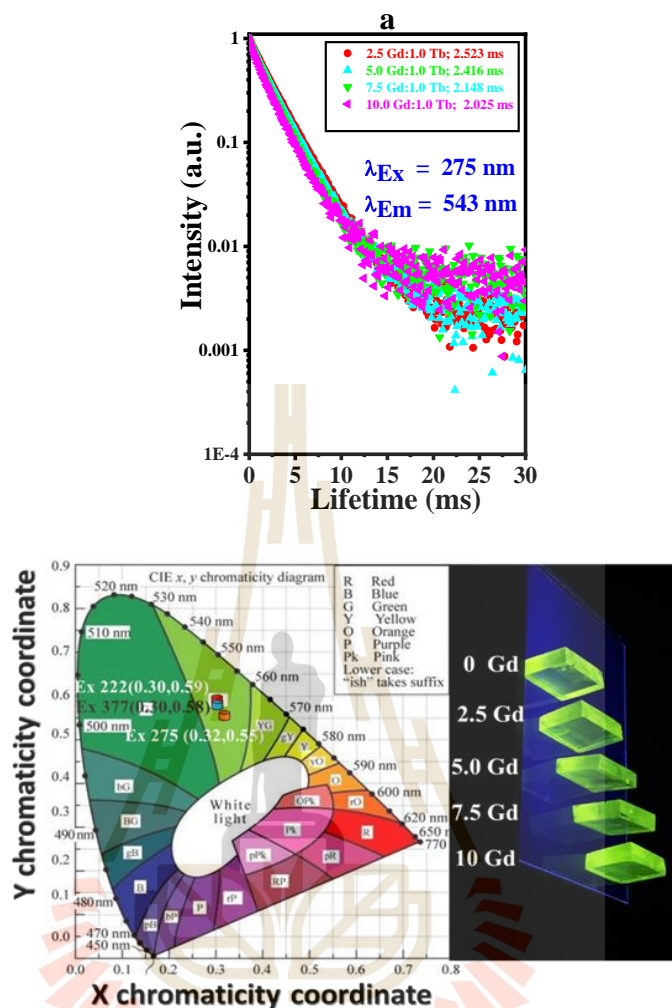


Figure 7.8 Lifetime curve (a) and 1931 CIE chromaticity diagram (b) for varying Gd^{3+} concentrations by fixing 1.0 mol% Tb^{3+} glass.

In general, the luminescence decay time analysis is a physical phenomenon used to understanding the energy transfer process. Figure 7.8(a) represents the decay curves for $^5\text{D}_4$ state with the difference Gd^{3+} ion, representing the signature emission green was shown around at 543 nm ($^5\text{D}_4 \rightarrow ^7\text{F}_5$ of Tb^{3+}) transition with exciting at 275 nm. The decay times are obtained to decrease 2.578 to 2.025 milliseconds unit for Gd^{3+} concentrations increase (0 mol% to 10 mol%). The potential of these dual-doped glasses for white light emission is explored by employing CIE 1931. The CIE diagram in Figure 7.8(b) presents the color coordinates of dual doped glasses under excitation at 222, 275, and 377 nm. In particular, all-glass samples show green

light emission (543 nm) as a result, the CIE coordinates $\lambda_{ex}= 222$ nm (0.30, 0.59), $\lambda_{ex}= 275$ nm (0.32, 0.55), and $\lambda_{ex}= 377$ nm (0.30, 0.58), which the mostly lie in shade of lime-green region. Moreover, the quality of green light was inspected with the correlated color temperature (CCT) value are calculated by McCamy equation (McCamy et al., 1992). Therefore, the CCT values of the present composition LATB glass were obtained in the range of 5749-6098 K, which the CCT value in between daylight CIE D55 and commercially available white light LED (see table 7.1).

Table 7.1 The CIE color coordinates (x,y), correlated color temperature (CCT) for LATB glass.

Glass	(x,y)	CCT
LABT doped 2.5 Gd glass: $\lambda_{ex}= 222$ nm	(0.30,0.59)	6083
LABT doped 2.5 Gd glass: $\lambda_{ex}= 275$ nm	(0.32,0.55)	5749
LABT doped 2.5 Gd glass: $\lambda_{ex}= 377$ nm	(0.30,0.58)	6098
Daylight CIE D55 (Fuches et al., 2009)	(0.332,0.347)	5500
Commercial white light LED (Yang et al., 2006)	(0.340,0.560)	6400

The optimum concentrations of Gd^{3+} ion in $25Li_2O-5Al_2O_3-YGd_2O_3-(69.0-Y)B_2O_3-1.0Tb_2O_3$ host glass matrix is $Y = 2.5$ mol%, which results in the maximum intensity of emission under both photoluminescence and radioluminescence results are inversely related in glass samples. Therefore, it is important to study both the properties in order to understand the radiation- induced and photoluminescence phenomena comprehensively. After the process, we were prepared glass samples with varying Tb_2O_3 content in the best host $25Li_2O-5Al_2O_3-2.5Gd_2O_3-(67.5-Z)B_2O_3-ZTb_2O_3$ so call LAGB series glass to study photoluminescence property.

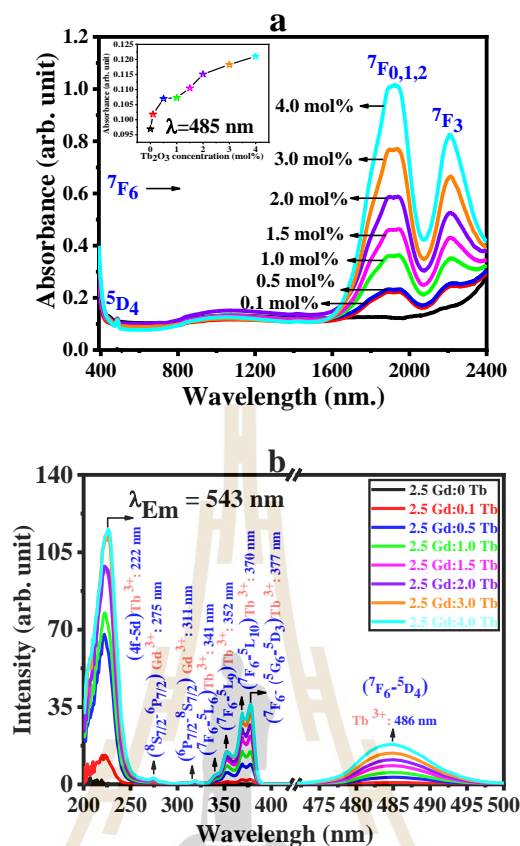


Figure 7.9 The optical absorption (a) and excitation (b) spectra of the LAGB glass series doped with different concentrations of Tb_2O_3 .

The absorption spectra of the samples appear the only one peak in the visible region and two peaks in the NIR region. The absorbance significantly increases with increasing Tb_2O_3 concentration. When the Tb_2O_3 concentration increased up to 4.0 mol%, a weak absorption appeared around 485 nm invisible and at 1,923 and 2,212 nm in the NIR region. The black-line compares the absorption spectra of un-doped and co-doped glasses are shown in Figure 7.9(a), illustrating in addition to the Tb^{3+} concentration, the absorption bands around 1,600 to 2,400 nm tended to increase gradually. The origin of the latter absorption bands was ascribed to Tb^{3+} for its typical feature.

Figure 7.9(b) shows the excitation spectra of Tb^{3+} ions doped LAGB glasses recorded by monitoring the green emission wavelength (λ_{em}) at 543 nm. The excitation spectra of all the LAGB sample glasses give eight luminescence bands centered at 275 and 311 nm are associated with hosting bands of Gd^{3+} ion and other six transitions at

222, 341, 352, 370, 377, and 486 nm are attributed to Tb^{3+} ion excitations. From the excitation spectra, we can be observed the transition at 222, 275, and 377 nm is important than the other transitions.

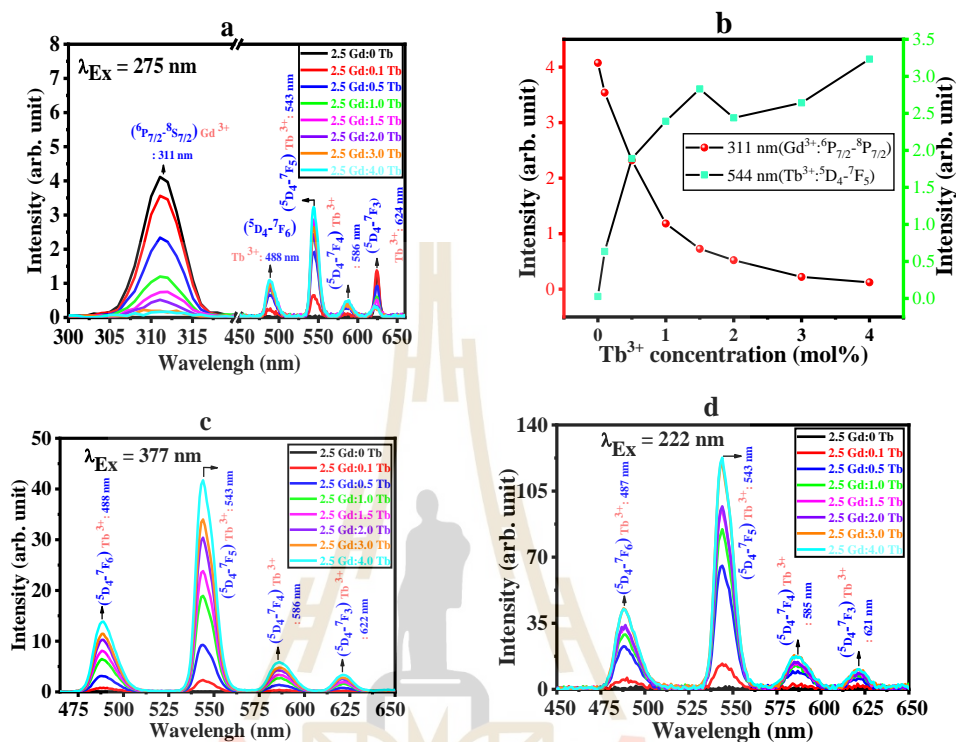


Figure 7.10 The emission ($\lambda_{ex} = 275, 377$ and 222 nm) spectra for LAGB glasses (a, c, and d) and variation of Gd^{3+} intensity at 311 nm and Tb^{3+} intensity at 543 nm (b) as a function of Tb_2O_3 concentrations for LAGB glasses.

The concentration Tb^{3+} ions effect on the luminescence was investigated, the emission spectra in the visible region were measured for the examined Tb^{3+} ion-doped LAGB glasses to all the concentrations (0, 0.1, 0.5, 1.0, 1.5, 2.0, 3.0, and 4.0 mol%) of Tb_2O_3 contents. The effects of the concentration of Tb^{3+} ions emission behavior of LAGB under direct excitation wavelength at 275 nm display a sharp peak at 311 nm attributed to the $Gd^{3+} \ ^6P_j \rightarrow \ ^8S_{7/2}$ transition. On start increasing Tb concentration since 0.1 mol%, Tb^{3+} emission dominates and the peak at 543 nm are illustrated in Figure 9 (a). Additionally, the other peaks result in well-known four lines spectra with $^5D_4 \rightarrow \ ^7F_6$, $^5D_4 \rightarrow \ ^7F_5$, $^5D_4 \rightarrow \ ^7F_4$, and $^5D_4 \rightarrow \ ^7F_3$ emissions are located at $487, 543, 585,$ and 621 nm based on $4f-4f$ transitions of Tb^{3+} ion. The increasing the Tb_2O_3 concentration, the

intensity of the ${}^6P_J \rightarrow {}^8S_{7/2}$ transition was reduced due to the energy transfer mechanism from Gd^{3+} to Tb^{3+} confirm, presented in Figure 7.10(b). Among under emission 377 and 222 nm gives a variation of the multiple emission luminescence peaks are very similar to the X-ray induced emission spectra as shown in Figure 7.7. Figure 7.10(a, b, c) shows increased luminescence intensities of all emission and excitation bands with increased Tb_2O_3 content up to 4.0 mol% until increased beyond 5.0 mol%, a considerable overload of doped was observed milky effect.

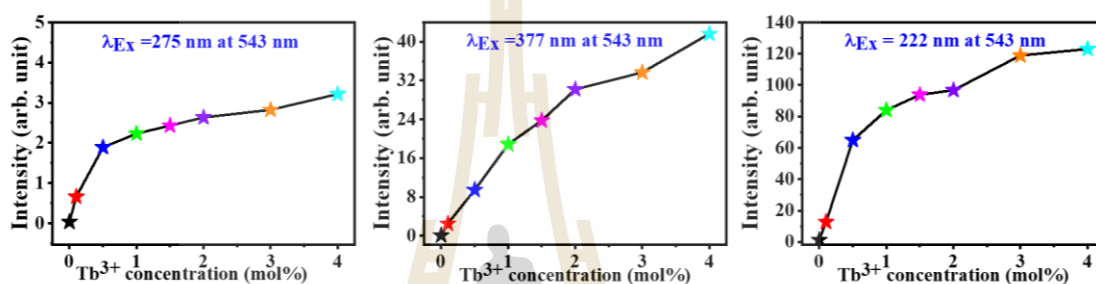


Figure 7.11 Three emission spectra for the Tb^{3+}/Gd^{3+} co-doped LAGB glass doped with different concentrations of Tb^{3+}

Figure 7.11 shows the luminescence spectra for LAGB glasses dual doped with Tb^{3+} and Gd^{3+} were emission with $\lambda_{ex} = 222, 275,$ and 377 nm. The appearance of the most intense band located at 543 nm is due to the main green transitions from Tb^{3+} , which tend to increase with the increase of Tb^{3+} content. Until 4.0 mol%, it was found the maximum load concentration of glass having a white color, milky appearance, usually with a fiery translucence.

The photoluminescence decay curves of the Tb -doped glass samples for 543 nm emission wavelength and under 222 nm excitation wavelength of the LAGB doped glass are presented in Figure 7.12(a). The lifetime curves were extrapolated by approximating with a single exponential decay function for all concentrations in the glass samples.

η (Gd–Tb) > η (Tb–Tb). The Gd³⁺ 311 nm emission intensity has been dramatically decreased and the Tb₂O₃ content is rising where the signature Gd³⁺ 311 nm emission declines. The efficiency of energy transfer from host (Gd³⁺) to activator (Tb³⁺) ions referred as a function of Tb₂O₃ concentration, the greater the concentration of Tb₂O₃, the higher the efficiency of energy transfer (59.199%) is shown in the Table 7.2 It can be observed that the Gd³⁺ plays an active role as a sensitizer.

Table 7.2 The concentration mol% and lifetime (ms) of the dopant (Tb³⁺) and the efficiency of the energy transfer from Gd³⁺ to Tb³⁺ and Tb³⁺ to Tb³⁺ in the LAGB doped glass series.

Glass	E _{ex} = 275, E _{em} = 543nm (ms)	E _{ex} = 275, E _{em} = 311 nm (ms)	E _{ex} = 222, E _{em} = 543 nm (ms)	η Gd ³⁺ - Tb ³⁺	η Tb ³⁺ - Tb ³⁺
0 Tb glass	-	2.499	-	-	-
0.1 Tb glass	3.310	2.210	2.682	49.773	0
0.5 Tb glass	3.015	2.01	2.643	50.000	1.454
1.0 Tb glass	3.001	1.956	2.625	53.425	2.125
1.5 Tb glass	2.947	1.879	2.613	56.838	2.572
2.0 Tb glass	2.789	1.771	2.585	57.481	3.616
3.0 Tb glass	2.571	1.615	2.560	59.195	4.548
4.0 Tb glass	2.544	1.598	2.450	59.199	8.650

Moreover, indicating the energy levels diagrams of Gd³⁺ and Tb³⁺ ions and their relative transition are described in Figure 7.12(b). The Gd³⁺ ion is stimulated by 275 nm of the UV radiation, the original upper energy level population relaxes to its lower energy levels before it exceeds the ⁶P_{7/2} level by phonon help and 311 nm of characteristic Gd³⁺ ion emission occurs. In this process, part of the energy in Gd³⁺ ion ⁶P_{7/2} through the electrical dipole-dipole interaction to the superior levels of Tb³⁺ ion and then relaxes easily to ⁵D₄. Thus, Gd³⁺ can increase the population of Tb³⁺ ions to ⁵D₄ levels and make Tb³⁺ luminescence more sensitive.

7.4 References

- Aboutaleb, D. and Safi, B. (2015). Lithium oxide effect on the thermal and physical properties of the ternary system glasses ($\text{Li}_2\text{O}_3\text{-B}_2\text{O}_3\text{-Al}_2\text{O}_3$). *International Journal of Chemical and Molecular Engineering*, 9(3), 425-428.
- Azizan, S. A., Hashim, S., Razak, N. A., Mhareb, M., Alajerami, Y., and Tamchek, N. (2014). Physical and optical properties of Dy^{3+} : $\text{Li}_2\text{O-K}_2\text{O-B}_2\text{O}_3$ glasses. *Journal of Molecular Structure*, 1076, 20:25.
- Bergh, A., Craford, G., Duggal, A., and Haitz, R. (2001). The promise and challenge of solid-state lighting. *Physics Today*, 54, 42.
- Dalal, S., Khasa, S., Dahiya, M. S., Agarwal, A., Yadav, A., Seth, V. P., and Dahiya, S. (2015). Effect of substituting iron on structural, thermal and dielectric properties of lithium borate glasses. *Materials Research Bulletin*, 70, 559:566.
- Deopa, N., Saini, S., Kaur, S., Prasad, A., and Rao, A. S. (2019). Spectroscopic investigations on Dy^{3+} ions doped zinc lead alumino borate glasses for photonic device applications. *Journal of Rare earths*, 37(1), 52-59.
- Farouk, M., Samir, A., Metawe, F., and Elokr, M. (2013). Optical absorption and structural studies of bismuth borate glasses containing Er^{3+} ions. *Journal of Non-Crystalline Solids*, 14, 371:372
- Fuches, E. C., Sommer, C., Wenzl, F. P., Bitschnau, B., Paulitsch, A. H., Muhlanger, A., and Gatterer, K. (2009). Polyspectral white light emission from Eu^{3+} , Tb^{3+} , Dy^{3+} , Tm^{3+} co-doped $\text{GdAl}_3(\text{BO}_3)_4$ phosphors obtained by combustion synthesis. *Materials Science and Engineering B*, 156, 73:78.
- Gedam, R. S. and Ramteke, D. D. (2012). Effect of Sm_2O_3 addition on electrical and optical properties of lithium borate glasses. *In AIP Conference Proceedings*, 1447, 561:562.
- Ibrahim, A. M., Hammad, A. H., Abdelghany, A. M., and Rabie, G. O. (2018). Mixed alkali effect and samarium ions effectiveness on the structural, optical and non-linear optical properties of borate glass. *Journal of Non-Crystalline Solids*, 495, 67:74.

- Kaewnuam, E., Kim, H. J., and Kaewkhao, J. (2017). Development of lithium yttrium borate glass doped with Dy^{3+} for laser medium, W-LEDs and scintillation materials applications. *Journal of Non-Crystalline Solids*, 464, 96:103.
- Kaur, P., Kaur, S., Singh, G. P., and Singh, D. P. (2014). Cerium and samarium codoped lithium aluminoborate glasses for white light emitting devices. *Journal of Alloys and Compounds*, 588, 394:398.
- Kesavulu, C., Kim, H., Lee, S., Kaewkhao, J., Wantana, N., Kothan, S., and Kaewjaeng, S. (2016). Influence of Er^{3+} ion concentration on optical and photoluminescence properties of Er^{3+} -doped gadolinium-calcium silica borate glasses. *Journal of Alloys and Compounds*, 683, 590:598.
- Kesavulu, C. R., Kim, H. J., Lee, S. W., Kaewkhao, J., Kaewnuam, E., and Wantana, N. (2017). Luminescence properties and energy transfer from Gd^{3+} to Tb^{3+} ions in gadolinium calcium silicoborate glasses for green laser application. *Journal of Alloys and Compounds*, 704, 557:564.
- Lakshminarayana, G., Kaky, K. M., Baki, S. O., Lira, A., Caldiño, U., Kityk, I. V., and Mahdi, M. A. (2017). Optical absorption, luminescence, and energy transfer processes studies for Dy^{3+}/Tb^{3+} -codoped borate glasses for solid-state lighting applications. *Optical Materials*, 72, 380:391.
- Li, Y. C., Chang, Y. H., Chang, Y. S., Lin, Y. J., and Laing, C. H. (2007). Luminescence and Energy Transfer Properties of Gd^{3+} and Tb^{3+} in $LaAlGe_2O_7$. *The Journal of Physical Chemistry C*, 111(28), 10682:10688.
- Loos, S., Mungra, M., Ahrens, B., Leonard, R. L., Evans, A., Johnson, J. A., Steude, F., and Schweizer, S. (2017). Concentration-dependent luminescence and energy transfer in Tb^{3+}/Eu^{3+} doped borate and fluorozirconate glasses. *Journal of Luminescence*, 187, 298:303.
- McCamy, C. S. (1992). Correlated color temperature as an explicit function of chromaticity coordinates. *Color Res. Appl*, 17, 142:144.
- Pisarska, J., Kos, A., Pietrasik, E., and Pisarski, W. A. (2014). Energy transfer from Dy^{3+} to Tb^{3+} in lead borate glass. *Materials Letters*, 129, 146:148.
- Pisarska, J., Kos, A., Sottys, M., Ur, L., and Pisarski, W. A. (2014). Energy transfer from Tb^{3+} to Eu^{3+} in lead borate glass. *Journal of Non-Crystalline Solids*, 388, 1:5.

- Ragab, M., Mahani, Y., Samir, Y., and Marzouk, A. (2013). conductivity and dielectric properties of $\text{SiO}_2\text{-Na}_2\text{O-B}_2\text{O}_3\text{-Gd}_2\text{O}_3$ glasses. *Journal of Alloys and Compounds*, 579, 394:400.
- Shaaban, E. R., Shapaan, M., and Saddeek, Y. B. (2008), Structural and thermal stability criteria of $\text{Bi}_2\text{O}_3\text{-B}_2\text{O}_3$ glasses. *Journal of Physics: Condensed Matter*, 20, 155108.
- Shaaban, K. H., Abo-Naf, S. M., and Hassouna, M. E. M. (2019). Physical and structural properties of lithium borate glasses containing MoO_3 . *Silicon*, 11(5), 2421-2428.
- Ullah, I., Shah, S. K., Rooh, G., Khan, A., Boonpa, W., Srisittipokakun, N., and Kaewkhao, J. (2021). $\text{Gd}^{3+}/\text{Sm}^{3+}$ energy transfer behavior and spectroscopic study of lithium gadolinium magnesium borate for solid state lighting material. *Optical Materials*, 111, 110657.
- Shamshad, L., Rooh, G., Kirdsiri, K., Srisittipokakun, N., Damdee, B., Kim, H. J., and Kaewkhao, J. (2017). Photoluminescence and white light generation behavior of lithium gadolinium silicoborate glasses. *Journal of Alloys and Compounds*, 695, 2347:2355.
- Singh, D., Singh, K., Bajwa, B. S., Mudahar, G. S., Singh, Manupriya, D. P., Arora, M., and Dangwal, V. K. (2008). Optical and structural properties of $\text{Li}_2\text{O - Al}_2\text{O}_3 - \text{B}_2\text{O}_3$ glasses before and after γ -irradiation effects. *Journal of Applied Physics*, 104, 103515.
- Singh, L., Thakur, V., Punia, R., Kundu, R. S., and Singh, A. (2014). Structural and optical properties of barium titanate modified bismuth borate glasses. *Solid State Science*, 37, 64:71,
- Sun, X. Y., Yang, Q. M., P., and Gao, P. (2015). Luminescence, energy transfer properties of $\text{Tb}^{3+} / \text{Gd}^{3+}$ - coactivated oxyfluoride borogermanate scintillating glasses. *Journal of Luminescence*, 165, 40:45.
- Sun, X. Y., Huan, S. M., Gong, X. S., Gao, Q. C., Ye, Z. P., and Cao, C. Y. (2010). Spectroscopic properties and simulation of white-light in Dy^{3+} -doped silicate glass. *Journal of Non-Crystalline Solids*, 356, 98.
- Thakur, V., Kushwaha, H. S., Singh, A., Vaish, R., Punia, R., and Singh, L. (2015). A study on the structural and photocatalytic degradation of ciprofloxacin using

- ($70\text{B}_2\text{O}_3$ - $29\text{Bi}_2\text{O}_3$ - $1\text{Dy}_2\text{O}_3$) - x (BaO - TiO_2) glass ceramics. *Journal of Non-Crystalline Solids*, 428, 197:203.
- Valieva, D., Polissadova, E., Stepanov, S., Belikov, K., Yegorova, N., Othman, H., and Vaganov, V. (2015). Luminescence spectroscopy of scintillating glasses doped with $\text{Tb}^{3+}/\text{Ce}^{3+}$ with different concentration of cerium under photo- and electron excitation. *Journal of Luminescence*, 162, 128:133.
- Wantana, N., Kaewnuam, E., Damdee, B., Kaewjaeng, S., Kothan, S., Kim, H. J., and Kaewkhao, J. (2018) Energy transfer based emission analysis of Eu^{3+} doped Gd_2O_3 - CaO - SiO_2 - B_2O_3 glasses for laser and X-rays detection material applications. *Journal of Luminescence*, 194, 75:81.
- Wantana, N., Kaewnuam, E., Ruangtaweep, Y., Valiev, D., Stepanov, S., Yamanoi, K., and Kaewkhao, J. (2019). Radio, cathodo and photoluminescence investigations of high density WO_3 - Gd_2O_3 - B_2O_3 glass doped with Tb^{3+} . *Radiation Physics and Chemistry*, 164, 108350.
- Yang, C. H., Pan, Y. X., and Zhang, Q. Y. (2007). Enhanced white light emission from $\text{Dy}^{3+}/\text{Ce}^{3+}$ codoped $\text{GdAl}_3(\text{BO}_3)_4$ phosphors by combustion synthesis. *Materials Science and Engineering: B*, 137(1-3), 195-199.
- Yao, L., Zeng, Z., Chen, G., Zhong, H., Cui, S., and Wen, C. (2016). Tunable luminescence and temperature sensing behavior of $\text{Tb}^{3+}/\text{Eu}^{3+}$ co-doped borate glasses. *Journal of Materials Science: Materials in Electronics*, 27(8), 8402:8407.
- Zaman, F., Kaewkhao, J., Srisittipokakun, N., Wantana, N., Kim, H. J., and Rooh, G. (2016). Investigation of luminescence and laser transition of Dy^{3+} in Li_2O - Gd_2O_3 - Bi_2O_3 - B_2O_3 glasses. *Optical Materials*, 55, 136:144.
- Zhang, P., Pun, Y. P., Zhu, X. J., Zheng, H. Y., Zhao, J. J., Wu, Y., Luo, Y. J., and Liu, Y. (2015). Luminescence properties of Dy^{3+} doped and $\text{Dy}^{3+}/\text{Ce}^{3+}$ co-doped CaO - Al_2O_3 - SiO_2 - B_2O_3 glass for LED applications. *Ceramics International*, 41, S729:S733.

CHAPTER VIII

DYSPROSIUM DOPED BORATE GLASS

The improving optical and luminescence properties of Dy^{3+} and Gd^{3+} dual doped lithium aluminum borate glasses with composition $25\text{Li}_2\text{O}-5.0\text{Al}_2\text{O}_3-2.5\text{Gd}_2\text{O}_3-(67.5-X)\text{B}_2\text{O}_3-X\text{Dy}_2\text{O}_3$ glasses were successfully developed. The as-synthesis composite used conventional melt-quenching processes. All glass samples doped with Dy_2O_3 show an enhanced emission intensity (photo and radioluminescence spectra) with increasing the concentration of Dy_2O_3 up to 1.0 mol%, and beyond that, concentration quenching has occurred for all samples. The experimental decay times calculated from the decay profiles have been gradually declined with an increase in Dy^{3+} ion concentration. The chromaticity coordinates (CIE 1931) were located in the white light region of the color chromaticity diagram. The Dy-doping glasses synthesized show the prevalent presence of Dy^{3+} also, the presence of the trivalent oxidation state in the glass series. Therefore, the results confirm that the Dy^{3+} -doped glasses could be usable for white-LEDs applications.

8.1 Introduction

In recent years, the researcher objective tried to reduce harmful materials such as a mercury fluorescent lamp for environmentally friendly, but illumination is also commonly used in human activities. Therefore, the new materials are an excellent replacement for the mercury fluorescent lamp of the past, such as white-light-emitting diodes (W-LEDs) (Bergh et al., 2001). W-LED lamps are a safer option more than the conventional fluorescent mercury bulb. These materials were highly interested because of their excellent properties such as green material, low cost of manufacturing, low energy efficiency, homogenous light emission, and high service life. In the commercial W-LEDs, the blue-light diodes (LED) surface with a coating of yellow phosphors is made (Bergh et al., 2001; Sun et al., 2010). However, this white light has

disadvantages with poor and very short life-time due to the coating of phosphors ununiform consequently, using rare-earth (RE) for doping in crystal and glass is the alternative for developing for solve problem. The RE-doped glasses have excellent properties such as high thermal stability, good transparency, and lower manufacturing costs rather than phosphors (Damak et al., 2014; Krishnaiah et al., 2013; Deopa et al., 2018; Uma et al., 2016). In numerous periodic table materials, rare-earth oxide (REO) has achieved broader interest due to its uses in optoelectronics, such as display devices, solid-state laser, optical sensors, memory modules, and fiber amplifiers (Chakraborty et al., 1894; Chakraborty et al., 1985). The rare-earth ions (REI) exhibit optical properties related to their 4f–4f level transitions, providing strong luminescence in the visible until the infrared region due to the variation component of glass. The variety of glass composition causes REI doping different structures. Moreover, various REIs provided different colors of emission properties. The development of the host materials is interesting for enhancing properties like transparency, chemical inertness, low-temperature synthesis, non-hygroscopic, and good solubility (Shamshad et al., 2016; Rajesh et al., 2012; Kiran et al., 2013). Since lithium has good choices that exhibit low weight and high energy density, lithium borate glasses have received much attention. A series of glasses doped with lanthanide oxides (Ce^{3+} -, Pr^{3+} -, Nd^{3+} -, Sm^{3+} -, Eu^{3+} -, Tb^{3+} -, Dy^{3+} -, Ho^{3+} -, and Er^{3+}) is widely used in glasses with excellent properties such as physical, chemical, optical, and other properties (Zaman et al., 2016). The variety glasses for W-LEDs light from the different lanthanide ion-doped, the dysprosium (Dy^{3+}) doped in glassy materials are most acceptable for single-phase generation (white light) and light transformation because their emission ~ 482 nm blue, ~ 575 nm yellow, and very low emission ~ 665 nm red light, which corresponds to (${}^4\text{F}_{9/2} \rightarrow {}^6\text{H}_{15/2}$), (${}^4\text{F}_{9/2} \rightarrow {}^6\text{H}_{13/2}$), and (${}^4\text{F}_{9/2} \rightarrow {}^6\text{H}_{11/2}$) transition, respectively (Vijaya et al., 2013; Kaewkhao et al., 2016; Shamshad et al., 2017). The strong peak at ${}^4\text{F}_{9/2} \rightarrow {}^6\text{H}_{13/2}$ transition of Dy^{3+} is suitable for lasing action, whereas emission of white light has an advantage when using white light diode emitting (W-LEDs). The borate glass with Al_2O_3 added provides a good network structure, strong chemical, and mechanical (Monisha et al., 2020). Additionally, the glass matrix plays a function in the development in

addition to doping materials. As a result of its very effective energy transfer from Gd^{3+} ions to the integrated activators (the luminescence core, such as lanthanide: Ln^{3+}) at a reasonable cost (Xiong et al., 2014; Babu et al., 2015; Vijayakumar et al., 2015; Nayab et al., 2013; saleh et al., 2012; Ragab et al., 2013), Gd_2O_3 has become a material of great interest in the glass matrix because the Gd is a high atomic number that can increase glass density and strengthens the relationship between glass and radiation (Ragab et al., 2013; Wantana et al., 2020).

However, there have been no systematic studies in (Gd^{3+}/Dy^{3+}) dual-doped transparent lithium aluminum borate glasses. Additionally, the bright white-light emission and other optical properties of lithium aluminum borate glasses with (Gd^{3+}/Dy^{3+}) dual-doped has not been reported. Therefore, the low-cost melt-quenching technique has been used to fabricate an attractive glass. All glasses were characterized the physical, structural, optical, photoluminescence, and radioluminescence properties. Interestingly, the effect of Gd_2O_3 and Dy_2O_3 concentrations was also optimized chemical composition and bright white-light emission of glass, which is usable for W-LEDs applications.

8.2 Experimental

8.2.1 Doped with Gd_2O_3 concentration

The variation of Gd^{3+} concentration in lithium aluminum gadolinium borate glasses of $25Li_2O-5Al_2O_3-XGd_2O_3-(69-X)B_2O_3-1.0Dy_2O_3$ system has been investigated for a host glass which X varied from 0 to 10.0 mol%, calling LAGdxBDy1.0 glasses (LAGd0BDy1.0= 0 mol% Gd, LAGd2.5BDy1.0= 2.5 mol% Gd, LAGd5.0BDy1.0= 5.0 mol% Gd, LAGd7.5BDy1.0= 7.5 mol% Gd and LAGd10.0BDy1.0= 10 mol% Gd).

8.2.2 Doped with Dy_2O_3 concentration

The best condition of host glass was selected to fabricate for Dy^{3+} dopant. A series of $25Li_2O-5Al_2O_3-2.5Gd_2O_3-(67.5-X)B_2O_3-XDy_2O_3$ doped with Dy_2O_3 (where X = 0, 0.05, 0.1, 0.3, 0.5, 1.0, and 1.5 mol%), calling LAGd2.5BDyx glasses (LAGd2.5BDy0= 0 mol% Dy, LAGd2.5BDy0.05= 0.05 mol% Dy, LAGd2.5BDy0.1= 0.1 mol% Dy, LAGd2.5BDy0.3= 0.3 mol% Dy, LAGd2.5BDy0.5= 0.5 mol% Dy, LAGd2.5BDy1.0= 1.0

mol% Dy, and LAGd2.5BDy1.5= 1.5 mol% Dy). Both glasses systems were synthesized through the melt quenching process using the chemical grade of high quality Li_2CO_3 , H_3BO_3 , Gd_2O_3 , Al_2O_3 , and Dy_2O_3 as starting materials. In the process, about 20 g batches were homogeneously mixed by grinding in an alumina crucible. Then, the mixed powder was melted in an electrical furnace at ~ 1200 °C for 90 minutes. Next step, the glass melted was poured onto a graphite plate followed by annealing at 500 °C for 3 hours and cooled slowly to room temperature to relieve thermal stress. All glasses were cut and polished to a rectangle shape of $1.0 \times 1.5 \times 0.3$ cm³. The transparent glass sample of uniform thickness was obtained, as shown in Figure 1(a, b). The density of synthesized glasses was studied by Archimedes method, then molar volumes of glasses were examined. Moreover, the optical absorption spectra of all samples were calculated in the range of 200-2500 nm via UV-vis -NIR spectrophotometer (Shimadzu UV-3600). The characteristics of photoluminescence (PL) spectra have studied a spectrofluorophotometer (Cary-Eclipse) thoroughly using a Xenon flash lamp with the excitation in 200-800 nm wavelength region. The system consists of Cu target x-ray generator (Inel, XRG3D-E), fiber optic spectrometer (Ocean Optics, QE65 Pro) and brass sample holder used to estimate the radioluminescence spectra. The optical luminescence spectra were measured from the radiated glass X-ray (50 kV and 30 mA). The spectroscopic technique of X-ray absorption near-edge structure (XANES) measurements is a useful method for determining the oxidation state of materials. We present a comparison of experimental XANES data obtained in fluorescence mode at the Dy L_{III}-edge (7795.5 eV) with bent Ge (220) crystals using a crystal analyzer spectrometer.

8.3 Result and discussion

Both series of LAGdxBDy1.0 and LAGd2.5BDyx are doped gently by Gd^{3+} and Dy^{3+} both glasses exhibit soft-yellow color, free of bubbles, homogeneous and high transparency, as seen in Figure 8.1(a, b).

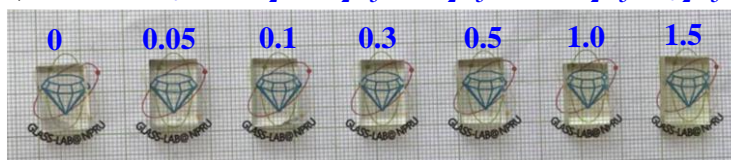
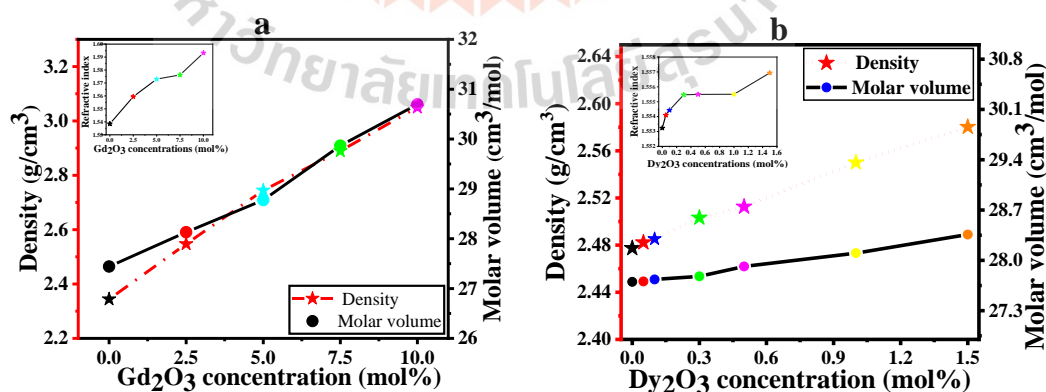
(a) $\text{LAGd}_x\text{BDy1.0} : 25\text{Li}_2\text{O}\cdot 5.0\text{Al}_2\text{O}_3\cdot x\text{Gd}_2\text{O}_3\cdot (69-x)\text{B}_2\text{O}_3\cdot 1.0\text{Dy}_2\text{O}_3$ (b) $\text{LAGd2.5BDy}_x : 25\text{Li}_2\text{O}\cdot 5\text{Al}_2\text{O}_3\cdot 2.5\text{Gd}_2\text{O}_3\cdot (67.5-x)\text{B}_2\text{O}_3\cdot x\text{Dy}_2\text{O}_3$ Figure 8.1 Photograph of glasses with different (a) Gd_2O_3 and (b) Dy_2O_3 concentrations.

Figure 8.2(a) displays density, molar volumes, and refractive index of $\text{LAGd}_x\text{BDy1.0}$ glasses. Those results tend to increase with the addition of Gd_2O_3 doped concentration linearly because Gd_2O_3 exhibits a higher relative molecular mass than B_2O_3 . The reason can be explained by an increase in the average molecular weight of glass, thereby increasing the glass density. Figure 8.2(b) shows a similar pattern of density, molar volume, and refractive index of LAGd2.5BDy_x glasses. The molar volume initially increased from zero concentration of Dy_2O_3 because the non-bridging oxygen (NBOs) number increased, indicating that the packed structure is bond breaking (Kaewnuam et al., 2017). Moreover, the increase in molar volume relates to the increase in interatomic spacing. Therefore, the increase of the molar volume of glasses occurs as a Gd_2O_3 and Dy_2O_3 concentration function due to the increase in the NBOs.

Figure 8.2 Densities, molar volumes, and refractive index for different concentrations of Gd_2O_3 and Dy_2O_3 in $\text{LAGd}_x\text{BDy1.0}$ (a) and LAGd2.5BDy_x (b) series glasses.

The XRD diffraction pattern shows broad peaks at low angles, confirming all glasses' non-crystalline characteristics, as shown in Figure 8.3(a, b).

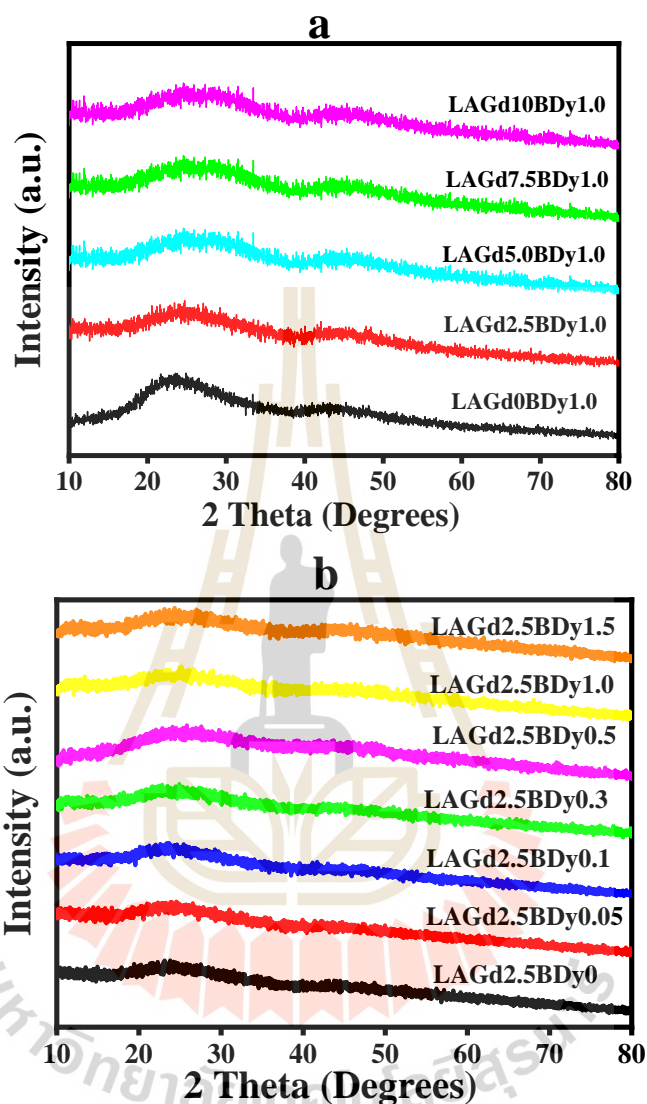


Figure 8.3 XRD pattern of LAGd_xBDy1.0 and LAGd2.5BDy_x series glasses doped with different concentrations of Gd₂O₃ (a) and Dy₂O₃ (b) in mol%.

8.3.1 Effect of Gd₂O₃ concentration

The excitation spectrum for LAGd_xBDy1.0 glass series (under λ_{em} at 575 nm) presents nine excitation bands peaking at 275, 311, 325, 350, 365, 387, 426, 453, and 474 nm due to the transition spectra of $^8S_{7/2} \rightarrow ^6I_{7/2}$, $^8S_{7/2} \rightarrow ^6D_{7/2}$, $^6H_{15/2} \rightarrow ^6P_{3/2}$, $^6H_{15/2} \rightarrow ^6P_{7/2}$, $^6H_{15/2} \rightarrow ^6P_{5/2}$, $^6H_{15/2} \rightarrow ^4F_{7/2}$, $^6H_{15/2} \rightarrow ^4G_{11/2}$, $^6H_{15/2} \rightarrow ^4I_{15/2}$, and $^6H_{15/2} \rightarrow ^4F_{9/2}$, respectively, illustrated in Figure 8.4(a). It was found that the highest

excitation peak belongs at 387 nm (${}^6\text{H}_{15/2} \rightarrow {}^4\text{F}_{7/2}$), proportional to the highest absorption transition in the visible light region. Under both emission spectra with $\lambda_{\text{ex}} = 275$ and 387 nm represent a strong emission band at $\lambda_{\text{em}} = 575$ nm, which is characteristic of ${}^4\text{F}_{9/2} \rightarrow {}^6\text{H}_{13/2}$ transition (Wantana et al., 2020). The emission spectra for the various Gd_2O_3 in the LAGdxBDy1.0 glass series exhibit in the range of 250–800 nm under $\lambda_{\text{ex}} = 275$ nm, represented in Figure 8.4(b). The emission spectra provide five visible, prominent emission bands, located 311, 482, 575, 665, and 751 nm corresponding to ${}^6\text{P}_{7/2} \rightarrow {}^8\text{S}_{7/2}$, ${}^4\text{F}_{9/2} \rightarrow {}^6\text{H}_{15/2}$, ${}^4\text{F}_{9/2} \rightarrow {}^6\text{H}_{13/2}$, ${}^4\text{F}_{9/2} \rightarrow {}^6\text{H}_{11/2}$, and ${}^4\text{F}_{9/2} \rightarrow {}^6\text{H}_{9/2}$ transitions, respectively. The emission of spectra was found substantially improved with an increasing concentration of Gd_2O_3 . The emission bands at 311 nm decreased because the energy transfers from the host Gd^{3+} to dopant Dy^{3+} ion. Moreover, the emission spectra were recorded by exciting at 387 nm, consisting of four prominent bands at 482, 575, 665, and 751 nm, which similarly result at the excitation wavelength of 275 nm, as shown in Figure 8.4(c). The blue, yellow, red emission peaks profile led to a soft-white color when human eyes were detected. Therefore, the emission and excitation peaks intensity increase with increasing Gd_2O_3 concentration, which reaches a maximum at 2.5 mol% and then decreases, as shown in Figure 8.4(d). The radioluminescence spectra of the LAGdxBDy1.0 glass samples are observed at room temperature, as seen in Figure 8.5. The radioluminescence spectra and photoluminescence emission spectra of both glass systems show a similar trend, with a high peak at around 574 nm being close to the direction of the photoluminescence spectra result. The results were demonstrated that the electron-hole pairs formed by X-ray interaction in the produced glass samples able to transfer their energy to the luminescence core, with the optimal concentration of Gd_2O_3 is 2.5 mol%.

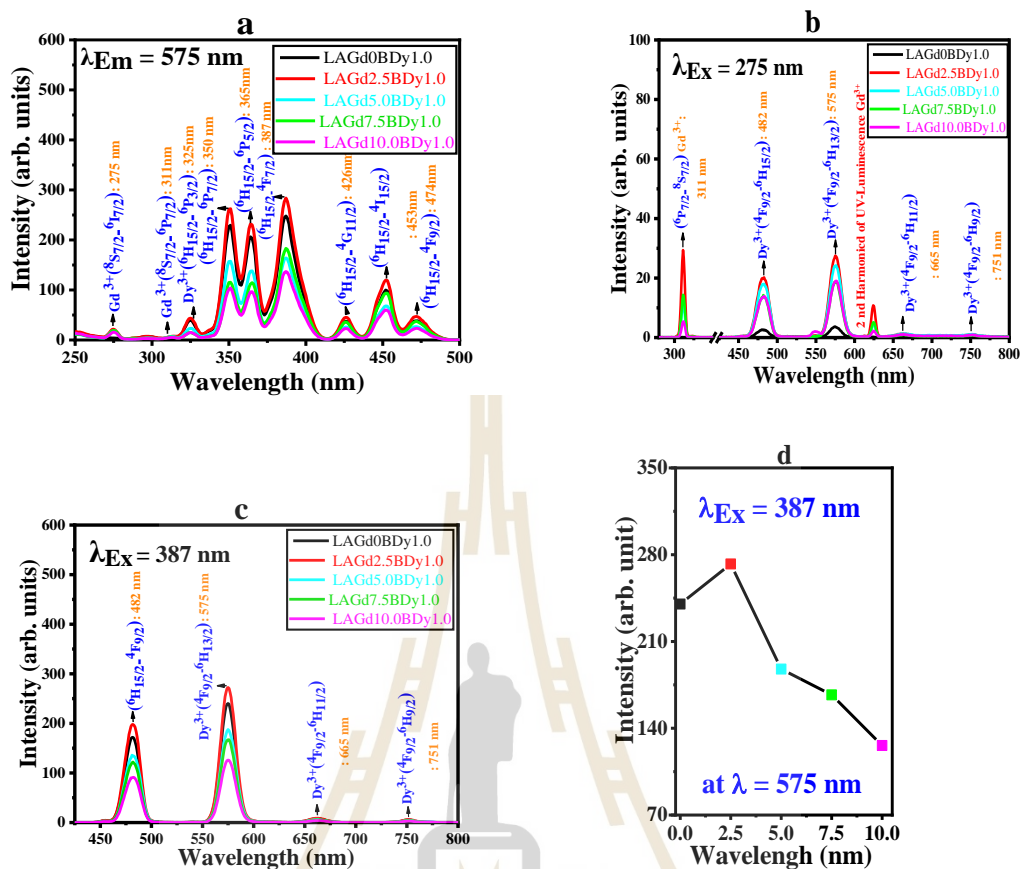


Figure 8.4 The excitation (a), emission (b, c), and trends to emission spectra (d) of LAGxBDy1.0 glasses doped with different concentrations of Gd₂O₃.

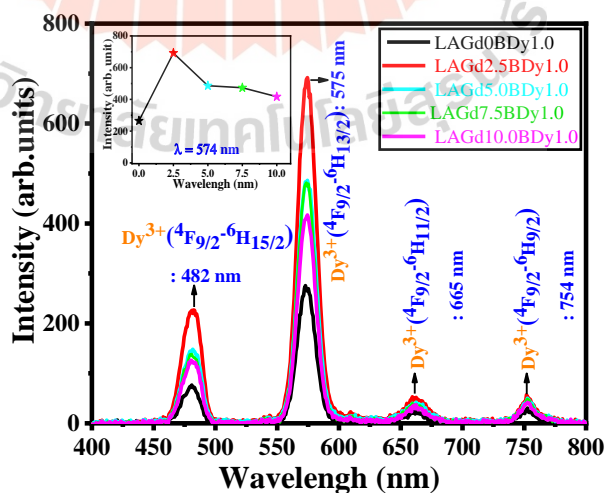


Figure 8.5 The radioluminescence of LAGxBDy1.0 glasses doped with Gd₂O₃.

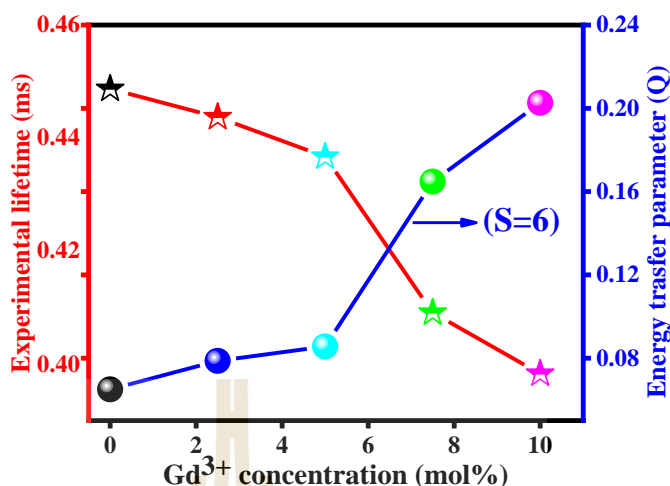


Figure 8.6 The relation between decay spectral profiles and energy transfer parameter of ${}^4F_{9/2} \rightarrow {}^6H_{13/2}$ ($\lambda_{\text{ex}} = 387 \text{ nm}$ & $\lambda_{\text{em}} = 575 \text{ nm}$) transition of Dy^{3+} ions in glasses series.

Figure 8.6 depicts the luminescence lifetime profiles obtained for the emission and excitation wavelengths of 575 and 387 nm. The observed decay time decreased as Gd_2O_3 concentration increased (0, 2.5, 5.0, 7.5 and 10 mol%) glass are 0.4487, 0.4437, 0.4367, 0.4091 and 0.3983, respectively) because of the increasing energy transfer through cross-relaxation in the existing glass network. When the energy transfer is faster than the energy migration. Therefore, the energy transfer mechanism can be explained with the I-H model (Inokuti et al., 1965) and luminescence intensity decay by the following relation (8.1).

$$I(t) = I_0 \exp\left\{-\frac{t}{\tau_0} - Q\left(\frac{t}{\tau_0}\right)^{3/S}\right\} \quad (8.1)$$

Where I_0 is the initial intensity at $t = 0$, t is time after excitation and τ_0 is intrinsic decay time of donors without the presence of acceptors, S is the multipolar interaction parameter, which when $S = 6, 8$, and 10 corresponds to electrical dipole-dipole, dipole-quadrupole, and quadrupole-quadrupole interaction, respectively. In this work, indicating the non-exponential decay curves fitted to the I-H model reveals the interaction between dipole-dipole (fit is good for $S = 6$, with $R^2 \geq 0.99$ (Deopa et al., 2018) in nature. Figure 8.7 and Table 8.1 illustrate the life expectancy and the energy transfer parameter Q .

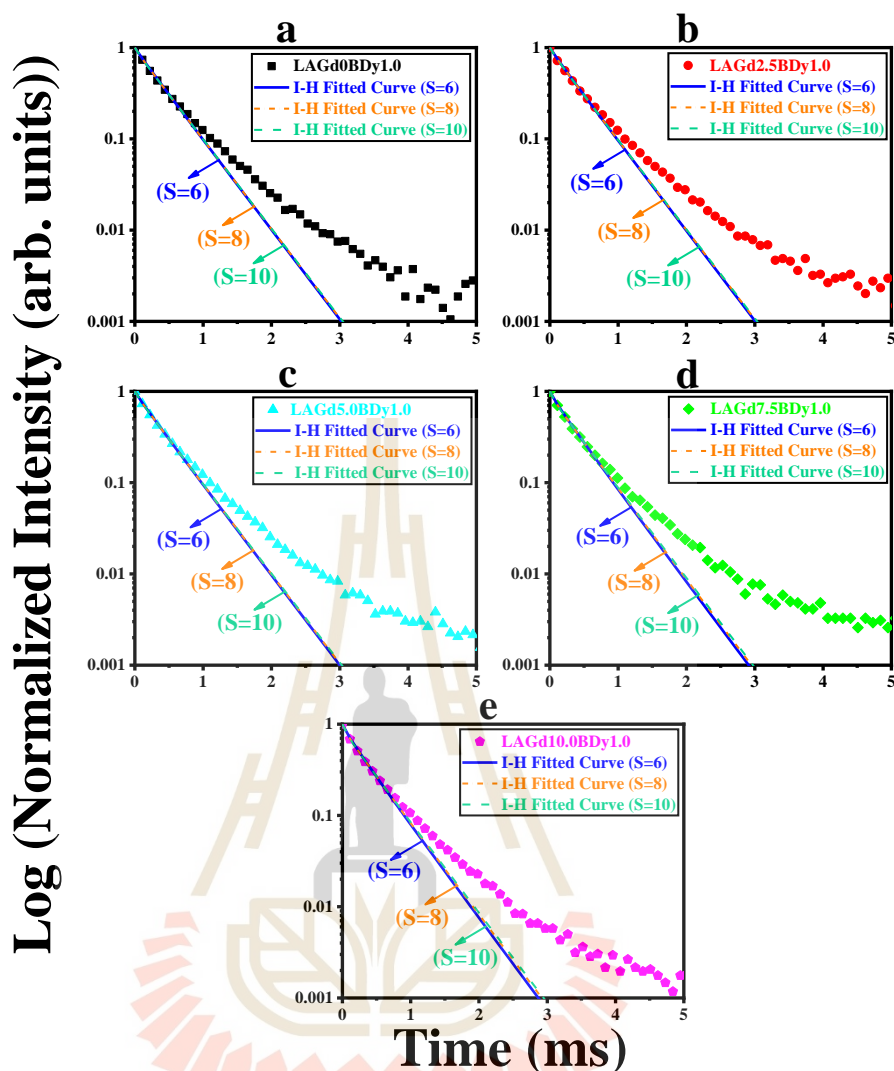


Figure 8.7 The decay curves of ${}^4F_{9/2} \rightarrow {}^6H_{13/2}$ ($\lambda_{\text{ex}} = 387 \text{ nm}$ and $\lambda_{\text{em}} = 575 \text{ nm}$) transition of Dy^{3+} ions with different Gd_2O_3 concentrations (mol%= 0 (a), 2.5 (b), 5.0 (c), 7.5 (d), and 10.0 (e)) along by I-H fitting curves ($S= 6, 8,$ and 10).

The IH resulted was fitted and released the energy transfer parameter (Q), indicating the probability of energy transfer from Dy^{3+} donor to Dy^{3+} acceptor. The Q value of LAGd0BDy1.0, LAGd2.5BDy1.0, LAGd5.0BDy1.0, LAGd7.5BDy1.0 and LAGd10.0BDy1.0 glass is 0.0650, 0.0787, 0.0856, 0.1648, and 0.2026, respectively. The increasing Q value under increasing Gd_2O_3 concentration and fixing Dy_2O_3 concentration (1.0 mol%) indicates the enhancement of energy transfer between ions in the glasses system (Table 8.1).

Table 8.1 The values of lifetime (τ_{exp} ; ms), energy transfer parameter (Q), and R-square of ${}^4\text{F}_{9/2} \rightarrow {}^6\text{H}_{13/2}$ transition in alkaline-earth borate glasses.

Glasses	Decay time (ms)	Energy transfer parameter (Q)		
		S = 6	S = 8	S = 10
LAGd0BDy1.0	0.4487	0.0650	0.0683	0.0691
LAGd2.5BDy1.0	0.4437	0.0787	0.0818	0.0825
LAGd5.0BDy1.0	0.4367	0.0856	0.0874	0.0873
LAGd7.5BDy1.0	0.4091	0.1648	0.1624	0.1592
LAGd10.0BDy1.0	0.3983	0.2026	0.1981	0.1936

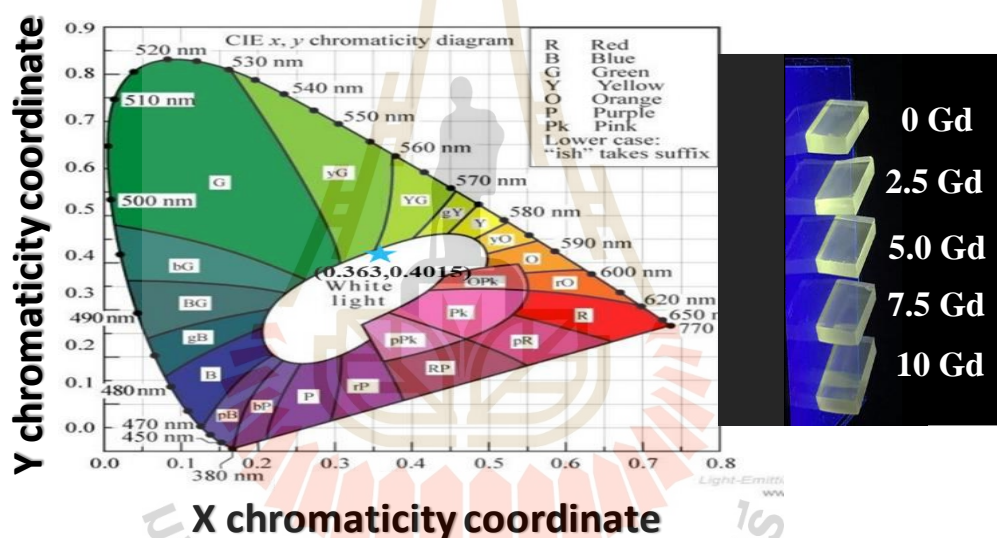


Figure 8.8 The 1931 CIE chromaticity diagram of the best condition emission of LAGdxBDy1.0 glasses illuminated by 365 nm UV lamp.

White light's color characteristics were assessed using CIE 1931 chromaticity coordinates and correlated color temperature (CCT). Figure 8.8 depicts the PL excitation and emission spectra of blue and yellow color in glass samples calculated using the Commission International de l'Eclairage (CIE) 1931 chromatic coordinates (x , y). The chromaticity coordinates for sample (the best condition) $25\text{Li}_2\text{O}-5\text{Al}_2\text{O}_3-2.5\text{Gd}_2\text{O}_3-66.5\text{B}_2\text{O}_3-1.0\text{Dy}_2\text{O}_3$ glasses (0.3630, 0.4015) were found in white region. The

CCT value can be calculated from CIE color coordinate through the McCamy formula as follows:

$$\text{CCT} = -449n^3 + 3525n^2 - 6823n - 5520.33 \quad (8.2)$$

where $n = (x-0.332)/(y-0.186)$. In the final results, the CCT of the best sample glasses (4556 K) is closest to CCT of standard white light (ranges from 4450 to 5335 K) for application of these glasses in W-LED application (Table 8.2). Real naked-eye under UV-lamp excitation also observed the soft-white emissions of all the samples.

Table 8.2 The CIE color coordinates (x,y), correlated color temperature (CCT) for LAGd2.5BDy1.0 glass.

Glass	(x,y)	CCT (K)
LAGd2.5BDy1.0 : $\lambda_{\text{ex}} = 387 \text{ nm}$	(0.3630,0.4015)	4556
NbFSDy01 (Venkata et al., 2013)	(0.358,0.409)	4817
LGBiBDy15 (Zaman et al., 2016)	(0.374,0.410)	4360

In this part, the development of optimization concentration with Gd_2O_3 was found that 2.5% is the best emission intensity (the radioluminescence and photoluminescence emission spectra results), then Gd_2O_3 is fixed at 2.5% for Dy_2O_3 concentration quenching study.

8.3.2 Effect of Dy_2O_3 concentration

A series of $25\text{Li}_2\text{O}-5\text{Al}_2\text{O}_3-2.5\text{Gd}_2\text{O}_3-(67.5-X)\text{B}_2\text{O}_3-X\text{Dy}_2\text{O}_3$ doped with Dy_2O_3 (where $X = 0, 0.05, 0.1, 0.3, 0.5, 1.0, \text{ and } 1.5 \text{ mol\%}$) is called LAGd2.5BDyx series glasses. As shown in Figure 8.9(a, b), the absorption bands for LAGd2.5BDyx glasses indicate the transitions from the ground state ${}^6\text{H}_{15/2}$ to different higher-level states. The various spectroscopic transitions observed are as follows: ${}^6\text{H}_{15/2} \rightarrow {}^4\text{F}_{9/2}$ (450 nm) for the UV-VIS range, and ${}^6\text{H}_{15/2} \rightarrow {}^6\text{F}_{3/2}$ (741 nm), ${}^6\text{H}_{15/2} \rightarrow {}^6\text{F}_{5/2}$ (802 nm), ${}^6\text{H}_{15/2} \rightarrow {}^6\text{F}_{7/2}$ (901 nm), ${}^6\text{H}_{15/2} \rightarrow {}^6\text{F}_{9/2}$ (1093 nm), ${}^6\text{H}_{15/2} \rightarrow {}^6\text{F}_{11/2} + {}^6\text{H}_{9/2}$ (1270 nm), and ${}^6\text{H}_{15/2} \rightarrow {}^6\text{H}_{11/2}$ (1682 nm) for VIS-NIR range indicating the Dy^{3+} in glass matrices. The typical absorption

spectra of 1.5 mol% of Dy^{3+} ions doped LAGd2.5BDy x glass recorded at room temperature show the transition ${}^6F_{11/2} + {}^6H_{11/2}$ of wavelength 1270 nm is the highest intensity among all these eight transitions and intensity peak of the glasses tends to increase with increase of Dy_2O_3 concentration.

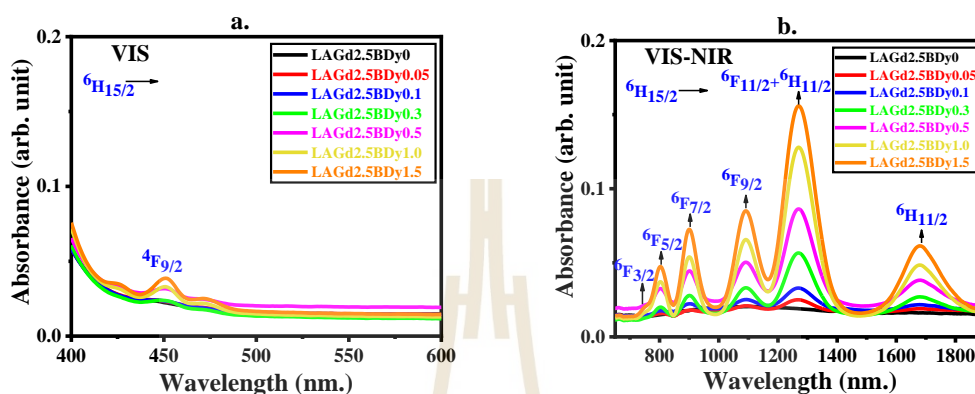


Figure 8.9 UV-VIS (a) and VIS-NIR (b) optical absorption spectra of LAGd2.5BDy x glasses with various Dy_2O_3 concentrations.

Figure 8.10 indicates the FTIR spectra of LAGd2.5BDy x series glasses activated with varying concentrations of Dy^{3+} glass samples were reported in the range 400–4400 cm^{-1} . The studied-based glasses consist of B_2O_3 is only network-forming oxides. The FTIR spectra analysis revealed that as the variation of Dy^{3+} concentrations, the band position does not show any significant change. The band around 449, 695, 951, 1263, 1373, and 1579 cm^{-1} were observed. In the first part, the vibrational modes associated with the glass network appear sound center around 449 cm^{-1} was used to bend the vibrate of Li^+ ions with the glass network (Rajesh et al., 2011; Pawar et al., 2016). The second band group formed at 695 cm^{-1} corresponds to the B-O-B bending vibrations of bridges containing one trigonal and one tetrahedral boron (Pawar et al., 2016; Pawar et al., 2016; Karunakan et al., 2009). And then, the strong band located at 963 cm^{-1} can be ascribed to the B–O bond stretching vibration of the tri-, tetra-, penta-borate BO_4 structure units (Hari et al., 2015). The addition of the Dy_2O_3 amount in the present glass increases the BO_4 units by entering the glass-forming network positions. The presence of peaks at 1268 cm^{-1} infrared vibration reflects the B–O stretching of BO_3 units in penta-borate, pyro-borate, ortho-borate groups. The last group of the band was observed at 1373 cm^{-1} displays stretching B–O vibration in trigonal BO_3 groupings,

whereas the vibration from 2000 to 3500 cm^{-1} indicates hydrogen bonding, molecular water, and O-H stretching of OH^- groups (Talewar et al., 2019). All FTIR results show the various vibrational bands of prepared glass samples and can be confirmed by the formation of borate groups BO_3 and BO_4 , in the glass network.

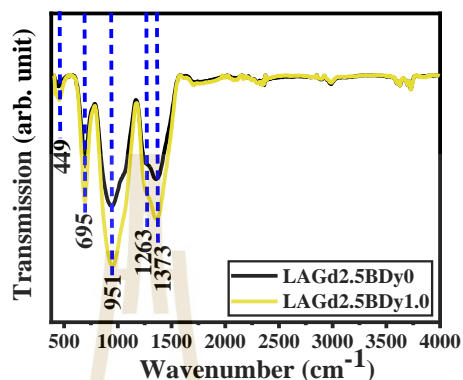


Figure 8.10 FTIR spectra of LAGd2.5BDy0 (black line) and LAGd2.5BDy1.0 (yellow line).

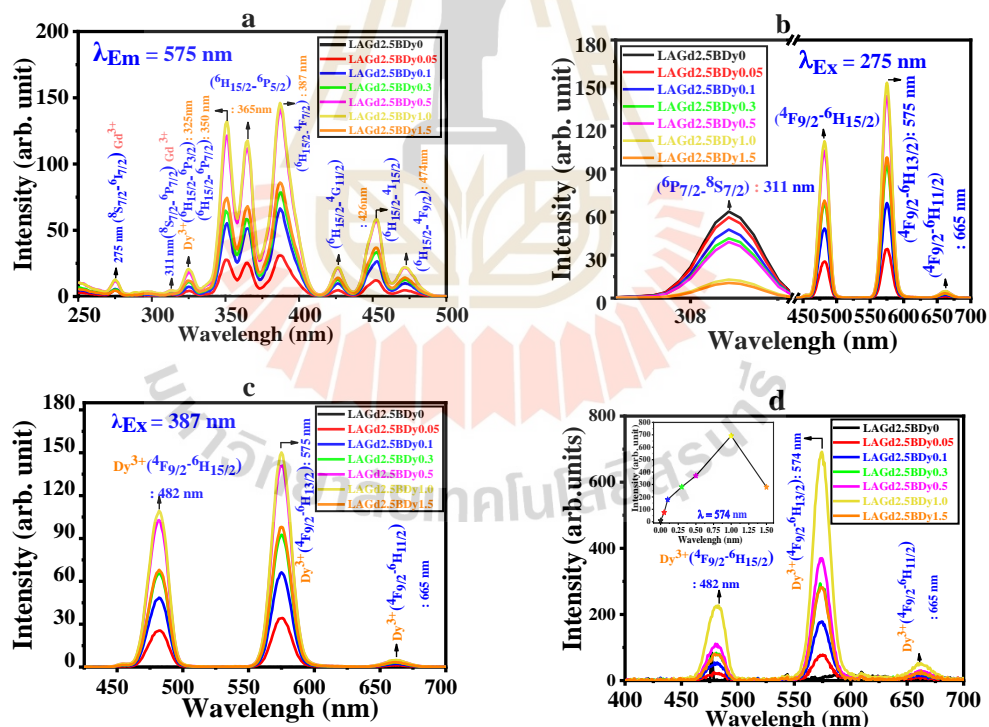


Figure 8.11 The photoluminescence results of (a) excitation (under $\lambda_{em} = 575 \text{ nm}$) and (b) emission (under $\lambda_{ex} = 275 \text{ nm}$), (c) emission (under $\lambda_{ex} = 387 \text{ nm}$), and (d) radioluminescence spectra of LAGd2.5BDyx glasses series doped with different Dy_2O_3 concentrations.

Figure 8.11(a) indicates the excitation spectra of LAGd2.5BDyx glass doped with different concentrations of Dy₂O₃. The excitation spectra consist of two parts. The first part has exhibited two major bands centered at 275 nm ($^8S_{7/2} \rightarrow ^8I_{7/2}$) and 312 nm ($^8S_{7/2} \rightarrow ^6D_{7/2}$). Additionally, the other peak excitation of Dy³⁺ were observed at 325 nm ($^6H_{15/2} \rightarrow ^6P_{3/2}$), 350 nm ($^6H_{15/2} \rightarrow ^6P_{7/2}$), 365 nm ($^6H_{15/2} \rightarrow ^6P_{5/2}$), 387 nm ($^6H_{15/2} \rightarrow ^4F_{7/2}$), 426 nm ($^6H_{15/2} \rightarrow ^4G_{11/2}$), 453 nm ($^6H_{15/2} \rightarrow ^4I_{15/2}$), and 474 nm ($^6H_{15/2} \rightarrow ^4F_{9/2}$). From the excitation spectra result, all samples represent the characteristic peak of Gd³⁺ at 275 nm and the strongest band of Dy³⁺ at 387 nm. So, all the samples were excited by this wavelength to investigate the emission spectra as given in Figure 8.11(b) and (c). We have noticed the emission spectra by exciting at 275 nm in the wavelength, exhibits five transitions which can be assigned to 311 nm ($^6P_{7/2} \rightarrow ^8S_{7/2}$) (from Gd³⁺), 482 nm ($^4F_{9/2} \rightarrow ^6H_{15/2}$), 575 nm ($^4F_{9/2} \rightarrow ^6H_{13/2}$), and 665 nm ($^4F_{9/2} \rightarrow ^6H_{11/2}$) (from Dy³⁺) transitions (saleh, et al., 2012; Ragab et al., 2013). The emission intensity of characteristic peak at 312 nm (Gd³⁺) reduced while increasing of Dy₂O₃ concentration by all emission intensity of Dy₂O₃ doped increase until 1.0 mol% due to the energy transfer phenomena from Gd³⁺ to Dy³⁺. Figure 8.11(c) show the emission spectra of LAGd2.5BDyx series glass by monitoring the excitation wavelength at 387 nm, comparing with Figure 8.11(b). It found similar to the 275 nm with emission band at 482 nm ($^4F_{9/2} \rightarrow ^6H_{15/2}$), 575 nm ($^4F_{9/2} \rightarrow ^6H_{13/2}$), and 665 nm ($^4F_{9/2} \rightarrow ^6H_{11/2}$) transitions) except for the sharp characteristic of Gd³⁺ ions at 311 nm. The emission pattern corresponds with the published in the literature (Srihari et al., 2019; Babu et al., 2009). These data indicated that the emission and excitation intensity of LAGd2.5BDyx series glass increase with increasing Dy₂O₃ concentration until 1.0 mol%. Also, in glass that dope Dy₂O₃ higher than 1.0 mol%, it was affected by start concentration quenching effect that reduces emission intensity. The radioluminescence spectra of LAGd2.5BDyx series glasses were recorded with the irradiation from an X-ray source, using a 50 keV and 30 mA, as shown in Figure 8.11(d). The spectra detected contained large emissions of around 400-700 nm, three-wavelength emission peaks similar to photoluminescence results (peaks at 482 nm: $^4F_{9/2} \rightarrow ^6H_{15/2}$, 574 nm: $^4F_{9/2} \rightarrow ^6H_{13/2}$, and 665 nm: $^4F_{9/2} \rightarrow ^6H_{11/2}$ transitions). An incoming particle of ionizing radiation could explain some

components trapped in the LAGd2.5BDyx series. The energy of the X-ray then induced the electron to overcome the energy difference that contributed to the ionization of glass samples. The result indicates that LAGd2.5BDyx series glasses are found to be at 1.0 mol% concentration of Dy^{3+} doped performs the best luminescence properties, which can be applied to be a scintillation material prepared glass samples were optimized for Dy^{3+} ions concentration of 1.0 mol% after that it drops with higher Dy_2O_3 amount due to the concentration quenching effect.

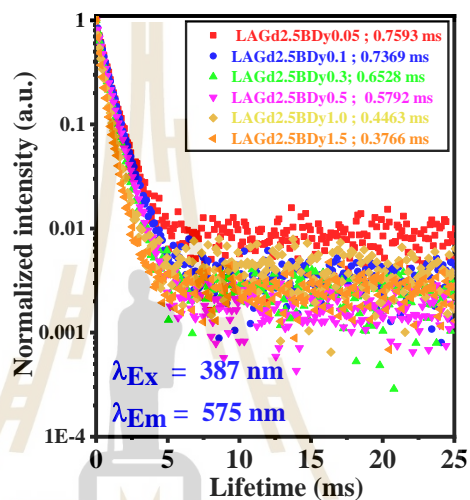


Figure 8.12 Luminescence decay curves ($\lambda_{ex} = 387$ nm, $\lambda_{em} = 575$ nm) with respect to the concentration of Dy^{3+} ion.

The decay curve of ${}^4F_{9/2} \rightarrow {}^6H_{13/2}$ level in LAGd2.5BDyx series of glasses is obtained by exciting with 387 nm wavelength, monitoring the emission at 575 nm, and is given in Figure 8.12. The experimental lifetime (τ_{exp}) values are 0.7593–0.3776 ms in the millisecond range. In Figure 8.12, the reduction in the τ_{exp} values of ${}^4F_{9/2}$ emissions with the increase in the Dy^{3+} ion concentrations. It may be due to the transfer of energy between Dy^{3+} - Dy^{3+} , or it could be due to resonant energy channels in the formed glass network. This finding confirms the energy transfer between trivalent lanthanide ions; for example, energy transfer is often defined as an exchange of electric interactions between (Dy^{3+} - Dy^{3+}). Increased concentration of Dy^{3+} may result in non-exponential growth due to the formation of resonant excitation energy movements between lanthanide ions. The host glass, which is important for the persistent

luminescence, can also be used to determine the energy transfer efficiencies in the produced series of glasses (calculate by using the Eq. (8.3)).

$$\eta_{(Dy^{3+}-Dy^{3+})} = 1 - (\tau_{xDy^{3+}}/\tau_{0Dy^{3+}}) \quad (8.3)$$

where $\eta_{(Dy^{3+}-Dy^{3+})}$ is the energy transfer efficiencies, where $\tau_{0Dy^{3+}}$ is the lifetime of the Dy^{3+} in sample with 0.05 mol% concentration and $\tau_{xSm^{3+}}$ is the lifetime of Dy^{3+} with $x = 0.1, 0.3, 0.5, 1.0,$ and 1.5 mol% concentration (Lakshminarayana et al., 2017). According to Table 8.3, (Deopa et al., 2018) the calculated values of the multipolar interaction parameter S can be reasonably approximated to $S = 6$ using the following relation Eq. (8.1). There is a possibility of dipole-dipole energy transfer between Dy^{3+} - Dy^{3+} ions at higher concentrations (≥ 0.5 wt%). The Q parameter may be determined by using the Inokuti–Hirayama (IH) model (Inokuti et al., 1965) fitted the decay curves. We may assume to see an increase in the Q parameter (LAGd2.5BDy0.5 = 0.1952, LAGd2.5BDy1.0 = 0.6279, LAGd2.5BDy1.5 = 0.8328) and the energy transfer efficiency was found to be LAGd2.5BDy0.1 = 2.95%, LAGd2.5BDy0.3 = 14.02%, LAGd2.5BDy0.5 = 23.71%, LAGd2.5BDy1.0 = 41.22%, and LAGd2.5BDy1.5 = 50.26%, whilst the distance between optically active Ln^{3+} ions decreased due to an increase in Dy_2O_3 increases. The influence of host matrix in the luminescence behaviour of Dy_2O_3 doped borate glass system have been analyzed using IH model and reported by Shanmugavelu et al. (Shanmugavelu et al., 2014).

The oxidation state of the dysprosium oxide ions scattered in the glass matrices was determined by analyzing the experimental X-ray absorption near edge structure (XANES) spectra for LAGd2.5BDyx series glass. The Dy L_{III} -edge XANES spectra of the LAGd2.5BDyx series glass were virtually identical in Figure 8.13, with just one sharp absorption peak (the prominent white line peak) at 7795.5 eV (Kaewjaeng et al., 2018) and the edge energy at 7795 eV, which corresponds to the peak position of the first derivative spectra. The differences in energy location can be used as fingerprints to identify Dy^{3+} organisms. The energy between the white line and edge positions was less than 0.5 eV compared to the XANES distribution of the pure Dy_2O_3 standard. As a result, the XANES results verified that the oxidation number of the Dy ions is +3.

Table 8.3 Dy³⁺ ions concentration, the values of lifetime (τ_{exp} ; ms), energy transfer efficiencies (η), and energy transfer parameter (Q) of LAGd2.5BDyx glasses.

Name of sample	Ln ³⁺ content mol%		τ_x (ms)	τ_0 (ms)	η (Dy- Dy)	Q
	G3 ⁺	Dy ³⁺				
LAGd2.5BDy0	2.5	0	-	-	-	-
LAGd2.5BDy0.05	2.5	0.05	0.7593	0.7593	-	-
LAGd2.5BDy0.1	2.5	0.1	0.7369	0.7593	2.95	-
LAGd2.5BDy0.3	2.5	0.3	0.6528	0.7593	14.02	-
LAGd2.5BDy0.5	2.5	0.5	0.5792	0.7593	23.71	0.1952
LAGd2.5BDy1.0	2.5	1.0	0.4463	0.7593	41.22	0.6279
LAGd2.5BDy1.5	2.5	1.5	0.3776	0.7593	50.26	0.8328

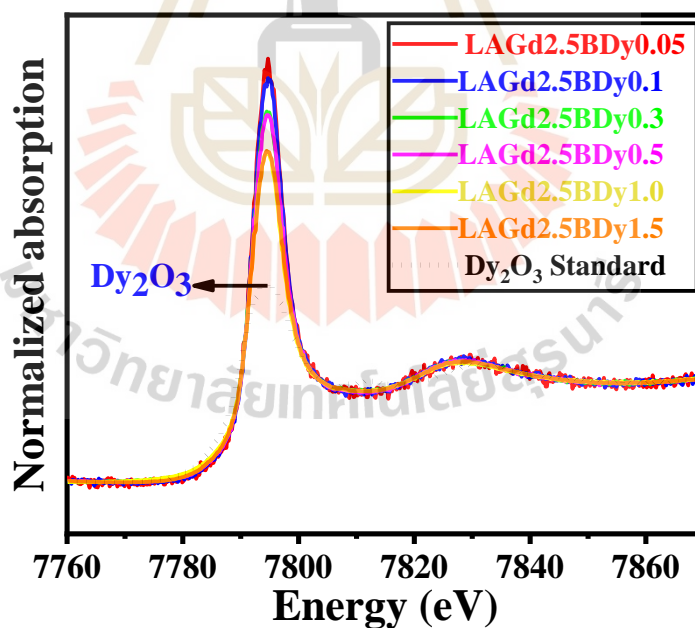


Figure 8.13 The comparison of normalized Dy L_{III}-edge XANES spectra with Dy³⁺ in oxide form reference standard.

8.4 References

- Babu, P., Jang, K. H., Kim, E. S., Shi, L., Vijaya, R., Lavin, V., Jayasankar, C. K., and Seo, H. J. (2010). Optical properties and energy transfer of Dy³⁺-doped transparent oxyfluoride glasses and glass-ceramics. *Journal of Non-Crystalline Solids*, 356, 236:243.
- Babu, S., Reddy Prasad, V., Rajesh, D., and Ratnakaram, Y. C. (2015). Luminescence properties of Dy³⁺ doped different fluoro-phosphate glasses for solid state lighting applications. *Journal of Molecular Structure*. 1080, 153:161.
- Bergh, A., Craford, G., Duggal, A., and Haitz, R. (2001). The promise and challenge of solid-state lighting, *Physics Today*. 5442.
- Chakraborty, I. N., Day, D. E., Lapp, J. C., and Shelby, J. E. (1985). Structure-Property Relations in Lanthanide Borate Glasses. *Journal of the American Ceramic Society*, 68, 368:371.
- Chakraborty, I. N., Shelby, J. E., and Condrate, R. A. (1894). Properties and Structure of Lanthanum Borate Glasses. *Journal of the American Ceramic Society*, 67, 782:785.
- Damak, K., Yousef, E. S., Rüssel, C., and Maàlej, R. (2014). White light generation from Dy³⁺doped tellurite glass. *Journal of Quantitative Spectroscopy and Radiative Transfer*, 134, 55:63.
- Deopa, N. and Rao, A. S. (2018). Spectroscopic studies of single near ultraviolet pumped Tb³⁺ doped Lithium Lead Alumino Borate glasses for green lasers and tricolour w-LEDs. *Journal of Luminescence*, 194, 56:63.
- Deopa, N., Saini, S., Kaur, S., Prasad, A., and Rao, A. S. (2019). Spectroscopic investigations on Dy³⁺ ions doped zinc lead alumino borate glasses for photonic device applications. *Journal of Rare earths*, 37(1), 52-59.
- Hari, B. and Ravi Kanth Kumar, V. V. (2016). Warm white light generation in γ -irradiated Dy³⁺, Eu³⁺ codoped sodium aluminoborate glasses. *Journal of Luminescence*, 169, 16:23.
- Inokuti, M. and Hirayama, F. (1965). Influence of Energy Transfer by the Exchange Mechanism on Donor Luminescence. *The Journal of Chemical Physics*, 43(6), 1978:1989.

- Kaewjaeng, S., Kaewkhao, J., Chanthima, N., Ruangtawep, Y., Klysubun, W., Kothan, S., and Kim, H. J. (2018). XANES and Luminescence Studies of M_2O_3 -CaO-SiO₂-B₂O₃ ($M_2O_3 = Y_2O_3$ and La_2O_3) Glasses Doped with Dy³⁺ Ions. *Key Engineering Materials*, 780, 37:42.
- Kaewkhao, J., Wantana, N., Kaewjaeng, S., Kothan, S., and Kim, H. J. (2016). Luminescence characteristics of Dy³⁺ doped Gd₂O₃-CaO-SiO₂-B₂O₃ scintillating glasses. *Journal of Rare Earths*, 34(6), 583:589.
- Kaewnuam, E., Kim, H. J., and Kaewkhao, J. (2017). Development of lithium yttrium borate glass doped with Dy³⁺ for laser medium, W-LEDs and scintillation materials applications. *Journal of Non-Crystalline Solids*, 464, 96:103.
- Karunakan, R. T., Marimuthu, K., Surendra Babu, S., and Arumugam, S. (2009). Structural, optical and thermal investigations on Dy³⁺ doped NaF-Li₂O-B₂O₃ glasses. *Physical Review B*, 404 (21), 3995:4000.
- Kiran, N. and Suresh Kumar, A. (2013). White light emission from Dy³⁺ doped sodium-lead borophosphate glasses under UV light excitation. *Journal of Molecular Structure*, 6, 1054:1055.
- Krishnaiah, K. V., Kumar, K. U., and Jayasankar, C. K. (2013). Spectroscopic properties of Dy³⁺-doped oxyfluoride glasses for white light emitting diodes. *Optical Materials Express*, 3, 61:70.
- Lakshminarayana, G., Kaky, K. M., Baki, S. O., Lira, A., Caldiño, U., Kityk, I. V., and Mahdi, M. A. (2017) Optical absorption, luminescence, and energy transfer processes studies for Dy³⁺/Tb³⁺-codoped borate glasses for solid-state lighting applications. *Optical Materials*, 72, 380:391.
- Monisha, M., DSouza, A. N., Hegde, V., Prabhu, N. S., Sayyed, M. I., Lakshminarayana, G., and Kamath, S. D. (2020). Dy³⁺ doped SiO₂-B₂O₃-Al₂O₃-NaF-ZnF₂ glasses: An exploration of optical and gamma radiation shielding features. *Current Applied Physics*, 20, 1207:1216.
- Nayab Rasool, S. K., Rama Moorthy, L., and Jayasankar, C. K. (2013). Optical and luminescence properties of Dy³⁺ ions in phosphate-based glasses. *Solid State Science*, 22, 82:90.

- Pawar, P. P., Munishwar, S. R., and Gedam, R. S. (2016). Physical and optical properties of Dy³⁺/Pr³⁺ Co-doped lithium borate glasses for W-LED. *Journal of Alloys and Compounds*, 660, 347:355.
- Pisarska, J., Kos, A., Pietrasik, E., and Pisarski, W. A. (2014). Energy transfer from Dy³⁺ to Tb³⁺ in lead borate glass. *Materials Letters*, 129, 146:148.
- Ragab, M., Mahani, Y., Samir, Y., and Marzouk, A. (2013). AC conductivity and dielectric properties of SiO₂-Na₂O-B₂O₃-Gd₂O₃ glasses. *Journal of Alloys and Compounds*, 579, 394:400.
- Rajesh, D., Ratnakaram, Y. C., Seshadri, M., Balakrishna, A., and Satya Krishna, T. (2012). Structural and luminescence properties of Dy³⁺ ion in strontium lithium bismuth borate glasses. *Journal of Luminescence*, 132, 841:849.
- Saleh, Y., Alajerami, M., Hashim, S., Saridan, W. M, Hassan, W., Ramli, A., and T, Kasim, A. (2012). Optical properties of lithium magnesium borate glasses doped with Dy³⁺ and Sm³⁺ ions. *Physica B: Condensed Matter*, 407, 2398:2403.
- Shamshad, L., Rooh, G., Kirdsiri, K., Srisittipokakun, N., Damdee, B., Kim, H. J., and Kaewkhao, J. (2017). Photoluminescence and white light generation behavior of lithium gadolinium silicoborate glasses. *Journal of Alloys and Compounds*, 695, 2347:2355.
- Shamshad, L., Rooh, G., Kirdsiri, K., Srisittipokakun, N., Kim, H. J., and Kaewkhao, J. (2016). Development of Li₂O-SrO-GdF₃-B₂O₃ oxyfluoride glass for white light LED application. *Journal of Molecular Structure*, 1125, 601:608.
- Shanmugavelu, B. and Ravi Kanth Kumar, V. V. (2014). Luminescence studies of Dy³⁺ doped bismuth zinc borate glasses. *Journal of Luminescence*, 146, 358:363.
- Sharma, R. and Rao, A. S. (2018). Photoluminescence investigations on Dy³⁺ ions doped zinc Lead tungsten tellurite glasses for optoelectronic devices. *Journal of Non-Crystalline Solids*, 495, 85:94.
- Srihari, T. and Jayasankar, C. K. (2017). Fluorescence properties and white light generation from Dy³⁺-doped niobium phosphate glasses. *Optical Materials*, 69, 87:95.

- Sun, X. Y., Huan, S. M., Gong, X. S., Gao, Q. C., Ye, Z. P., and Cao, C. Y. (2010). Spectroscopic properties and simulation of white-light in Dy³⁺-doped silicate glass. *Journal of Non-Crystalline Solids*, 356, 98.
- Talewar, R. A., Mahamuda, S., Swapna, K., and Rao, A. S. (2019). Near UV based Dy³⁺ ions doped alkaline earth chloro borate glasses for white LED's and visible lasers. *Optics & Laser Technology*, 119, 105646.
- Uma, V., Maheshvaran, K., Marimuthu, K., and Muralidharan, G. (2016). Structural and optical investigations on Dy³⁺-doped lithium tellurofluoroborate glasses for white light applications. *Journal of Luminescence*, 176, 15:24.
- Venkata, K., Upendra Kumar, K., and Jayasankar, C. K. (2013). Spectroscopic properties of Dy³⁺-doped oxyfluoride glasses for white light emitting diodes. *Optical Materials Express*, 3(1), 61:70.
- Vijaya, N., Upendra Kumar, K., and Jayasankar, C. K. (2013). Dy³⁺-doped zinc fluorophosphate glasses for white luminescence applications. *Spectrochimica Acta Part A: Molecular and Biomolecular Spectroscopy*, 113, 145:153.
- Vijayakumar, M. and Marimuthu, K. (2015). Structural and luminescence properties of Dy³⁺ doped Oxyfluoro-borophosphate glasses for lasing materials and white LEDs. *Journal of Alloys and Compounds*, 629, 230:241.
- Wantana, N., Ruangtaweep, Y., Kaewnuam, E., Kang, S. C., Kim, H. J., Kothan, S., and Kaewkhao, J. (2020). Development of WO₃-Gd₂O₃-B₂O₃ high density glasses doped with Dy³⁺ for photonics and scintillation materials application. *Solid State Sciences*, 101, 106135.
- Xiong, H. H., Shen, L. F., Pun, E. Y. B., and Lin, H. (2014). High-efficiency fluorescence radiation of Dy³⁺ in alkaline earth borate glasses. *Journal of luminescence*, 153, 227-232.
- Zaman, F., Kaewkhao, J., Srisittipokakun, N., Wantana, N., Kim, H. J., and Rooh, G. (2016). Investigation of luminescence and laser transition of Dy³⁺ in Li₂O-Gd₂O₃-Bi₂O₃-B₂O₃ glasses. *Optical Materials*, 55, 136:144.
- Zhang, P., Pun, Y. P., Zhu, X. J., Zheng, H. Y., Zhao, J. J., Wu, Y., Luo, Y. J., and Liu, Y. (2015). Luminescence properties of Dy³⁺ doped and Dy³⁺/Ce³⁺ co-doped CaO-Al₂O₃-SiO₂-B₂O₃ glass. *Ceramics International*, 41, S729:S733.

CHAPTER IX

CONCLUSIONS

The results reported herein demonstrate the lanthanide contraction for the set of trivalent rare-earth ions studied. For $25\text{Li}_2\text{O}-5\text{Al}_2\text{O}_3-\text{XGd}_2\text{O}_3-(69-\text{X})\text{B}_2\text{O}_3-1.0\text{R}_2\text{O}_3$ glasses containing a considerable concentration of R_2O_3 (CeF_3 , Sm_2O_3 , Eu_2O_3 , Tb_2O_3 , and Dy_2O_3), the following results were confirmed:

9.1 CERIUM DOPED BORATE GLASS

We synthesized two different series of glass composition, the first series $25\text{Li}_2\text{O}-5\text{Al}_2\text{O}_3-5\text{Gd}_2\text{O}_3-(65-\text{Y})\text{B}_2\text{O}_3-\text{YCeF}_3$ (LAGB doped CeF_3) glasses in mol %, where $\text{Y} = 0, 0.05, 0.1, 0.3, 0.5, 1.0, \text{ and } 1.5$ and the second series $25\text{Li}_2\text{O}-5\text{Al}_2\text{O}_3-\text{XGd}_2\text{O}_3-(69.5)\text{B}_2\text{O}_3-0.5\text{CeF}_3$ glasses (LACB doped Gd_2O_3) where $\text{X} = 0-10$ mol% all them were synthesized by using a conventional melt-quenching technique. The first series LAGB glasses, density is in a range of $2.66 - 2.73 \text{ g/cm}^3$ with no obvious relation to the concentration of CeF_3 contents. The XRD results for all the glass samples are confirmed by the absence of crystallization peaks in the spectra. The photoluminescence results, the emission spectra under 310 and 275 nm excitation wavelengths perform the similar emission peak at 350 nm wavelength corresponding to the $5d \rightarrow 4f$ transition of $(4f \rightarrow 5d) \text{Ce}^{3+}$ and $(4f \rightarrow 4f)$ transition states of the Gd^{3+} are overlapped with $4f \rightarrow 5d$ transition state of the Ce^{3+} , which present the charge transfer of the $4f \rightarrow 5d$ character. The emission strength can be generated under the direct excitation with 310 nm is higher than one under 275 nm excitation due to the stronger absorption. The emission intensity increases with increment of CeF_3 concentration from 0.05 mol% until 0.5 mol% for both excitations. After that, the intensity decreases because of the concentration quenching effect and energy transfer phenomena. After the step, using the best condition (LAGB doped with 0.5 mol% CeF_3) varying Gd_2O_3 concentration have been called LACB glass series.

The physical properties of LACB glass, with the increase in Gd_2O_3 content the density and molar volume increase, which means the Gd_2O_3 portion is a glass modifier. The XRD pattern for all samples has no continuous sharp peaks indicate the glassy quality of the glass samples prepared. The FTIR spectrum indicates two main signature bands owing to the presence of borate groups are the trigonal BO_3 and tetrahedral BO_4 . The emission intensity increases with the increment of Gd_2O_3 concentration until 2.5 mol% over than that the intensity decreases. Moreover, the optimal concentrations of Gd_2O_3 for the PL and RL results are different as 2.5 mol% and 5.0 mol%, respectively. It can be clarified that the host material and activator ion have various interaction mechanisms with excitation by UV and X-ray. The XANES spectra could be used to determine the cerium oxidation state found in Ce^{3+} ions of glasses increase with the increase of Gd_2O_3 doping concentration, and the highest relative content of Ce^{3+} is about 92.4% for the 7.5 mol% Gd_2O_3 in LACB glass sample. The finally, the decay time constants were typical for the $4f \rightarrow 5d$ transitions of Ce^{3+} . From the 286 nm excitation with 2 ns of pulse rate height spectra have successfully measured the estimated light yields of the 5.0% Gd_2O_3 -doped samples were approximately 17.45 to 15.20 ns, which the fast decay time of glass could be a potential candidate for radiation scintillating materials

9.2 SAMARIUM DOPED BORATE GLASS

The standard melt-quenching approach was successfully utilized to synthesize a variety of glasses based on LAGdxBSm1.0 and LAGd2.5BSmx series. Both series of glasses exhibit excellent transparency and warm yellow color. The density and molar volume of glasses increased due to atomic compaction increases with the Gd_2O_3 and Sm_2O_3 dopant in the LAGdxBSm1.0 and LAGd2.5BSmx glass series. The structural properties of all glass samples based on XRD indicated their amorphous nature without any crystalline phase. The optimum Gd_2O_3 concentration doped in the host matrix required for maximum photoluminescence and radioluminescence emission intensity is 2.5 mol%. Then, produced glass samples with varying Sm_2O_3 concentrations in the optimal host, dubbed the LAGd2.5BSmx glass series, were examined for their

luminescence property. The impact of changing Sm^{3+} concentrations to the improvement of the absorption and emission characteristics of the produced glasses has been determined. The highest excitation peak appears at 401 nm corresponding to the ${}^6\text{H}_{5/2}$ - ${}^6\text{P}_{3/2}$ transition. The emission spectrum shows four distinct emission peaks that can be ascribed to the transitions at 562 nm (${}^4\text{G}_{5/2}$ - ${}^6\text{H}_{5/2}$), 600 nm (${}^4\text{G}_{5/2}$ - ${}^6\text{H}_{7/2}$), 648 nm (${}^4\text{G}_{5/2}$ - ${}^6\text{H}_{9/2}$), and 705 nm (${}^4\text{G}_{5/2}$ - ${}^6\text{H}_{11/2}$). Quenching is observed above 0.5 mol % of Sm^{3+} ions concentration due to the resonant energy transfer process between Sm^{3+} ions. The CIE chromaticity coordinates and the color temperatures are calculated to be (0.591, 0.407) and 1725 K, respectively, which corresponds to the orange-red emission. The XANES results revealed that the Sm ions in these glass series are Sm^{3+} ions, similar to those in the standard Sm_2O_3 powder. These studies show that Samarium (Sm^{3+}) ions doped borate glass is an attractive candidate for Ln^{3+} ions to be chosen as the light-emitting center since these ions emit strongly in the orange-red spectral region.

9.3 EUROPIUM DOPED BORATE GLASS

In this study, we synthesized two different series of glass compositions, the first part $25\text{Li}_2\text{O}-5\text{Al}_2\text{O}_3-\text{YGd}_2\text{O}_3-(69.0-\text{Y})\text{B}_2\text{O}_3-1.0\text{Eu}_2\text{O}_3$ glasses series and the second series $25\text{Li}_2\text{O}-5\text{Al}_2\text{O}_3-2.5\text{Gd}_2\text{O}_3-(67.5-\text{Z})\text{B}_2\text{O}_3-\text{ZEu}_2\text{O}_3$. Both series were successfully synthesized via a conventional melt-quenching technique and studied properties of density, optical, photoluminescence, and X-ray luminescence. The results show the glass densities provided an increasing trend with the increase of Eu_2O_3 concentrations. In contrast, the molar volume trend is opposite to that of the density with the addition of Gd_2O_3 concentration. Because it can be decreased the inter-atomic distance between the atoms or increased oxygen packing density, causing the structure more compact of the host matrix. The amorphous nature of glass samples was confirmed by the XRD analysis. In the investigation of FTIR spectra, it is found that the glasses are composed of $[\text{BO}_4]$ and $[\text{BO}_3]$ units in the glass network. Nevertheless, no change was observed in the glass structure with the variation of Eu_2O_3 and the addition of Gd_2O_3 in the host matrix. Moreover, the oxidation state of Eu as +3 was characterized by

XANES spectroscopy near L_3 -edges. The optimum concentration of Gd_2O_3 is 2.5 mol% which creates the maximum intensity of X-ray induced luminescence and photoluminescence spectra. In addition, the host glass with different Eu_2O_3 concentrations exploits optimal conditions (LAEUB doped at 2.5 mol% Gd_2O_3). We found that the excitation and emission intensities of all peaks increased up to 3.0 mol% when over 3.0 mol% the intensity decreased because of concentration quenching and energy transfer phenomena. The I-H model indicates that the energy transfer process between Eu^{3+} - Eu^{3+} ions occur in nature as an electric dipole-dipole. Moreover, the highest energy transfer efficiency value of the Eu^{3+} luminescence was obtained at 15.36%. The results of CIE 1931 chromaticity coordinates x and y were found to be in the soft red-orange light region. These kinds of luminescence functionality novel phosphor glasses could be a potential candidate for solid-state material applications.

9.4 TERBIUM DOPED BORATE GLASS

A new series of Gd^{3+} - Tb^{3+} co-doped lithium aluminum borate glasses have been prepared by conventional melt-quenching technique with the chemical composition $25Li_2O$ - $5Al_2O_3$ - $Y Gd_2O_3$ - $(69-Y)B_2O_3$ - $1.0Tb_2O_3$ host glasses with the difference of Gd_2O_3 concentrations. From the results, both parameters (density and molar volume) tend to increase with the increase of Gd_2O_3 concentrations. The XRD spectra confirm the amorphous nature of all sample glasses without any crystalline phase. The structural analysis by FTIR confirmed the presence of tetrahedral BO_4 units and trigonal BO_3 units in the borate glass system. Under three excitation wavelengths ($\lambda_{ex} = 222, 275$ and 377 nm) were identified as four signature peaks at 488 nm (Tb^{3+}): $^5D_4 \rightarrow ^7F_6$, 543 nm (Tb^{3+}): $^5D_4 \rightarrow ^7F_5$, 585 nm (Tb^{3+}): $^5D_4 \rightarrow ^7F_4$ and 622 nm (Tb^{3+}): $^5D_4 \rightarrow ^7F_3$, while the strong emission spectra of Gd^{3+} ($\lambda_{ex} = 275$ nm) were observed consists of a peak in addition at 311 nm: $^8S_{3/2} \rightarrow ^6P_{7/2}$ transitions. The result of three emission spectra strong green emission belongs to 543 nm ($^5D_4 \rightarrow ^7F_5$) show increases of photoluminescence output with increasing of Gd^{3+} concentration up to 2.5 mol%. The XANES data has revealed that terbium ions still in +3 oxidation number. And then, the

radioluminescence spectra were measured. The strong emission bands with wavelength are located at 543 nm, so similarly to the photoluminescence results. As a result, it can be said that both the properties (photoluminescence and radioluminescence) have similar trends with increased Gd_2O_3 concentrations. The correlated color temperature (CCT) values were found in the range of 5749-6098 K in between daylight CIE D55 and commercially available white light LED. In the last process, we were prepared glass samples with varying Tb_2O_3 content in the best host $25Li_2O-5Al_2O_3-2.5Gd_2O_3-(67.5-Z)B_2O_3-ZTb_2O_3$ series. The optimum concentration of Tb^{3+} ions is found to be 4.0 mol% doped glass had the highest emission intensity after that, its milky effect because the overconcentration of luminescence occurred and luminescence decay time in a millisecond. The efficiency of energy transfer has been based on the analysis of these data. The energy transfer from Gd^{3+} to Tb^{3+} ions occur through a nonradiative process with an efficiency up to 59.199%.

9.5 DYSPROSIUM DOPED BORATE GLASS

As-synthesized $LAGdxBDy1.0$ and $LAGd2.5BDyx$ series glasses were prepared through melt quenching technique. The density and refractive index parameters increase with increasing Gd_2O_3 concentration because Gd_2O_3 has a higher molecular mass than B_2O_3 . Moreover, the molar volume of as- glasses increases linearly, dependent on Gd_2O_3 content, corresponding to an increase in NBOs. The XRD was used to confirm the amorphous characteristic of all samples. The radioluminescence and photoluminescence emission spectra provided the best emission intensity at 2.5 mol% Gd_2O_3 concentration. The values of CIE (0.3630, 0.4015) and CCT (4556 K) confirmed the emission lies are closest to CCT of the standard white light region, that possible for W-LED application. Therefore, 2.5 mol% Gd_2O_3 concentration was chosen to study Dy_2O_3 concentrations quenching. The varying Dy_2O_3 concentrations in synthesized glasses were studied by UV-VIS-NIR techniques, showing peak intensity of the glasses tends to increase with the increase of Dy_2O_3 concentration. Moreover, FTIR results confirmed the formation of borate groups as BO_3 and BO_4 in the glass system. The photoluminescence spectra represented the highest intensity of Dy_2O_3

concentration quenching is 1.0 mol%, giving three emission bands in blue, yellow and red regions at 482 nm (${}^4F_{9/2} \rightarrow {}^6H_{15/2}$), 575 nm (${}^4F_{9/2} \rightarrow {}^6H_{13/2}$), and 665 nm (${}^4F_{9/2} \rightarrow {}^6H_{11/2}$) transitions, correspond to the radioluminescence spectra results. XANES data verify that the oxidation state of the Dy ions is trivalent typical. Consequently, the developed glasses could be applied for white LEDs applications.



CURRICULUM VITAE

Name: Miss. Wipakorn Rittisut

Education Background:

- | | |
|-----------|--|
| 2011-2014 | Ubon Ratchathani University, Ubon Ratchathani, Thailand.
Bachelor of Science (Physics) |
| 2014-2018 | Suranaree University of Technology, Nakhon Ratchasima,
Thailand. Master of Science (Physics) |
| 2019-2021 | Ph.D. (Physics) Suranaree University of Technology, Nakhon
Ratchasima, Thailand. Degree of Doctor of Philosophy (Physics) |

Academic Experience:

1. Research Assistant at 1.3W : Small/Wide Angle X-ray Scattering, Synchrotron Light Research Institute (Public Organization), Thailand.
2. Research Assistant at 1.1W : Multiple X-ray Texhniques, Synchrotron Light Research Institute (Public Organization), Thailand.
3. Research Assistant at BL5.2 : SUT-NANOTEC-SLRI XAS Beamline, Synchrotron Light Research Institute (Public Organization), Thailand.
4. Teaching Assistant at Laboratory, School of Physics, Suranaree University of Technology, Thailand.